THE UNIVERSITY OF MICHIGAN
INDUSTRY PROGRAM OF THE COLLEGE OF ENGINEERING

SMALL PARTICLE RESEARCH

at

THE UNIVERSITY OF MICHIGAN

Transcript of the Third Ann Arbor Industry-Education Symposium

August, 1958
IP-312

TABLE OF CONTENTS

PROGRAM COMMITTEE MEMBERS

P. R. Crowley	General Mills, Inc.
H. H. Holscher	Owens-Illinois
R. Lo	Whirlpool Corporation
C. G. Spike	Ethyl Corporation
F. L. Black	Industry Program
J. A. Bolt	Department of Mechanical Engineering
F. K. Boutwell	Department of Mechanical Engineering
R. E. Burroughs	Engineering Research Institute
R. E. Carroll	Industry Program
S. W. Churchill	Department of Chemical and Metallurgical Engineering
W. A. Cook	School of Public Health
R. C. Juvinall	Department of Mechanical Engineering
L. L. Kempe	Department of Chemical and Metallurgical Engineering
D. C. Weiss	Engineering Research Institute

INTRODUCTION

The ten talks reproduced in this volume were delivered at the Third Ann Arbor Industry-Education symposium, sponsored by the Industry Program of the College of Engineering. At this meeting, the authors reported on studies and experimental programs, most of which were carried out at the University of Michigan.

This type of meeting represents one way in which the Industry Program reports to participating companies on University research activities, at the same time stimulating an interchange of ideas between technical people in industry and the University.

This book is not a publication; it was prepared primarily for distribution to those who attended the symposium.

OPENING REMARKS

J. Louis York
Chairman of Symposium

SMALL-PARTICLE RESEARCH

The field of research so broadly specified in the title, and so ill-defined by that title, has been skirted by almost all the branches of science and engineering. We define the term by including studies of particle formation and destruction, studies of particle characteristics when combined with fluids to form suspensions or pastes, studies of the suspensions, interactions with other particles and with fluids.

Subject selections were made from the viewpoint of engineering application to problem solving, without tending to slight by exclusion the many other researchers and many other areas of interest. We include some of the basic science which underlies all engineering studies, and recognize that the borderline between science and engineering is hazy indeed.

This program is primarily concerned with particles larger than molecules, but we do include work on large molecules, because the techniques are applicable to a wide range of particle sizes. We are interested mainly in non-living particles, but we do include work on pollens, again because the principles and techniques are applicable to all particles. The particle size of interest ranges from the wavelength of light (about 0.5 micron or 0.00002 inch) to large snowflakes. Our level of knowledge ranges from complex mathematical formulation to crude observational experiments.

Few of the speakers present neatly packaged solutions; all admit that the work to be done is enormously greater than the work accomplished. We do not attempt to present an integrated book of knowledge; we are only opening the doors to our laboratories and our thinking to show you where we stand and where we hope to be going in the foreseeable future.

This brief introduction can only warn of the scope of things to be presented. Further, we should be impudent to attempt a thorough integration of the material. There are those who believe that it will be integrated someday, and those who are equally convinced that we have simply dabbled in unrelated fields of work to pluck out items related only by an artificial and undefinable phrase -- small particles.

LIGHT SCATTERING OF COLLOIDAL SOLUTIONS

Peter Geiduschek
Assistant Professor of Chemistry
The University of Michigan

LIGHT SCATTERING OF COLLOIDAL SOLUTIONS

Peter Geiduschek

INTRODUCTION

The interaction of systems of small particles with radiation is one of the most powerful methods for the study of their size and form. In particular, this brief discussion is intended to provide a simple review of certain aspects of the light scattering from solutions of macromolecules, and to describe methods whereby the mass and size distribution of solute particles in heterogeneous mixtures may be investigated. The enitre topic of light scattering in its many phases and applications has a large and rapidly growing literature, including numerous reviews dealing with limited aspects of the field. The reader is particularly referred to Van de Hulst's general monograph[1] and a number of review articles[2-6] dealing with the light scattering of macromolecular solutions. This discussion deals with a domain of scattering phenomena very different and in many ways simpler, than that discussed by Professor Churchill in the succeeding paper. We restrict ourselves to a consideration of dilute suspensions of particles possessing no secondary scattering. In addition we consider only those scattering phenomena of such particles uninfluenced by the presence of the solute — solvent interface.

LIGHT SCATTERING FROM SMALL PARTICLES

Both the theory of fluctuation[2,7] and the exact molecular theory of scattering[8] give the excess scattering over that of the pure solvent for an ideal solution of point isotropic particles. as

$$R_\theta = KcM \qquad (1)$$

where $K = \dfrac{2\pi^2\left(\frac{dn}{dc}\right)^2 n_o^2}{N_o\lambda^4}$ and $R_\theta = \dfrac{i_\theta r^2}{I_o(1+\cos^2\theta)}$

with i_θ the excess intensity scattered by a unit volume of solution at an angle θ to the incident beam, I_o the incident intensity of unpolarized light, r the distance from the scattering volume to the detector, n_o and n the refractive indices of solvent and solution respectively, N_o Avogadro's number, λ the wavelength of the incident light in vacuo, c the concentration of solute in grams/ml. of solution, and M the molecular weight of the solute.

It will be noted that K is a constant determined entirely by the wavelength of the scattered light and the refractive properties of the system while the reduced scattering intensity, R_θ, is independent of scattering angle if the scattering particles are sufficiently small.

In thermodynamically non-ideal systems, the reciprocal specific scattering intensity is a function of concentration. The theory of fluctuations then yields

$$\frac{Kc}{R_\theta} = \frac{1}{M} + 2Bc + 3Cc^2 + ... \qquad (2)$$

where B and C are the coefficients of the c and c^2 terms of the osmotic pressure — concentration relation:

$$\frac{\pi}{cRT} = \frac{1}{M} + Bc + Cc^2 + ... \qquad (3)$$

It is clear from equation (2) that for sufficiently dilute solutions, specific reciprocal scattering data may be extrapolated to infinite dilution on a scale linear in concentration, to yield the molecular weight. From the experimental point of view, it is therefore necessary to measure refractive index increments, concentrations and scattering intensities. A wide variety of light scattering photometers has been described in the literature and their calibration is the subject of numerous descriptions and discussions[9-12]. Figure 1 shows a simplified diagram of the commercially available instrument used in this laboratory[10,13], which is quite adequate for standard light scattering applications. In practice, Kc/R_{90} (R_{90} is the Rayleigh's ratio for excess scattering at $\theta = 90^\circ$) is usually measured as a function of solute concentration is solutions sufficiently dilute that only the first two terms of equation (2) are of appreciable magnitude. Kc/R_{90} is then plotted against concentration, and extrapolated to c=0. The intercept is the reciprocal of the molecular weight, and the slope of the line connecting the experimental points is twice the second virial coefficient, B (equation 2).

If the solute particles of the scattering system have any dimensions exceeding one tenth of the wave length of the incident light in the medium, then R_θ depends on the scattering angle. The problem of calculating the angular variation of scattering of such a particle involves summing up the waves from all the scattering points in the molecule (taking their differing phases into account) to obtain the electromagnetic disturbance

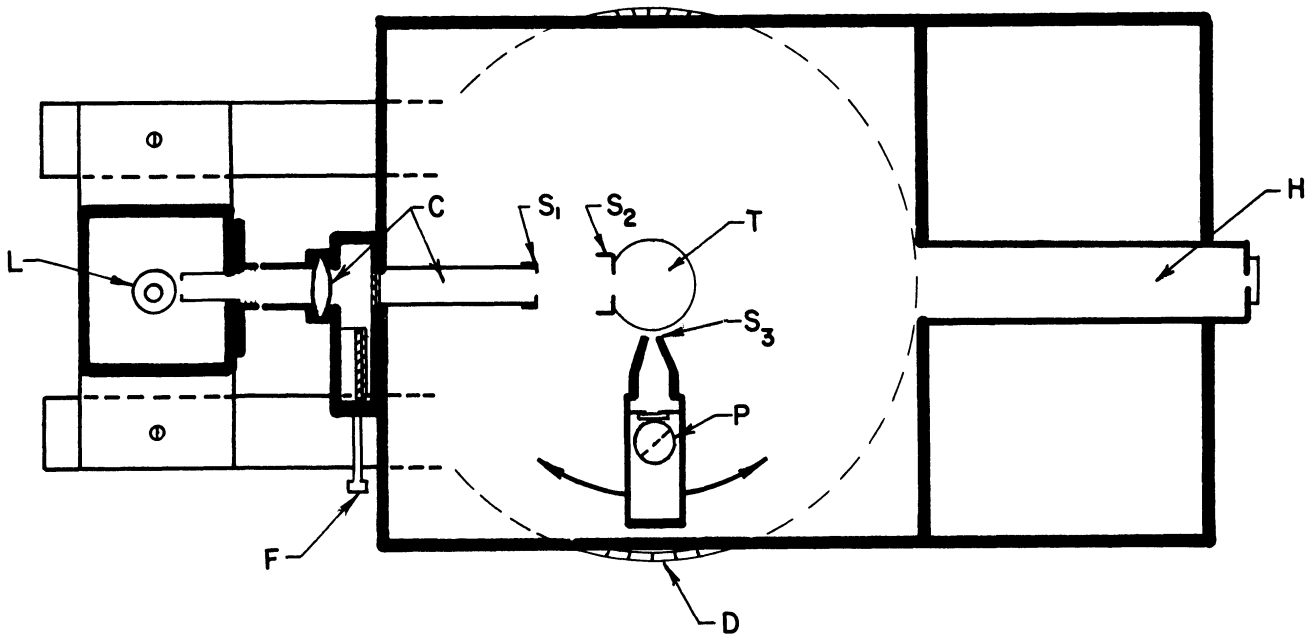

Figure 1. Simplified Schematic Diagram of the Brice-Speiser Light Scattering Photometer.

L light source, F neutral filters. C collimating lenses, S_1,S_2,S_3 slits defining the incident beam and phototube aperture, T cell table, P photomultiplier detector tube, D graduated disk, H light trap.

(and therefore the light intensity) and averaging over all molecular orientations and configurations. Figure 2 is a simple representation of the situation which arises. m and n are two scattering centers in a single large molecule which are located a distance r_{mn} apart. The light scattered from the incident beam by m and n respectively, in the direction θ, has traveled different distances in reaching the detector and is therefore out of phase by

$$\Phi = \overline{Am} - \overline{nB}/\lambda' \qquad (4)$$

where $\lambda' = \lambda/n_o$ is the wave length of the light in the medium, and interference -- a reduction of the scattering power -- results. Only in the forward direction ($\theta = 0$) does the scattering remain uninfluenced by the extension of the solute particles, since Φ approaches zero as θ goes to zero.

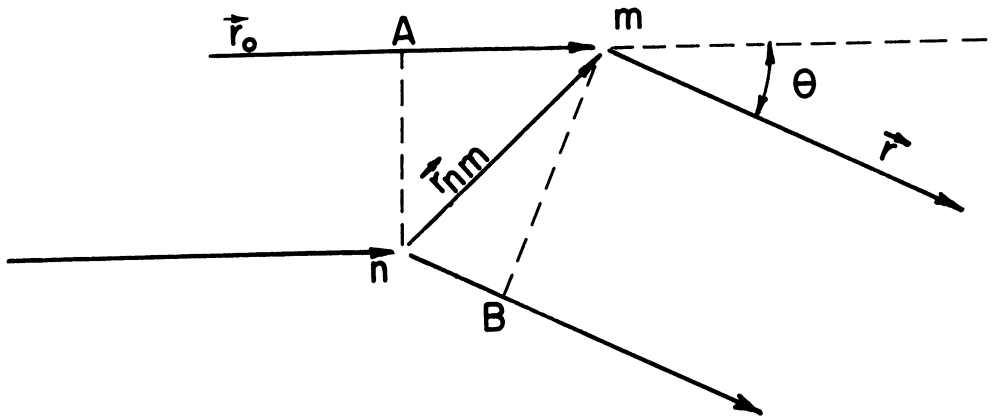

Figure 2.

The above effect is the only one occurring in the scattering by the solute particles under certain restricted conditions:

1) The solution is sufficiently dilute to permit the solute particles to scatter independently;

2) The molecules are randomly oriented in space;

3) The incident beam consists of monochromatic, parallel rays;

4) There is no absorption;

5) The particles are isotropic;

6) Interaction of the scattered and incident radiation inside the particle can be ignored as can be the re-scattering of scattered radiation.

The above conditions are met by most solutions of synthetic high polymers, whatever their molecular weight and the equations which may be then derived are of very general utility.* For such systems, we may relate the shape and size of the particles with the angular dependence of their light scattering. In general, as a consequence of the situation outlined in Figure 1, the Rayleigh ratio for scattering at $\theta = 0$ will be greater than at all other angles and we may write

*The scattering of systems of large globular particles and of dense suspensions, on the other hand, presents a rather different, and more complex situation. The calculations appropriate to that domain of scattering are the topic of Professor Churchill's talk.

$$R_\theta = P(\theta)R_o \; ; \quad R_o = P^{-1}(\theta)R_\theta \tag{5}$$

$P(\theta)$ is called the particle scattering factor; $P^{-1}(\theta)$ is called the reciprocal particle cattering factor. Details of the processes involved in the calculation of particle scattering factors are given in a number of references [2,11, 14-16] and the resulting functions have been tabulated.[6] Figure 3 gives a graphical representation of P^{-1} as a function of angle for a number of particles of different shapes as a function of angular and size parameters, whose significance is discussed below. In general, the reciprocal particle scattering factor, $P^{-1}(\theta)$, may be expressed as a power series of a function of the scattering angle — $\sin^2 \theta/2$:

$$P^{-1}(\theta) = 1 + \frac{h^2\rho^2}{3} + a_2 h^4(\rho^2)^2 + \ldots\ldots \tag{6}$$

where ρ^2 is the square of the radius of gyration of the particle, defined by the ratio of the moment of inertia of the particle to its mass:

$$\rho^2 = \frac{I}{M} = \frac{1}{M} \sum_i m_i r_i^2$$

m being the mass of the particle, m_i the mass of the scattering elements of the particle and r_i their distance from the center of mass; $h = \frac{4\pi n_o}{\lambda} \sin\theta/2$ and a_i are the coefficients of the expansion in even powers of h and ρ. In other words, at sufficiently low values of the angle θ, $P^{-1}(\theta)$ is a linear function of $\sin^2 \theta/2$, and the slope of $P^{-1}(\theta)$ against h^2 yields the radius of gyration. For particles of known shape this latter quantity may be related to more familiar size parameters. For instance,

$$\rho^2 = \frac{L^2_{rod}}{\ell 2} = \frac{3R^2_{sphere}}{5} = \frac{D^2_{disc}}{4} = \frac{1}{6}\overline{R^2}_{coil}$$

With the aid of equation (6) we may also provide a suitable recipe for the determination of molecular weight and size in such systems. From equations (2) and (6) we see that by carrying the measurements to sufficiently low concentrations and angles we may attain that region of concentration and angle from which linear extrapolation of specific reciprocal scattering against c and $\sin^2\theta/2$ yields the molecular weight, i.e.,

$$\lim_{\substack{c \to 0 \\ \theta \to 0}} \left(\frac{Kc}{R_\theta}\right) = \frac{1}{M} \tag{7}$$

Similarly from the definition of the particle scattering factor

$$P^{-1}(\theta) = \lim_{c \to 0} \frac{KcM}{R_\theta} \tag{8}$$

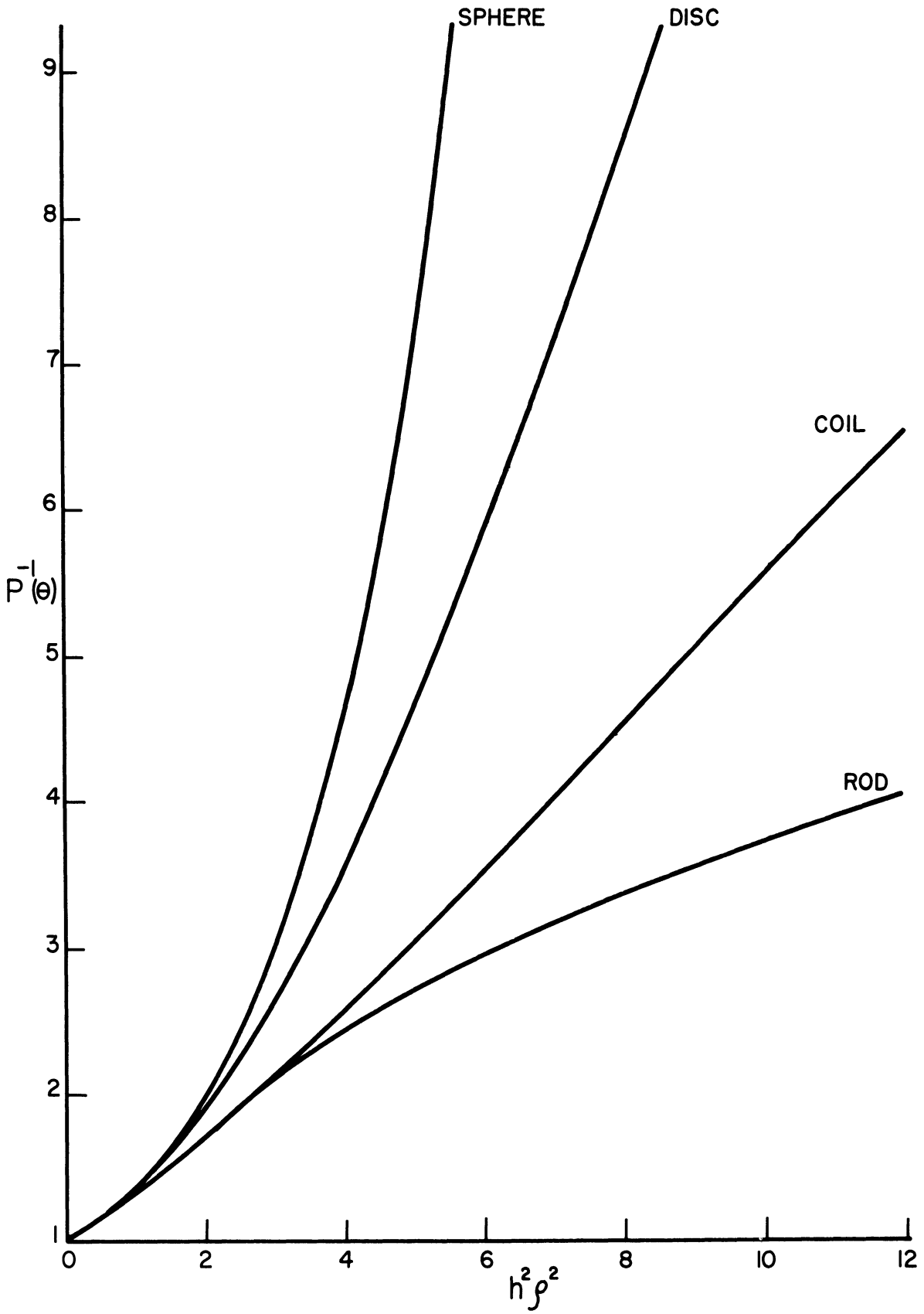

Figure 3. Plots of the Reciprocal Particle Scattering Factors, $P^{-1}(\theta)$, of Monodisperse Spheres, Discs, Gaussian Coils and Infinitely Thin Rods. ρ is the radius of gyration and $h = \frac{4\pi n_o}{\lambda} \sin \frac{\theta}{2}$

while

$$\lim_{h \to 0} \frac{dP^{-1}(\theta)}{dh^2} = \frac{1}{3}\rho^2 \qquad (9)$$

yields the radius of gyration. A very useful and convenient form for these extrapolations has been proposed by Zimm[11] and is in general use for treating the light scattering data of non-ideal solutions of large macromolecules.

POLYDISPERSE SYSTEMS

Thus far, we have confined our discussion to systems in which the macromolecular solute is completely homogeneous with respect to size, shape, and configuration. However, in most real experimental systems, heterogeneity with respect to one or all of these properties is either a given fact, or a dreaded possibility. The light scattering of such heteroform systems can provide information about certain averages of their molecular weight and size distributions. In many heterogeneous systems, the refractive index increment and therefore K are the same for all the solute particles. In that case, at concentrations sufficiently low that each of the solute particles scatters independently of the others, the total scattering will be merely the sum of the individual scattering intensities due to each of the species, i, and

$$R_{\theta tot} = \sum_i R_{\theta i} = K\sum_i c_i M_i \qquad (10)$$

where c_i and M_i are the concentration and molecular weight, respectively, of component i. In consequence, the limiting value of the reciprocal specific scattered intensity gives an <u>average</u> molecular weight — the weight average, $\langle M \rangle_w$:

$$\lim_{\substack{c \to 0 \\ \theta \to 0}} \frac{Kc_{tot}}{R_{tot}} = \frac{1}{\langle M \rangle_w} = \frac{\sum c_i}{\sum c_i M_i} \qquad (11)$$

On the other hand, it is the "light-scattering-average" of the particle scattering factor, $\langle \rho^2 \rangle_{\ell.s.}$ which is determined for a polydisperse system: recalling the definition of $P(\theta)$ we have

$$\langle P(\theta) \rangle_{\ell.s} = \frac{\sum c_i M_i P_i(\theta)}{\sum c_i M_i} \qquad (12)$$

If we proceed to determine the average radius of gyration from the limiting slope of $\langle P^{-1}(\theta) \rangle$ for the polydisperse solute at low values of $\sin^2\theta/2$ or h^2,

then

$$\left\langle P^{-1}(\theta) \right\rangle = \frac{Kc_{tot}\langle M \rangle_w}{R_{\theta tot}} = 1 + \frac{h^2}{3}\langle \rho^2 \rangle_{\ell.s.} + \ldots \qquad (13)$$

inserting the definitions of $R_{\theta tot}$ and M_w, equations (10) and (11), into equation (13), we find that the average of the radius of gyration which we measure is given by

$$\langle \rho^2 \rangle_{\ell.s.} = \frac{\sum c_i M_i \rho_i^2}{\sum c_i M_i}$$

We conclude, then, that the application of equations (11) and (13) to measurements on polydisperse systems yields weight average molecular weights and light-scattering average radii of gyration. However, the heterogeneity of the solute system also influences the shape of the average particle scattering factor. For any given system, the heterogeneity increases, $P^{-1}(\theta)$ assumes more downward curvature with respect to the h^2 or $\sin^2\theta/2$ axis. In general, it is possible to write out all the terms in the series expansion of P^{-1} (equation 6) in terms of successive averages of the size, shape and configuration distributions. However, in order to derive useful numerical information from the experimental data, it is advisable to restrict consideration to specific cases. We shall present here, the analysis of the scattering curve for polydisperse systems of linear chain randomly kinked molecules, built up of identical monomer units[17]. For a monodisperse system of such coils, of degree of polymerization ν, effective bond length b, monomer molecular weight M_o, the reciprocal particle scattering factor may be written as

$$P^{-1}(\theta) = \frac{\chi^2}{2(\chi - 1 + e^{-\chi})} \qquad (14)$$

where

$$\chi = h^2\overline{\rho^2}$$

and the average square of the radius of gyration is $\overline{\rho^2} = \nu b^2/6$. At low values of $h\rho$, as before, $P^{-1} = 1 + \frac{h^2\rho^2}{3}$ and at high values of $h\rho$, that is, for high scattering angle and size, equation (14) can be simplified to give

$$P^{-1}(\theta) = \frac{(h^2\overline{\rho^2})^2}{2(h^2\overline{\rho^2} - 1)} \qquad (15)$$

For a polydisperse system containing a concentration, c_i, of material of degree of polymerization ν_i, the average reciprocal scattering factors are

at low $h\rho$ and at high $h\rho$

$$\left\langle P^{-1}(\theta)\right\rangle = 1 + \frac{h^2}{3}\left\langle\overline{\rho^2}\right\rangle_{\ell.s.} \qquad \left\langle P^{-1}(\theta)\right\rangle = \frac{c_{tot}\left\langle M\right\rangle_w}{2\sum\frac{c_iM_i}{h^2\overline{\rho^2}_i} - 2\sum\frac{c_iM_i}{(h^2\overline{\rho^2}_i)}} \qquad (16)$$

Now, for an ideal Gaussian chain, since $\overline{\rho^2}_i \alpha M_i$

$\left\langle\overline{\rho^2}\right\rangle_{\ell.s.} = \frac{b^2}{6M_o}\left\langle M\right\rangle_z$ where M_o is the molecular weight of a monomer unit, and $\left\langle M\right\rangle_z$ is the z-average molecular weight of the polymer sample defined by

$$\left\langle M\right\rangle_z = \frac{\sum c_iM_i^2}{\sum c_iM_i}$$

and $\left\langle\overline{\rho^2}\right\rangle_w = \frac{b^2}{6M_o}\left\langle M\right\rangle_w$; $\left\langle\overline{\rho^2}\right\rangle_n = \frac{b^2}{6M_o}\left\langle M\right\rangle_n$

where the weight and number averages of $\overline{\rho^2}$ are defined by

$$\left\langle\overline{\rho^2}\right\rangle_w = \frac{\sum c_i\rho^2_i}{c_{tot}} \quad \text{and} \quad \left\langle\overline{\rho^2}\right\rangle_n = \frac{\sum c_i}{\sum c_i/\overline{\rho^2}_i}$$

It follows that

$$\left\langle P^{-1}(\theta)\right\rangle_{h^2p^2\gg1} = \frac{\left\langle M\right\rangle_w}{2\left\langle M\right\rangle_n} + \frac{h^2\left\langle\overline{\rho^2}\right\rangle_w}{2} \qquad (17)$$

and the ratio of slopes of $P^{-1}(\theta)$ vs. $\sin^2\theta/2$ (or h^2) at high and low values of $h\rho$

$$\frac{S_\infty}{S_o} = \frac{3\left\langle M\right\rangle_w}{2\left\langle M\right\rangle_z} \qquad (18)$$

In other words, from the intercept and slope of initial and asymptotic tangents to $P^{-1}(\theta)$ of systems of polydisperse coils, we may obtain the number, weight, and "z" averages of the molecular weight and average square radius of gyration. Figure 4[17] illustrates the relationships presented in equations (16) to (18).

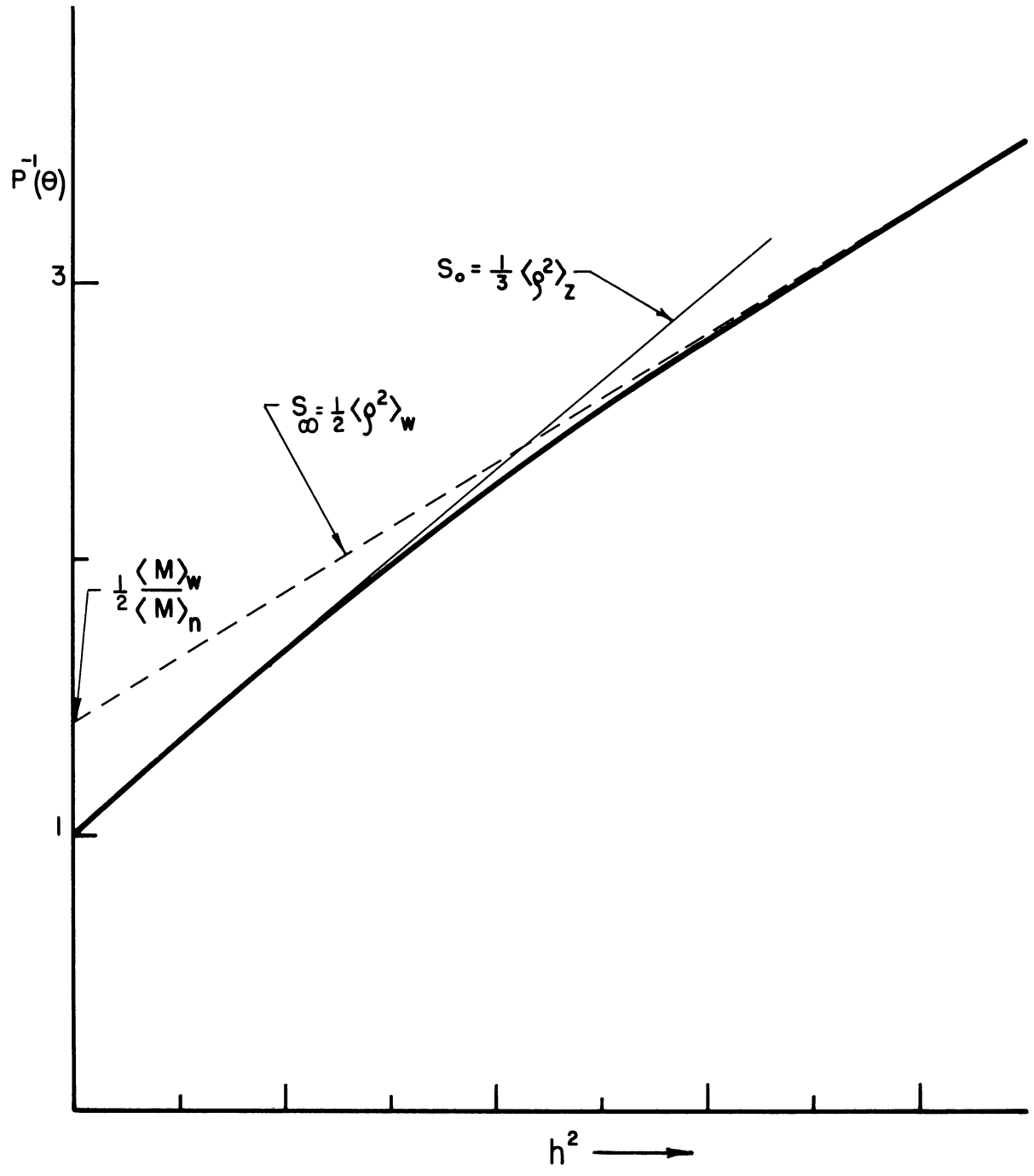

Figure 4. Reciprocal Particle Scattering Factor of a Polydisperse System of Ideal Gaussian Chain Molecules. S_o and S_∞ are the Initial and Asymptotic Slopes of P^{-1} against $h^2 = \frac{16\pi^2 n_o^2}{\lambda^2}\sin^2\frac{\theta}{2}$

What are the conditions under which this seemingly powerful analysis of coiled macromolecular systems is feasible?

a) All the molecules must be made up of identical building blocks--that is to say, b must be constant; one can have heterogeneity of molecular weight only;

b) Molecular coils may show no excluded volume effects. If $\overline{\rho^2}$ is not proportional to M, then certain minor corrections must be made to equations (16) through (18)[18];

c) It must be possible to perform measurements both on the asymptotic and limiting linear portions of the scattering curve, i.e., one must make measurements both at low and high values of $h\rho$.

The location of the lower and upper limits on $h\rho$ depend on how rapidly P^{-1} converges on its two limiting tangents. To examine this point we need to look at the entire reciprocal particle scattering factor curve, which depends, in the polydisperse case, on the molecular weight distribution. In general, we may say the following: the narrower the molecular weight distribution, the quicker P^{-1} converges on its two limits. Multi-peaked distributions probably converge more slowly on their limits than single-peaked distributions leading to the same ratios of weight to number average molecular weights. For the molecular weight distributions likely to be encountered in synthetic high polymers, it is usually necessary to make measurements in the range of $1.6 > h\rho > 2.6$. For example, as is often the case, if the experiments are performed with incident light of 4358 A wavelength, and scattering is measured for the angular range $\theta = 20$ to 145°, then the solute particles must be in the size range given by $500 < \langle \overline{\rho^2} \rangle_{\ell.s.}^{1/2} < 1000$ A. If the particles are smaller than the limits given, then it is only possible to measure the weight average molecular weight, $\langle M \rangle_w$ and the z average radius of gyration $\langle \rho^2 \rangle_z$ (Equations 11, 13); if the solute particles are larger, only the number average molecular weight, $\langle M \rangle_n$ and the weight average square radius of gyration, $\langle \rho^2 \rangle$ (Equation 17) can be determined.

If the system is also heterogeneous with respect to configuration (for instance, if there is a distribution of effective bond lengths), then the above analysis, which assigns all the deviations from the reciprocal scattering factor for a monodisperse system to molecular weight heterogeneity, gives too large an estimate to the breadth of the molecular weight distribution.

APPLICATION

To illustrate the use of these relationships we select data from our own research on a naturally occurring high polymer. The material being studied is sodium desoxyribose nucleate (DNA) a naturally occurring polynucleotide which may be isolated from viruses, bacteria, and the nuclei of the cells of higher organisms. It is a molecule of very high molecular weight. The sample to be described below was isolated from the gonads of salmon. Due to the great difficulties attending its fractionation, very little reliable information is presently available regarding the molecular weight distribution of sodium desoxyribose nucleate, although it is generally recognized that considerable molecular weight heterogeneity must be present. Our approach to the problem has been the following. By rather indirect and somewhat elaborate means, it is possible to dissolve DNA in absolute ethanol,[18] in which it appears to be coil-like and to possess a rather collapsed configuration. On such material we may determine the angular dependence of light scattering by extrapolation of the scattering data from very dilute solutions. By these means, it is possible to determine $\langle P^{-1} \rangle$, the reciprocal particle scattering factor of the nucleate in this solvent medium (Figure 5). The analysis of this scattering curve now proceeds in terms of the equations given in the previous section and yields the results summarized in Table I. Inspection of Figure 5 shows that the curve of P^{-1} has a linear portion both at high and at low angles. The value of the light scattering average radius of gyration, $\langle \rho^2 \rangle^{1/2}_{l.s.}$, of 900 A, also indicates that we are in the right range of sizes for applying the heterogeneity analysis of equations (16) and (18). From that point of view, then, the data of Table I are valid. However, there is no evidence to show that molecular weight heterogeneity is the only type of distribution present. In fact, a priori, it is quite likely that a certain degree of configurational heterogeneity also exists. In that case, the above analysis provides an upper limit estimate of molecular weight heterogeneity. However, in the absence of other data this represents a very useful first approach to the problem of determining the molecular distribution of sodium DNA. For simpler systems of high polymers, such as for unfractionated synthetic macromolecules, the situation is less complicated and for instance, Benoit, Holtzer, and Doty[19] have been able to achieve considerable success with highly heterodisperse nitrocelluloses.

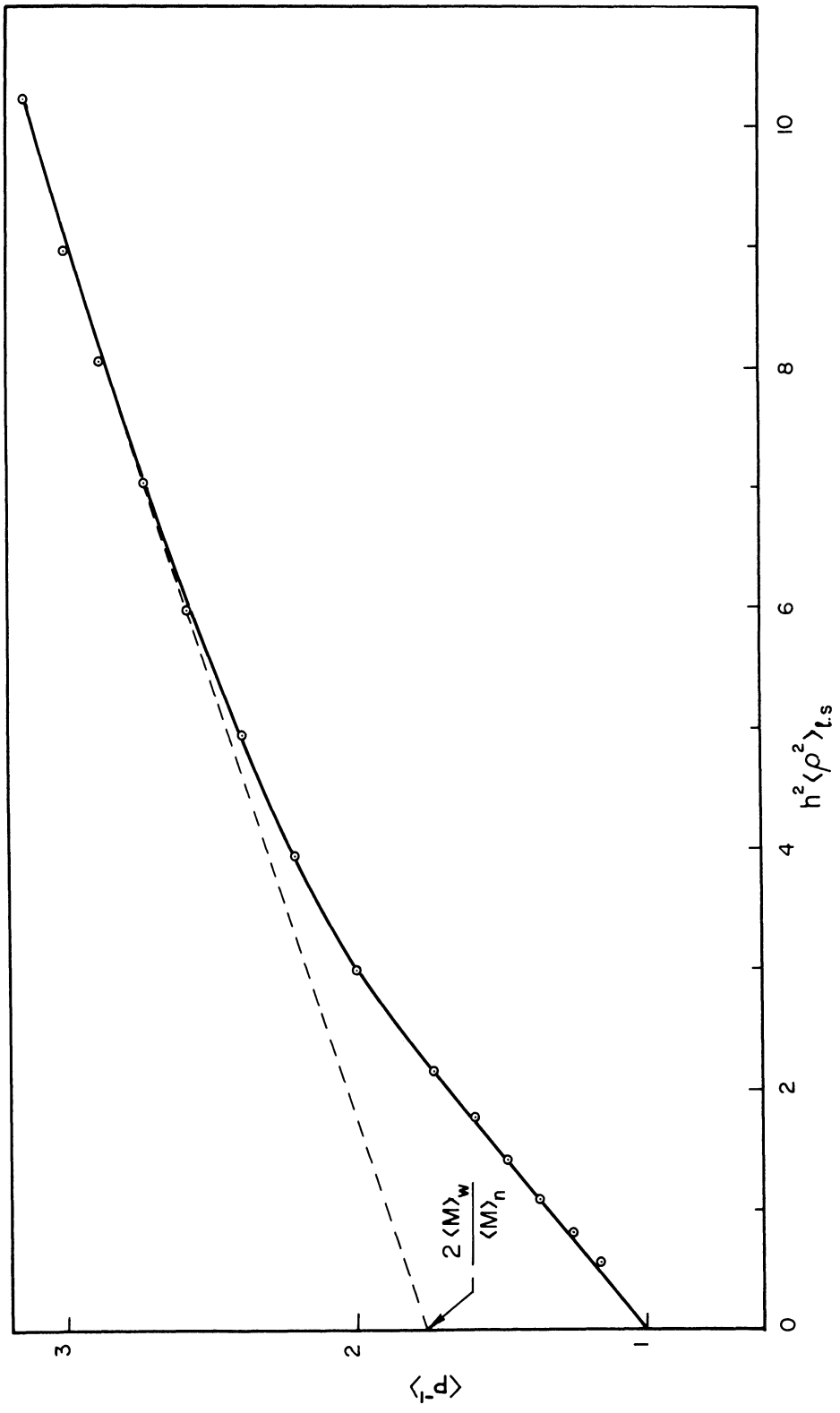

Figure 5. Reciprocal Particle Scattering Factor of a Sample of Sodium Desoxyribose Nucleate (DNA-C-Cu-25) in Absolute Ethanol as a Function of $h^2 < \rho^2 >_{\ell.s.}$

TABLE I

Polydispersity Analysis of a Sample of Sodium Desoxyrebose Nucleate (DNA), Isolated From Salmon, in Absolute Ethanol.

	n	w	z
$< M >$	2.1×10^6	7.4×10^6	27.7×10^6
$< \rho^2 >^{1/2}$, A	250	470	910

Note:

The weight-average molecular weight of the DNA in ethanol is approximately 15% higher, in this case, than in aqueous solution. Undoubtedly this arises from a slight tendency to aggregate in this solvent.

CONCLUSION

In the limited time and space available, only a very cursory review of a highly selected topic from the domain of light scattering in dilute solutions has been attempted. This method is now well established, and with the proper care it proves to be a powerful tool in the elucidation of the size, shape, heterogeneity and interactions of large molecules in solution.

BIBLIOGRAPHY

1. Van de Hulst, H. C., "Light Scattering from Small Particles," (John Wiley, New York, 1957).

2. Zimm, B. H., Stein, R. S. and Doty, P. (1945), Polymer Bulletin 1, 45.

3. Doty, P., and Edsall, J. T., (1951), Adv. in Protein Chemistry 6, 85.

4. Sadron, C., (1954), J. Polymer Sci., 12, 69.

5. Flory, P. J., "Principles of Polymer Chemistry," (Cornell, Ithaca, 1953), p. 283-303.

6. Geiduschek, E. P., and Holtzer, A., (1958), Advances in Biological and Medical Physics 6, in press.

7. Einstein, A., (1910), Ann Phys. 33, 1275.

8. Fixman, M., (1955), J. Chem. Phys. 23, 2074.

9. Stacey, K. A., "Light Scattering in Physical Chemistry," (Academic Press, New York, 1956).

10. Brice, B. A., Halwer , M., and Speiser, R., (1950), J. Opt. Soc. Am. 40, 768.

11. Zimm, B. H., (1948), J. Chem. Phys., 1093, 1099.

11a. Kushner, L. M., (1954), J. Opt. Soc. Am. 44, 450.

12. Billmeyer, F. W., and de Than, C. B., (1955), J. Am. Chem. Soc. 77, 4763.

13. Manufactured by the Phoenix Precision Instrument Company, Philadelphia, Pa.

14. Debye, P., (1947), J. Phys. Coll. Chem. 51, 18.

15. Roess, L. C., and Shull, C. G., (1947), J. Appl. Phys. 18, 308.

16. Neugebauer, T., (1943), Ann. Physik 42, 509.

17. Benoit, H., (1953), J. Polymer Sci. 11, 507.

18. Geiduschek, E. P., and Gray, I., (1956), J. Am. Chem. Soc. 78, 408.

19. Benoit, H., Holtzer, A. M., and Doty, P., (1954), J. Phys. Chem. 58, 635.

LIGHT SCATTERING COMPUTATIONS AND RESEARCH IN THE DEPARTMENT OF CHEMICAL AND METALLURGICAL ENGINEERING

Stuart W. Churchill
Professor of Chemical Engineering
The University of Michigan

Presented by Professor J. L. York

LIGHT SCATTERING COMPUTATIONS AND RESEARCH IN THE DEPARTMENT OF CHEMICAL AND METALLURGICAL ENGINEERING

Stuart W. Churchill

(Presented by Professor J. L. York)

INTRODUCTION

Light scattering by dispersed material is quite receptive to theoretical treatment. However, the available theories yield solutions which are in the form of infinite series of complex functions and invariably require the use of high speed digital computing machinery for their practical application. During the past decade, the faculty and graduate students in the Department of Chemical and Metallurgical Engineering of the University of Michigan have been involved in a number of engineering applications of light scattering and in the course of this work have computed and published six books of tables of light scattering functions. Other theoretical and experimental contributions have been reported in doctoral theses and journal publications.

Professor C. M. Sliepcevich initiated the program in 1948. Professor S. W. Churchill became co-supervisor in 1952 and has continued to supervise the program since Professor Sliepcevich's departure from the University of Michigan in 1955. More than a dozen graduate students and a comparable number of undergraduate students have participated. A number of other faculty members, in particular, Professor C. M. Chu of the Electrical Engineering Department have contributed to various phases of the work.

This paper will review this continuing research program with emphasis upon the computational aspects and will illustrate the character of some of the computed functions.

REVIEW OF PREVIOUS WORK

In 1908 Mie published exact solutions for the interaction of electromagnetic radiation and a single spherical particle. However, his solutions are in the form of infinite series of complex mathematical functions and are inconvenient for direct application or for hand computations. Consequently, most of the earlier applications of light scattering utilized approximate formulas rather than the exact solutions. Since the advent of modern high speed computing machinery in the 1940's, the functions and series occurring in the Mie solution have been computed and tabulated for a wide range of physical parameters, although many important values are not yet available.

One of the earliest and most expensive compilations was prepared and published by C. M. Sliepcevich and R. O. Gumprecht in the course of the development of a method for the determination of the size distribution of spray droplets by light scattering. This set of tables[1] included the light scattering of amplitude functions and the scattering coefficients for a large number of indices of refraction and values of the circumference to wave length ratio. The scattered intensity at a selected number of angles was also included. Two tables of mathematical functions which were computed in the process of computing the light scattering functions were also published.[2,3] The application of the light scattering functions in particle size measurements were reported in journal references [4,5,& 6] and in Dr. Gumprechts' thesis.[7]

Graduate students J. H. Chin and R. H. Boll continued work on light scattering. Dr. Chin developed what is undoubtedly the most exact method available for determining the size distribution of polydispersed systems by light scattering. This work, which is reported in references[8,9,&10] is based upon a very original and interesting mathematical development. It has perhaps received less attention than it merits because of its apparent complexity and very real demand upon experimental precision. However, the experimental demands are inherent in the analysis of a polydispersed system rather than a shortcoming of the method.

Dr. R. H. Boll studied liquid-in-liquid sprays by light scattering. This work which is reported in references 11, 12 and 13, required computation of values of the light scattering functions for relative indices of refraction of less than unity. These computations which have application for dispersions of gas in liquid or solid, liquid in liquid or solid, and solid in liquid or solid have recently been extended and published as a book of tables.[14]

In 1952 sponsored research on multiple scattering by dense or extended dispersions was begun with the assistance of Dr. C. M. Chu. Some of the results to date have been reported in references [15, 16, 17, 18, 19 and 20] and an equal number of papers are in preparation. This work is being actively continued.

The necessity of utilizing the complex Mie solution as an integral part of the formulation of the mathematical representation of multiple scattering provided a strong incentive for simplification of the Mie solutions. This simplification was accomplished by formally rearranging the solution for the angular distribution of scattered light in the form of a simple series of Legendre polynomials.[21,22] The new representation is much more convenient in most applications of

light scattering than the original form of the Mie solutions. The coefficients in this series, called Angular Distribution Coefficients, have now been computed and compiled for a wide range of conditions.[23] In addition an extended table of Legendre polynomials was computed and published for use with the Angular Distribution Coefficients as well as in other applications.[24]

As his doctoral research B. K. Larkin measured the contribution of radiation in heat transfer through porous insulating materials by light scattering techniques and succeeded in correlating the results in terms of a theoretical model based upon light scattering by single spheres and cylinders. As a supplement to this work the light scattering functions for cylinders, analogous to those derived by Mie for spheres, were derived and computed. This work has been reported in Dr. Larkin's thesis and in two papers recently submitted for publication.[25,26,27]

Work on another aspect of light scattering is in progress as the doctoral research of George C. Clark who is investigating experimentally and theoretically the effect of interference between adjacent particles on the transmission of light through dense dispersions.

Several of the many applications of light scattering in engineering are apparent from the above work and publications. The role and importance of high speed digital computing machinery in this type of work is also very apparent.

ILLUSTRATIVE LIGHT SCATTERING COMPUTATIONS

The character of some of the light scattering functions which have direct engineering application and which have been computed at the University of Michigan and elsewhere is illustrated in the following figures.

The angular distribution of the intensity of monochromatic radiation scattered by a single non-absorbing particle is illustrated for an index of refraction of 1.33 and a circumference to wave length ratio of 25 in Figure 1. The critical variation of the scattered light with angle is particularly apparent when it is noted that logarithmic coordinates were used in this polar diagram. The particular figure was plotted from values computed by hand from the tabulated values in references 22 and 23. The variation of the angular distribution coefficients with circumference to wave length ratio is illustrated for an index of refraction of 1.33 in Figure 2. It is this critical variation of scattered intensity with angle and the significant

if less critical variation with circumference to wave length ratio and index of refraction which makes it possible to analyze and characterize dispersions by light scattering.

The total amount of light scattered by a single particle also varies significantly with a circumference to wave length ratio, index of refraction and absorptivity. The scattering coefficient, i.e., the ratio of the scattered light to that geometrically obstructed by a single particle, is plotted as a function of the circumference to wave length ratio in Figure 3 for an index of refraction of 1.44. Although a satisfactory representation is apparently obtained in Figure 3 a great deal of fine structure is discovered if the computations are carried out for a greater number of circumference to wave length ratios as shown in Figure 4. This fine structure is unimportant in many applications but may be significant in applications involving monochromatic light and closely sized particles.

For absorbing materials the light scattering functions are a function of absorptivity as well as of the index of refraction and the circumference to wave length ratio. The variation of the interception coefficient, i.e., the ratio of light absorbed and scattered to that geometrically obstructed by a single particle is plotted as a function of circumference to wave length ratio for a series of values of the absorptivity and an index of refraction of 1.29 in Figure 5.

In order to obtain solutions for problems of multiple scattering Chu and Churchill developed an approximation in which the continuous angular distribution of scattered radiation is represented by six discrete components, one forward and one backward and four sidewise. The variation of the forward and backward components in this six-flux representation is illustrated in Figures 6 and 7 for several indices of refraction and a range of the circumference to wave length ratio. The complex variation of even these "smoothed" functions is quite impressive. In some of the applications of multiple scattering this second order variation has been significant and the extremely detailed calculations required to obtain the fine structure of the curves have been necessary.

As a further simplification, which has proved surprisingly successful in multiple scattering problems the scattered radiation has been represented by only a forward and a backward component. This two-flux representation can in fact be shown to be a better representation than the diffusion model which is widely utilized in the essentially analogous problem of neutron scattering. The light curve in Figure 8 is an estimate of this two-flux back scattered component based upon

computations at a limited number of intervals of the circumference to wave length ratio as indicated by the triangles. Subsequent calculations at a greater number of intervals as indicated by the circles show that the initial estimate was significantly in error at many points. For application involving a wide range of wave lengths such that merely the total area under the curve is important, the limited calculations are sufficient but applications involving a single particle size or wave length require detailed calculations. The detailed results for three indices of refraction are shown in Figure 9.

The light scattering functions shown in the previous figures have all been expressed in terms of the circumference to wave length ratio and the index of refraction. Most commercially important materials have significant and highly selective absorptivity in the visible or infra-red region and have a closely related, critical variation in the index of the refraction with wave length. Therefore, for a real material the use of the previous curves requires experimental data for the variation of the index of refraction and the absorptivity with wave length as shown for water in Figure 10. In general interpolation will be necessary between the various discrete indices of refraction and discrete absorptivities for which the light scattering functions may be plotted or tabulated. For polydispersed materials and distributed sources of radiation such as black body radiation it is apparent that a series of fairly detailed integrations are then necessary to obtain the integral light scattering properties.

CONCLUSION

Computational work is often a necessary part of research in light scattering applications. The continuing improvement and greater availability of high speed computing machinery will encourage the computation of more extensive tables of light scattering functions and this will in turn encourage greater application of light scattering in all branches of science and technology. We look forward to continued participation in this very active field of research.

ACKNOWLEDGMENTS

The above program of research in light scattering and its engineering applications has been made possible by the continuous and concurrent acquisition of computing facilities by the University of Michigan and by the financial support of the Evans Signal Laboratory, U. S. Army; the U. S. Naval Ordance Test Station; the Army Chemical Center; and Armed Forces Special Weapons Project through the Office of Naval Research; and the National Science Foundation. Industrial Fellowships in Chemical Engineering have provided for the financial requirements of several graduate students and materials have generously been contributed by a number of companies. The Engineering Research Institute underwrote the publication of the six books of tables.

LIST OF FIGURES

BIBLIOGRAPHY

1. Gumprecht, R. O., and Sliepcevich, C. M., Tables of Light-Scattering Functions for Spherical Particles, University of Michigan Press, Engineering Research Institute Publications (1951).

2. Gumprecht, R. O., and Sliepcevich, C. M., Tables of Riccati Bessel Functions for Large Arguments and Orders, University of Michigan Press, Engineering Research Institute Publications (1951).

3. Gumprecht, R. O., and Sliepcevich, C. M., Tables of Functions of First and Second Partial Derivatives of Legendre Polynomials, University of Michigan Press, Engineering Research Institute Publications (1951).

4. Gumprecht, R. O., Sung, Neng-Lun, Chin, Jin H., and Sliepcevich, C.M., "Angular Distribution of Intensity of Light Scattered by Large Droplets of Water," J. Opt. Soc. Amer., 42, 226-231 (1952).

5. Gumprecht, R. O., and Sliepcevich, C. M., "Scattering of Light by Large Spherical Particles," J. Phys. Chem., 57, 90-95 (1953).

6. Gumprecht, R. O., and Sliepcevich, C. M., "Measurement of Particle Sizes in Polydispersed Systems by Means of Light Transmission Measurements Combined with Differential Settling," J. Phys. Chem., 57, 95-97 (1953).

7. Gumprecht, R. O., Particle Size Measurements by Light Scattering, Ph.D. Thesis, University of Michigan, Ann Arbor (1952).

8. Chin, Jin H., Particle Size Distributions from Angular Variation of Intensity of Forward-Scattered Light, Ph.D. Thesis, University of Michigan, Ann Arbor (1955).

9. Chin, J. H., Sliepcevich, C. M., and Tribus, M., "Particle Size Distributions from Angular Variation of Intensity of Forward-Scattered Light at Very Small Angles," J. Phys. Chem., 59, 841-844 (1955).

10. Chin, J. H., Sliepcevich, C. M., and Tribus, M., "Determination of Particle Size Distributions in Polydispersed Systems by Means of Measurements of Angular Variation of Intensity of Forward-Scattered Light at Very Small Angles," J. Phys. Chem., 59, 845-848 (1955).

11. Boll, R. H., Gumprecht, R. O., and Sliepcevich, C. M., "Theoretical Light-Scattering Coefficients for Relative Refractive Indexes Less Than Unity and for Totally Reflecting Spheres," J. Opt. Soc. Amer., 44, 18-21 (1954).

12. Boll, R. H., and Sliepcevich, C. M., "Evaluation of Errors of Optical Origin Arising in the Size Analysis of a Dispersion by Light Transmission," J. Opt. Soc. Amer., 46, 200-208 (1956).

13. Boll, R. H., A Rapid Technique for Determining Specific Surface in Liquid-Liquid Sprays, Ph.D. Thesis, University of Michigan, Ann Arbor (1955).

14. Boll, R. H., Leacock, J. A., Clark, G. C., and Churchill, S. W., Tables of Light-Scattering Functions - Relative Indices of Less Than Unity, and Infinity, University of Michigan Press, Engineering Research Institute Publications (1958).

15. Chu, C. M., and Churchill, S. W., "Multiple Scattering by Randomly Distributed Obstacles - Methods of Solution," IRE Trans. on Antennas and Propagation, AP-4, 142-148 (1956).

16. Chu, C. M., and Churchill, S. W., "Numerical Solution of Problems in Multiple Scattering of Electromagnetic Radiation," J. Phys. Chem, 59, 855-863 (1955).

17. Scott, P. H., Clark, George C., and Sliepcevich, C. M., "Light Transmission Measurements on Multiple-Scattering Latex Dispersions," J. Phys. Chem., 59, 849-854 (1955).

18. Chu, Chiao-Min, Clark, George C., and Churchill, Stuart W., "A Six Flux Solution of Multiple Scattering by Dispersion with a Partially Reflecting Boundary," J. Phys. Chem., 61, 1303-1309 (1957).

19. Scott, Philip H., and Churchill, Stuart W., "Transmission of Light Through Multiple Scattering Dispersions of Latex with a Partially Reflecting Boundary," J. Phys. Chem. (To be published in October, 1958).

20. Sleicher, C. A., Jr., and Churchill, S. W., "Radiant Heating of Dispersed Particles," Ind. Eng. Chem., 48, 1819-1824 (1956).

21. Chu, C. M., and Churchill, S. W., "Representation of the Angular Distribution of Radiation Scattered by a Spherical Particle," J. Opt. Soc. Amer., 45, 958-962 (1955).

22. Clark, G. C., Chu, C. M., and Churchill, S. W., "Angular Distribution Coefficients for Radiation Scattered by a Spherical Particle," J. Opt. Soc. Amer., 47, 81-84 (1957).

23. Chu, C. M., Clark, G. C., and Churchill, S. W., Tables of Angular Distribution Coefficients for Light-Scattering by Spheres, University of Michigan Press, Engineering Research Institute Publications (1957).

24. Clark, G. C., and Churchill, S. W., Tables of Legendre Polynomials, University of Michigan Press, Engineering Research Institute Publications (1957).

25. Larkin, B. K., A Study of the Rate of Thermal Radiation through Porous Insulating Materials, Ph.D. Thesis, University of Michigan, Ann Arbor (1957).

26. Larkin, B. K., and Churchill, S. W., "Heat Transfer by Radiation through Porous Insulations," presented at Joint Meeting of A.I.Ch.E. and C.I.C. at Montreal, Quebec, (April 1958).

27. Larkin, B. K., and Churchill, S. W., "Scattering and Absorption of Electromagnetic Radiation by Infinite Cylinders," (submitted for publication).

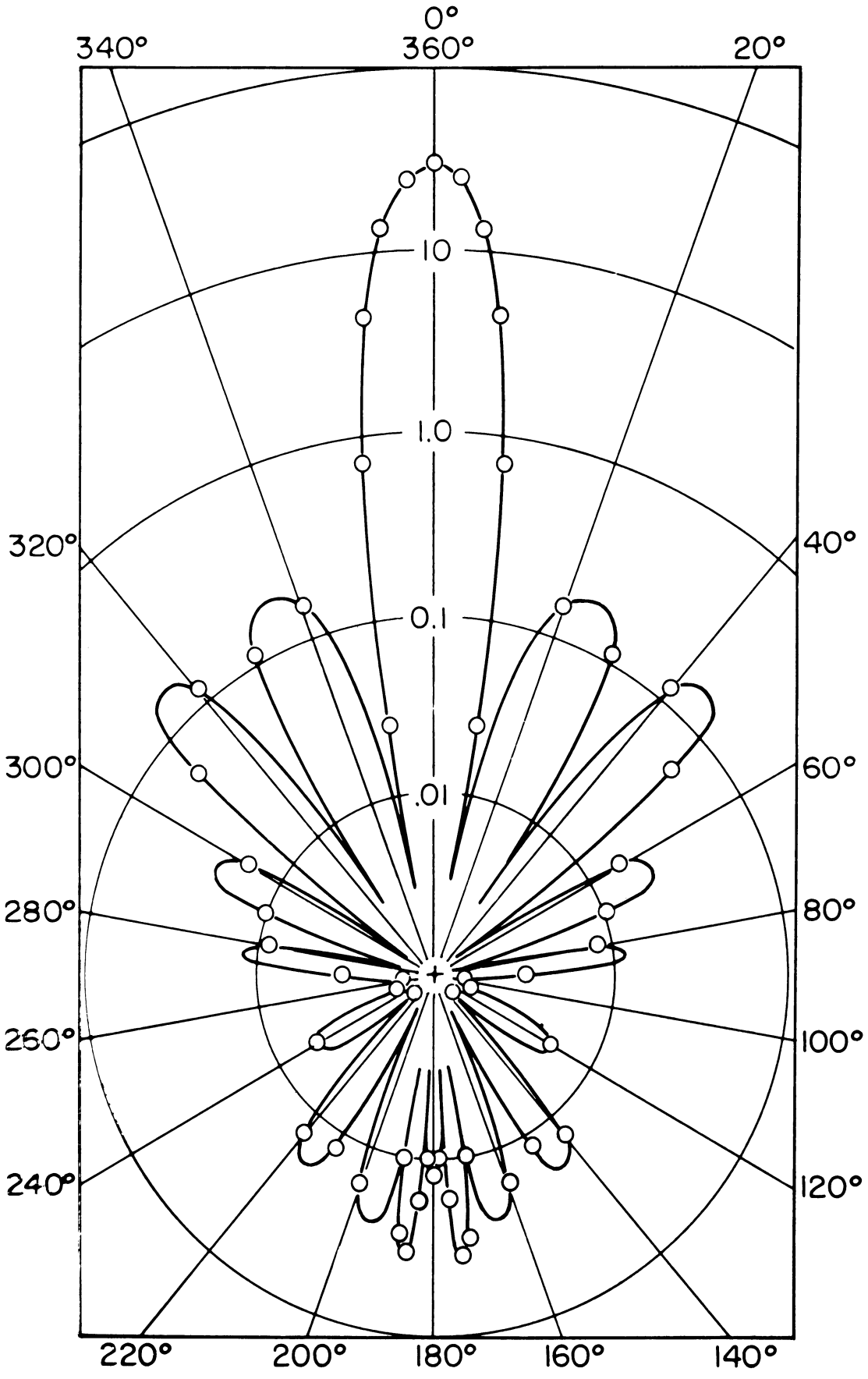

Figure 1. Angular Distribution of Scattered Radiation.

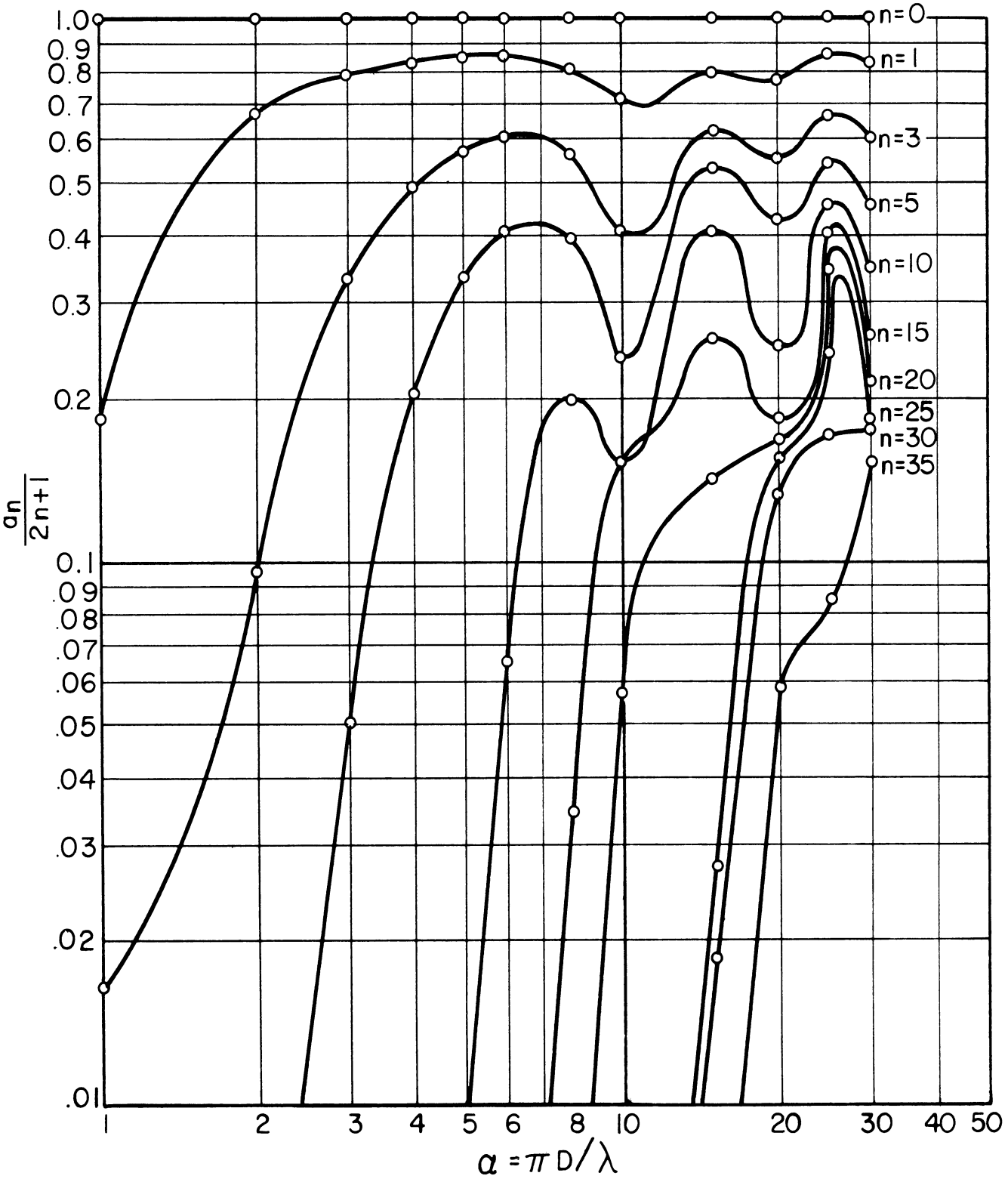

Figure 2. Angular Distribution Coefficients for Non-Absorbing Spheres.

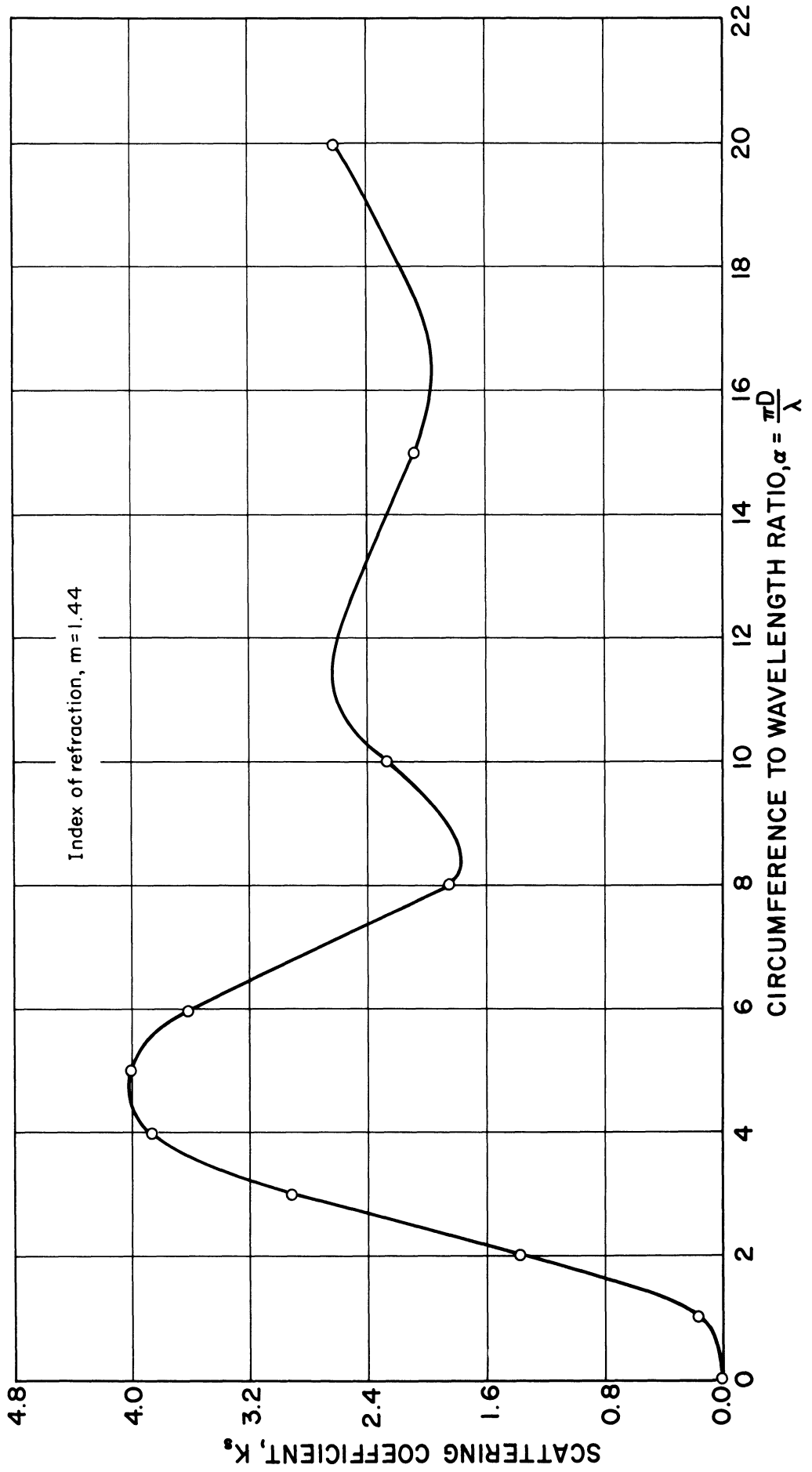

Figure 3. Scattering Coefficient for Non-Absorbing Spheres.

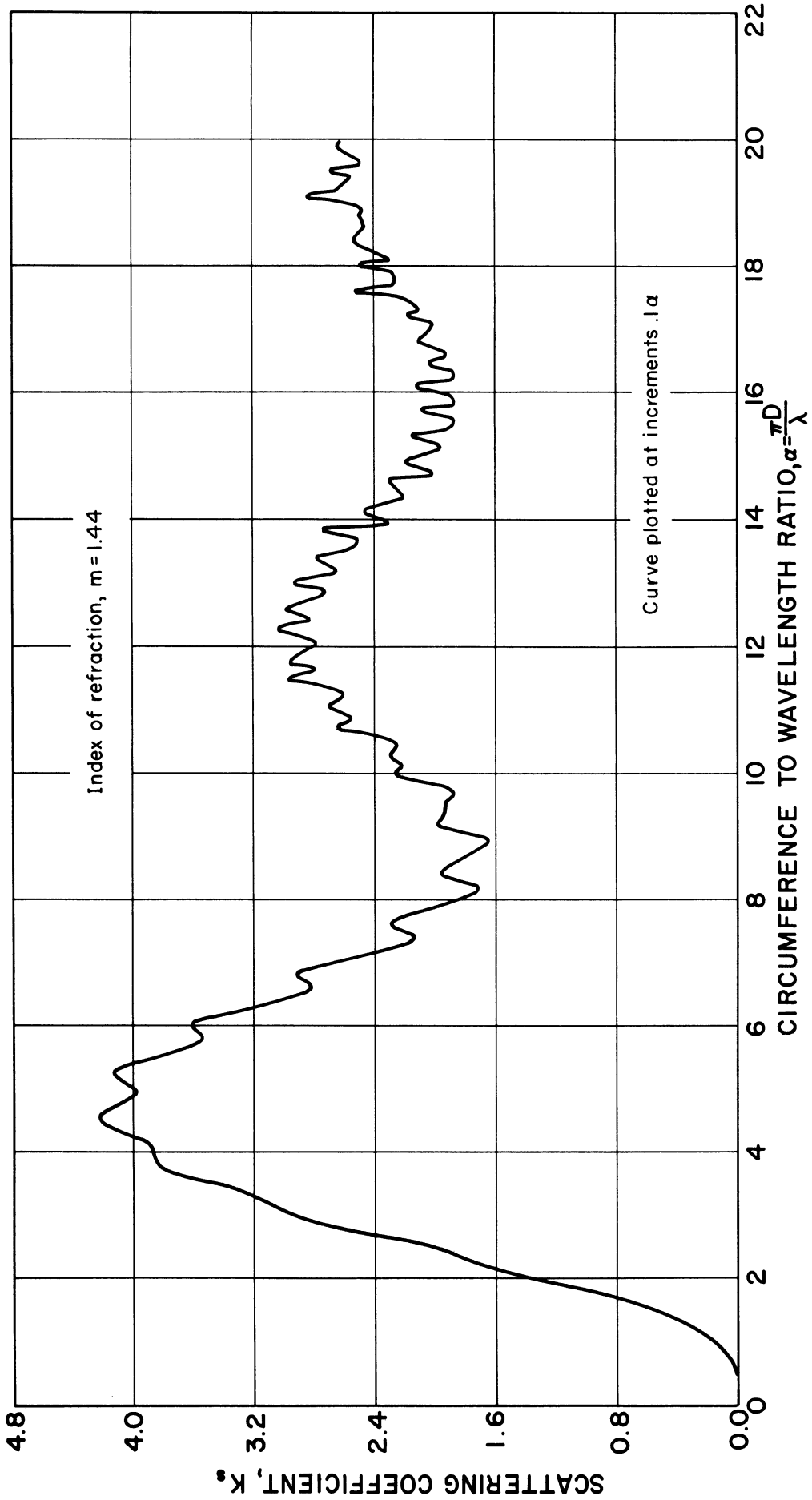

Figure 4. Scattering Coefficient for Non-Absorbing Spheres - Fine Structure.

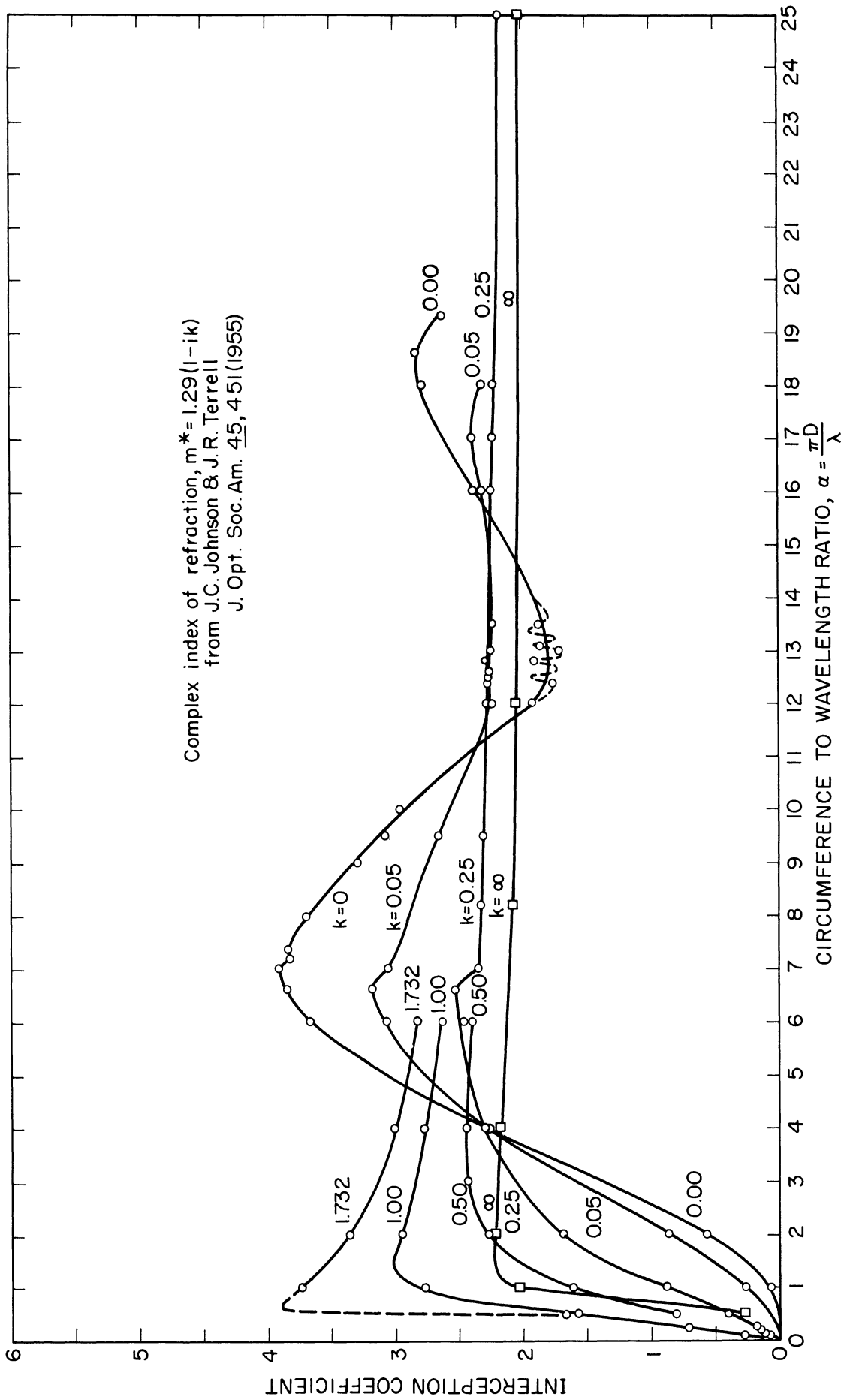

Figure 5. Scattering Coefficient for Absorbing Spheres.

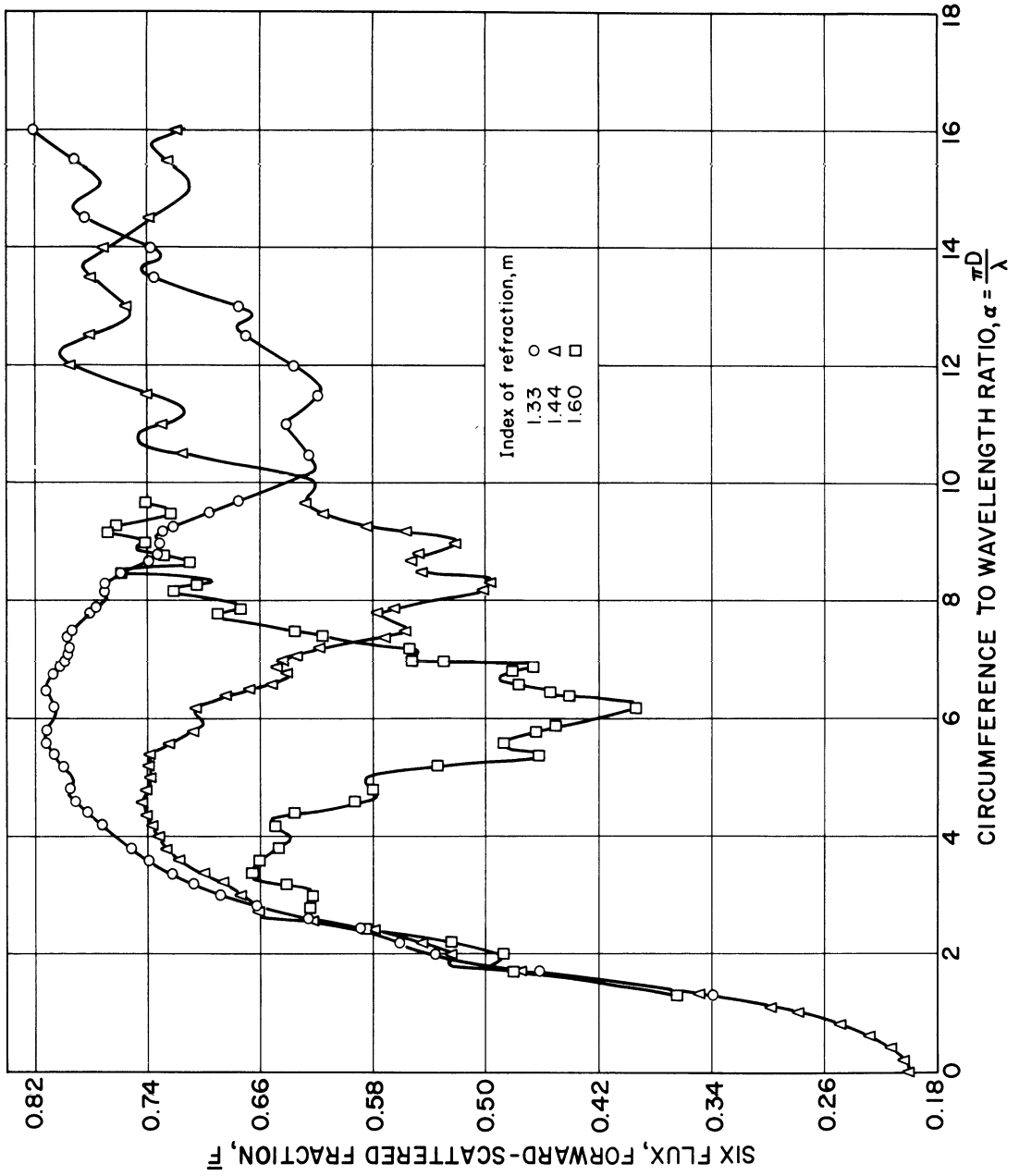

Figure 6. Forward Scattered Fraction, Six-Flux Representation.

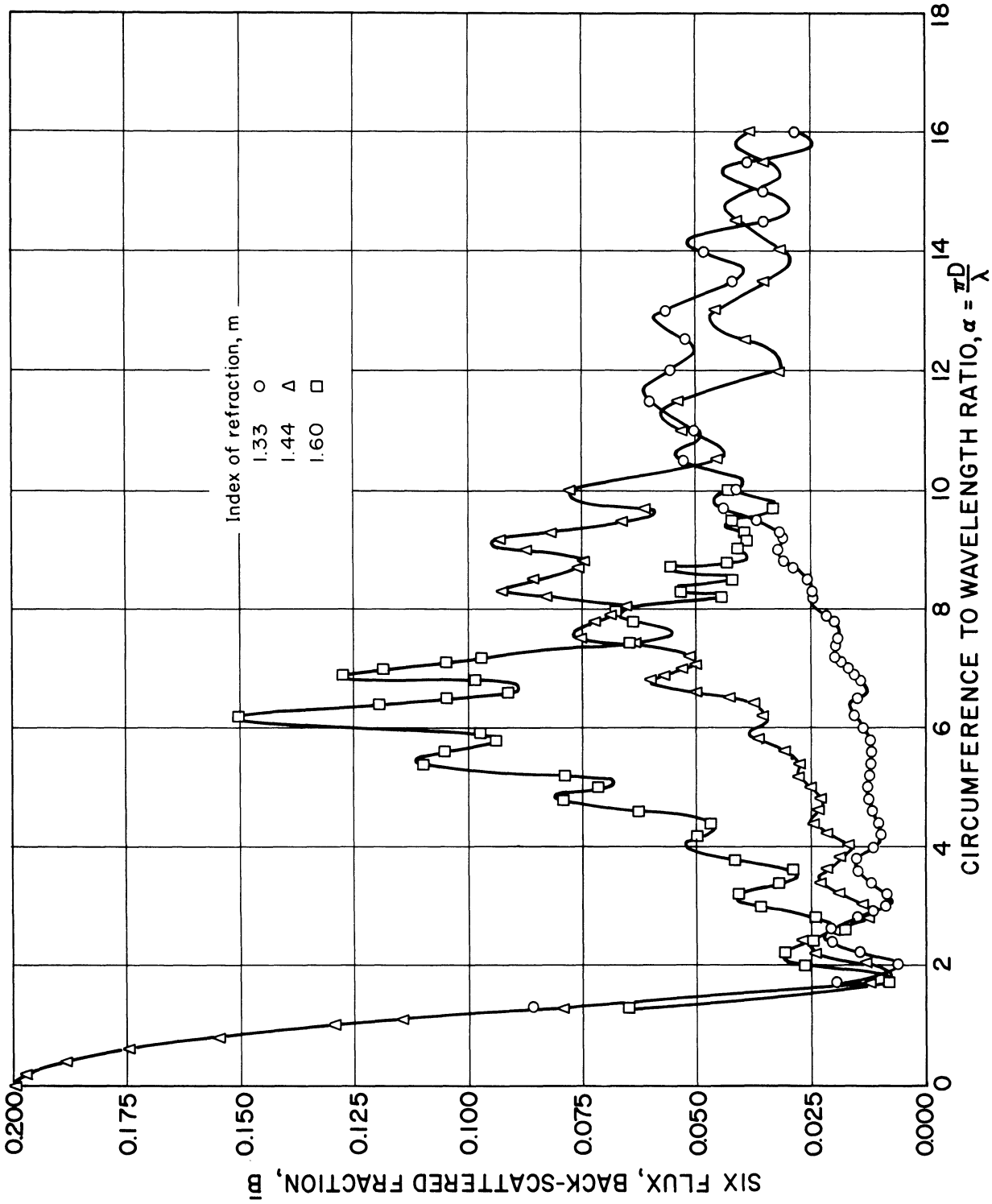

Figure 7. Back Scattered Fraction, Six-Flux Representation.

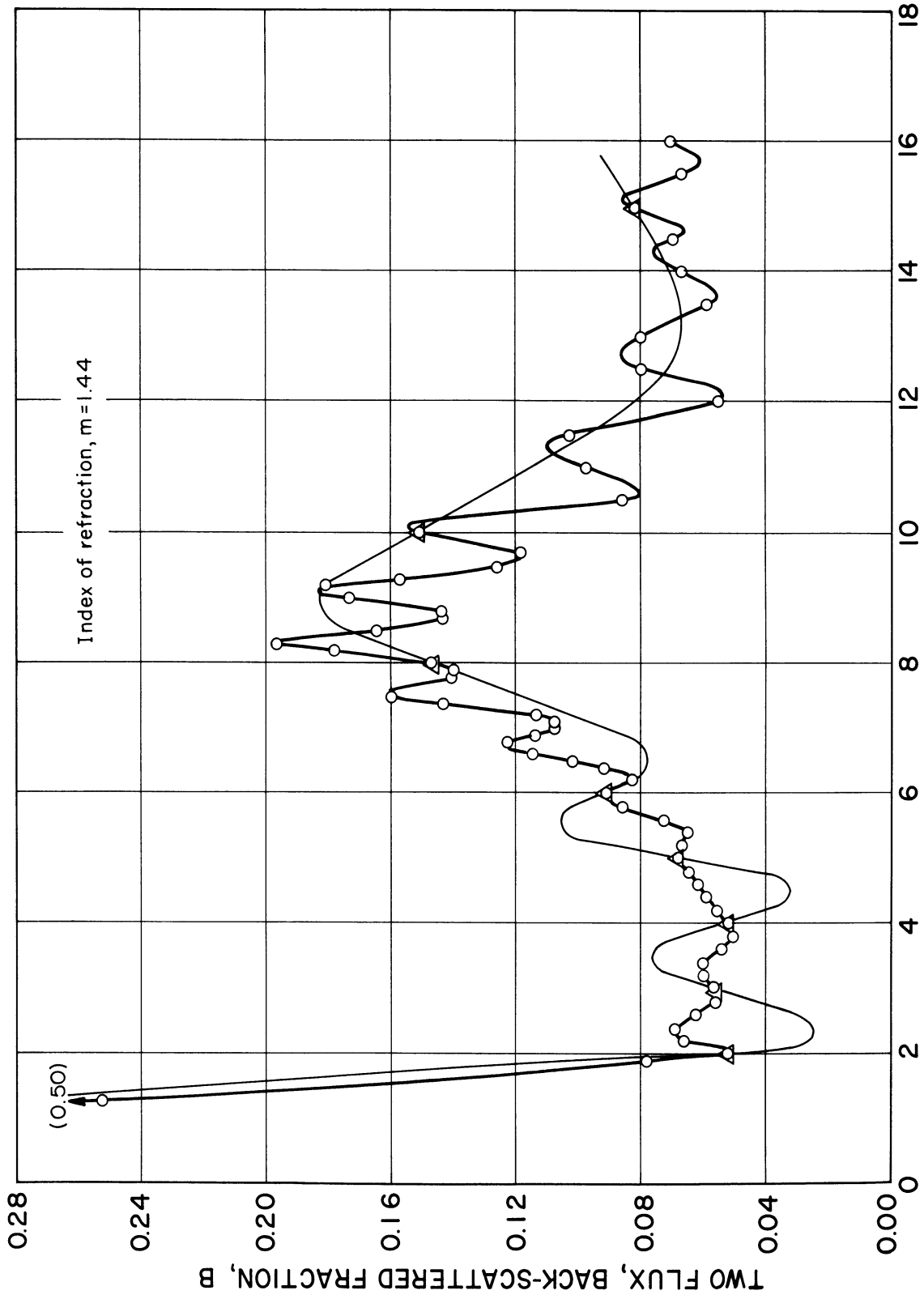

Figure 8. Effect of Fine Structure - Back Scattered Fraction, Two-Flux Representation.

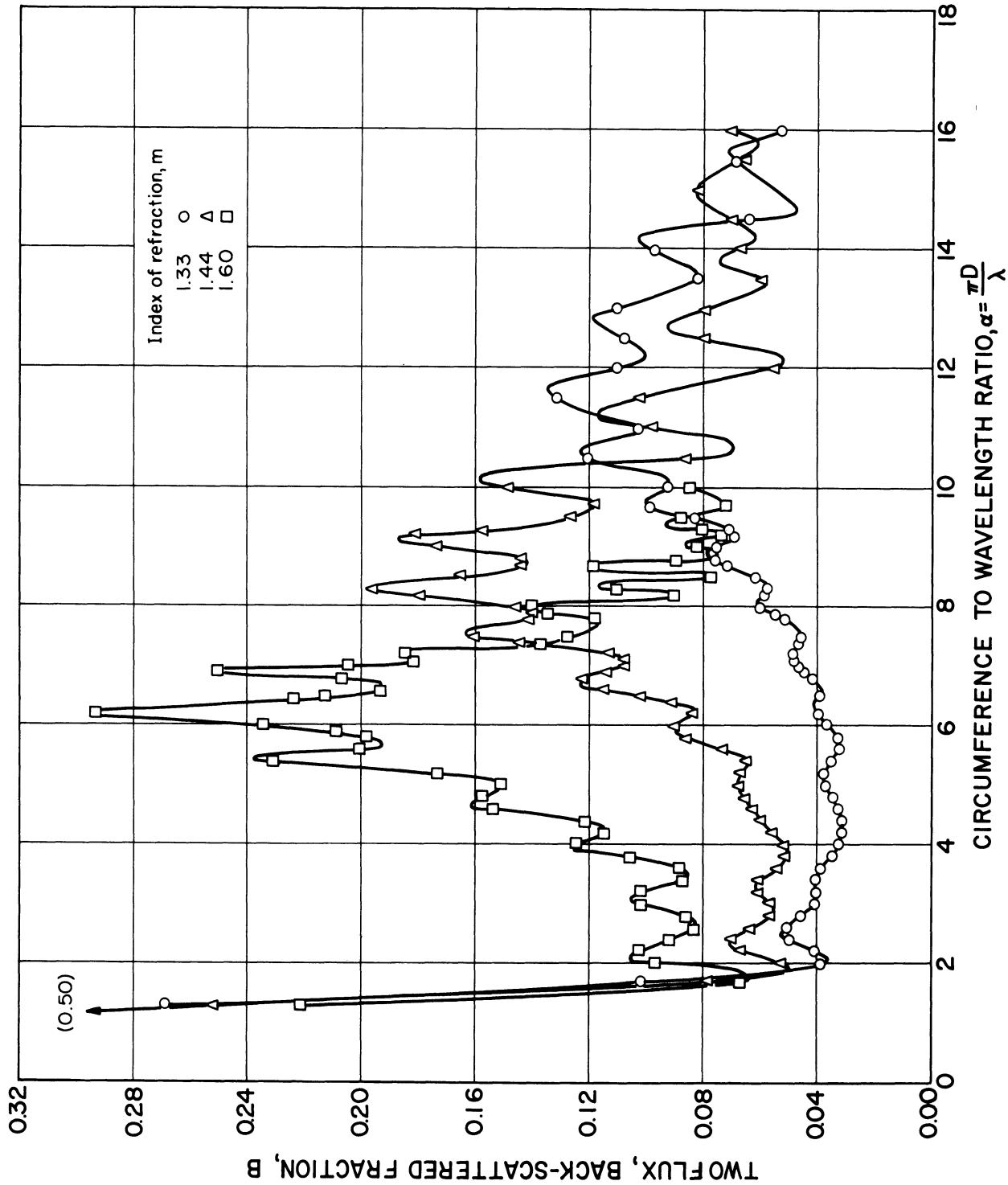

Figure 9. Back Scattered Fraction, Two-Flux Representation.

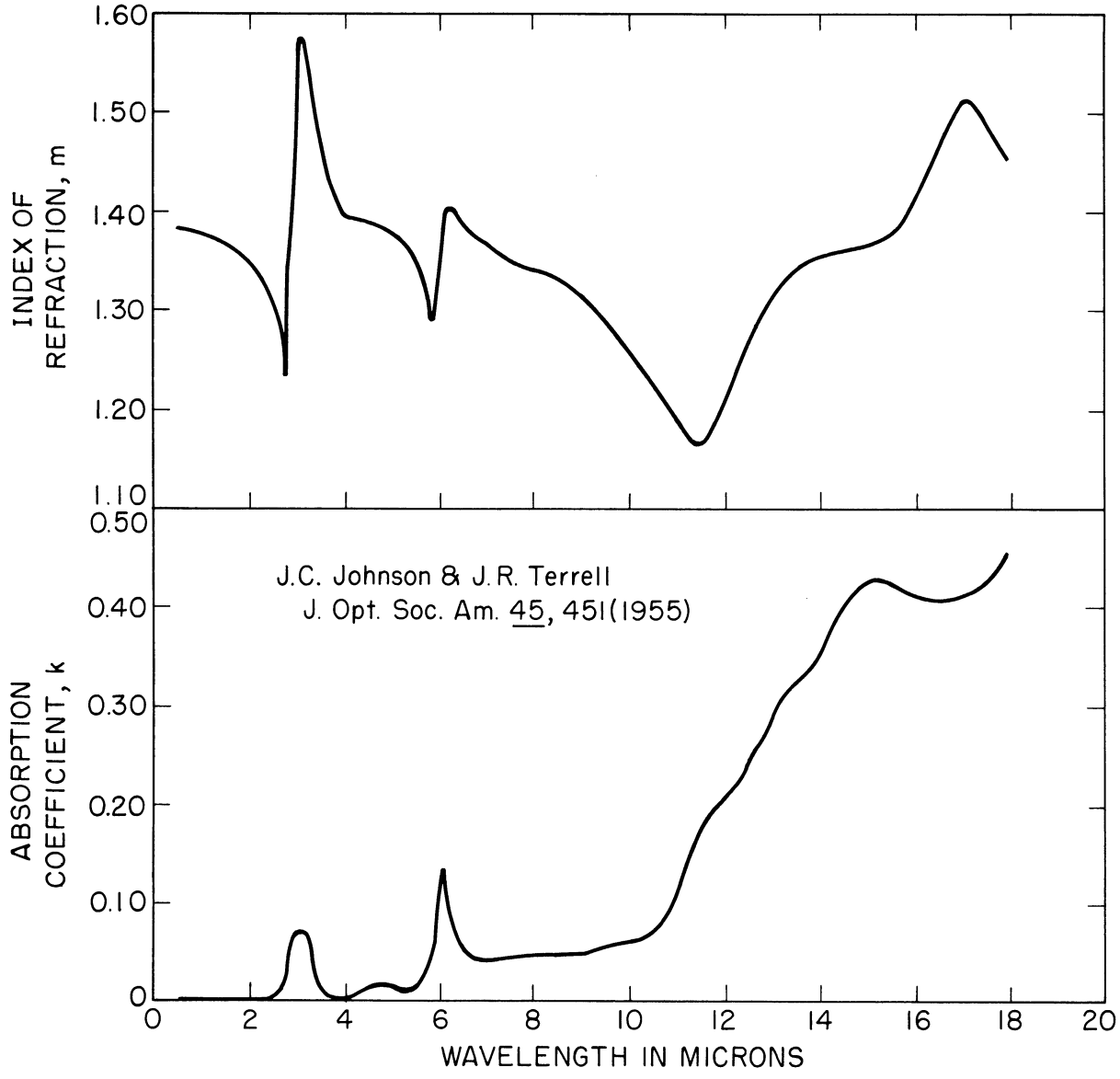

Figure 10. Optical Properties of Water.

POLLEN DISPERSION AND PENETRATION

A. Nelson Dingle
Associate Professor of Meteorology
The University of Michigan

POLLEN DISPERSION AND PENETRATION

A. Nelson Dingle

INTRODUCTION

Initially, our interest in ragweed pollen was stimulated because of the ragweed hay fever problem of the Central and Eastern parts of the United States. In the course of our studies of the Public Health problems associated with this particulate, we have found it to have a number of properties that are useful for studies of atmospheric dispersion.

As a particulate, ragweed pollen is remarkable uniform in size, density and aerodynamic properties. The pollen grain is very nearly spherical, Figure 1, although it is covered with blunt spines. In the most prominent species, Ambrosia artemisiifolia, the range of size of the pollen grains is from about 18 to 21 microns diameter.(1) The fall speed in still air is very nearly 1.58 cm per sec,(2) from which, by Stokes' Law, the density is computed to be about 1.3 gm per cm^3.

In size, therefore, this pollen falls well above the range of particles which can be treated adequately be means of gaseous diffusion ideas and experience, and well within the range of particles that are frequently and relative efficiently airborne. In addition it is readily available in bulk quantities and it is unmistakably identifiable. All of these properties are useful in the experimental study of particulate dispersion and penetration.

GROWTH OF RAGWEED AND NATURAL DISPERSION AND PENETRATION

Manner of Growth and Flowering

The manner of growth of ragweed, Figure 2, is more or less familiar to all. The prominent spikes bear numbers (20 to 50 or so) of cup-like units called involucres. Each involucre contains 6 to 12 male flowers which tend to open at somewhat different times. Figure 3 shows a male flower completely open, with all the pollen swept out. The surrounding flowers remain closed and less elevated. Obviously the wind-exposure of the flower is enhanced if only one flower in the involucre opens at a time. In opening, apparently the central organ (pistillodium) of this flower pushes the pollen in a moist sticky mass out of the flower to dry. Portions of this mass fall to nearby leaf surfaces and to the ground.

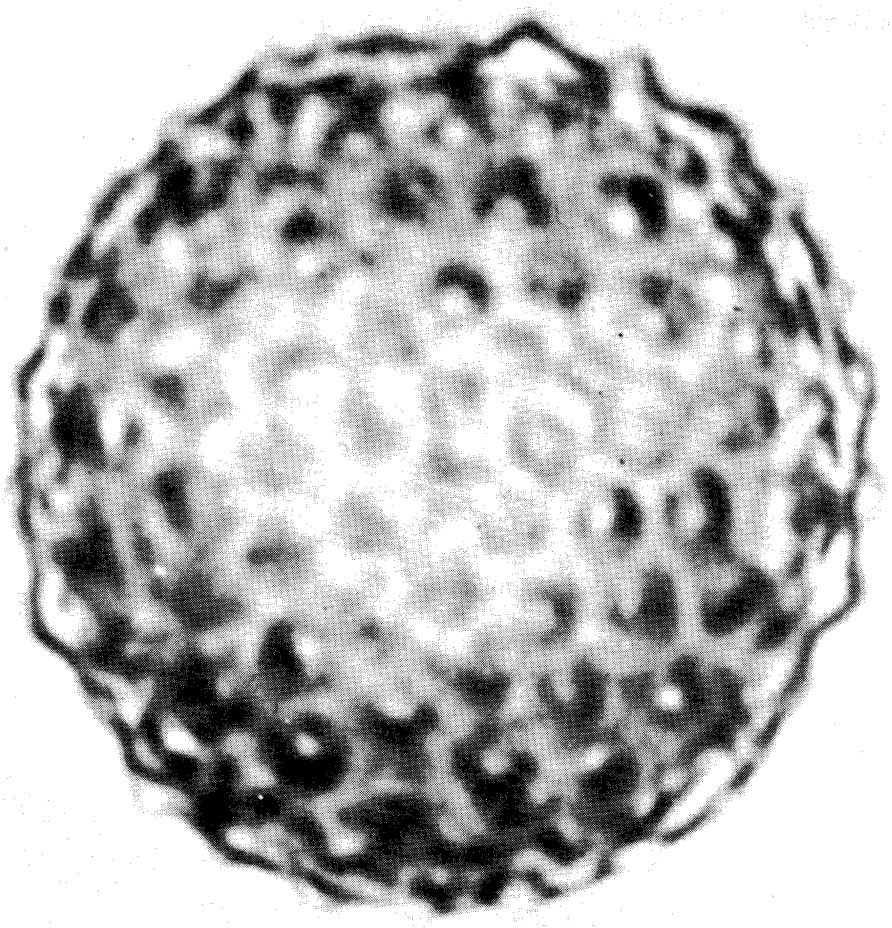

Figure 1. Microphotograph of a typical ragweed pollen grain.

Figure 2. Closeup view of ragweed plant showing general structural characteristics.

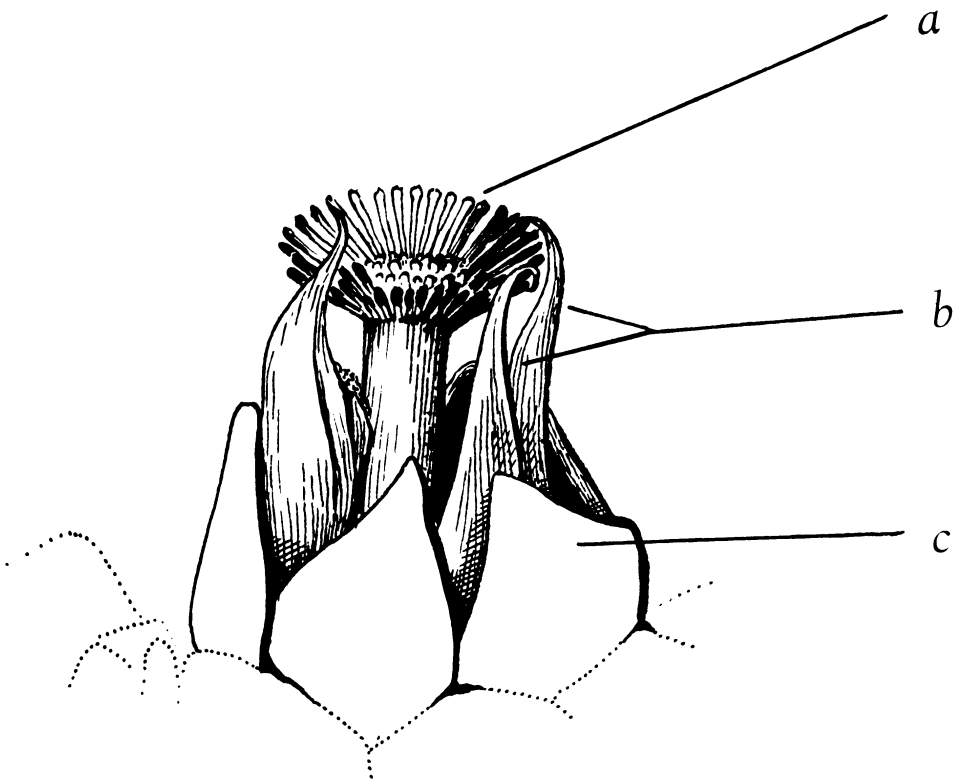

Figure 3. The staminate flower of ragweed (A. artemisiifolia) after the pollen have been carried away. a. The pistillodium. b. The anther tails. c. The lobes of the petals. Dotted lines show the level of the adjacent unopened flowers. Length of pistillodium is about 2 mm.

Ordinarily, the plant grows primarily in recently disturbed, but untended, soil. Thus, it is found along fence and hedge rows, railroad tracks and in vacant lots in urban areas. Important rural growing sites are roadside ditches and the stubble fields left after the harvest of cereal grains. Thus, the primary dispersion of ragweed pollen is accomplished in the natural distribution of the weed.

Wind Dispersion of the Pollen

Obviously the wind is the agent whereby the pollen of ragweed become an air contaminant. The process that results in the elevation of pollen from the plant surfaces (leaves, anthers, etc.) is similar to that which lifts blowing snow or dust into the air. The pollen is favored over soil by virtue of its initially elevated position and hence its enhanced exposure to the air stream, but in both cases, apparently, the breakdown of the surface boundary layer is essential. Thus, all sizes of dust particles remain earth-bound until the wind speed passes the threshold at which the boundary layer is penetrated by occasional gusts. This occurs over smooth soil when the wind speed at anemometer level (15 to 20 ft or so) is about 15 mph.(3)

Despite the favored position of great quantities of polled for pickup by the wind, it is impressive that only a small percentage of the total ragweed pollen crop ever becomes airborne, and that probably less than 0.1 per cent of the pollen crop is carried more than 100 meters from from the source plant. The pollen productivity of ragweed is prodigious, however, so that even 0.1 per cent of the crop is a large quantity.

An additional consideration in the natural dispersion problem is that of reflotation. It appears possible that all surfaces that receive pollen by settling are potential secondary sources from which the wind can refloat the pollen grains. Mechanisms such as the impaction and flushing action of rain must tend to clean such surfaces, but in an extended dry period within the pollen season, reflotation may be an important process contributing to produce high pollen concentrations at great distances from the primary source plants.

Field Observations

Investigation of the natural transport of pollen, during the ragweed pollination season has been based upon a relatively complete observational program centered at our field station on the prison farm northeast of Jackson, Michigan. Figure 4 shows the 100-ft instrument tower at this site. Instruments on the tower include millipore filter samplers at 4 ft, 50 ft and 100 ft and anemometers at 12 ft, 25 ft,

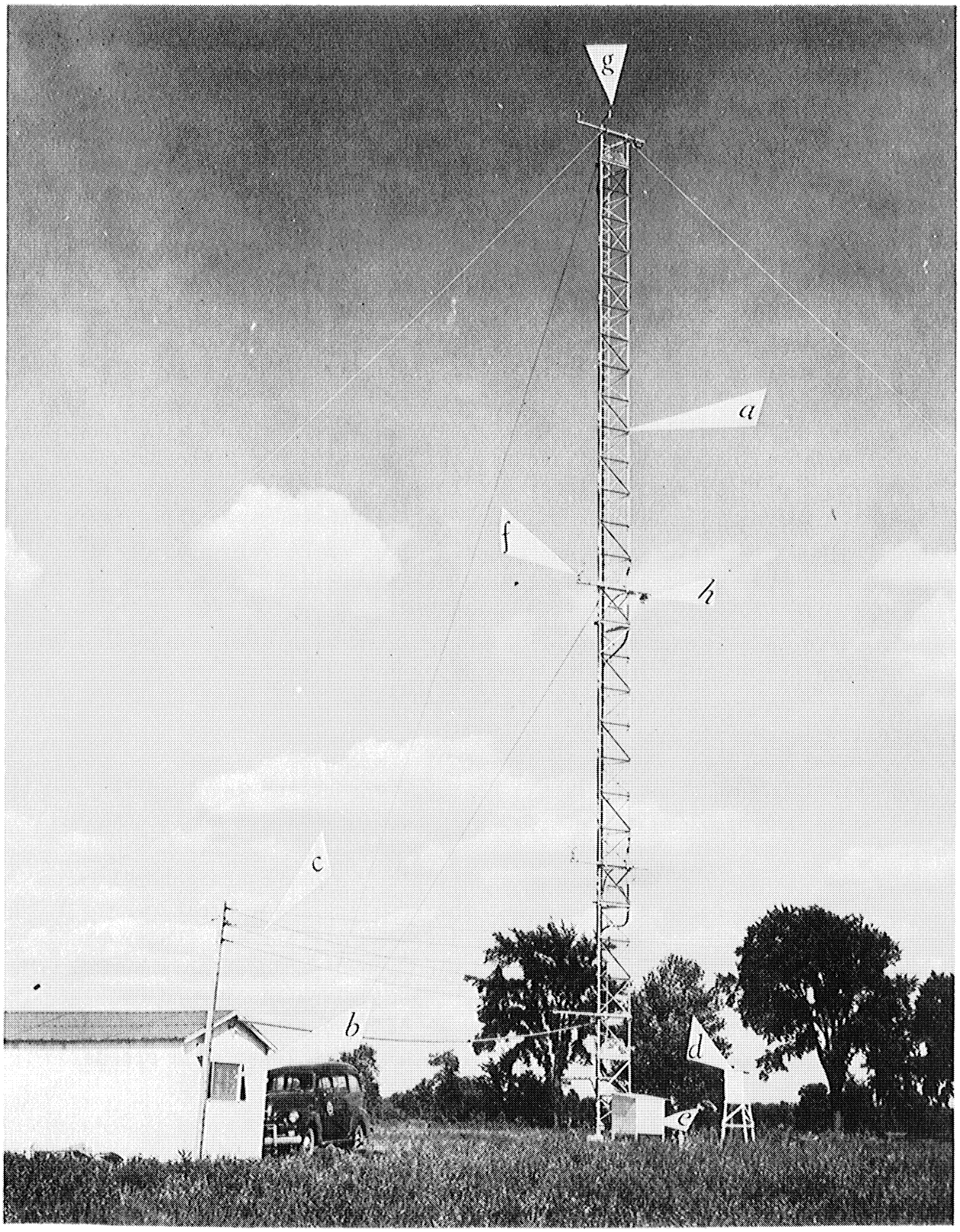

Figure 4. Facilities of the field station. a. 100-ft. guyed tower. b. Instrument hut. c. 110-220 v., 60 cycle, power lines. d. Standard weather station instrument shelter. e. Shelter for blower and air pumps. Details of tower instrumentation include. f. 3-cup contact anemometers. g. Aspirated thermocouples. h. 6-head volumetric sampling units.

50 ft and 100 ft. Records of the wind speeds at these levels are recorded in the instrument shack. In addition provision is made for routine observation of temperature, humidity and rainfall at the station. Sunshine records are maintained at Ann Arbor, and it is assumed that these in a general way, at least, are adequately representative of sunshine at Jackson.

Figures 5 and 6 show graphically some of the results of the field sampling program during the ragweed pollen season of 1956. The days selected for these figures were choses for relative simplicity and constancy of the weather situation. The general decreasing trend of the pollen concentrations from early to mid-September is evident. Aside from the more obvious anomalies, such as the excessively large sample at 100 ft for period I (0030 to 0430 EST) on September 3, which may be attributed to a mistake in handling or identification, the effects of wind speed and of observable instability of the air are apparent. On September 3 and 10, for example, 12-ft wind speeds above 10 mph appear to be associated with markedly increased pollen concentrations. On these days also, the vertical dispersion of the pollen "plume"appears to be relatively limited. On September 2 and 7, however, a more marked vertical dispersion is observed with generally lower wind speeds (7 to 9 mph) at the 12-ft level. This improved vertical transport is correlated with atmospheric instability shown by cumulus clouds on both days, and by a distinct onset of vertical circulation indicated by the marked increase of wind speed at all four levels between 0800 and 1100 EST on the 7th. On September 9 the 12-ft wind speed is remarkably low to have produced the reported pollen concentrations at the 4-ft level; however, the higher level pollen samples introduce new problems of interpretation which call for additional data.

In a general way these observations support the general hypothesis, set forth earlier, that the boundary layer breakdown is a necessary condition to launch pollen into the air stream. Under stable air conditions the relatively higher wind speed produces this breakdown by intensifying the wind shear across the boundary layer; and under unstable conditions, the boundary layer is disturbed by convective breakthrough which serves to carry the pollen aloft at lower wind speeds.

Penetration Under Field Conditions

An experiment was devised to study the penetration of ragweed pollen into an enclosure under natural conditions of wind and pollen supply, during the summer of 1955. A standard contractor's field-office structure was used for this study (Figure 7). After thoroughly cleaning the test room, simultaneous pollen samples were collected inside the room and outside. The air in the room was continuously stirred by four 12-in. oscillating fans.

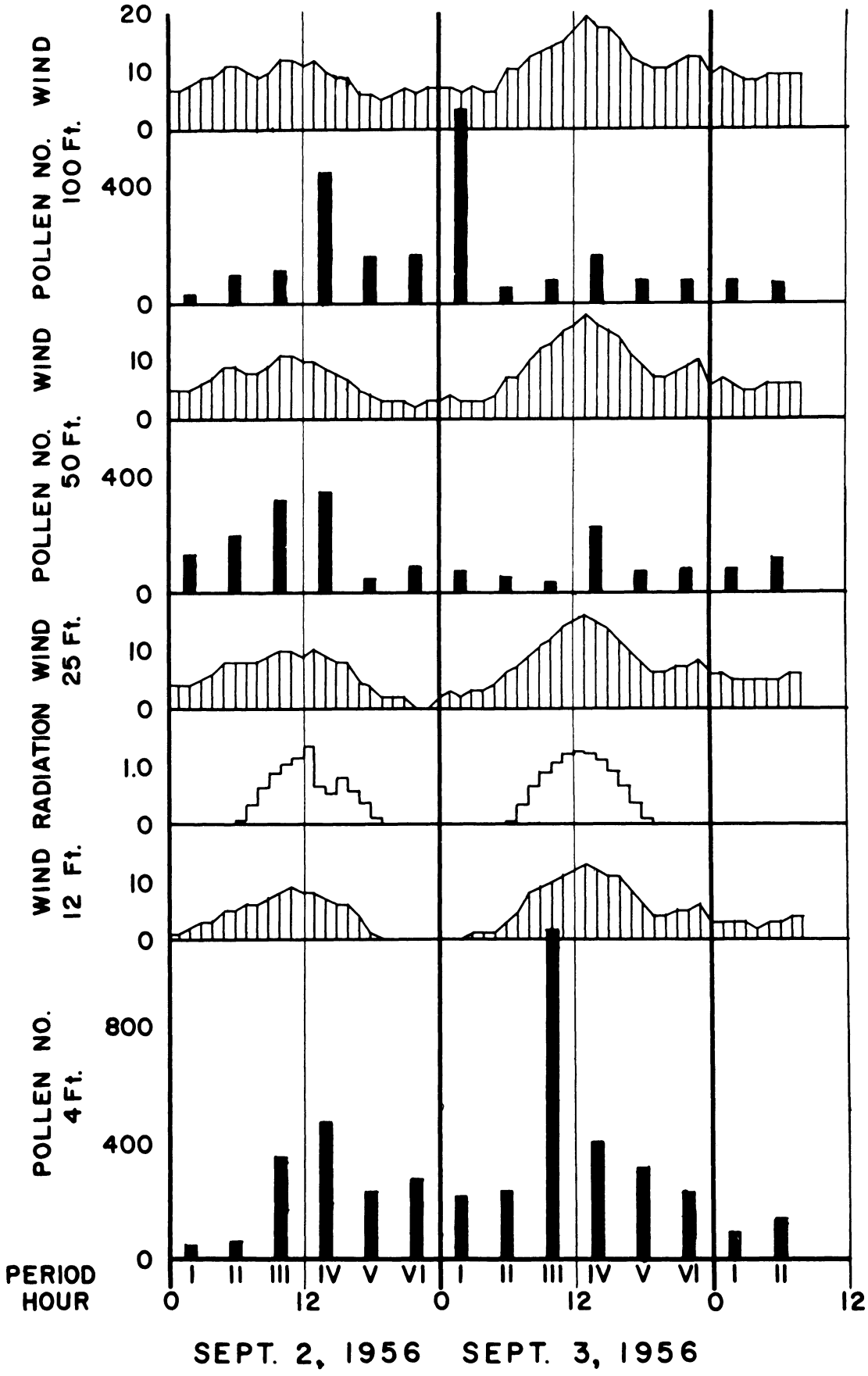

Figure 5. Ragweed pollen counts at three levels, average wind speeds at four levels, and solar radiation for September 2 and 3, 1956.

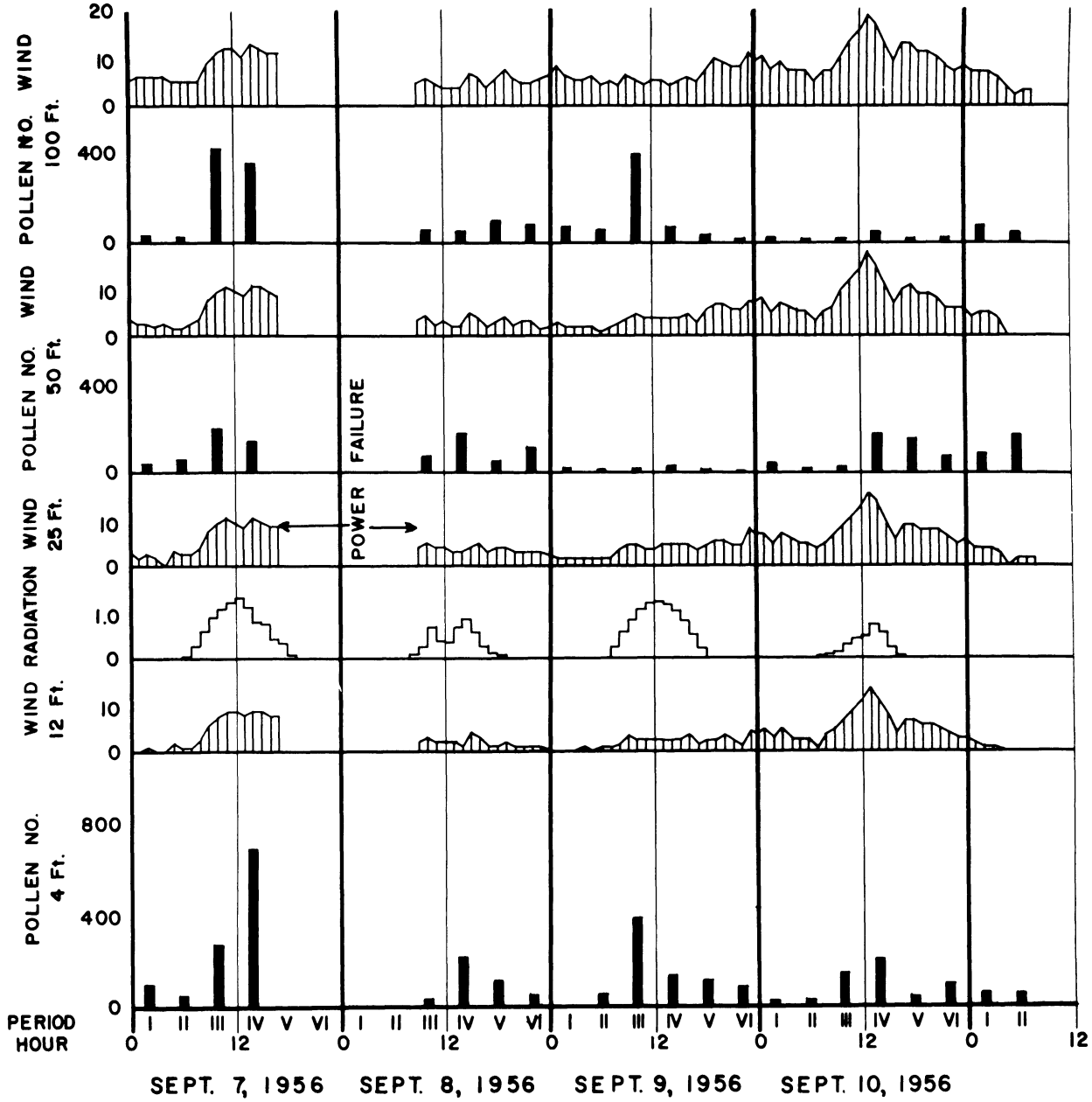

Figure 6. Ragweed pollen counts at three levels, average wind speeds at four levels, and solar radiation for September 7, 8, 9 and 10, 1956.

Figure 7. Field test house for ragweed pollen penetration studies showing outside instrumentation.

Penetration of pollen grains into the test room was assumed to depend entirely upon the exchange of air between the room and the outside. Hence the change of pollen concentration in the room should be directly proportional to the difference between the pollen concentration outside and that inside the room. Since the rate of exchange of air is expressed by the ventilation rate of the room, this rate also must be directly proportional to the rate of change of pollen concentration inside the room. Superficial study of the data by means of graphs suggested that the ventilation rate might be expressed as a quadratic function of mean wind speed. It was necessary to devise a simple index of ventilation rate that could be computed for each pair (outside and inside) of samples. The index chosen was the simple ratio

$$\frac{x}{m} = \frac{\text{inside pollen concentration}}{\text{outside pollen concentration}} \quad .$$

The relation of this index to the ventilation rate, k is superficially indicated by the limiting cases:

$$\text{as } k \to 0 \ , \qquad \frac{x}{m} \to 0 \ .$$
$$\text{as } k \to \infty \ , \qquad \frac{x}{m} \to 1 \ .$$

It was then possible to compute quadratic regressions for $\frac{x}{m}$ as a function of sample mean wind speed, $\bar{v}$. The results were as follows:

(a) windows closed, n = 117 sample pairs

$$\frac{x}{m} = 16.69 + 1.39\ \bar{v} + 0.32\ \bar{v}^2$$

(b) windows open 1 in., n = 88

$$\frac{x}{m} = 4.26 + 14.45\ \bar{v} - 0.60\ \bar{v}^2$$

(c) windows open 3 in., n = 34

$$\frac{x}{m} = -23.56 + 20.31\ \bar{v} - 0.92\ \bar{v}^2$$

In case (a) the regression is as anticipated. The term in $\bar{v}^2$ begins to exceed the $\bar{v}$ term at about 4.5 mph wind speed and becomes increasingly important at higher wind speeds. In cases (b) and (c), on the other hand, the effect of $\bar{v}^2$ is very small within the range of wind speeds encountered during the experiment, suggesting a fundamental difference between the "open-window" and the "closed-window" ventilation processes.

In general, the $\bar{v}^2$ term expresses the effectiveness of the wind in generating dynamic pressure differences between the room and the outside air which serve to ventilate the room through chinks and cracks by virtue of a "pumping action". Evidently when the windows were open as much as 1 in., the air exchange was so free that no substantial pumping forces could be developed, and the ventilation approached proportionality with $\bar{v}$ rather than $\bar{v}^2$

These findings are very similar to those of Georgii[4] who found that ventilation of a closed room was related to wind speed by an expression of the form $a + b\ \bar{v}^2$.

STUDIES UTILIZING ARTIFICIAL CONTROLS

Ragweed pollen very quickly disappear from the atmosphere after the plants stop blooming. Studies by the botany group affiliated with this work show that in all likelihood the great bulk of the pollen is very promptly attacked and digested by certain species of fungi. It is possible, however, to procure pollen for use in experiments outside the normal pollination period. At such times, the pollen serves as a labeled particulate uniquely traceable to its artificial source.

Artificial Emission of Pollen From a Bulk Source

A series of experiments was conducted for the purpose of studying the details of pollen dispersal from a point source. An additional objective of these experiments was to investigate the feasibility of bathing a test structure with pollen in penetration studies. Figures 8 and 9 show graphically the results of these experiments. The source was a small dust atomizer from which pollen were blown into the air stream. A three-dimensional array of impaction samplers (coated microscope slides) was devised using four collapsible frames. Each frame supported 19 sampling stations, at each of which were mounted one sampler facing upward and one facing upwind. In the first experiment (Figure 8), the array was oriented to be downwind from the source. In the third experiment, the objective was to bathe a small test room (Figure 9, low-roofed part of superstructure), with the pollen cloud using the sampling array as a means of monitoring the cloud. Partly for this reason, but principally because other roof obstructions prohibited it, the array was not wind-oriented in this experiment.

The air brush has been used to show gradation of pollen concentrations as they are inferred from the impaction patterns, and to help emphasize the three-dimensional character of the flow.

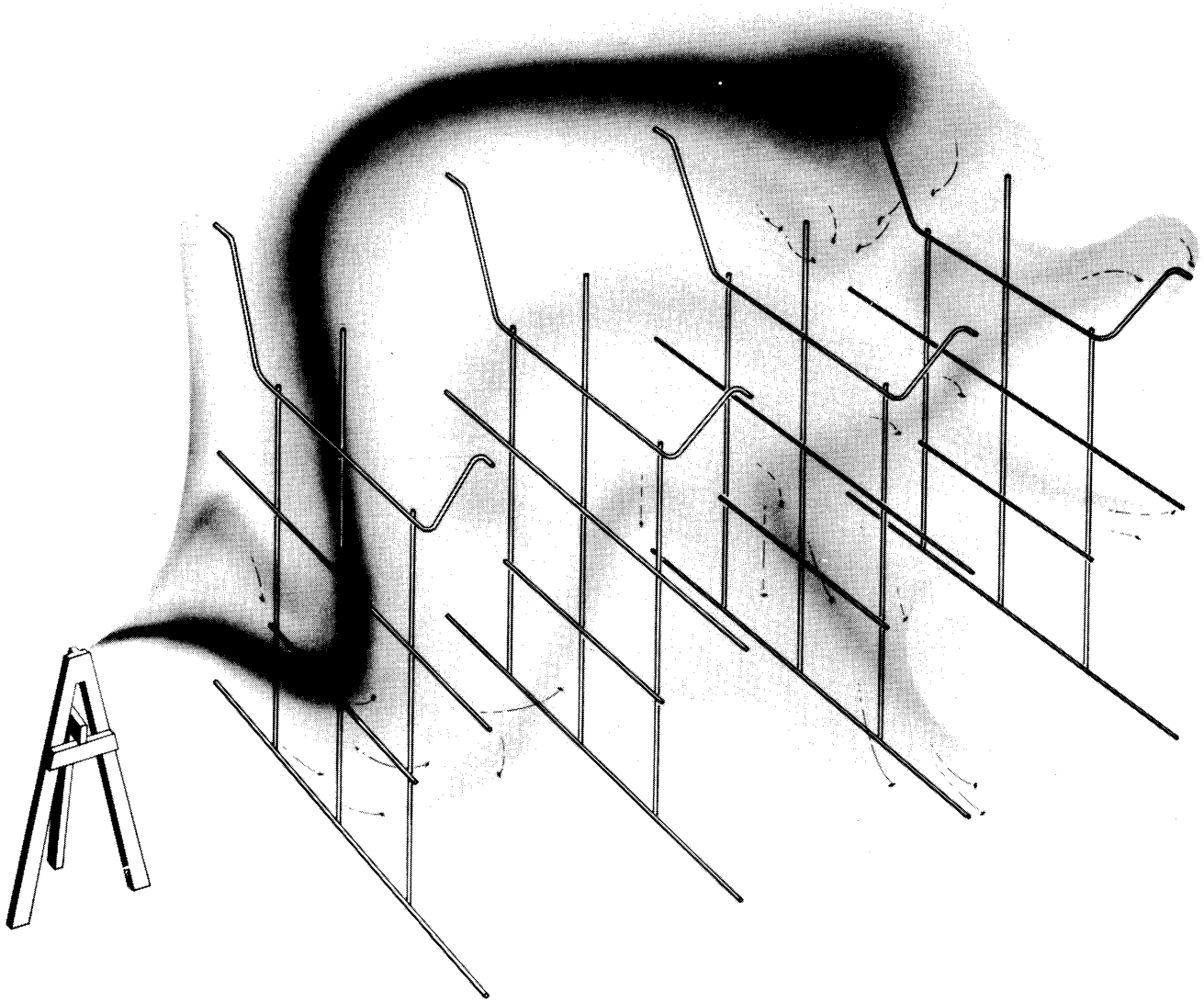

Figure 8. Reconstruction of dispersal pattern of ragweed pollen emitted from a point source, inferred from a three-dimensional array of impaction samples. Puffwise emission over 90-sec period.

In the final test of this series, the penetration of the pollen cloud (Figure 9) into the test room through the partly opened window was investigated. The results of this test are shown in Table 1.

Table 1

Volumetric Pollen Counts in Test Room, May 16, 1955

Sample No.	Time (min)	Pollen Count	Average Wind Speed (mi/hr)	Average Ventilation Rate
1	0-3	94	3.8	0.866
2	3-6	25	3.4	0.654
3	6-9	12	3.6	0.642
4	9-12	6	4.0	—
5	12-15	1	4.7	—
6	15-18	1	4.8	—

Zero time in this table corresponds with the beginning of emission of pollen by the dispenser, which lasted 1 min 50 sec. The average ventilation rate is defined as the number of air changes in the test room per minute. The last two samples were too small to give reliable values for the ventilation rate.

The first value for ventilation rate is probable less valid than the second and third because of the rapid changes of outdoor pollen concentration that necessarily occurred during the time of sample 1. One is assured, however, that the outside pollen concentration was zero within a few seconds after the dispenser was shut off, hence samples 2, 3 and 4 show only the effects of sedimentation and of dilution by clean air. The second and third values for the ventilation rate are therefore considered to be quite valid. These were computed using the equation for ventilation rate under the condition of constant outside concentration, m, which was zero after the first sampling period;

$$k = \left(\frac{\Delta x}{\Delta t} + \frac{w}{h} \bar{x} \right) \frac{1}{m - \bar{x}}$$

where k is the average ventilation rate for the time interval, Δt,

Δx is the change of the inside concentration in the time interval, Δt,

w is the terminal fall rate of the particulate,

h is the vertical dimension of the test room,

and $\bar{x}$ is the average inside concentration for the time interval, Δt.

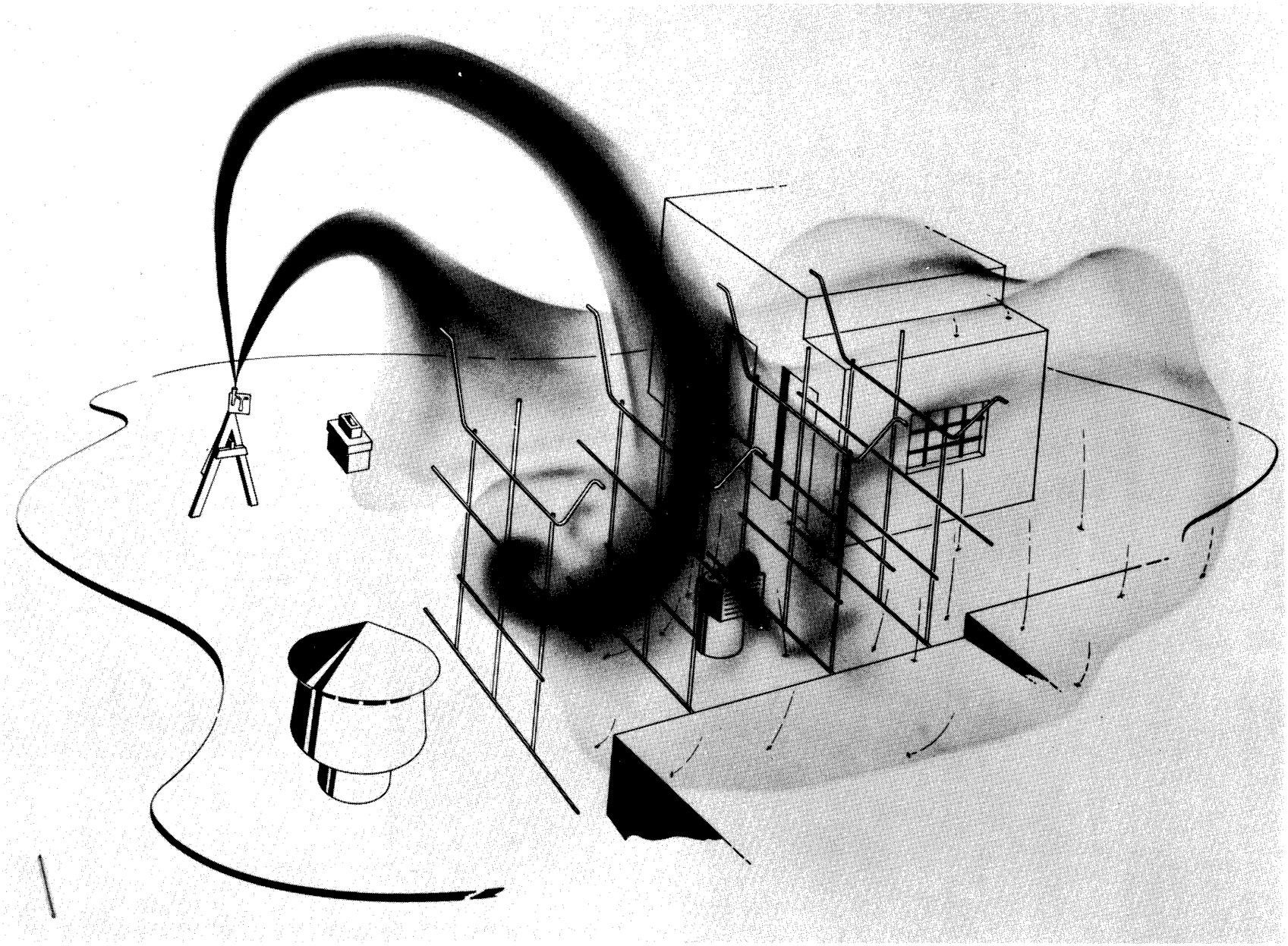

Figure 9. Reconstruction of dispersal pattern of ragweed pollen emitted from a point source, inferred from a three-dimensional array of impaction samples. Puffwise emission over 110-sec period, bathing test room in penetration study.

The Use of Hothouse-Grown, Forced-Blooming Plants

Another means of exploiting ragweed pollen as a particulate tracer material was suggested by the blooming habit of the weed. It is, in botanical terms, a "long-night" plant, which means that it will bloom if it is subjected to nights of the order of 14 hours or so. By bringing plants of ragweed to physiological maturity in the greenhouse, and then subjecting them to long night by artifical means, they can be forced to bloom. This method has been used in a series of "pre-seasonal" experiments designed to show how the pollen is dispersed from plants in a known source under field conditions.

The first such test was set up in June, 1956, around a source of about 150 plants arranged in a 4-ft square. These were set out in a mown meadow and surrounded by upward-facing impaction samplers at distances of 10, 20, 40, 80 and 160 ft. The samplers were supported 2 ft above the ground and were set on radial lines at 40° intervals. Pollen counts from this experiment have been totaled in Figure 10. To construct this figure, the counts for each sampling period have been oriented according to the rules that the sampling ray nearest the total wind vector for the period must be directed along the +x direction, and that the wind speed must average at least 5 mph. As a result, Figure 10 presents a composite average picture, over a period of 31 hr, of the deposition from the pollen 'plume'.

The figures represent pollen deposition reduced to the average number of pollen grains caught in 6 hr on 1 cm^2 of coated slide surface. The symmetry of the 0.5 line, which forms the outer limit of shaded area, is remarkable, especially when viewed in contrast to the asymmetry of the progressively denser areas near the source. The occurence of the high counts far to the left of the average wind direction serves to emphasize the fact that the deposition patterns are produced by at least two factors, the wind, and pollen availability. The interaction of these two is probably of great importance near the source where extremely high concentrations of pollen are encountered. Very small-scale, short-lived gusts or eddies which happen to pick up an especially heavy load of pollen may contribute heavily to the deposition pattern without contributing substantially to the average wind vector. On the other hand, the more distant deposition pattern depends most heavily upon the average wind vector, and only slightly upon the wind details at the instant of pollen flotation. Reflotation of pollen grains is an additional factor which would tend to respond to the average wind vector and to improve the symmetry of the deposition patterns with increasing distance.

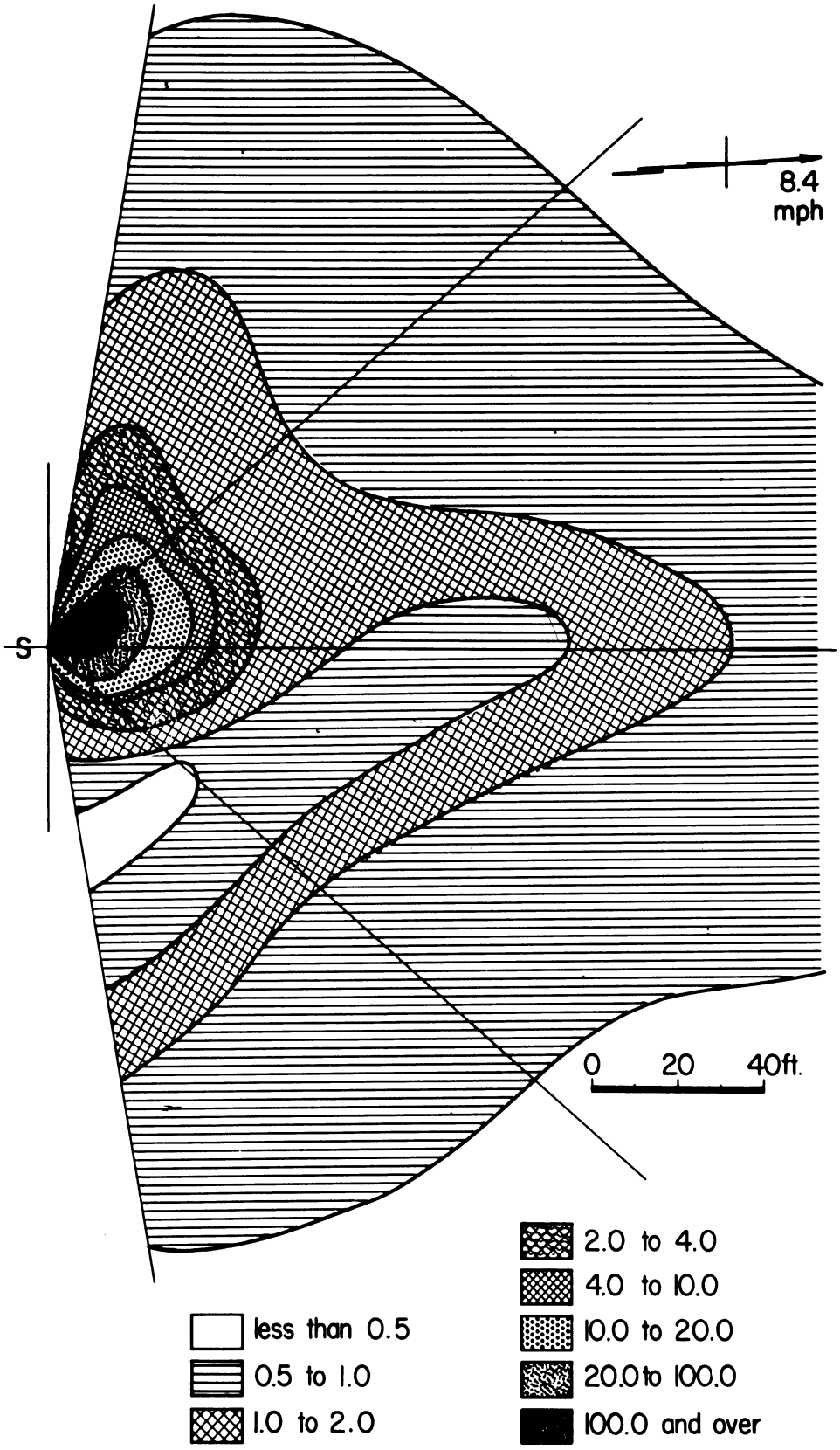

Figure 10. Composite of ragweed pollen deposition at wind speeds greater than 5 mph as constructed from impaction samples taken 2 ft above the ground. Source, S, was a 4-ft-square bed of hot-housed-forced Ambrosia elatior set out in a mown meadow. Deposition values are grains per cm^2 in 6 hr.

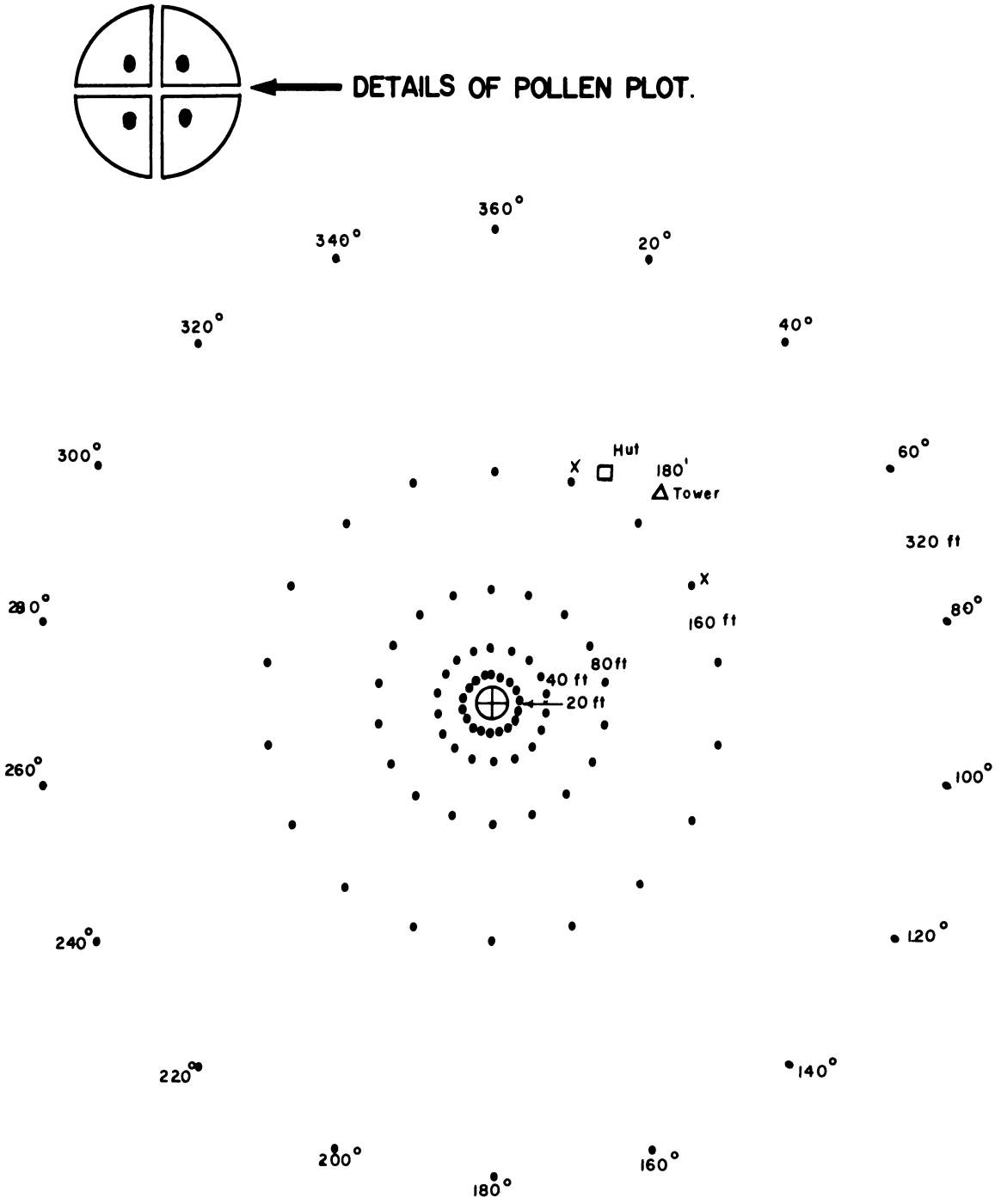

Figure 11. Plan of the sampling array for the June, 1957, experiment.

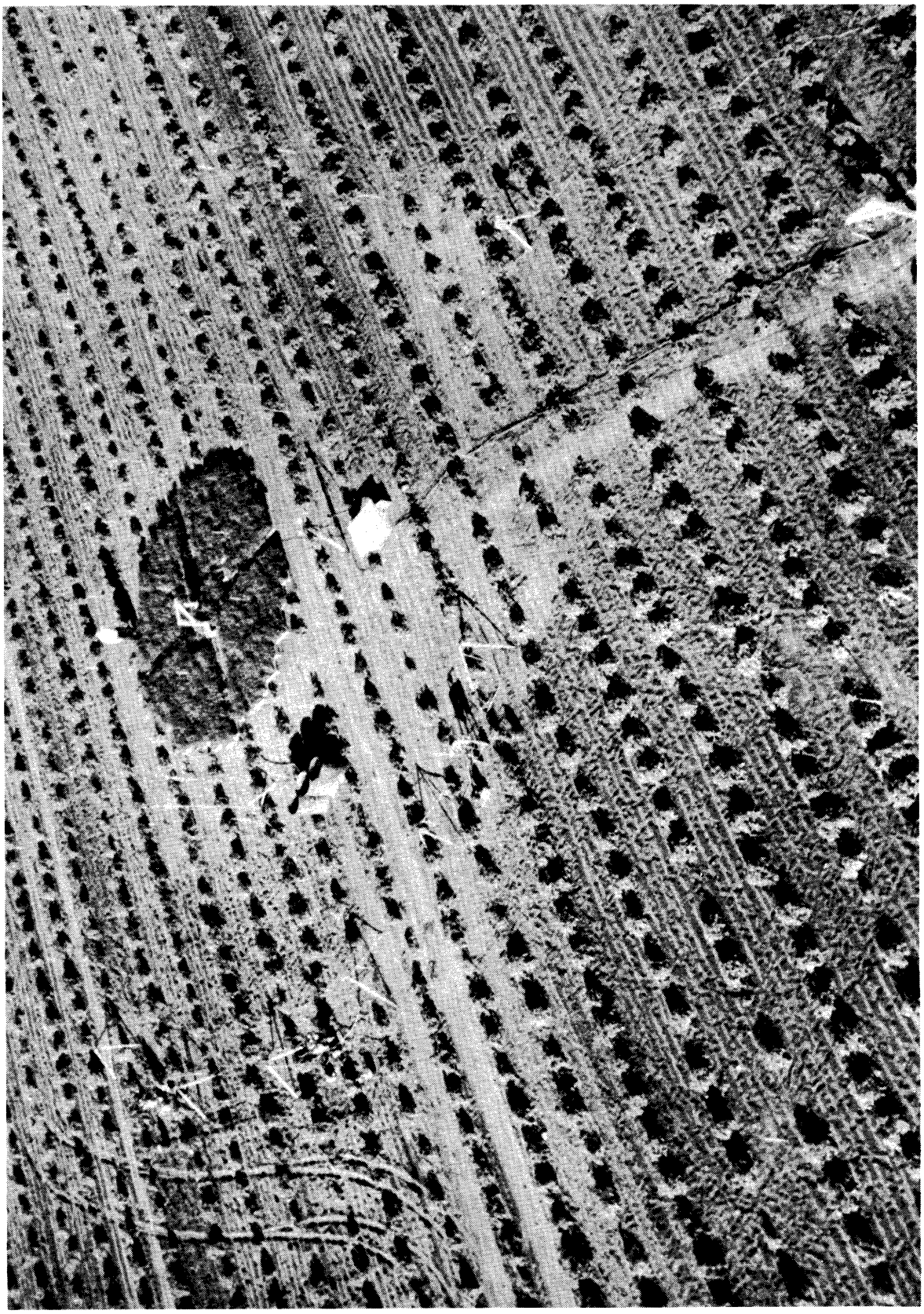

Figure 12. View of site of the June, 1957, experiment on the prison farm north of Jackson, Michigan, as seen from the top of the 100 ft instrument tower.

A second experiment of this same general type was performed in June, 1957. The entire scale of the operation was increased for this second experiment. Some 3,000 ragweed plants were grown and forced to bloom. These were set out in flats to form a circular source of about 26 ft diameter. In addition, the entire operation was moved to the tower site on the prison farm near Jackson. Figure 11 is a plan of the array of samplers. Figure 12 shows a view of the ragweed plot and vicinity as seen from the top of the instrument tower.

The instrumentation and the array of impaction samplers used in this experiment was considerably more extensive than that for the earlier one. Impaction samplers were placed 2 ft above the ground on rays 20 degrees apart at distances of 20, 40, 80, 160 and 320 ft from the center of the plot. Volumetric samplers were distributed at eight points in this general array and at four levels on the tower. A newly developed sampling system designed to give a continuous rather than an intermittent record of particulate matter was also tried out in this program. The data of this experiment are being analyzed.

In addition to these extensive experiments, a number of specific laboratory-type studies have been made to clarify various details. These are reported elsewhere[5-6].

CONCLUSIONS

Although this paper represents only a limited report of progress with our research on Air Pollution by Aeroallergens, a few points may be stated as firm conclusions derived from this work:

1. Ragweed pollen has numerous characteristics which make it a useful particulate for studies of aerosol dispersion and penetration. Its uniform size, shape and density are highly attractive properties for a research material to be used in studies of the behavior of medium-sized particulates. Its unique identity at all seasons except the natural ragweed pollination season meets all necessary tracer requirements.

2. Both the dispersal and the penetration of particulates near 20 microns diameter depend heavily upon atmospheric motion, and in particular, atmospheric turbulence. The relationship between wind speed at the lower elevations and air turbulence is understood in a general way by meteorologists, but the entire problem needs and deserves more study. As yet no completely satisfactory quantitative expression for air turbulence has been developed.

3. The cross-fertilization of ideas, language and research approach that is accomplished by bringing workers from diverse disciplines together to attack a problem having elements of interest for all is highly productive. In the present research, the collaboration of botanists, allergists, statisticians, meteorologists and engineers has proven to be most rewarding, and promises to yield important successes in a difficult field.

REFERENCES

1. Wodehouse, R.P, "Hayfever Plants," Chronica Botanica Co., Waltham, Mass., 1945.

2. Crawford, J.H., Pub. Health Rep. 64, 1195, 1949.

3. Dingle, A.N., Bul. Amer. Meteorol. Soc. 38, 8, 465, 1957.

4. Georgii, H.W., "Arch. f. Meteorologie," Geophys. u. Bioklim., Ser. B, 5, 191-214, 1954.

5. Sheldon, J.M. and Hewson, E.W., "Atmospheric Pollution by Aeroallergens," August 1, 1955, to April 30, 1957, Progress Report No.1, Engineering Res. Inst., Univ. of Mich., Ann Arbor, 1958.

6. Sheldon, J.M. and Hewson, E.W., "Atmospheric Pollution by Aeroallergens," May 1, 1957, to April 30, 1958, Progress Report No. 2, Engineering Res. Inst., Univ. of Mich., Ann Arbor, 1958.

RESEARCH ON OIL-BATH AIR CLEANERS

Seymour Calvert
Associate Professor of Chemical Engineering
Case Institute of Technology

RESEARCH ON OIL-BATH CLEANERS

Seymour Calvert

INTRODUCTION

Dust was the controlling factor causing incredibly short tank engine life in desert operations during the second World War. To a less dramatic extent dust is a major cause of engine wear under less severe conditions of road and cross-country vehicle operations. Numerous types of air cleaners had been devised, used, and tested but none were really satisfactory when judged by all of the criteria important to army vehicle operation. The air cleaner required had to provide the features of high dust collection efficiency, long service life, low restriction (air pressure-drop), and simple maintenance requirements. There was a further requirement that the air cleaner be suitable for (or easily modified for) use in severe winter service where plugging with fine snow and ice is a major problem.

The Detroit Arsenal had been studying the problem of engine wear for several years and had established with fair certainty the importance of dust. By 1954 the Arsenal had set up a program which consisted of development by air cleaner manufacturers, testing at the Arsenal and other installations, and research at the University of Michigan.

The research at the University was conducted as an Engineering Research Institute project under the supervision of Professor J. Louis York and had the major objectives of:

1. With regard to general air cleaner design

    a. Determining the basic principles involved in the mechanism of operation of existing air cleaners and measuring the limits and quantitative effect of these principles on performance, with first emphasis upon the oil bath units now employed extensively.
    b. Organizing these principles and quantitative measurements to furnish a basis for evaluating new design, developing improvements in existing cleaners, and developing new designs.

c. Furnishing technical background for preparation of revised specifications for air cleaners.

2. With regard to snow problems

a. A study of the causes of snow clouds and their characteristics.
b. A study of characteristics of vehicles which influence the formation of snow clouds.
c. A study of Meteorological conditions such as temperature, winds, ice and snow crystalline structure which are conducive to cloud formation.
d. Analysis of the flow of air through the induction systems of the vehicles encountering the accumulation of ice and snow.
e. Effects of the geometrical arrangements of the air induction system.
f. Effects of components such as filters and carburetors.
g. Effects of the nature and type of snow and ice crystals suspended in air.

GENERAL PROBLEMS IN AIR CLEANER DESIGN

This report deals with the general problems of air cleaner design as related to dust collection. Once the decision had been made to study oil-bath air cleaners the specific problems could be set by an analysis of the significant components of oil-bath air cleaners. Considering the oil-bath cleaners from the standpoint of dust collection, they are seen to consist of two major zones of action. Figure 1 shows the cross-section through a typical oil-bath air cleaner. The first zone encountered by the air is the baffle region in which the air stream is deflected by a relatively large conduit element (baffle) and simultaneously contacted with oil. The second zone is the packed section in which the air stream leaving the baffle passes through an array of small solid bodies such as wire screen or other fibrous packing. The functions of the baffle section are to remove the larger dust particles and to introduce oil which is carried to the packed section. The functions of the packed section are to remove the smaller dust particles and also to separate the entrained oil from the air stream.

In order to design an air cleaner it would be necessary to know how to predict dust collection efficiency, pressure drop, and limiting air flow rate. Most of the discussion here will be on dust collection so work on the other two points will be summarized briefly before taking up dust collection efficiency.

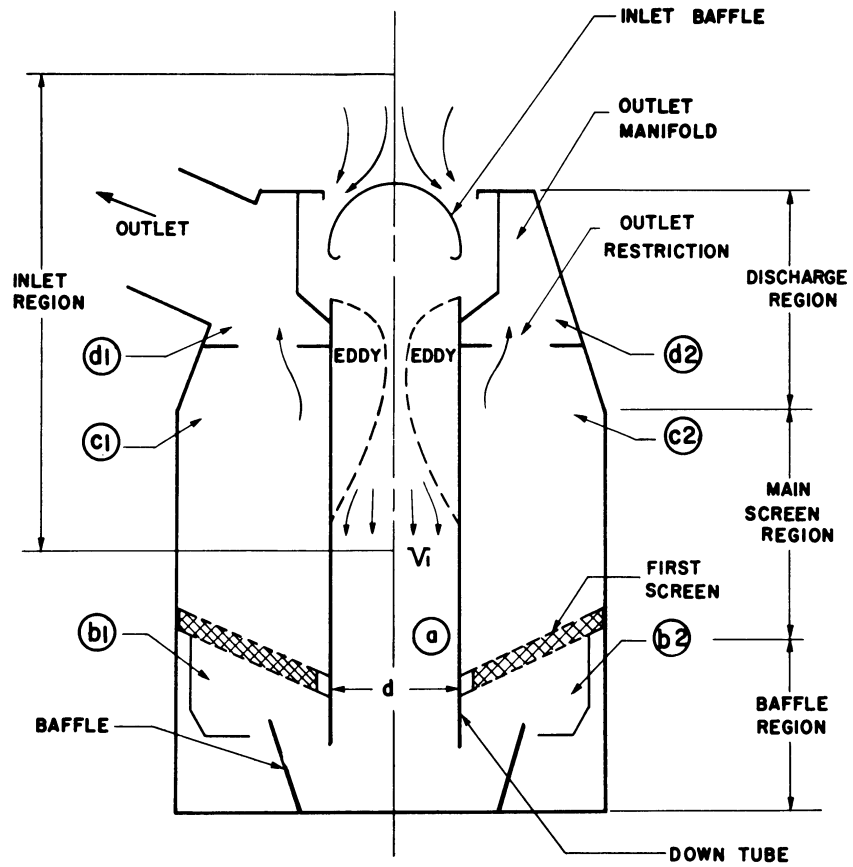

Figure 1.

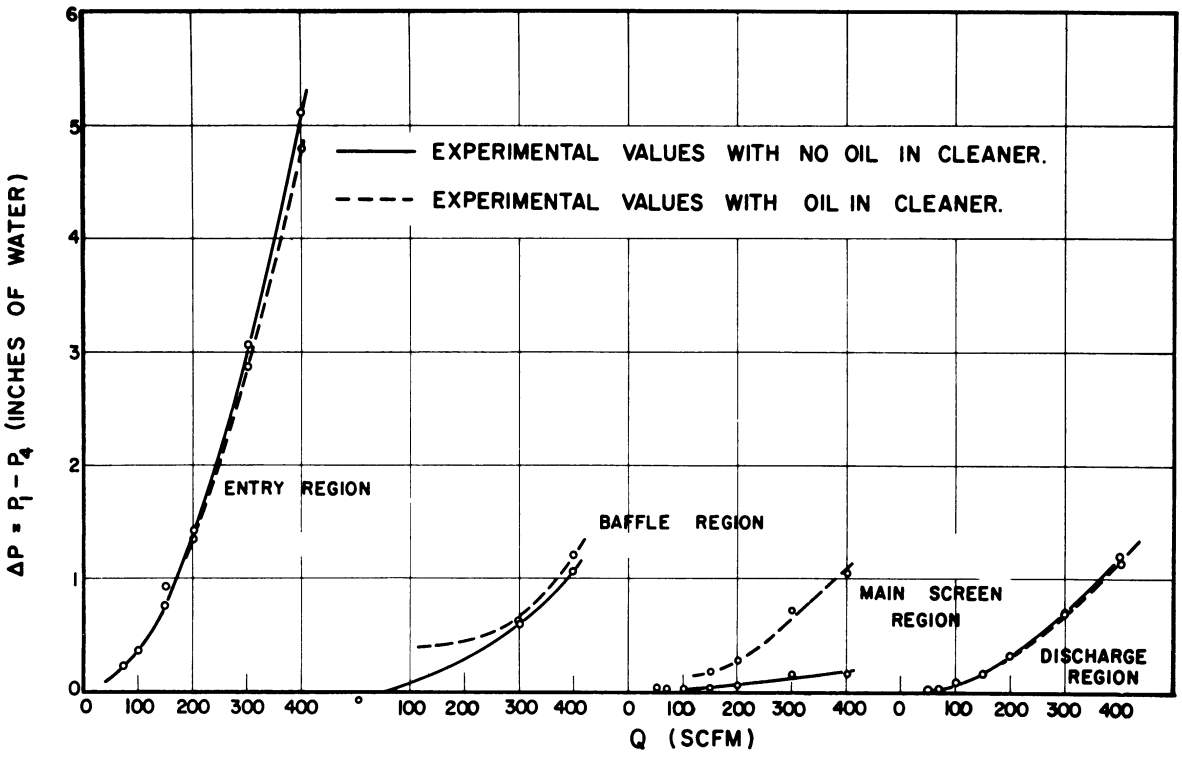

Figure 2.

PRESSURE DROP AND AIR FLOW PATTERNS

Air flow patterns and pressure drops were studied experimentally in models of the principal elements and in full-scale commercial air cleaners. Equations were developed analytically to describe the pressure drop in the baffle and packed sections and the predictions of these equations agreed satisfactorily with the experimental data. Because of the complexity of the air cleaner geometry it was not possible to make any quantitative predictions of flow patterns and these had to be studied entirely on an experimental basis.

A comparison of the pressure drops in the various sections of a commercial air cleaner is given in Figure 2. It is interesting to note that almost two-thirds of the total pressure drop occurs in the entry region which has no influence on dust collection efficiency. Although the inlet baffle is required to prevent major oil loss in the event of a backfire, its effect on pressure drop can be minimized by the use of guide vanes. Pressure drop for air flow through fibrous beds can be predicted for high-porosity beds by means of an equation based on the drag coefficient for a single fiber. Figure 3 shows a plot of predicted pressure drop group versus air velocity for the flow of air through round steel wire. (It should be noted that this relationship involves constants which are evaluated for the specific system.) If the average distance between fibers is less than about 8 fiber diameters it is necessary to take contraction losses into account and the validity of the single fiber model fades as the bed becomes more dense.

LIMITING AIR FLOW RATE

The air flow rate is limited by the point at which oil is carried out of the air cleaner. This corresponds to the flooding point in packed columns. Experimental data on several types of lube oil in beds of steel wool and wire grids were satisfactorily correlated by the method of Sherwood. Figure 4 shows the experimental data plotted along with the lines representing flooding points for a variety of packed columns and fluids.

It is interesting to note that the packed section is designed (at least implicitly) as an oil entrainment separator rather than as a dust collector. At least two-thirds of the volume of the air cleaner is devoted to this function. It will be seen later that the contribution of this section to dust collection efficiency is relatively minor.

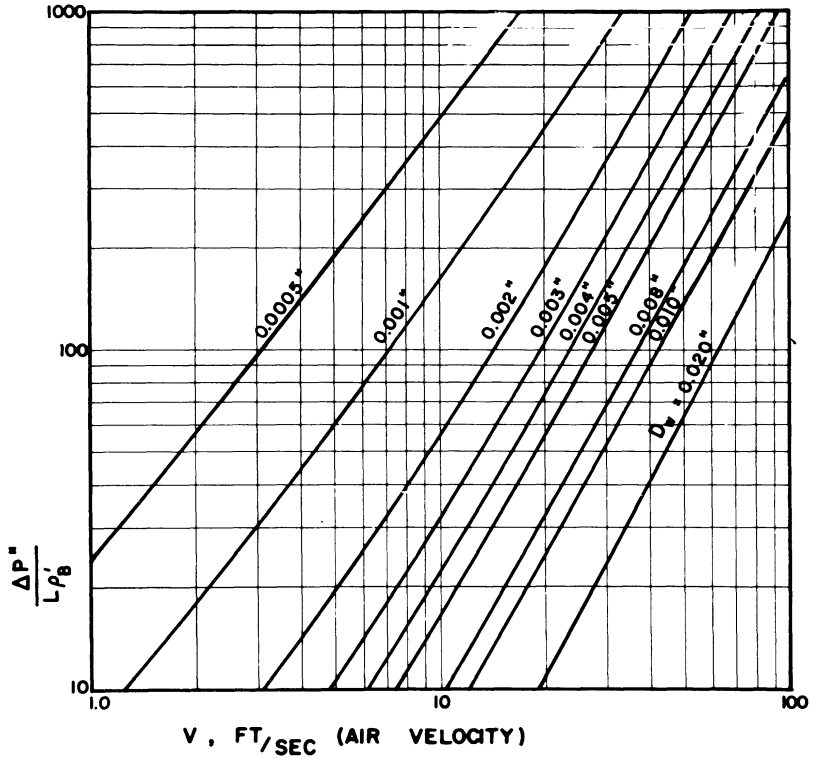

BASED ON:

$$\frac{\Delta P''}{L\rho'_B} = 2.2 \times 10^{-4} C_D \frac{v^2}{r''_w} = \frac{''H_2O}{FT \times GM/CC}$$

(ρ_{AIR} = 0.075 LB/CU.FT , μ_{AIR} = 0.018 CP).

Figure 3.

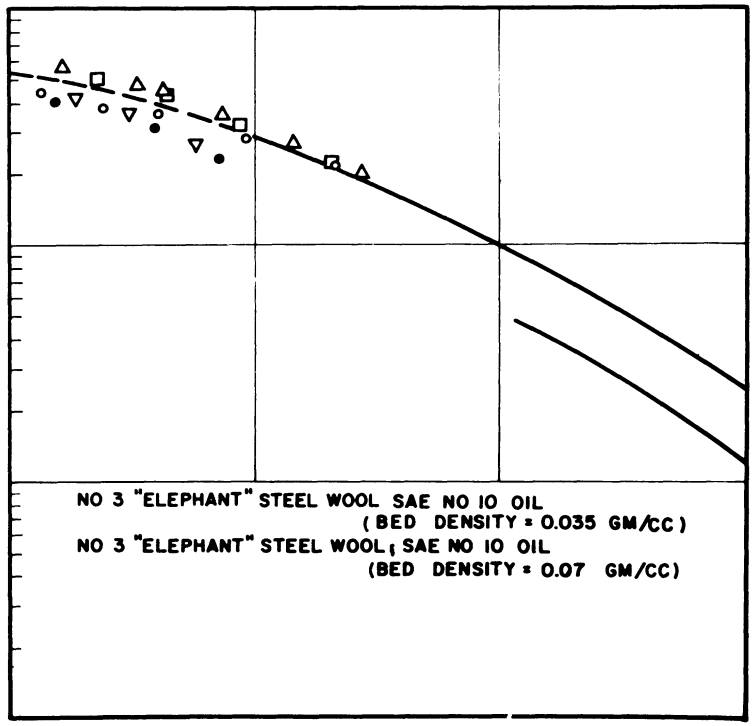

Figure 4.

The essential design criterion is that the air velocity be kept below about 10 ft./sec.

DUST COLLECTION

Before getting into the problem of predicting dust collection efficiency we have to consider what kind and size of dust must be collected. Briefly; we do not know exactly. What we do know is that A. C. Fine Test Dust is fairly representative of the size distributions which have been encountered in dusty operations and that particles larger than about one micron in diameter contribute significantly to engine wear. What we do not know is exactly what size distribution, particle shape, and density will be encountered in a specific operating situation and particularly, the extent of agglomeration of particles in the air stream entering the cleaner.

We can study the problem of dust collection efficiency from the point of view that we are interested in the collection of particles about one micron and larger in diameter and with densities around that of silica. Thus the major mechanism of collection will be inertial impaction. There are two variants of the inertial impaction mechanism in the air cleaner. In the baffle region the entire air stream is turned and the particles which can't make the turn collide with the baffle wall and presumably stick to it or the oil on it. In the packed section small elements of the air stream are diverted around the packing fibers and the particles which can't turn quickly enough strike the fibers.

A comparison of the predicted collection efficiencies for the baffle section and the packed section indicated that the efficiency of the packed section is so much higher than that of the baffle that the overall efficiency of the cleaner is determined by the packing. Using an approximate method based on the distance particles would be pitched into still air before stopping and an estimated flow pattern it was determined that the baffle would remove all particles larger than 15 microns and practically none smaller than 5 microns. These results checked with the predictions based on Ranz and Wong's data on collection efficiencies of jets impinging on plates.

The major concern was with the collection efficiency of the packing. Collection efficiencies for single elements have been predicted by several investigators and some experimental data are available. Figure 5 shows the data of Langmuir and Blodgett and Ranz and Wong. When it comes to using these data for a bed of fibers one faces the problem of having to decide what effect the presence of other fibers has on the situation confronting an individual fiber. Two extreme cases were considered. One case is that

where there is negligible mixing in the air stream and each fiber sweeps out a "clean" path so that the fibers downstream confront air which has either the original dust content or the "swept" content. The other case is that where there is complete mixing of the air stream so that the dust content of the air downstream from a fiber is the average of the swept and unswept air. The effect of making one assumption or the other is greatest for shallow beds (something like 10 layers or less of 10 mesh screen) and becomes negligible for deep beds.

For the assumption of no mixing the total collection efficiency is given by:

$$\eta_{Dt} = 1 - (1 - \eta_D)^{nY} \qquad (1)$$

Where

η_{Dt} = fraction of particles of diameter "D" collected by the bed.
η_D = fraction of particles of diameter "D" collected by one fiber.
n = number of "layers" of fibers (assume that the fibers are arranged in a square grid).
Y = fraction of flow cross-section blocked by wire in any layer.

For the assumption of complete mixing the total collection efficiency is given by:

$$\eta_{Dt} = 1 - (1 - Y\eta_D)^{n} \qquad (2)$$

EXPERIMENTAL DETERMINATION

In order to establish the nature of the behavior of groups of fibers, experimental studies of dust collection efficiency were undertaken. Collection efficiencies for oil-washed beds of round wires were determined using 0-30 micron silica dust. The data indicated that the collection efficiency predictions of Langmuir and Blodgett plus the assumption of no mixing described the situation for shallow beds (12 layers of parallel 0.0125" wires on 1/8" centers).

Further study of stacks of parallel wire and screen assemblies was undertaken using salt dust as the test aerosol and using dry wires. The purpose of this study was to explore the effect of wire spacing on mixing. A sketch of the apparatus is shown in Figure 6.

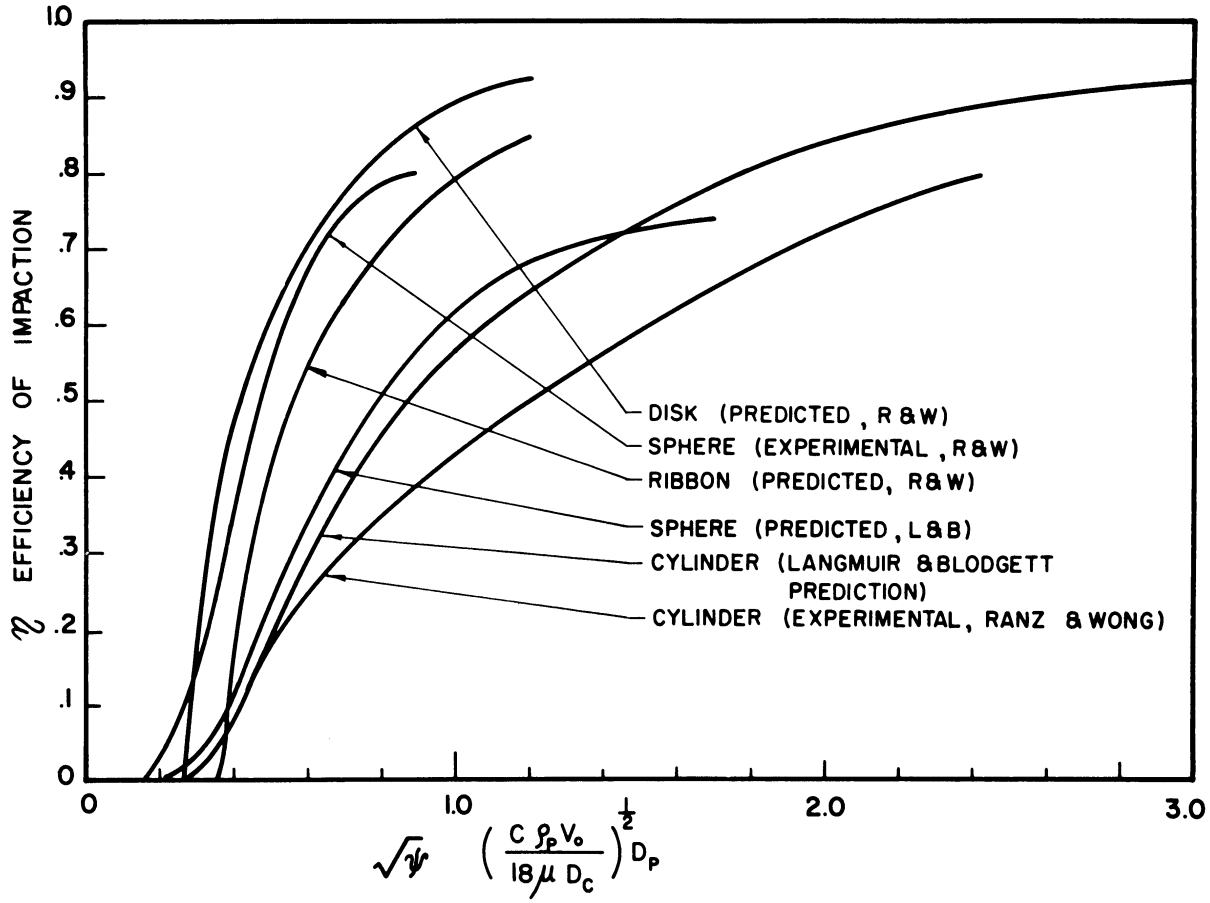

Figure 5.

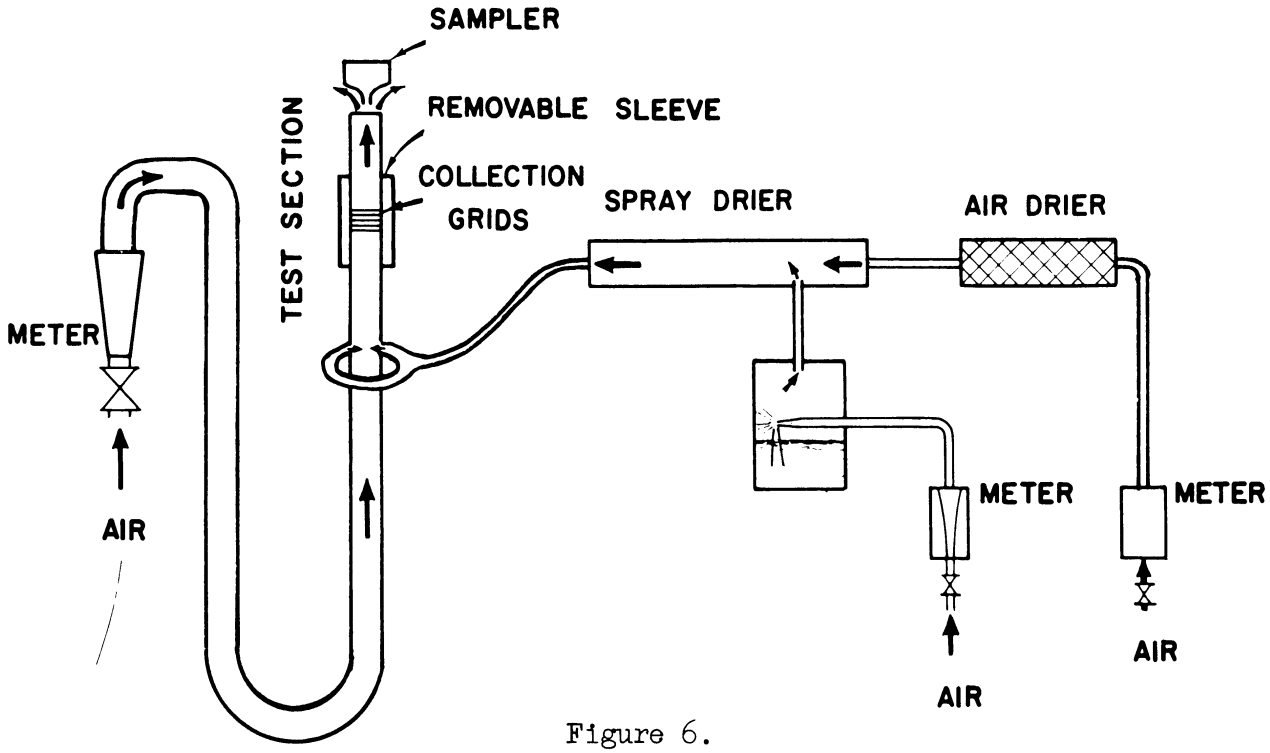

Figure 6.

1. The test section was made of 2-inch (ID) lucite tubing. It was built so that a number of brass rings, which supported the wires, could be stacked on top of a tube and another length of tubing placed on top of the stack. The assembly was held in place by a lucite sleeve and the result was a continuous duct of 2-inch internal diameter. The test grids were 27-3/4 inches above the salt-dust entrance. The removable sleeve permitted removal of the stack of test grids after a run so that the salt could be washed off in a beaker of water.

2. The test grids were brass rings to which 0.003-inch-diameter Alumel wire was glued in parallel lines 1/8 inch apart (center to center). The rings were 2 inches (ID) x 2-1/4 inches (OD) x 1/32 inch thick. In some runs blank rings were used as spacers. Some tests were also performed using circular pieces of 14-mesh copper wire screen (0.011-inch wire diameter) rather than the parallel grids.

3. The exit-air sampler was an isokinetic type, employing MSA 1106B glass-fiber paper as the filtering medium. The ratio of total air rate to sampler air rate was 28.4. Isokinetic conditions were maintained by matching the sampler air rate to the mainstream air rate by a throttle valve and rotameter leading to an aspirator.

4. The salt-dust generation system involved an aspirating atomizer installed in a chamber containing a large volume of saturated salt (NaCl) solution. The spray was directed at one wall of the chamber so that large drops struck the wall and ran back down. The smaller drops were carried into the spray-drying chamber by the atomizing air. In the spray-drying chamber the drops were mixed with air which had been dried in a desiccant-packed tube. The dried salt particles were then transported through a 1/2-inch (ID) plastic tube to the test-section entrance. The entrance consisted of a "Y" tube connected to two 1/2-inch tubes entering the test section from opposite sides. Thus the salt-dust stream split into two portions which entered the test section through two diametrically opposed tubes.

5. The main air stream was supplied by an air-jet ejector pump and metered with a calibrated rotameter.

PROCEDURE

Collection efficiency was determined in this apparatus for groups of 12 and 24 parallel wire grids and for groups of 10 and 20 screen discs with several variations in spacing between grids. The amount of salt dust collected on the wires was determined by washing the wires in a known volume of distilled water and then analyzing for salt content by an electrical conductivity measurement. The concentration of salt dust in the air leaving the test section was determined

by similar analysis of the salt retained on the filter paper in the isokinetic sampler. From these measurements one can compute the total dust load in the air approaching the collection wires and also the percent collected.

The isokinetic sampler was checked against an absolute filter and the agreement was considered adequate although not perfect. The major difficulty in making this comparison was that the rate of salt-dust generation was not uniform but varied from about 0.0045 gm/min to 0.0075 gm/min. The agreement between the sampler and the absolute filter was about $\pm$ 10%. Measurements of dust distribution around the test section were made, but since these could not be made simultaneously, the results, which show as much as twofold variation, are not conclusive.

Dust-particle size was determined by a visual count of a sample collected on a microscope slide. The sample was collected by introducing the airstream from the dust-generator outlet tube into the top of a 1-foot-high, 3-inch-diameter tube which was set vertically over the slide and allowing the dust to settle on the slide. Several checks indicated consistency in this method and there does not seem to be any sampling bias. The size distribution was quite constant and is shown on a logarithmic probability plot in Figure 7. Weight distribution was computed from number distribution by means of the formula

$$\ln X'_g = \ln X_g + 3(\ln \sigma_g)^2$$

where

X_g = geometric mean diameter by number,
X'_g = geometric mean diameter by weight, and
σ_g = standard deviation.

RESULTS

The experimental collection-efficiency data are shown in Figure 8 and Figure 9 which are plots of collection efficiency vs. air velocity for the parallel wire grids and the wire screen, respectively. Also plotted on these figures are the dashed lines representing predicted collection efficiency, using the Langmuir and Blodgett data and assuming either complete mixing of the airstream or no mixing, as indicated on the plots. This prediction involves the use of collection efficiencies for single wires which are presented in Figure 5, a plot of collection efficiency versus air rate with particle diameter as the parameter.

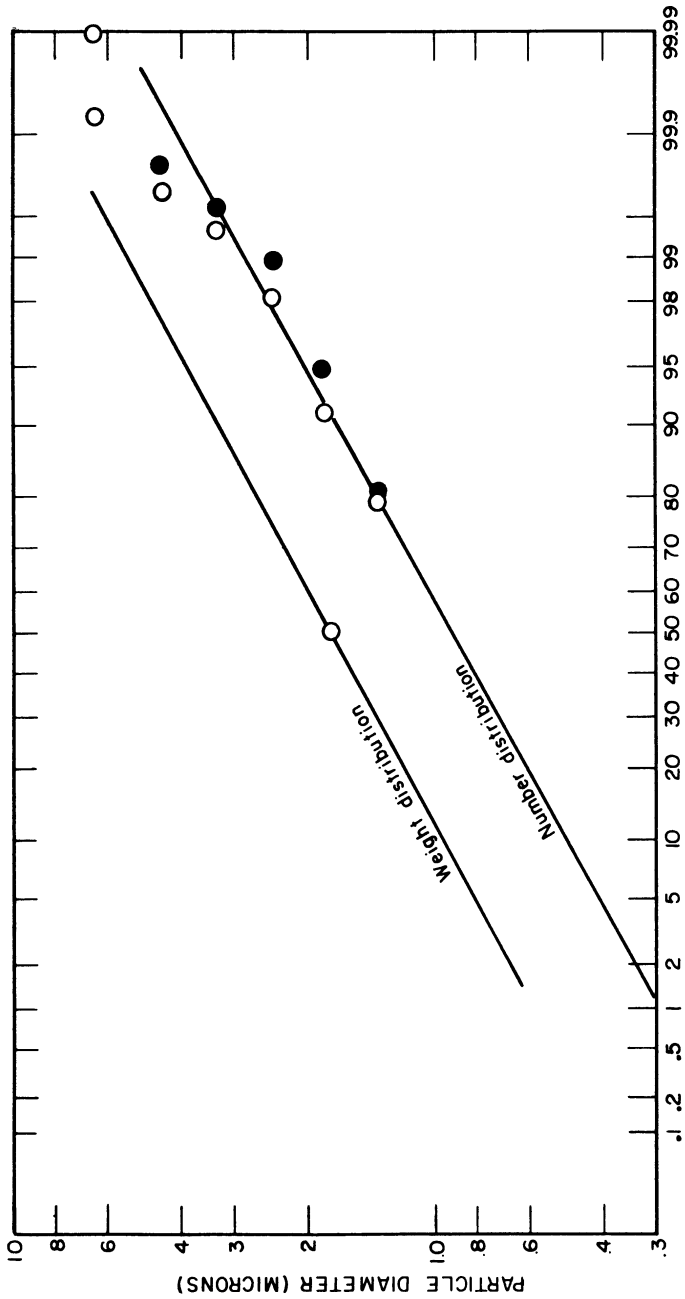

Figure 7. Salt-dust size distribution

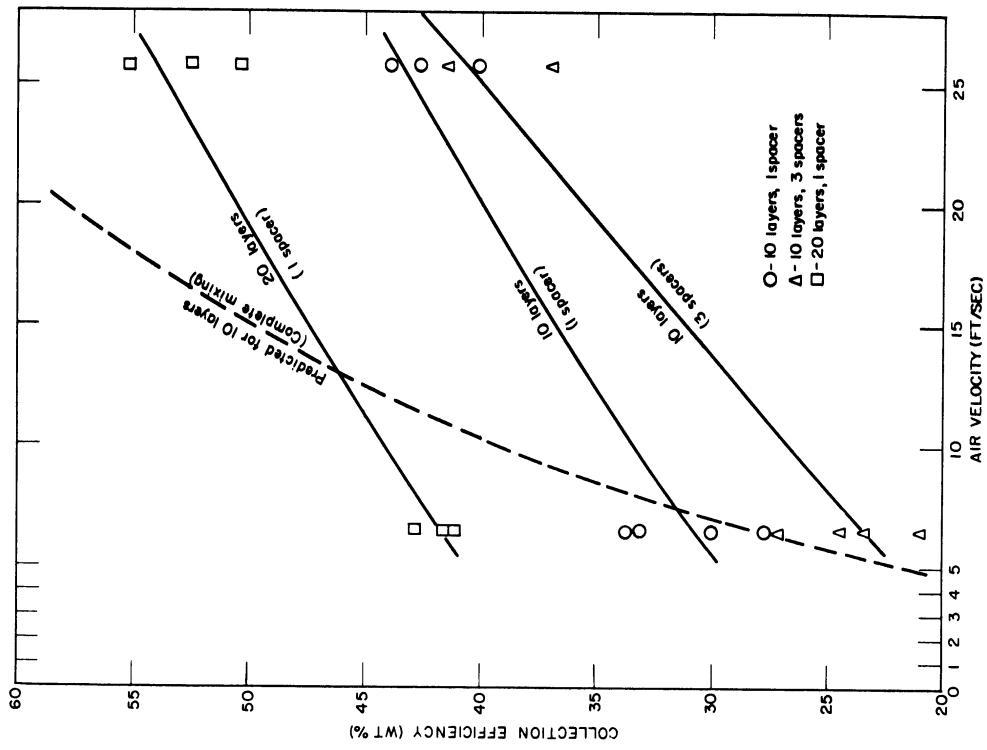

Figure 9. Salt-dust collection efficiency vs air velocity (.011-in.-dia wire screen, .075-in. space, 14 mesh, 2-in.-ID tube, 1/32-in. vertical spacers).

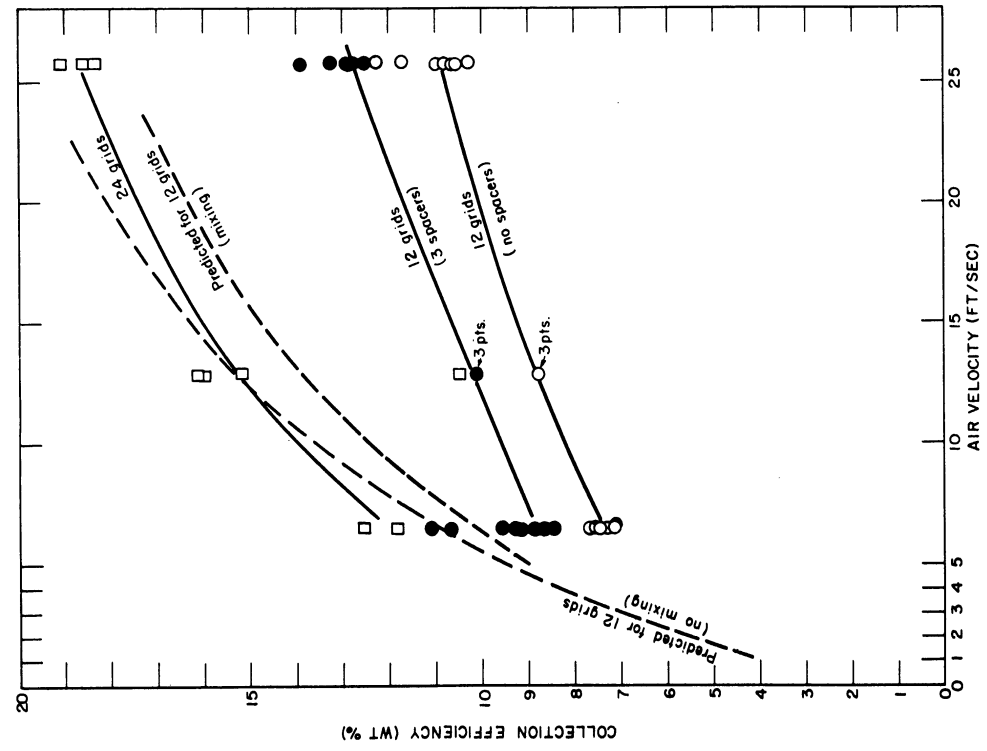

Figure 8. Salt-dust collection efficiency vs air velocity (.003-in.-dia wire, 1/8-in. wire spacing, 2-in.-ID tube, 12 and 24 grids, 1/32-in. vertical spacers).

DISCUSSION OF RESULTS

The most significant observation is that the predictions are close at low velocity but depart appreciably from the experimental data as velocity increases. The effect of increasing bed depth is in general agreement with the theory, although it is not possible to determine the amount of mixing from these data. There is a definite effect of axial spacing; but, since it is in opposite directions for the parallel wires and for the screens, any discussion of the mechanism involved would be purely speculative at this point.

The data obtained are not sufficient to establish any correlation, but they definitely indicate that collection efficiency is lower than predicted on the basis of the impaction mechanism. The obvious explanation is that some of the particles bounce off the collecting wires. An attempt was made to obtain some information on this by taking high-speed motion pictures and high-speed flash pictures of a dust-laden jet striking a wire. Unfortunately, there was not sufficient resolution in these pictures to show the particle trajectories.

A few exploratory runs were made using wires coated with Canada balsam to see whether this would raise collection efficiency, but it did not. The use of oil fog was also explored but the analytical difficulties made this brief study inconclusive, except for one point: that collection efficiencies for round jets striking flat plates were lower than predicted. Stated another way, this meant that the particle size passing through the impaction zone was larger than predicted.

The conclusion is that particulate collection efficiency is by no means completely described by the theoretically derived impaction efficiencies. The fact that predictions agree well with data for wetted wires can be considered fortuitous and may result from a different mechanism than has been assumed.

CONCLUSIONS

Relationships have been developed which enable the design of oil-bath air cleaners with regard to pressure drop characteristics, flooding point, and dust collection efficiency. The accuracy of collection efficiency predictions must be regarded as fortuitous since they are not valid for dry wires. The necessity for further experimental investigation of dust collection efficiency is indicated.

APPENDIX

As part of the presentation of the paper, a series of motion pictures was shown. This sequence showed a section of an oil-bath air cleaner operating with snow in the intake air. Figures 10, 11, and 12 are representative of the operation as pictured.

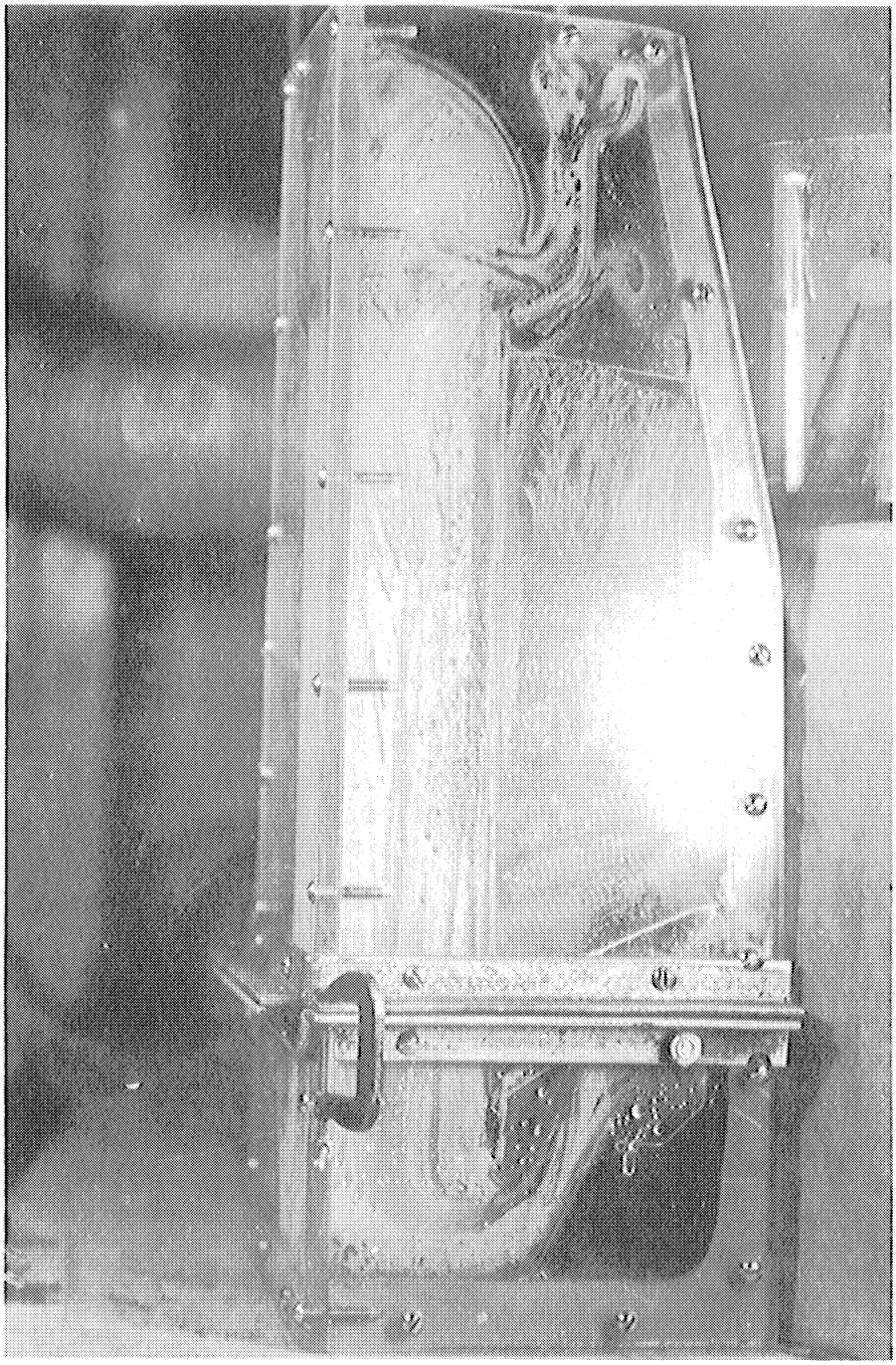

Figure 10. Flow path through air cleaner shown by steam condensate on window.

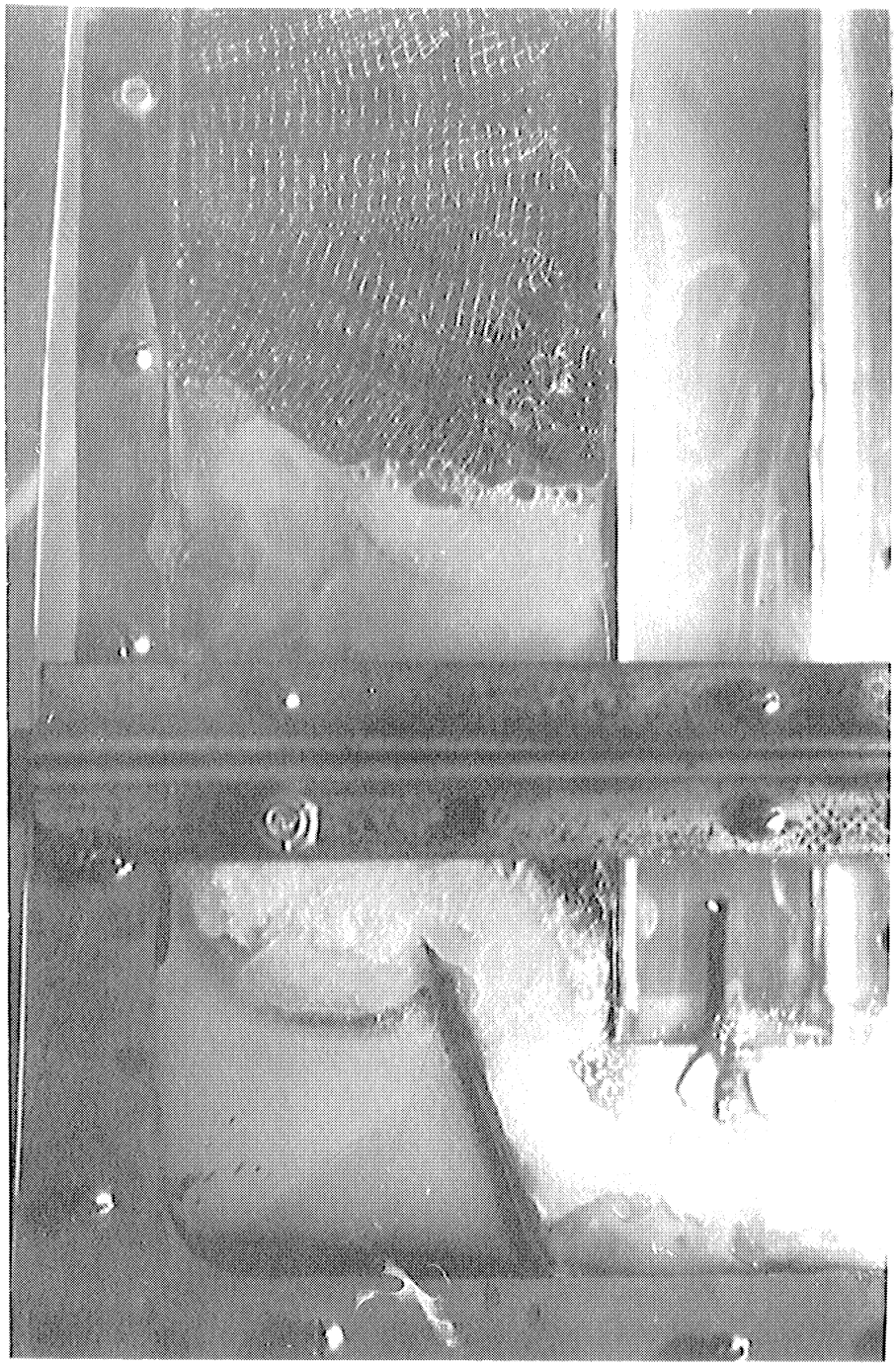

Figure 11. Air cleaner clogged with snow, ethylene glycol in cleaner.

Figure 12. Air cleaner clogged with snow, no oil in cleaner.

SNOW AND OTHER SMALL CRYSTALS

Ernst Katz
Associate Professor of Physics
The University of Michigan

SNOW AND OTHER SMALL CRYSTALS

Ernst Katz

Crystals have attracted the attention and fancy of man since times immemorial. In the early days of the scientific age the first laws were established, the laws which govern the macroscopic symmetry of crystals. A classification of all possible crystals into 32 groups was established as a result of these laws.

Further research has clarified the microscopic, structural symmetries. This analysis was greatly stimulated by the invention of X-rays and their application to the study of crystals. The result was an ultimate classification of all possible crystal structures into 230 symmetry groups. In all these theoretical and experimental studies the efforts were directed entirely towards the ideal or perfect crystal. Until one began to wonder whether anybody had ever seen such a thing as a perfect crystal. An indeed, today we know that perfect crystals do not exist, perfect in the sense that they consist of a regular, exactly periodic array of atoms or atom groups.

During the last thirty years great advances have been made in regard to the study of crystal imperfections, especially those known as dislocations. It is becoming more and more evident that each individual crystal is permeated by a fine network of dislocation threads or lines, which give it its individual character. Much to the despair of the crystal physicist, no two crystals of the same material will yield exactly the same results when subjected to careful physical measurements. Even the law of constant angles, which is historically the first law and has long been considered as the very foundaion of crystallography, must be taken with a play of the order of a few tenths of a degree of actually measured deviations.

The cause of all this variability, the dislocation, has emerged from a purely hypothetical entity to something which can in many cases be observed directly by means of the electron microscope as well as by other techniques. In most cases studied, it can be shown that a crystal will grow more readily for a nucleus which has a least one screw-dislocation present.

Figure 1 shows the atomic arrangement, like a spiral staircase, at a screw dislocation. Below is seen how the ridge will gradually wind up to a spiral when such a crystal starts to grow. The presence of screw dislocations in a crystal during growth gives rise to spiral terraces on the surface of the crystal, and these can be observed.

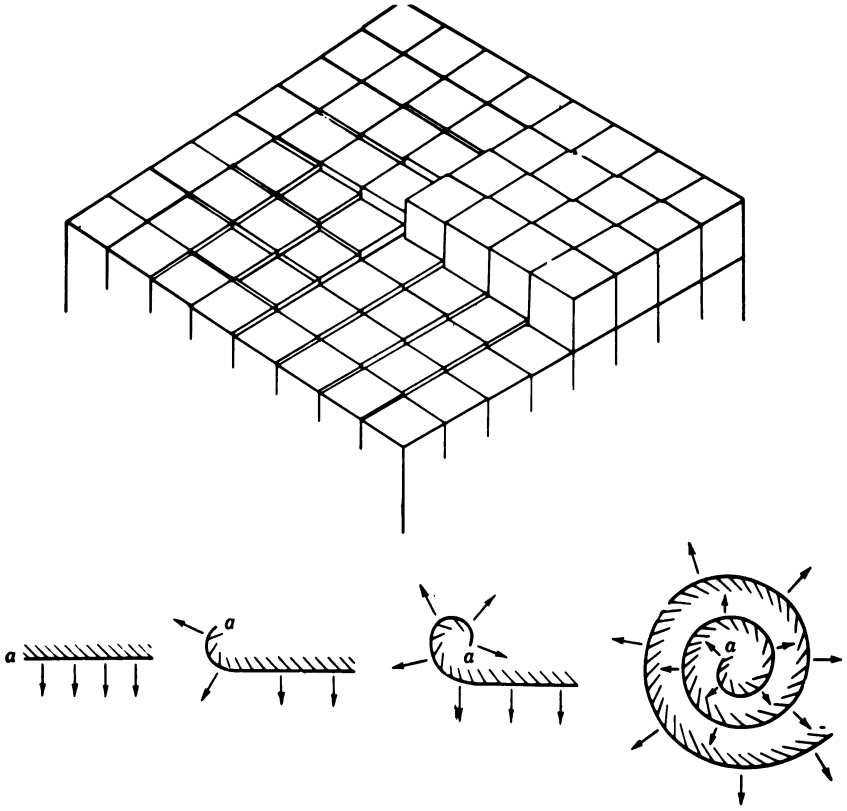

Figure 1. Development of a spiral step produced by intersection of a screw dislocation with the surface of a crystal. Each cube represents a molecule. (After F. C. Frank.)

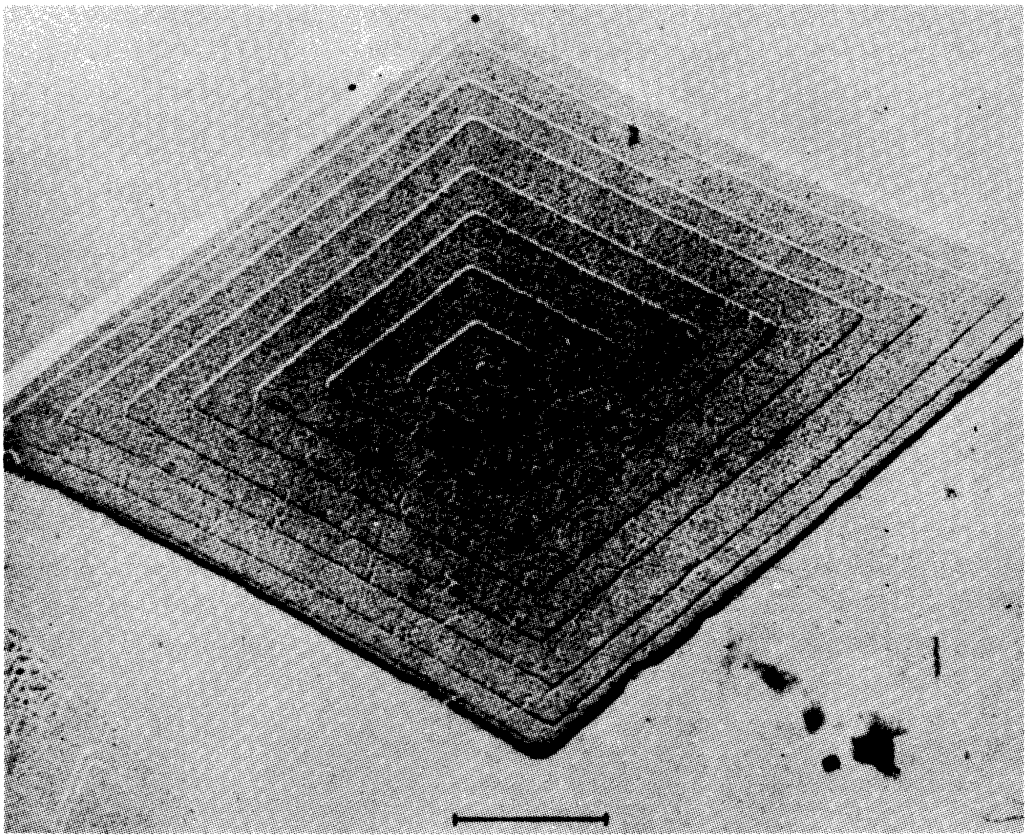

Figure 2. Growth pattern from single dislocation on single crystal of paraffin n-$C_{36}H_{74}$. [Electron micrograph courtesy of H. F. Kay and B. J. Appelbe, after Dawson and Vand, Proc. Roy. Soc. (London) A206, 555 (1951).]

Figure 2 shows an example of a paraffin crystal examined under the electron microscope where the spiral terraces can clearly be seen. The terrace steps here are found to be one atomic layer high, and this is often the case, although for some materials such as SiC terrace steps of several atomic layers height have also been observed. Beautiful and very complex spiral patterns have been observed today on many crystals, and it is known, for example, that the elastic strength of a crystal is greatly weakened by the presence of many dislocations.

Experiments on dendrites or whiskers, small, needle-shaped crystals, of certain metals such as Sn, Fe, Cu, have shown that under suitable conditions of growth these crystals have an elastic strength of the order of 100 to 1000 times that of bulk material. There is strong evidence that this high strength is due to the presence of very few, possibly only one, dislocations. Thus I want to point to a field of research in small crystals which, though not actively pursued by myself, may lie close to your interests and, as will soon become clear, also to mine.

I have indicated that a good deal of progress has been made, and much insight has been gained in regard to certain branches of crystal physics, namely those concerned with the structure of the ideal crystal, and with structure faults or dislocations. There is, however, a different area of questions, equally old, and equally fundamental, in which very little work has been done. I mean all the questions associated with the form into which a crystal grows. This area is at present merely in its infancy.

It is, of course, well known that the forms of crystal depend sensitively on many external circumstances. One of the oldest experiments in this field shows that ordinary salt, NaCl, crystallizes from a water solution in cubes, but when some urea is added, it takes the form of octahedra, although its inner structure, the microscopic arrangement of the Na^+ and Cl^- ions, is the same in both cases. As early as 1883 Lehmann published several books, showing how the forms of crystal formations could be used for the identification of chemicals and/or chemical impurities, but his work has not been picked up for some time.

I became interested in questions of crystal forms through more recent work of E. Pfeiffer, who developed a method whereby a solution of $CuCl_2$ is allowed to evaporate slowly under controlled conditions of temperature and humidity. If the $CuCl_2$ is pure and the concentration chosen right, the crystals form characteristic, starry patterns on the bottom of the dish, covering only a small portion of its surface. The addition of relatively small amounts of foreign substances or impurities changes this pattern drastically.

For example, Figure 3 shows a pure $CuCl_2$ pattern, and a pattern obtained from a slightly more dilute solution to which a few drops of fresh lemon juice had been added. An entirely new type of pattern, covering the entire dish with a delicate crystalline growth results. Figure 4 shows a similar picture with a somewhat more concentrated solution of $CuCl_2$. Its forms are reminiscent of frost patterns observed on windows in winter.

The effects of such added impurities are often very specific. Lemon juice consists largely of water, and the principal chemical body dissolved in this water is citric acid. If the same experiment is performed with an equivalent amount of pure citric acid added to the $CuCl_2$ solution, a pattern as shown in Figure 5 results, which, as you see, is quite different from that of whole lemon juice, and can also easily be distinguished from that of pure $CuCl_2$ alone.

Pfeiffer has worked this method out empirically and developed a sort of assaying technique for biological and medical purposes. Figure 6 shows some work of Pfeiffer, where he started with $CuCl_2$ solutions somewhat more concentrated than mine. The upper left corner shows the blank with pure $CuCl_2$, the other pictures show the results of additions of small amounts of various juices of plants or blood from animals.

You can see that this has possibilities in various fields of application, but from a fundamental standpoint these pictures raise a host of questions as to the factors governing the forms of the patterns, which are at present far from being answered.

It occurred to me that perhaps an understanding of the shape of snow crystals might be simpler to attain, and pave the way to a possible later understanding of these more complicated forms. I soon found that even for snow the problem is very complicated, but at least more carefully controlled studies under simpler conditions have been reported here, especially by Nakaya in his famous book on snow crystals. I want to summarize now some of Nakaya's most striking results because I want to get work started along similar lines, in the hope that the form problems may be more easily solved in the case of the snow crystals than in the case of the $CuCl_2$ crystals with which I have done some work so far.

Nakaya presents us in his book with the world's most complete set of snow crystal photographs. He classifies all the forms which occur and relates their occurrence to the weather conditions in the upper atmosphere, insofar as known. Snow crystals are not always of sixfold symmetry, nor are they always flat, but Figure 7 gives a condensed survey of some nine principal forms of flat, sixfold symmetry. He gave names to these types as follows:

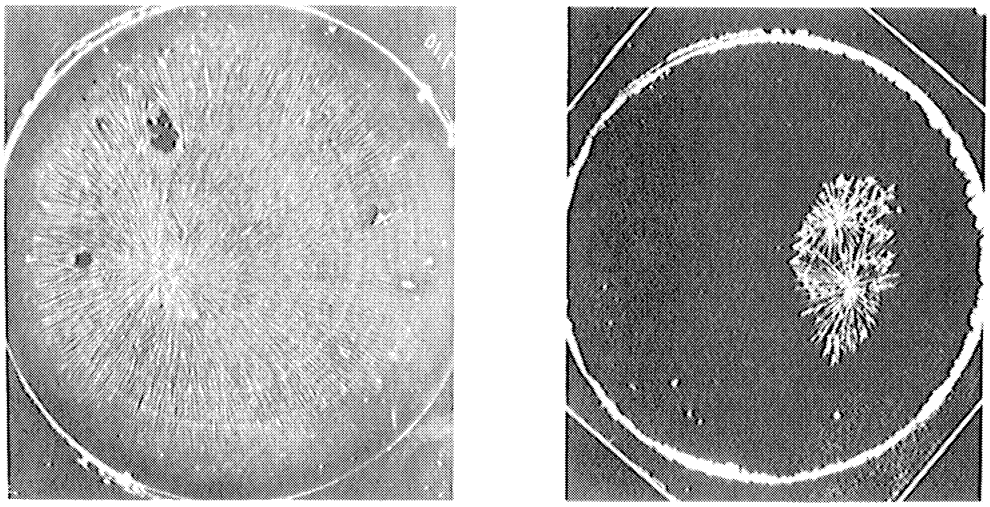

Figure 3

(a) 10 cc $CuCl_2$ 0.2% and 0.02 cc lemon juice

(b) 10 cc $CuCl_2$ 1% blank with stars

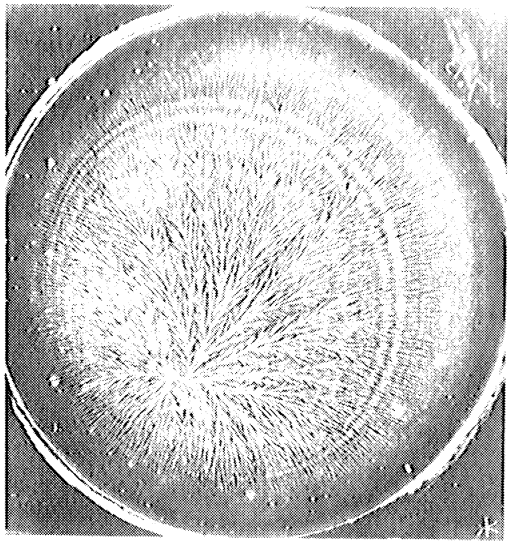

Figure 4. 10 cc $CuCl_2$ 0.5% and 0.1 cc lemon juice.

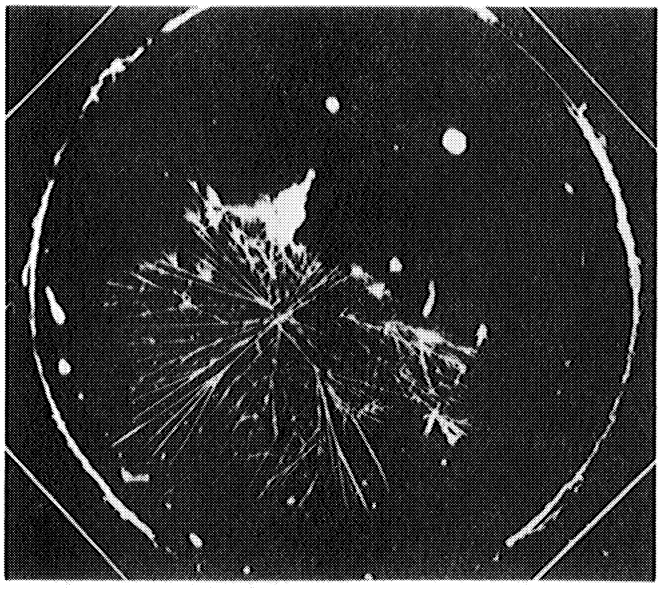

Figure 5. 10 cc $CuCl_2$ 0.67% and 0.2 cc 5% citric acid.

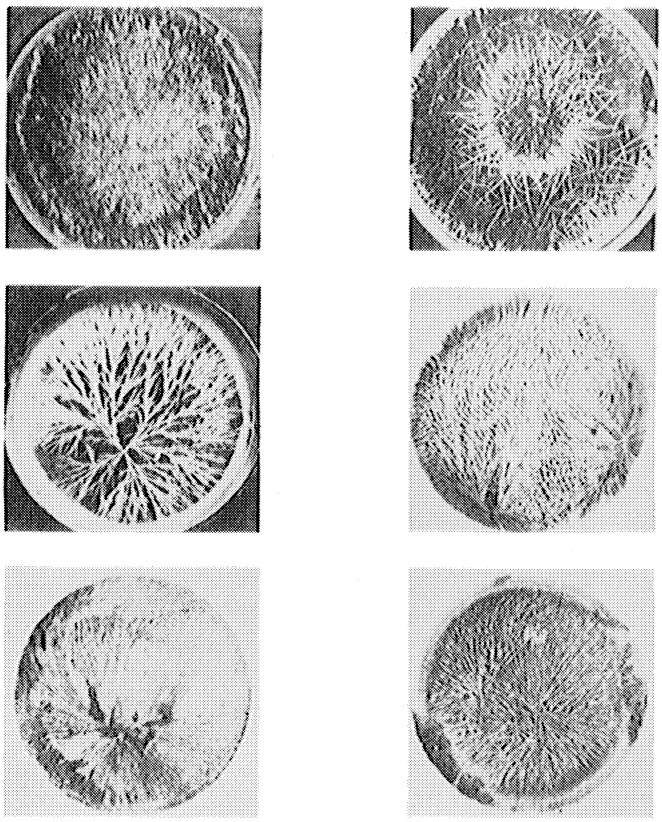

Figure 6

Crystal Patterns Obtained by E. Pfeiffer (ref. 1)

Upper left: 20% $CuCl_2$ blank

Center left: 5% $CuCl_2$ and one drop Camomile flower extract.
Lower left: 15% $CuCl_2$ and 0.05 cc blood from human female.

Upper right: 25% $CuCl_2$ and one drop extract from Agava Americana.
Center right: 15% $CuCl_2$ and 0.05 cc rooster blood.
Lower right: 15% $CuCl_2$ and 0.05 cc rat blood.

a. plates
b. sectors
c. plate with twigs
d. broad branches
e. star
f. dendritic form
g. fern
h. dendritic form with plates
i. plate with dendritic extensions

It is clear that a number of combinations can be made of the structural elements plate, broad branch, sector, line. Nakaya shows hundreds of the most beautiful photographs of all varieties and I want to present a quick idea of his pictures by means of a few of the characteristic ones.

Figure 8 shows some pure plates with various built-in designs.

Figure 9 shows a plate with broad fernlike branches.

Figure 10 shows a smaller plate with slighly dendritic, almost starlike, branches.

Figure 11 shows a still smaller plate, the branches are now more fernlike.

Figure 12 shows a snow crystal with no center plate and branches whose side arms are broadened into sector-like shapes.

Figure 13 shows a pure star.

Figure 14 shows a plate with broad branches at the ends of which we find again new plates.

And so we can go on and on. But there are also more unusual forms.

Figure 15 shows a crystal with what looks at first sight like a twelve fold symmetry. Such crystals are not rare and Nakaya discovered that a slight pressure, exerted by means of a toothpick, in the center, will usually separate them into two sixfold-symmetrical crystals. Still, the question remains why the two would attach to each other in such an almost perfectly symmetric way. Their similarity in structure indicates that they must have come together at a very early stage and fallen through the same atmospheric conditions as one crystal. It also indicated that the atmospheric conditions are responsibile in a reproducible way for the forms of the branches and side branches.

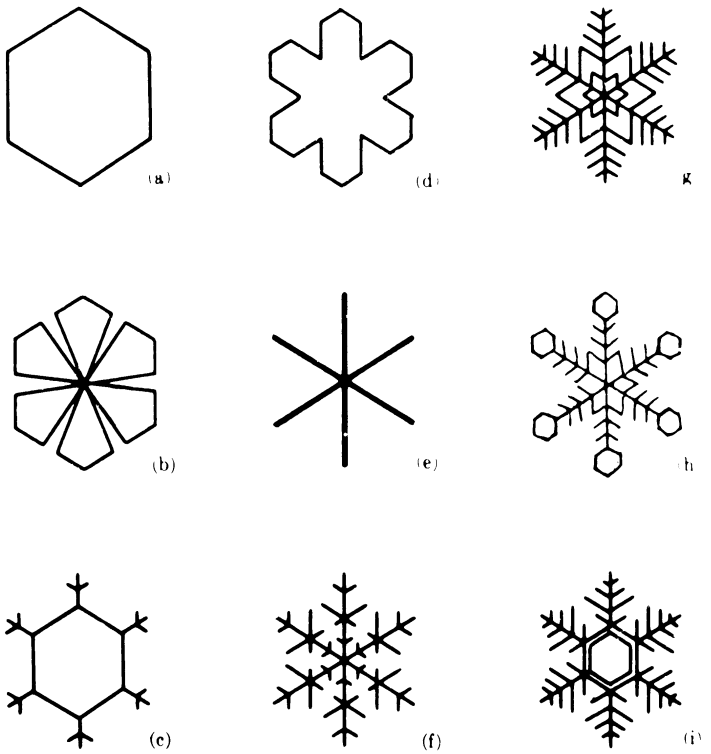

Figure 7. Classification of regular plane crystals: (a) simple plate; (b) branches in sector form; (c) plate with twigs; (d) broad branches; (e) simple stellar form; (f) dendritic form; (g) fern-like form; (h) dendritic form with plates; (i) plate with dendritic extensions.

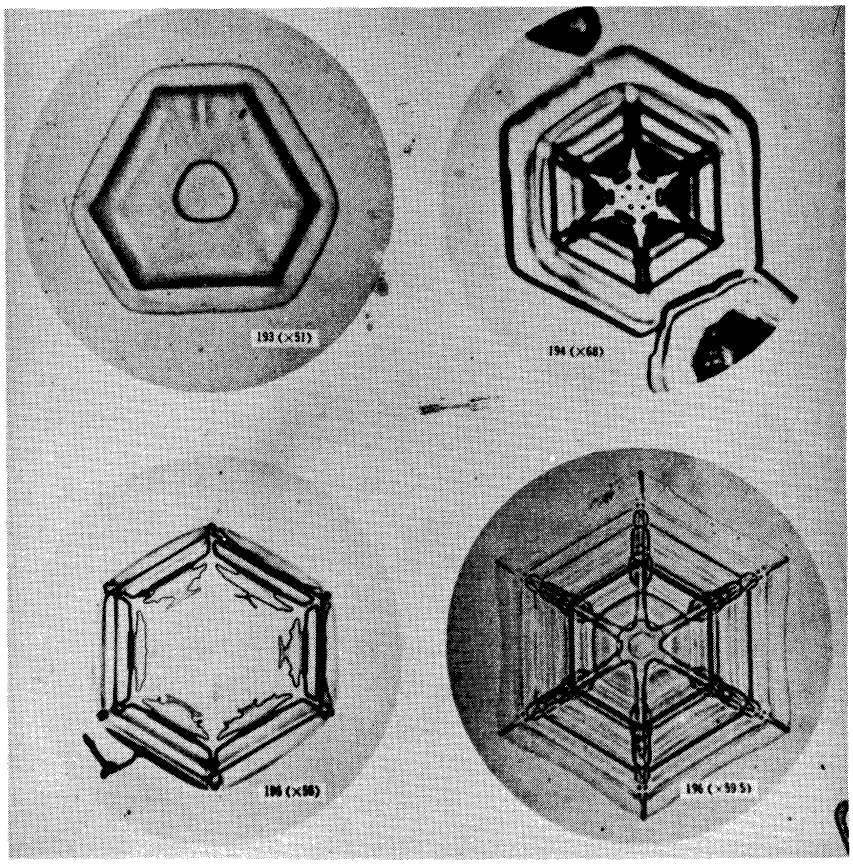

Figure 8.

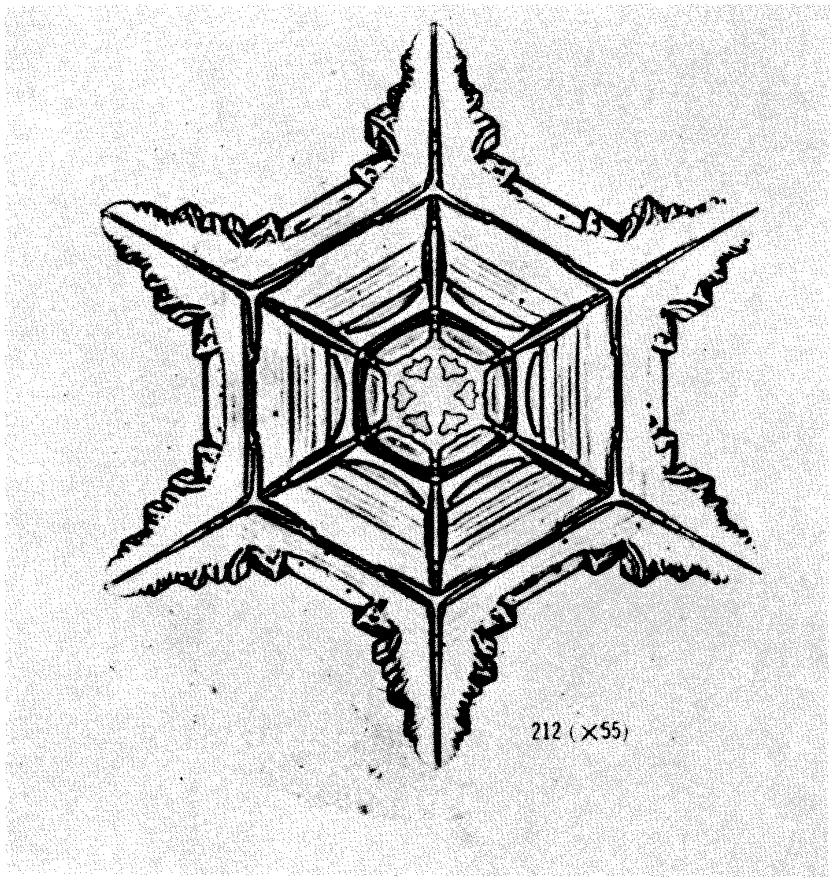

Figure 9.

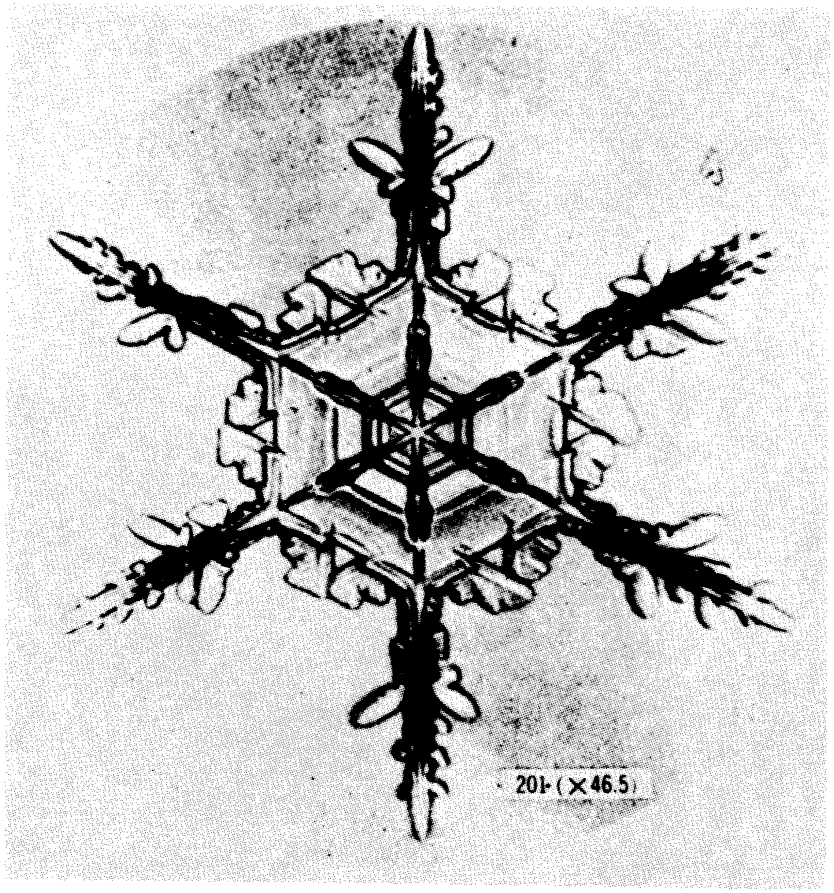

Figure 10.

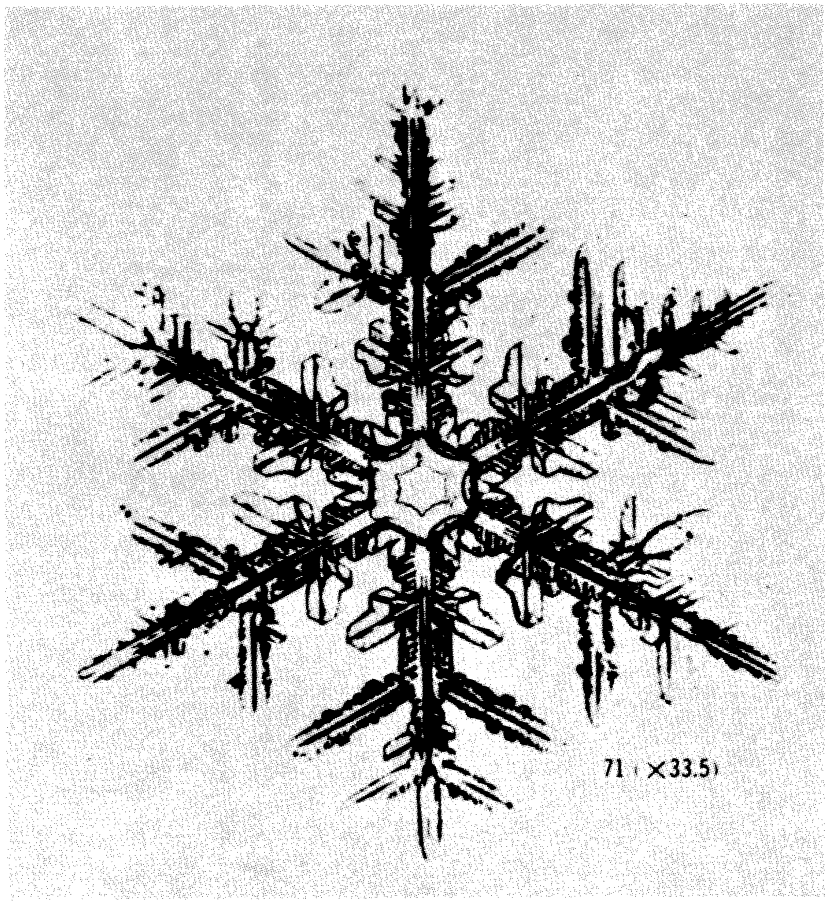

Figure 11.

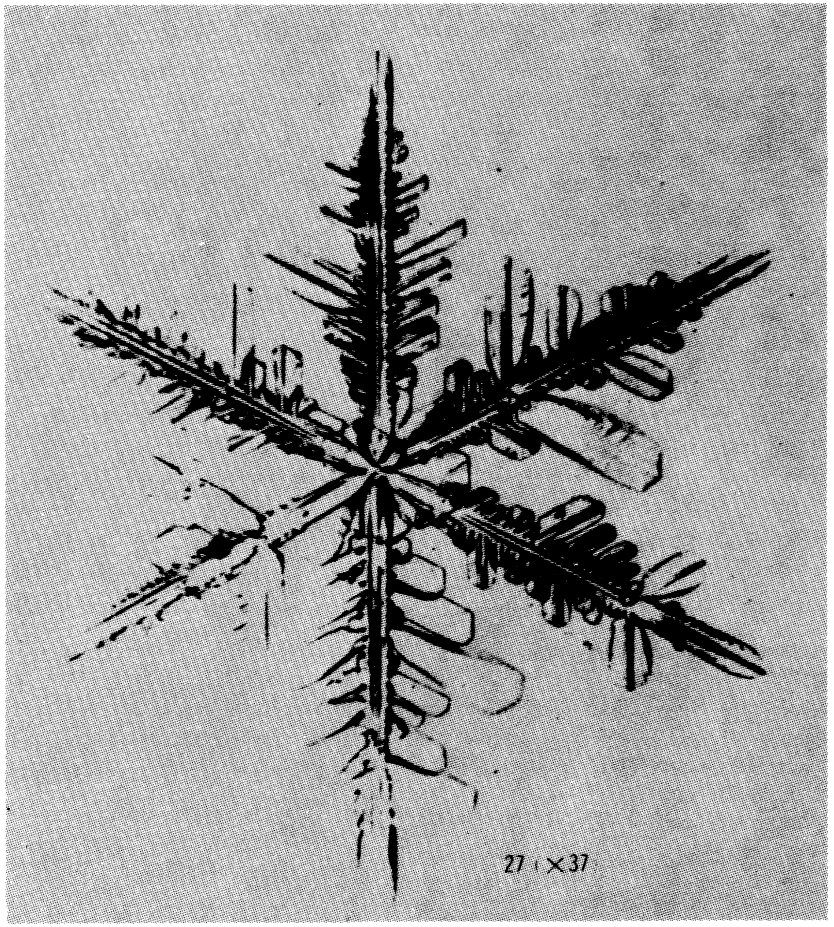

Figure 12.

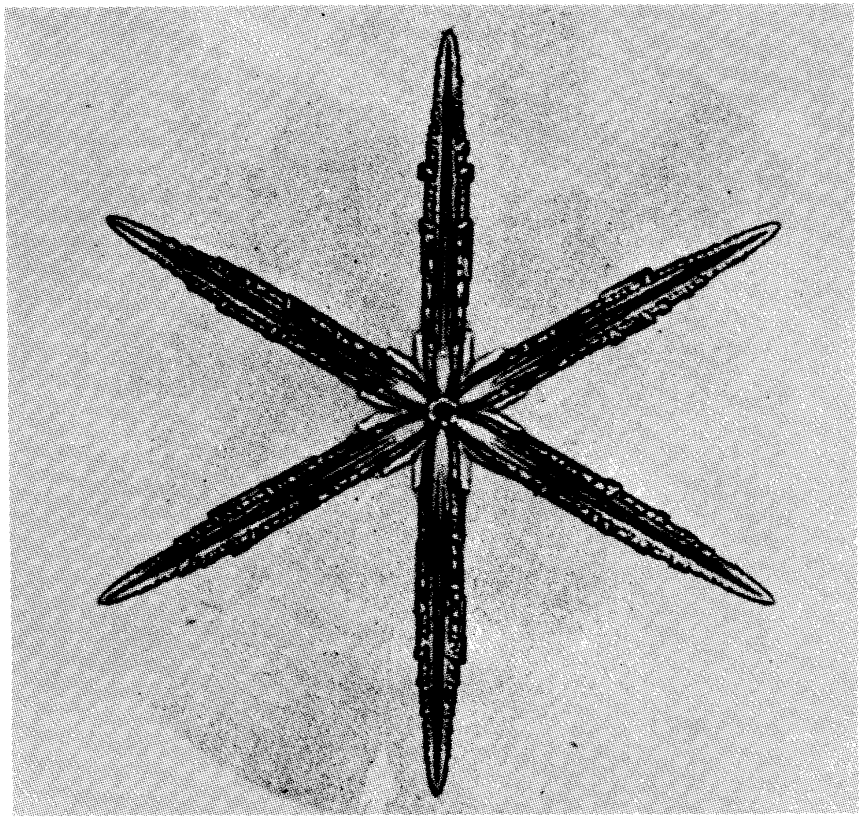

Figure 13.

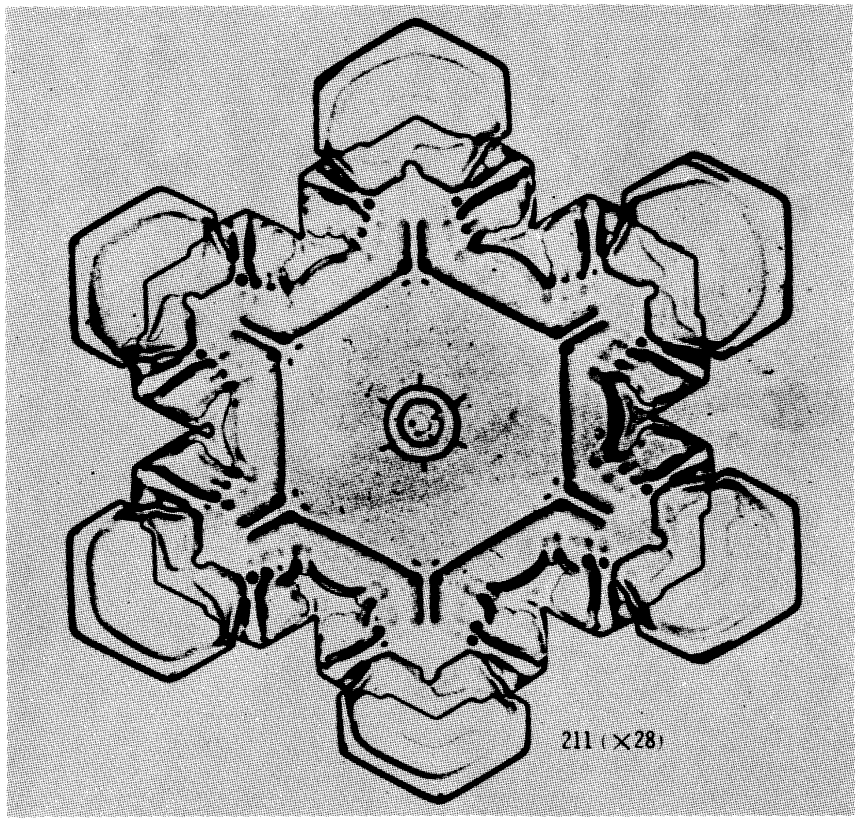

Figure 14.

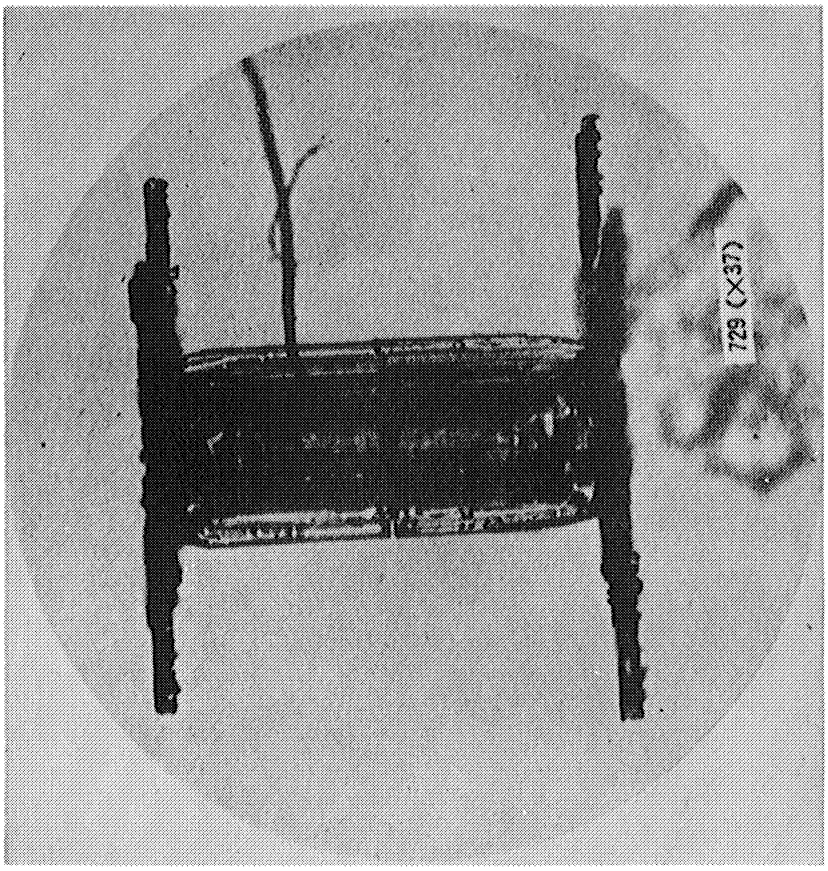

Figure 16.

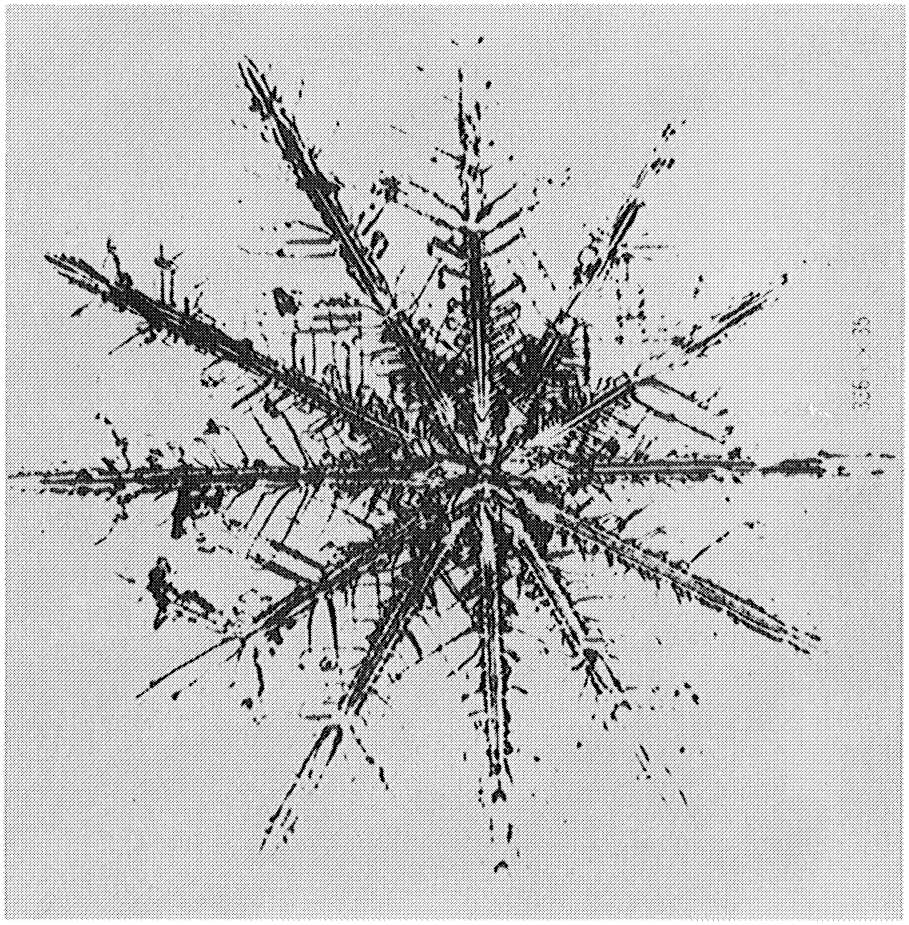

Figure 15.

Figure 16 shows another unusual type, definately not flat, called "Japanese drum" or "tsuzumi". I believe it is called "axle with wheels" in this country.

Figure 17 shows snow crystals in the form of hexagonal "bullets", with a point and a prismatic body, separate or aggregated. It is striking that often bullet aggregates form by sticking the points together, and very often the angles between the bullets are multiples of 60°. Although the latter feature is not evident from this picture, there are other pictures in Nakaya's book which show this very strikingly.

Figure 18 shows a column, which may possibly have been formed by two bullets growing together at 180°.

Figure 19 shows a frost crystal of a frost of a very unusual type designated as cup shape. A number of variations of this type have been encountered.

This study would have been a work of art rather than of science if it were merely a collection of these beautiful pictures, with some sort of classification. However, Nakaya went beyond this. He decided to try to grow man-made snow crystals, something which nobody ever had dreamt of before.

Figure 20 shows the very simple appartus he used. The upper part of the apparatus is kept at a temperature T_a, the air temperature, usually between 0° and -20° C. The lower section contains water which is kept at a temperature T_w, usually between 0° and +10° C causing super-saturation of the colder air with water vapor. Under these conditions no snow forms as yet. A nucleus must be provided. Nakaya mounts at H the hair of a Japanese snow rabbit. On this hair the snow will nucleate and grow and can be observed through the microscopic M. In the course of a time of the order of one or a few hours Nakaya succeeded in growing the first man-made snow crystal, Figure 21. If you look carefully you can still see the hair near the center, running perpendicular to the flake and therefore soon out of focus. The crystal is a little uneven because the apparatus is not quite symmetrical and gravity is a one-sided influence. Later crystals were rotated to get more perfect symmetry.

It is clear what the next step must be. Varying the two variables T_a and T_w, the temperatures of air and water, and growing lots of artificial snow crystals and finding what their forms look like. This was done and it was found that definite regions in the T_a - T_w plane belong to definite form types.

Figure 17.

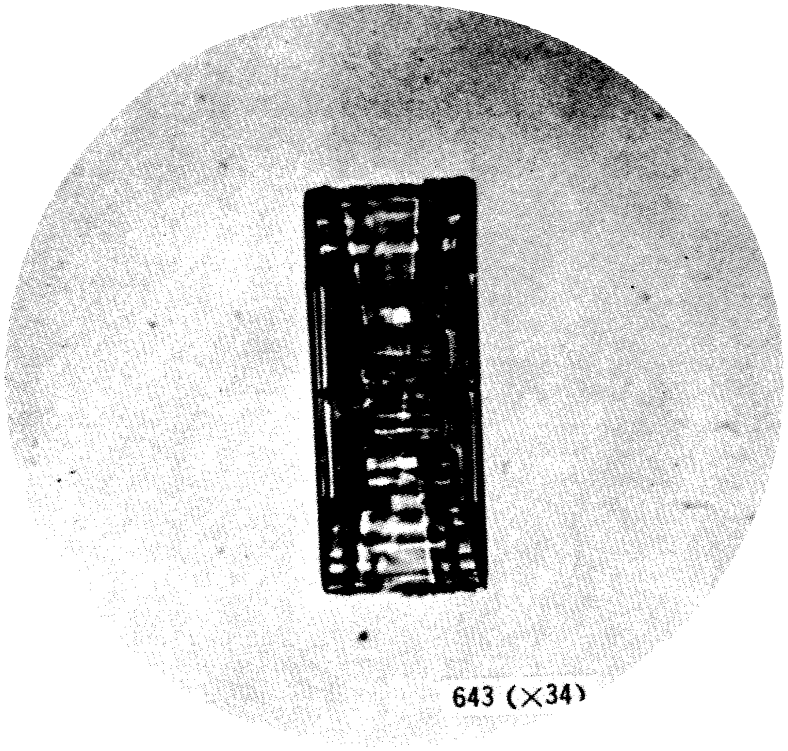

Figure 18.

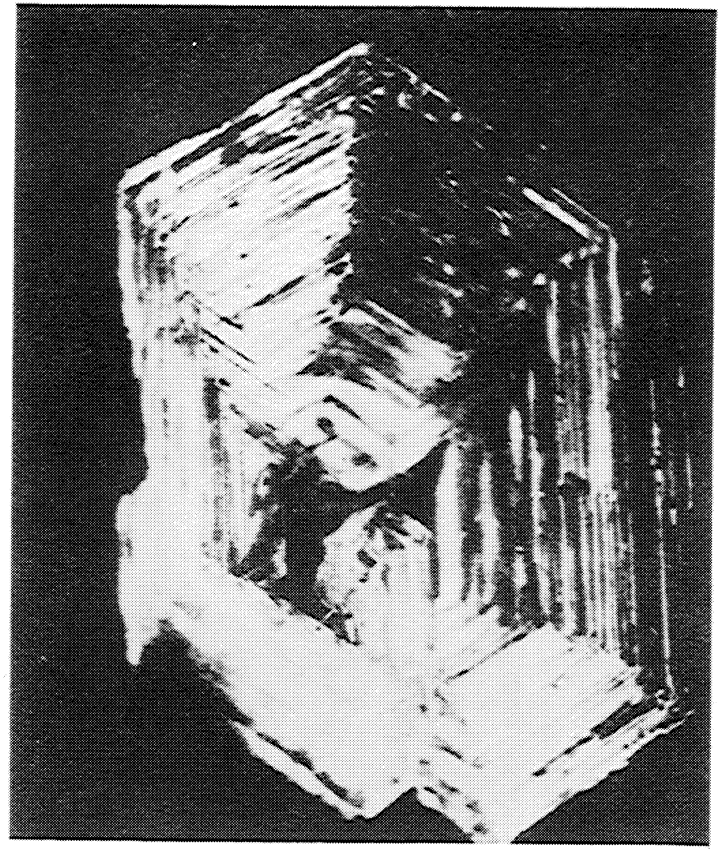

Figure 19. Cup crystal of frost (X 11).

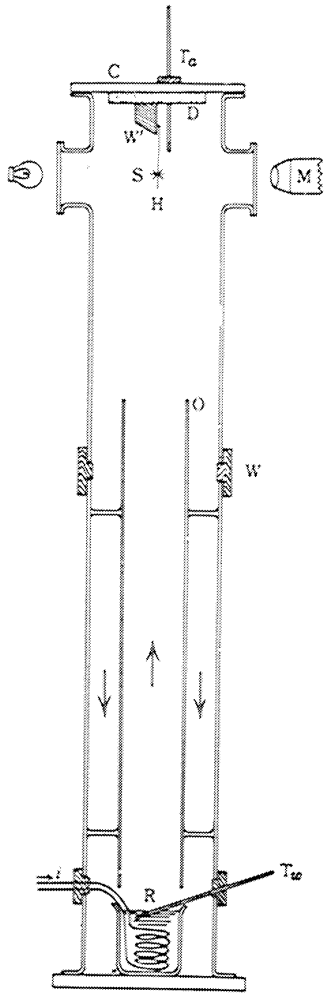

Figure 20. Apparatus No. 1.

Figure 22 shows the results of this study, carried out by one of Nakaya's associates. It is seen that definite regions of the plane belong to definite form types. As a result they were able to grow crystals of any form to order. If, for example, you want a central plate with six dendritic arms and then again plates at the ends, you must first make conditions, for example $T_a = -15°$, $T_w = 12°$. You watch the crystal grow and after a time of the order of half an hour, when you see that the plate has formed you change T_w to 17°, keeping T_a constant. That brings the process into the dendritic region and arms will now grow. When they are long enough to your taste you return to $T_w = 12°$ and at the ends of the arms nice hexagonal plates are formed. Thus by programming his variables Nakaya is able to grow snowflakes of any form to order. He shows many pictures, comparing natural snowflakes and artificial ones of the same form type. The agreement obtained is so striking that you would not be able to tell one picture from the other, were it not for the inevitable rabbit hair running through the artificial crystal. Studies like these can shed a great deal of light on the precise atmospheric conditions under which snow is formed.

Figure 23 shows a cup grown in his equipment. Even this is possible.

CONCLUSIONS

The researches on snow crystals have not, as yet, by any means resolved all questions regarding the factors determining the form of crystals, let alone the mechanism by which they operate. But they have brought into the laboratory, for further study, what was before high up in the air. It is reasonable to hope that researches such as those described, if attacked in the future with the necessary theoretical background, may lead to a more precise understanding of the forces that determine the growth and form of crystals in general.

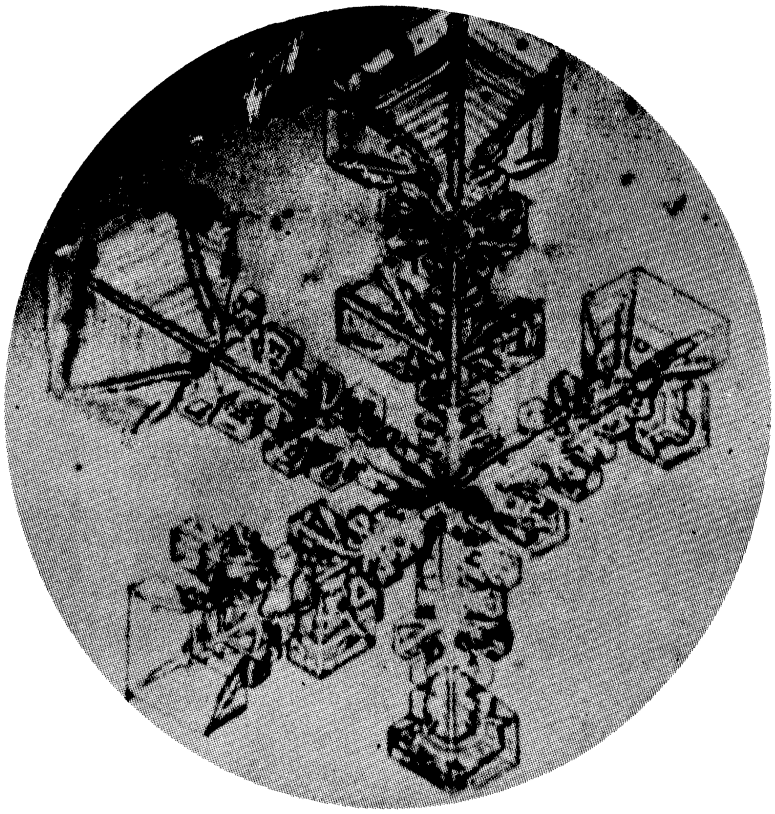

Figure 21. The first snow crystal made in the laboratory (X 22.5).

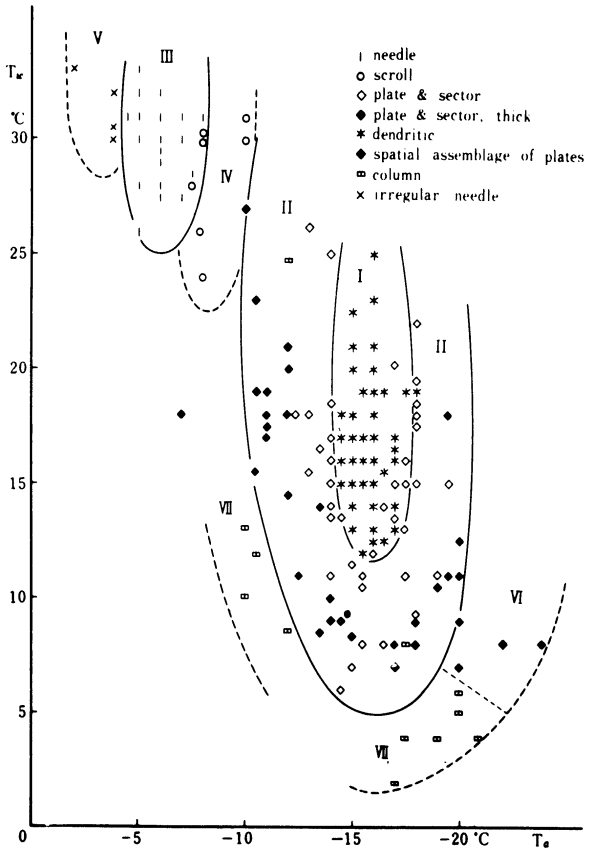

Figure 22. External conditions controlling the form of snow crystals: T_a - T_w diagram.

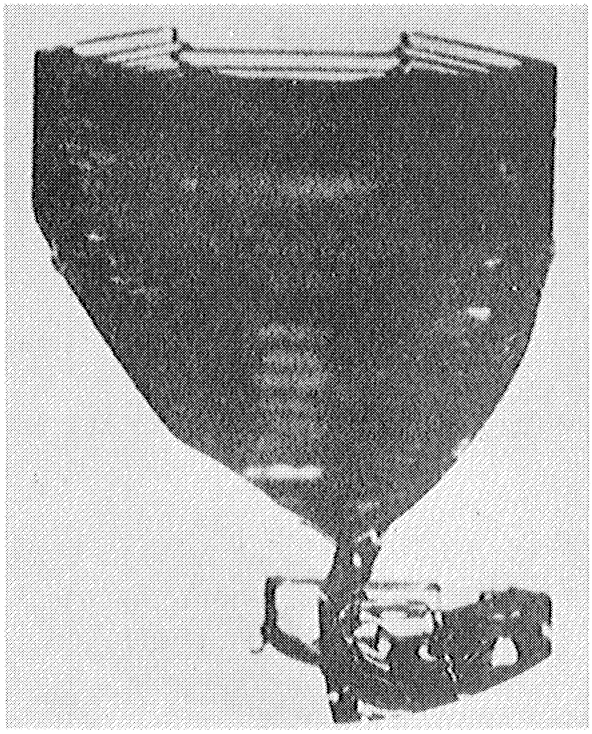

Figure 23. Well-developed cup crystal (X 26).

GAS DESORPTION OF NICKEL POWDERS

M. J. Sinnott
Professor of Metallurgical Engineering
The University of Michigan

and

J. F. Watson
at present with Convair Research Laboratory
San Diego, California

GAS DESORPTION OF NICKEL POWDERS

M. J. Sinnott and J. F. Watson

A study has been made of the gases desorbed from a variety of commercial nickel powders when heated to elevated temperatures. The study included the determination of the amount, composition, and temperature-dependence of the desorption.

The results of these tests showed that volumes of as much as seven milliliters of gas (standard temperature, pressure) per ten grams of sample were evolved from the powder at 1800°F. All gas mixtures collected were composed of one or more species from a group consisting of H_2, H_2O, CO, N_2, CO_2 and SO_2.

The results of this investigation confirmed the hypothesis that the mechanisms of gas evolution and the types of gas evolved from nickel powder heated to 1800°F are dependent upon how the nickel powder is produced.

Problems which arise during processing metal powders include dimensional instability, incomplete welding at the particle interfaces, and uncontrolled porosity. The causes of these problems are not fully understood, but it is believed that gases liberated during sintering are largely responsible for the observed deleterious effects. These gases are usually attributed to one or more of the following sources: gases dissolved in the metal powder; gases resulting from chemical reactions between the sintering furnace atmosphere and the powder; gases entrapped in the pressed compact; and gases adsorbed on the surface of the powder. When gases from any of these sources are liberated after the interior voids have been closed, they are entrapped in these voids and prevent further densification. In extreme cases this interior pressure may cause the compact to grow.

It was the purpose of this investigation to determine the amounts and compositions of the gases liberated from nickel powders at elevated temperatures, and to determine the mechanism of their evolution. The powders were heated under an inert atmosphere in a loose condition so that chemical reactions with the atmosphere and mechanical entrapment could be eliminated as sources of gas. It was reasonable to expect that powders manufactured by different techniques would exhibit different gas evolution characteristics; consequently a variety of powders produced by several methods were examined. The temperature dependence of the gas evolution from these powders was studied over the range of 70°F to 1800°F. The source of the liberated gases was studied by investigating the influence of surface treatments on the subsequent gas evolution.

The literature pertaining to the general field of gas-metal systems is voluminous, but very little of it applies directly to the subject of this investigation. The general topic of gas adsorption has been thoroughly covered, but this work is generally conducted at or below room temperature. The reverse mechanism, desorption, which is considered in the present work, has received very little attention, especially at the elevated temperatures such as those used in the powder metal industry.

The gases evolved from nickel wire heated to 750°C were found to consist of carbon dioxide, carbon monoxide and hydrogen in some tests by Smithells and Ransley[1]. Several hours were required for the completion of the gas evolution which led Jones to postulate that dissolved gases were diffusing to the surface[2]. This lead to the conclusion that the controlling factor was the rate of diffusion of dissolved oxygen. Warren and Libsch investigated the gases evolved from iron-cobalt compacts at 1400°C and found that compacts heated under helium possessed greater permeability than those heated under hydrogen[3]. This effect was explained by assuming that the hydrogen reduced surface oxides fast enough so that the reacted gases could escape before the pores were sealed. In the other case, dissolved carbon reduced the surface oxides, but the diffusion of carbon was too slow to allow the gaseous products of the reaction to escape before the interior voids were closed. In another experiment by the same authors, pure cobalt was heated to 1000°C under vacuum and the evolved gases were collected. About 1.6 milliliters of carbon dioxide per gram of cobalt were liberated. The source of the gas was attributed to chemisorbed carbon dioxide, and reactions between dissolved carbon and surface oxides. Duftschmid, Schlecht, and Schubart found that carbon dioxide and carbon monoxide were liberated from carbonyl iron powder[4]. These gases were shown to be the products of reactions between dissolved carbon and iron oxide. Tobin and Sinnott collected and analyzed the gases desorbed from a series of copper powders, and found that water vapor, carbon dioxide and sulfur dioxide were desorbed on heating to 1400°F[5]. The source of these gases was shown to be surface compounds. Fedorchenko, in experiments with nickel powder compacts, observed growth at elevated temperatures which he attributed to gas evolution and the release of internal stresses[6].

EXPERIMENTAL PROCEDURES

The experimental data obtained in this investigation were derived from five procedures: measurements of the total volumes of desorbed gases; measurements of the cumulative volumes of desorbed gases, vacuum fusion analyses, x-ray diffraction, and electron diffraction. The gas desorption studies made use of a gas desorption apparatus, while the vacuum fusion, x-ray diffraction, and electron diffraction analyses were performed on commercially available equipment.

Testing Methods

The gas desorption apparatus used in this investigation was a modification of equipment previously used by J. C. Tobin[7]. Quartz was substituted for Vycor in the sampling tubes because of the higher operating temperatures involved in the present program. A schematic diagram of this equipment is shown in Figure 1.

Two gas desorption techniques were employed. In the total gas desorption runs, it was desired to collect all of the gases liberated from the powder before they could react with the hot powder. This was done by placing a liquid nitrogen cold trap in the system so that the reactive gases were condensed before they could react. In the cumulative gas desorption runs, it was desired to keep the manifold pressure constant, and to allow the desorbed gases to approach equilibrium with the hot metal powder at a series of temperatures, so that the ensuing gas evolution could be studied as a function of temperature.

X-ray diffraction investigations were made on the ball mill fines resulting from the short-time ball milling of nickel powders. Coarse samples of powder, -70 + 100 mesh, were ball milled in porcelain ball mills for about ten minutes. The powder was then sieved through a -325 mesh screen and the fines were used for x-ray powder pictures using normal Debye-Scherrer techniques. The short times of milling and the coarse fractions of powder insured that only surface layers would be removed and subsequently analyzed. The porcelain mills and balls used prevented contamination of the powder. As an additional safeguard, the mills and balls were boiled in nitric acid for fifteen minutes, washed in distilled water, and dried at 200°C overnight before use.

Electron diffraction investigations were made on both powdered and massive nickel samples. Initial work was done on very fine -325 mesh powder, but polished surfaces of massive nickel were found to yield slightly better results. Both transmission and reflection studies were attempted.

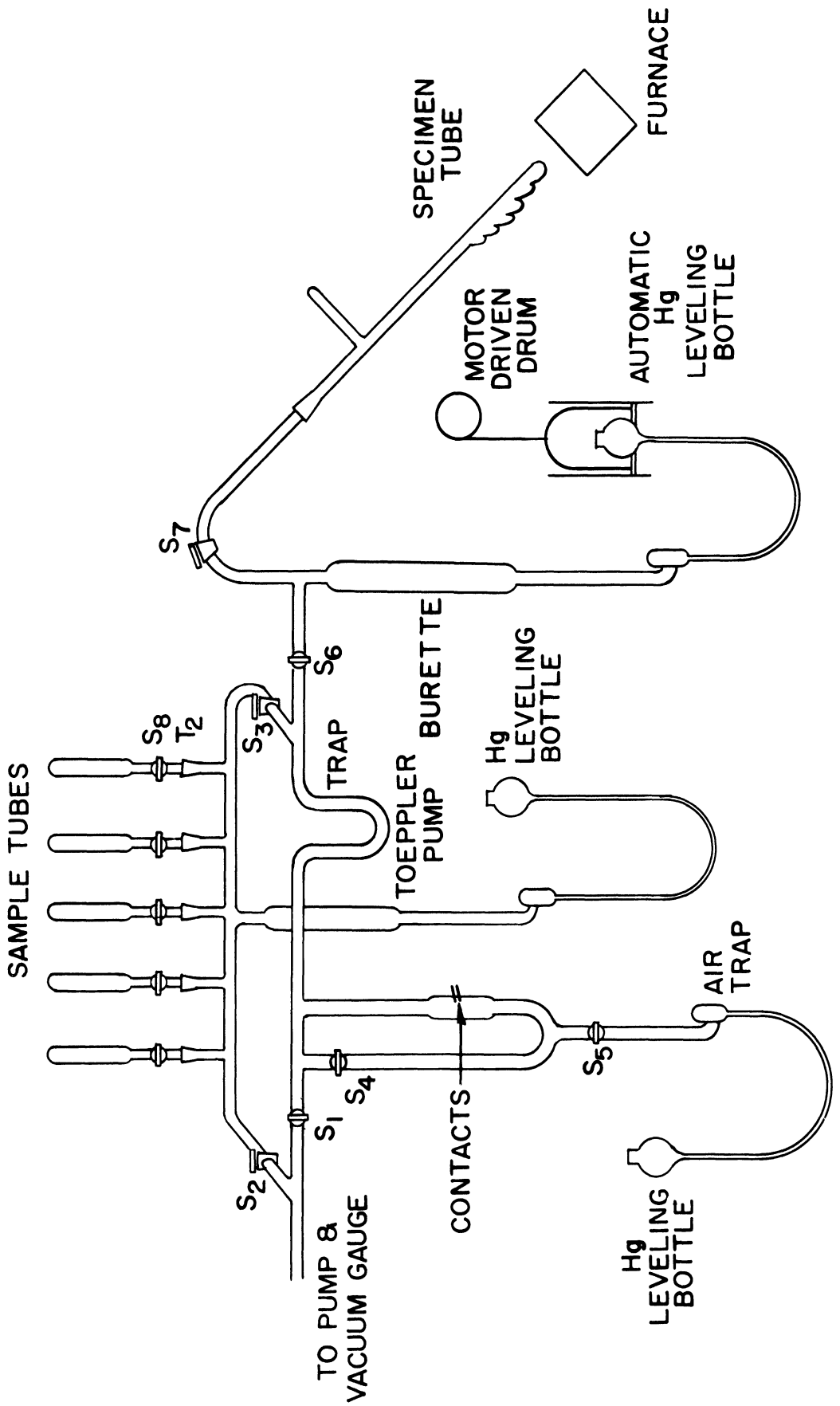

Figure 1. Gas Desorption Apparatus

The vacuum fusion analyses were performed on a standard National Research Corporation vacuum fusion gas analysis apparatus.

Description of Powders

The materials selected for examination in this program represented a variety of commercially available powders. The first nickel powder was produced by steam scattering in air and will hereafter be designated as MD9119 powder. This powder was produced by subjecting a stream of molten electrolytic nickel to a jet of steam which atomized the nickel and gave each powder pellet a roughly spherical shape. This technique resulted in a powder covered with a dull nickel oxide film, containing some nickel-nickel oxide eutectic in the grain boundaries.

The second nickel powder was prepared by steam scattering in air followed by an annealing treatment in cracked ammonia and will hereafter be designated as PM273 powder. This powder was prepared in the same manner as the MD9119 powder, but after atomization was subjected to an annealing treatment at 1400°F for 45 minutes under a cracked ammonia atmosphere. This powder exhibited a much brighter appearance than the MD9119 powder, because the annealing treatment had reduced the surface oxides.

The third powder was prepared by hydrogen reduction from a nickel-ammonia complex aqueous solution and will hereafter be designated as SG321 powder. The details of this manufacturing process have been described by Forward and by Mackiw, Lin, and Kunda[8,9].

The fourth nickel powder was produced by steam scattering in a nitrogen atmosphere followed by an annealing treatment in hydrogen and will hereafter be designated as FM powder. This powder presented a very bright appearance, because the nitrogen atmosphere had minimized surface oxidation, and the hydrogen annealing operation had removed any remaining surface oxides

Experimental Results

MD9119 Powder

The total volume gas desorption analyses on three mesh fractions of this powder in the "as received" condition are shown in Table I. Other total volume gas desorption analyses for this powder in the ball milled and rinsed conditions are shown in Table II for the -70 +100 mesh fraction. The data showing the behavior of this powder after being rinsed in nitric acid and then being re-exposed

TABLE I

TOTAL AND CUMULATIVE GAS VOLUMES FOR TEN GRAM SAMPLES HEATED TO 1800°F IN THE AS RECEIVED CONDITION:

MD9119 POWDER

	Total Volume						Cumulative Volume					
	Volume, ml. at STP						Volume, ml. at STP					
Mesh Fraction	H_2	H_2O	CO	CO_2	SO_2	Total	H_2	H_2O	CO	CO_2	SO_2	Total
- 70 + 100	0.0	0.2	0.1	1.9	0.6	2.8	0.0	0.2	0.1	1.5	0.1	1.9
- 100 + 200	0.0	0.3	0.3	2.5	0.9	4.0	0.0	0.5	0.3	2.4	0.1	3.3
- 200 + 325	0.0	0.2	0.7	4.2	1.5	6.6	0.0	0.6	0.6	3.6	0.2	5.0

PM273 POWDER

	Total Volume						Cumulative Volume					
	Volume, ml. at STP						Volume, ml. at STP					
Mesh Fraction	H_2	H_2O	CO	CO_2	SO_2	Total	H_2	H_2O	CO	CO_2	SO_2	Total
- 70 + 100	0.1	0.4	5.2	0.6	0.0	6.3	0.6	0.2	5.0	0.4	0.0	6.2
- 100 + 200	0.0	0.3	4.0	1.1	0.0	5.4	0.3	0.5	3.4	1.3	0.0	5.5
- 200 + 325	0.4	0.4	4.5	0.8	0.0	6.1	0.9	0.4	4.8	1.0	0.0	7.1

SG321 POWDER

	Total Volume						Cumulative Volume					
	Volume, ml. at STP						Volume, ml. at STP					
Mesh Fraction	H_2	H_2O	CO	CO_2	SO_2	Total	H_2	H_2O	CO	CO_2	SO_2	Total
- 100 + 200	0.0	3.9	0.1	1.8	0.4	6.2	1.1	1.6	0.2	1.5	0.1	4.5
- 200 + 325	0.0	3.1	0.3	2.0	0.3	5.7	0.5	1.5	0.1	1.6	0.3	4.0

FM POWDER

	Cumulative Volume	
	Volume, ml. at STP	
Mesh Fraction	H_2	CO_2
- 70 + 100	0.1	0.1

to air as a function of time are presented in Figure 2. A typical cumulative volume gas desorption analysis for the -100 +200 mesh fraction of this powder is presented in Figure 3. In addition, the cumulative volumes at 1800°F are presented in Table I for comparison with the total gas desorption volumes at this temperature.

Vacuum fusion runs were made on duplicate samples of -70 +100 mesh powder after cumulative and total gas desorption studies as well as in the as received condition, and these data are presented in Table III.

PM273 Powder

The total volume gas desorption analyses for three mesh fractions of this powder are shown in Table I. A typical cumulative volume gas desorption analysis for the -100 +200 mesh fraction is shown in Figure 4. The cumulative gas desorption volumes at 1800°F are also presented in Table I for comparison with the total volume runs.

SG321 Powder

The total volume gas desorption analyses for two mesh fractions of this powder are presented in Table I. A typical cumulative volume gas desorption analysis for the -100 +200 mesh fraction is shown in Figure 5. In addition the cumulative volumes at 1800°F are presented in Table I for purposes of comparison.

FM Powder

The cumulative volume gas desorption analyses of a -70 +100 mesh sample of this powder is given in Figure 4. The results of vacuum fusion work on this powder in the as received condition are presented in Table III. The cumulative volumes at 1800°F are presented in Table I.

Analysis of Results

The volumes and analyses of the gases liberated from the various nickel powders studied throughout the course of this investigation were found to be dependent upon the method of powder manufacture. The gases evolved were found to be mixtures of one or more species from a group composed of H_2, CO_2, CO, SO_2, and H_2O. The number of different gases evolved and their relative abundance was found to vary widely between different powders, and also varied with temperature for a given powder.

The mechanisms of gas desorption were also found to be influenced by the manufacturing technique. Powder atomized in air without

further treatment was observed to liberate gas by surface desorption. Powders heat treated in hydrogen bearing atmospheres after atomization evolved gases whose source was believed to be dissolved hydrogen, oxygen and carbon. The heat treatments were performed at temperatures sufficiently high to cause the evolution of any gases adsorbed during the manufacturing process. These treatments in hydrogen bearing atmospheres also increased the dissolved hydrogen content of the annealed powders.

Structural studies of both powdered and massive nickel surfaces by electron diffraction techniques were unsuccessful. No diffraction rings were obtained from fine, -325 mesh powder, because of charging phenomena. Very faint and diffuse diffraction rings were obtained from massive nickel surfaces which had been polished, etched, and re-exposed in air, but no positive identifications could be made. Diffuse diffraction rings of this type have also been observed by other investigators.

MD9119 Powder

This powder, produced by steam scattering in air, was studied in the greatest detail. It exhibited the greatest variety of desorption mechanisms, and for this reason received more study than the other powders.

Table I shows that there is a correlation between gas volumes evolved and apparent surface area. This established the primary mechanism of gas evolution as surface desorption. This conclusion was further substantiated by tests wherein the influence of surface preparation on gas evolution was studied.

The total volume gas desorption studies, wherein evolved gases were condensed in a cold trap, show, in Table I, that CO_2 was the major constituent of the gases evolved at 1800°F. These data also demonstrate that the volumes of CO, CO_2 and SO_2 evolved were related to the surface area, which established their mechanism of evolution as a surface phenomenon. The amount of water vapor liberated was erratic, and this was believed to be due to the low strength of the physical adsorptive bond by which water is known to be adsorbed on nickel.

The amounts of SO_2 liberated in the total volume studies were considerably higher than those amounts liberated in the cumulative volume studies. This was caused by the non-equilibrium nature of the experimental procedure, wherein the SO_2 was frozen out as soon as it was formed, thus allowing the reaction producing it to proceed to completion. This reaction is believed to be as follows:

$$Ni_3S_2(s) + 4CO_2(g) \rightarrow 3Ni(s) + 2SO_2(g) + 4CO(g) \qquad (1)$$

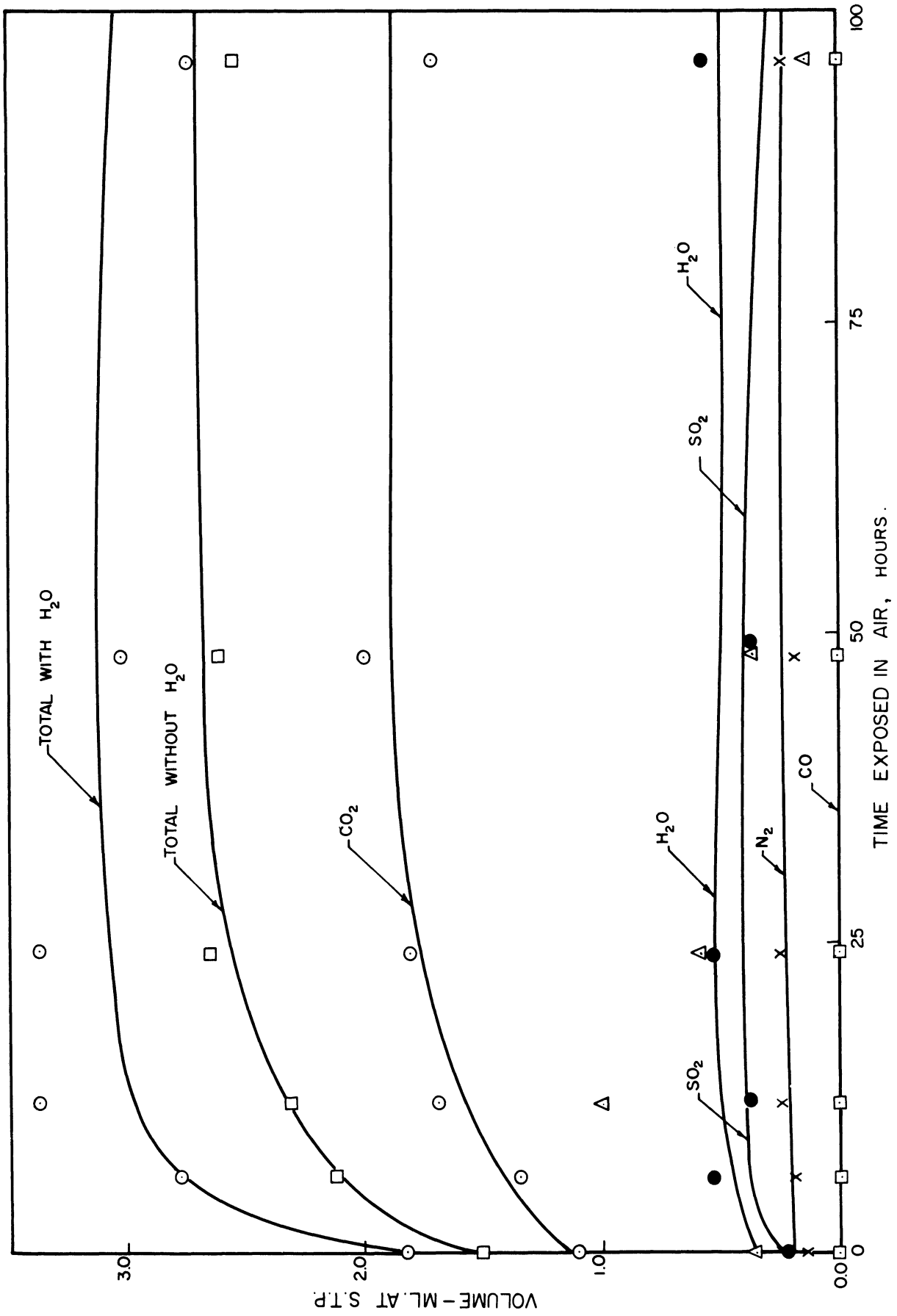

Figure 2. Total Gas Volumes as a Function of Time for Ten Gram Samples of MD 9119 Powder Rinsed in Nitric Acid and Re-exposed in Air; -70 +100 Mesh Fraction.

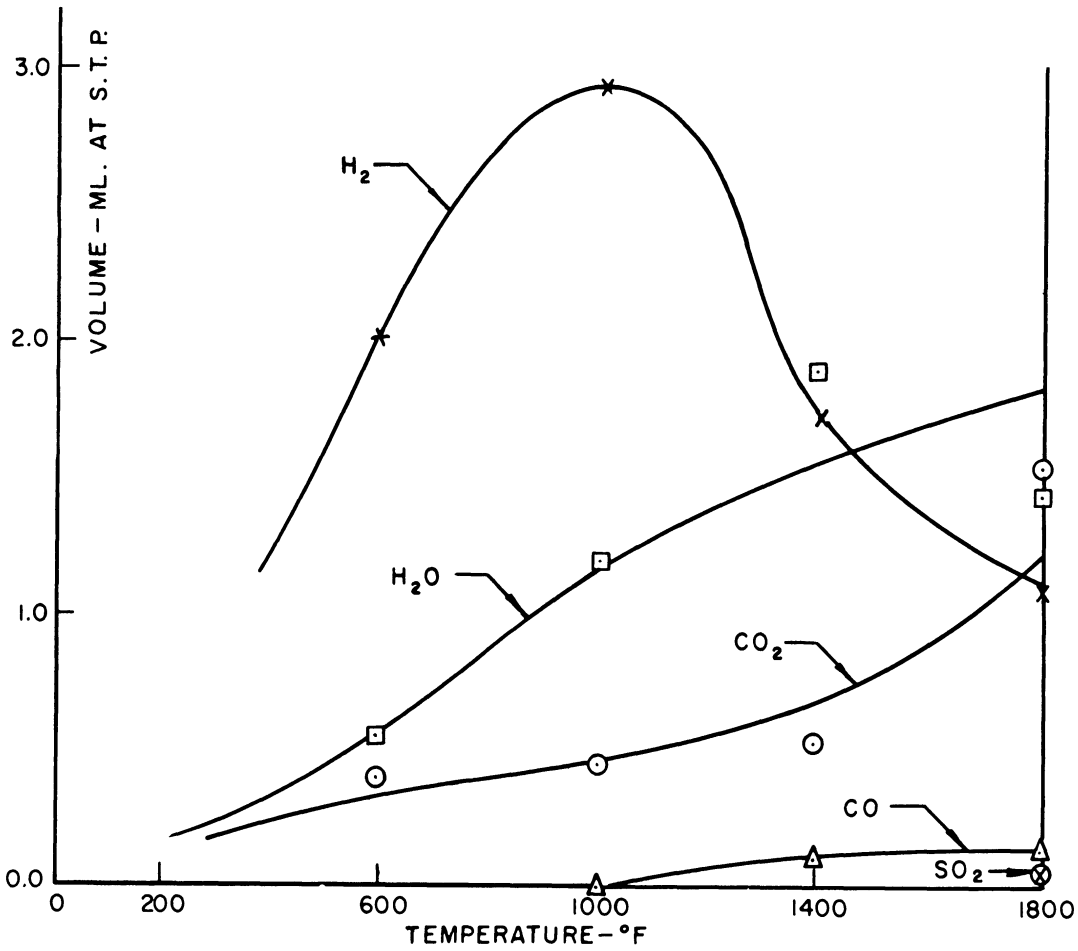

Figure 3a. Cumulative Gas Volumes as a Function of Temperature for a Ten Gram Sample of SG 321 Powder in the As Received Condition; -100 +200 Mesh Fraction.

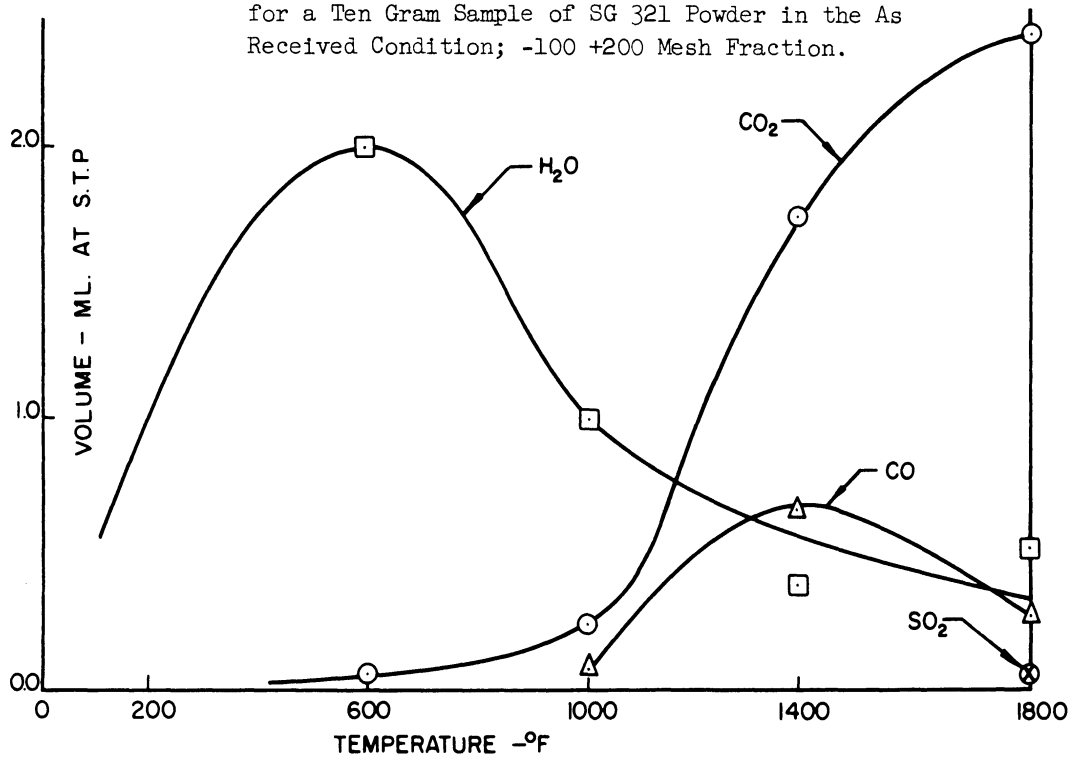

Figure 3b. Cumulative Gas Volumes as a Function of Temperature for a Ten Gram Sample of MD 9119 Powder in the As Received Condition; -100 +200 Mesh Fraction.

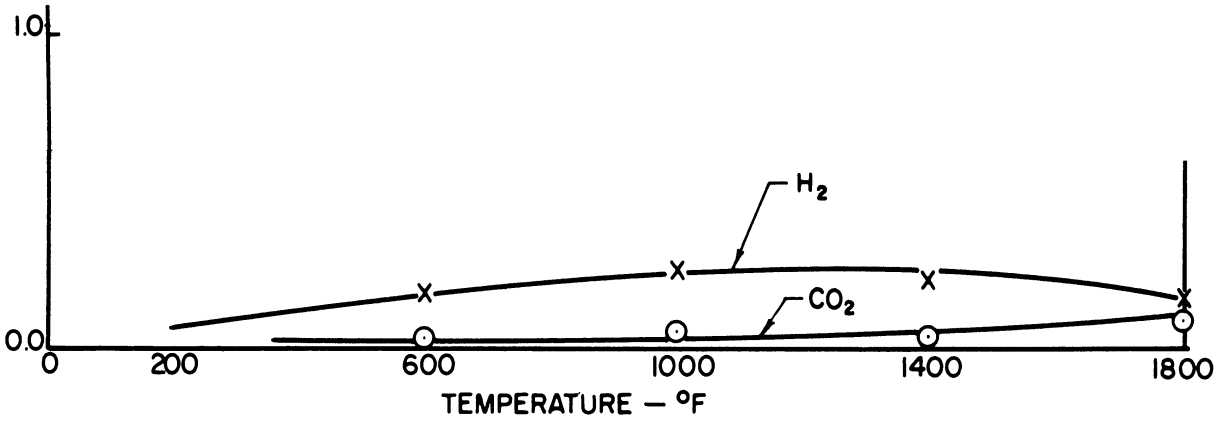

Figure 4a. Cumulative Gas Volumes as a Function of Temperature for a Ten Gram Sample of FM Powder in the As Received Condition; -70 +100 Mesh Fraction.

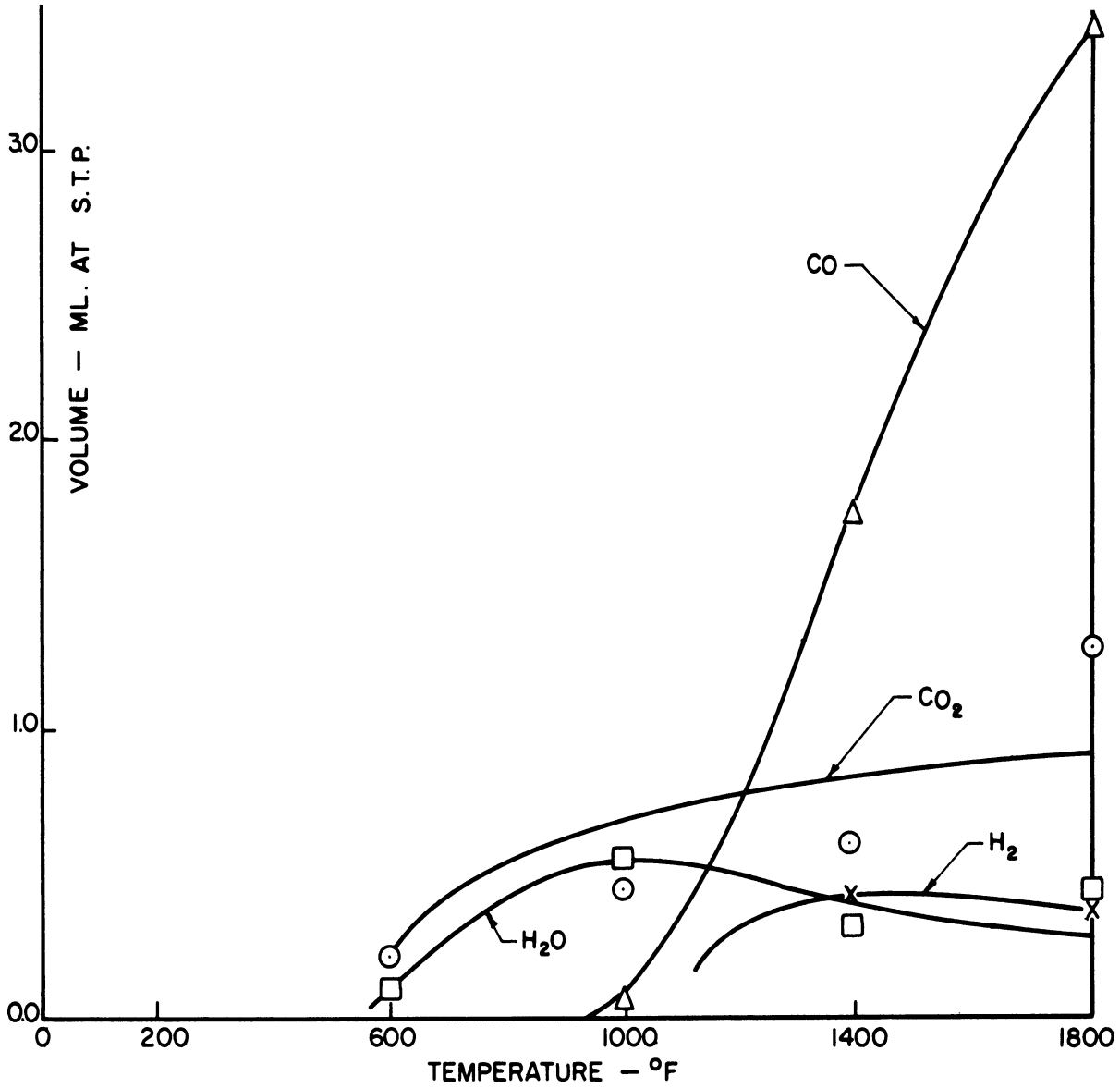

Figure 4b. Cumulative Gas Volumes as a Function of Temperature for a Ten Gram Sample of PM 273 Powder in the As Received Condition; -100 +200 Mesh Fraction.

In the cumulative volume procedure, however, the gas system approached equilibrium and the amount of SO_2 produced was limited.

The cumulative volume gas desorption studies, shown in Figure 3, indicate the temperatures at which the various gases were evolved, and again show that CO_2 was the major constituent in the evolved gas mixture. Because these cumulative plots show the total volumes of the various gases evolved to a given temperature, it is apparent that a curve which shows a decreasing volume with increasing temperature indicates that the gas is reacting in some way so as to reduce its total volume at the higher temperature. It is believed that water vapor was undergoing a reaction to produce hydrogen and oxygen in the temperature range of 600°F to 1400°F, and that CO was undergoing a reaction to produce CO_2 between 1400°F and 1800°F. It should also be noted that very small amounts of SO_2 were liberated only at 1800°F.

The primary reaction involving CO is as follows:

$$NiO\ (s) + CO\ (g) \rightarrow Ni\ (s) + CO_2\ (g) \qquad (2)$$

The surface material milled from the as received powder indicated the presence of nickel oxide on the surface of the powder. Surface material milled from the powder in the same way after a cumulative gas desorption test showed that all of the nickel oxide had been removed from the surface of the powder. That the CO was acting as the reducing agent is shown in the cumulative studies of Figure 3, where the CO is seen to reach a maximum at about 1400°F and then decrease.

A comparison of the total and cumulative gas desorption studies at 1800°F, presented in Table I, shows that the CO and CO_2 values are about the same in both runs. This was caused by the fact that the CO was not frozen out in the total volume runs, because it did not condense at the temperature of liquid nitrogen under the manifold pressure. Thus the CO was free to react with the hot nickel oxide, with the result that the CO volume was reduced to the same low level as observed in the cumulative run. The CO_2 produced by the reduction reaction in the total volume test was frozen out, and this had the effect of allowing the reaction to continue until all of the nickel oxide had been reduced. In both cases the powder was appreciably brighter after the desorption runs than in the as received condition which also indicated the occurrence of an oxide reduction reaction.

The desorbed water vapor underwent a reaction at higher temperatures which involved a breakdown of the water molecule with a subsequent solutioning of the hydrogen in the nickel, and a probable reaction of the oxygen with CO to form CO_2. The solutioning of the

hydrogen is established by the vacuum fusion data of Table III which indicate that the powder contained significantly more dissolved hydrogen after the cumulative run than in the as received condition. The nickel did not show a significantly higher dissolved oxygen content after the cumulative run, which led to the hypothesis that the oxygen reacted with CO to form CO_2. The desorption of water vapor at relatively low temperatures was consistent with the literature which indicates that water is very weakly bonded to nickel by a physical adsorption bond, and should therefore be desorbed at a relatively low temperature[10,11].

As a means of further investigating the surface dependence of the desorbed gases, powder surfaces were treated by ball milling and by rinsing in acid before total gas desorption runs were performed. Table II shows that both treatments effected the desorbed gas volumes significantly. The nitric acid rinse reduced the CO_2, CO and SO_2 volume desorbed, which again indicated that the desorption mechanism for these gases was a surface phenomenon.

The ball milling operation lowered the CO_2 gas volume desorbed, but increased the SO_2 volume. These data support the surface desorption mechanism for CO_2, and indicate that the SO_2 is the product of a reaction involving the oxidation of a nickel sulphide. The presence of the nickel sulphide was to be expected because sulfur was present in excess of its solubility limit. Apparently the ball milling brought more nickel sulphite into contact with the atmosphere where SO_2 was produced according to equation (1).

Both the ball milling and acid rinse increased the surface activity of the powder, as evidenced by a tendency for the powder to cling to the sides of the sample tube. That this surface activity was caused by unsatisfied surface forces of the type which causes adsorption was demonstrated by the fact that powders in both conditions desorbed nitrogen upon heating. Of all the samples investigated, these were the only ones to desorb nitrogen, which was presumably adsorbed during loading when the "active" powder was briefly exposed to air.

The tendency for the cleaned powder to readsorb gases was studied by exposing powder rinsed in nitric acid to air for periods of time up to 96 hours. The results of these tests are presented in Figure 2, and show that readsorption was completed in about 24 hours. This readsorption was limited primarily to CO_2 and smaller amounts of nitrogen. It is believed that both of these gases were adsorbed directly from the atmosphere. The water data again tend to be erratic because of the weak adsorptive bond. The SO_2 curve shows no definite trend, which lends support to the hypothesis that the SO_2 was produced by the oxidation of a nickel sulphide distributed throughout the powder matrix.

TABLE II

TOTAL GAS VOLUMES FOR TEN GRAM SAMPLES OF MD9119 POWDER HEATED TO 1800°F IN THE BALL MILLED, RINSED, AND AS RECEIVED CONDITIONS; - 70 + 100 MESH FRACTION

	Volume, ml. at STP						
Condition	H_2	H_2O	CO	CO_2	SO_2	N_2	Total
Rinsed in HNO_3	0.0	0.4	0.0	1.1	0.2	0.2	1.9
Ball Milled	0.0	0.6	0.2	1.1	1.5	0.1	3.5
As Received	0.0	0.2	0.1	1.9	0.6	0.0	2.8

The vacuum fusion data of Table III show that the oxygen content of the powder in all conditions of treatment is substantially higher than that which could be accounted for by the desorbed gases. As mentioned previously, CO and CO_2 adsorbed on the powder would analyze as oxygen. The excess of oxygen was due to dissolved oxygen, and oxygen present as nickel oxide. The solubility of oxygen in nickel is .020 weight percent at 600°C[12]. Additional amounts of oxygen result in the formation of nickel oxide. If the nickel were free of oxygen and nickel oxide, the vacuum fusion analysis would theoretically show the maximum amount of CO and CO_2 that would be liberated if the powder were heated to its melting point. Then a subtraction of the CO and CO_2 desorbed at 1800°F would leave a remainder which would be the amount of CO and CO_2 that would be evolved if the powder were heated from 1800°F to its melting point. The powder, however, contained excessive amounts of dissolved oxygen and nickel oxide which made such calculations meaningless.

A comparison of the various nitrogen and oxygen analyses shows that the within sample variation exceeds the between sample variation, which means that the between sample analyses are not significantly different. As mentioned previously, the samples tested after cumulative analysis had a higher hydrogen content than did the as received samples. This difference was attributed to the solutioning of hydrogen from reacted water vapor in the powder during the cumulative run.

PM273 Powder

This powder was of interest because it was manufactured in the same way as the MD9119 powder, but had had an additional annealing treatment of 45 minutes in a cracked ammonia atmosphere. The most noticeable feature of the gas evolution from this powder was that the volume desorbed was not a function of the apparent surface area; thus the mechanism of surface desorption was eliminated as the major source of gas. It is believed that dissolved elements, H, O, and C, were responsible for the evolved gases. This mechanism is reasonable in view of the fact that this annealing treatment would result in the desorption of the greater part of any adsorbed gases present on the atomized, unannealed powder.

Table I shows that the gas volumes released during both the total and the cumulative desorption tests were not related to surface area, and that the gas mixtures evolved contained H_2, H_2O, CO and CO_2. Carbon monoxide is seen to be the major constituent of the desorbed gases, with CO_2, H_2, and H_2O representing smaller fractions of the total.

Typical cumulative volume gas desorption data for the -100 +200 mesh fraction of this powder are shown in Figure 4. The outstanding feature of the gas desorption was that the evolution of CO did not occur until a temperature in excess of 1000°F was attained. This is further evidence that the CO was formed from dissolved carbon and oxygen, because these higher temperatures are required before diffusional mechanisms will transport carbon and oxygen atoms to the surface at an appreciable rate.

Another feature of the cumulative plot was the general decrease in the water volumes at a temperature where the hydrogen volumes increased. These facts are best explained by a reaction of the type:

$$H_2O(g) + CO(g) \rightarrow H_2(g) + CO_2(g) \qquad (3)$$

where the H_2O and CO were both originally formed from dissolved elements.

The correlation between total and cumulative volumes evolved is seen to be quite good in Table I, primarily because the only gases which could be frozen out, H_2O and CO_2, were present in minor amounts. The major constituent, CO, was not frozen out and therefore participated in the same reactions in both types of desorption runs. Thus the CO and CO_2 volumes checked very well in both runs.

The annealing treatment in cracked ammonia would result in the powder being saturated with dissolved hydrogen. Thus, when the reaction of water vapor with CO_2 yielded hydrogen, this hydrogen could not dissolve and was liberated in the gaseous state, as contrasted to the MD9119 powder wherein the hydrogen resulting from the dissociated of water vapor was dissolved in the powder.

A final point of interest concerning the gases liberated from this powder pertains to the lack of SO_2 evolution. This powder contained sulfur in excess of the solubility limit, indicating that some nickel sulphide must have been present. No SO_2 was produced by an oxidation reaction of the sulfide [equation (1)] with CO_2 because the CO present in large amounts shifted the equilibrium in the opposite direction.

SG321 Powder

This powder, manufactured by hydrogen reduction from an aqueous solution, represented a completely different method of manufacture, and was of interest as a means of determining the effect of manufacturing technique on the evolved gases.

Neither the cumulative nor total gas volumes correlate with apparent surface area, as seen in Table I, so again the mechanism of surface desorption as a source of gas was eliminated. Dissolved hydrogen, oxygen and carbon are believed to be the source of the evolved gases. In Table I the total volumes desorbed are seen to be substantially greater than cumulative volumes. The difference is due mainly to the higher water volumes in the total volume tests. The water was frozen out in the total volume tests, but reacted during the cumulative runs with dissolved carbon to form both molecular and dissolved hydrogen and a mixture of CO and CO_2. A comparison of the gases evolved during both cumulative and total desorption runs, shown in Table I, indicates that no hydrogen is evolved during the total volume runs, but is seen to be present in the cumulative runs. This would indicate that no hydrogen is evolved as such, but is produced by a reaction with the water vapor.

The cumulative plot, Figure 3, shows that fairly large amounts of hydrogen are liberated at temperatures up to 1000°F, but that the hydrogen volume decreases above this temperature. This is taken as an indication that hydrogen is dissolving in the nickel powder at higher temperatures, because the solubility of hydrogen in nickel increases rapidly at elevated temperatures. Solutioning would not be expected at lower temperatures because the powder was manufactured at 350°F by bubbling hydrogen through a solution from which the nickel powder was precipitated. These manufacturing conditions would saturate the powder with hydrogen at this temperature, and preclude further solutioning of hydrogen until the solubility limit was increased by raising the temperature.

Dissolved carbon was held to relatively low levels in this process, so that the reaction between dissolved carbon and oxygen would not be expected to yield large quantities of CO and CO_2. The small amounts of CO and CO_2 actually evolved during the cumulative runs was taken as indirect evidence supporting the existence of this type of reaction in the PM273 powder which contained larger amounts of dissolved carbon.

Evolution of SO_2 was observed at 1800°F, and again the existence of a nickel sulphide was postulated, which upon oxidation yielded SO_2. The same reaction [equation (1)] was involved with the MD9119 and PM273 powders, and in this case the CO/CO_2 ratio favors the reaction producing the SO_2.

FM Powder

This powder, manufactured by water atomization in a nitrogen atmosphere, followed by an annealing treatment under a hydrogen atmosphere,

offered a means of checking the effects of manufacturing variations, as well as heat treatment variables. Only a limited amount of this powder was available, so only one cumulative volume test and duplicate vacuum fusion analyses were made. The cumulative volume run, Figure 4, shows that only very small amounts of hydrogen and CO_2 were liberated from this powder. The relatively minor amounts of gas liberated from this powder would indicate that this method of manufacture yields the cleanest product of any of those tested.

The vacuum fusion data of Table III show that annealing this powder under a hydrogen atmosphere for one hour at 1200°F resulted in a dissolved hydrogen content about one order of magnitude above that obtained in the unannealed MD9119 powder. The amount of dissolved hydrogen observed approaches the solubility limit at room temperature.

CONCLUSIONS

Nickel powder produced by steam scattering in air desorbs CO_2, H_2O, CO, and SO_2. The mechanism of gas evolution is surface desorption. The H_2O and CO are physically adsorbed, while the CO_2 is present as a weakly bonded surface compound. The SO_2 is the product of the oxidation of a nickel sulphide which is distributed throughout the metallic matrix. Nickel powder produced by steam scattering, followed by an annealing treatment in cracked ammonia, evolves CO and minor amounts of H_2O, H_2 and CO_2. The CO and H_2O are formed from dissolved O, C, and H, while the H_2 and CO_2 are products of reactions between H_2O and CO. Nickel powder produced by precipitation from aqueous nickel ammonia complex solutions evolves H_2, H_2O, CO_2, and minor amounts of CO and SO_2. The gases are formed from dissolved elements in the metallic phase. Nickel powder produced by water atomization in a nitrogen atmosphere followed by an annealing treatment by hydrogen for one hour at 1200°F yields a very clean powder which evolves only minor amounts of H_2 and CO_2 upon heating to 1800°F.

TABLE III

VACUUM FUSION ANALYSIS OF MD9119 POWDER IN THE AS RECEIVED CONDITION, AND AFTER BOTH TOTAL VOLUME GAS DESORPTION TESTING AND CUMULATIVE GAS DESORPTION TESTING

	Gas Content					
	Weight Percent			Ml./10gm (STP)		
Condition	N_2	O_2	H_2	N_2	O_2	H_2
As Received	0.00163	0.296	0.00040	0.1	20.7	0.5
As Received	0.00061	0.214	0.00058	0.1	15.0	0.7
After Cumulative Run	0.00098	0.255	0.00075	0.1	17.9	0.8
After Cumulative Run	0.00194	0.299	0.00099	0.2	20.9	1.1
After Total Run	0.00177	0.258	0.00068	0.1	18.0	0.8
After Total Run	0.00150	0.218	0.00268	0.1	15.3	3.0

VACUUM FUSION ANALYSIS OF FM POWDER IN THE AS RECEIVED CONDITION:- 70 + 100 MESH FRACTION

	Gas Content					
	Weight Percent			Ml./10gm (STP)		
	N_2	O_2	H_2	N_2	O_2	H_2
Sample Number 1	0.0009	0.284	0.0023	0.1	19.9	2.6
Sample Number 2	0.0007	0.304	0.0013	0.1	21.2	1.5

ACKNOWLEDGEMENT

This work was supported by the Michigan Memorial-Phoenix Project of the University of Michigan and by Fellowship Grants from the General Electric Company and General Motors Corporation. This support is gratefully acknowledged by the authors.

BIBLIOGRAPHY

1. Smithells, C. J. and Ransley, C. E., Proc. Royal Soc., A 155, 195, 1936.

2. Jones, W., Principles of Powder Metallurgy, Metallurgy Press, London, 1940.

3. Warren, D and Libsch, J. F., Trans. AIME 191, 774, 1951.

4. Duftschmit, F., Schlect, L. and Schubart, W., Stahl u. Eisen 52, 845, 1932.

5. Tobin, J. C. and Sinnott, M. J., Trans. AIME 212, 167, 1958.

6. Fedorchenko, I., Zhur. Teklu. Fiziki, 26, 2067, 1956.

7. Tobin, J. C., Ph.D. Thesis, University of Michigan, Ann Arbor, 1956.

8. Forward, F. A., C.I.M. Trans. 56, 373, 1953.

9. Mackiwo, V. N., Lin, W. C. and Kunda, W., Jour. Met. 9, 787, 1957.

10. Tingle, E. T., Trans. Faraday Soc. 46, 43, 1950.

11. Zettlemoyer, A. C. and Chessick, J. J., J. Phys. Chem., 58, 242, 1954.

12. Smithells, C. J., Metals Reference Book, Vol. II, Interscience Publishers, Inc., New York (1955).

THE EFFECTS OF ULTRASONIC AND ELECTROSTATIC ENERGY ON EVAPORATION AND COMBUSTION

William Mirsky
Associate Professor of Mechanical Engineering
The University of Michigan

THE EFFECTS OF ULTRASONIC AND ELECTROSTATIC ENERGY ON EVAPORATION AND COMBUSTION

William Mirsky

INTRODUCTION

A more complete understanding of the factors involved in the combustion of liquid fuels, and possible means for increasing their rate of combustion, remain important objectives.

Because of the extremely complex nature of evaporation and combustion processes for liquid drops and the difficulties involved in measurements, most investigators have chosen to study the evaporation or burning processes associated with an isolated drop. Many of these researches have employed fine filaments to hold the drops in space while observations are made.

Studies were made at the University of Michigan to establish means for holding liquid drops in space without any attachments.(1) Attempts were made first to stabilize a drop on a rising air stream. This proved impractical, and an ultrasonic field was added to give transverse stability. The combination of air drag and ultrasonic field forces made it possible to hold a drop fixed in space while evaporation occurred.

As would be expected, tests revealed that the ultrasonic energy affected the rates of evaporation and combustion, and it therefore became necessary to evaluate these rates with and without the ultrasonic energy. In the course of determining the evaporation rate without ultrasonic energy a new expression for drop evaporation was developed.

Cumene was used for the greater part of this study because of its suitable rate of evaporation and relatively low cost for the pure grade of fuel used.

EXPERIMENTAL EQUIPMENT

The experimental equipment is shown schematically in Figure 1. This equipment comprises four functional systems, as follows:

1. Air-flow system
2. Ultrasonic field generating system
3. Photographic recording system
4. Instrumentation and accessories.

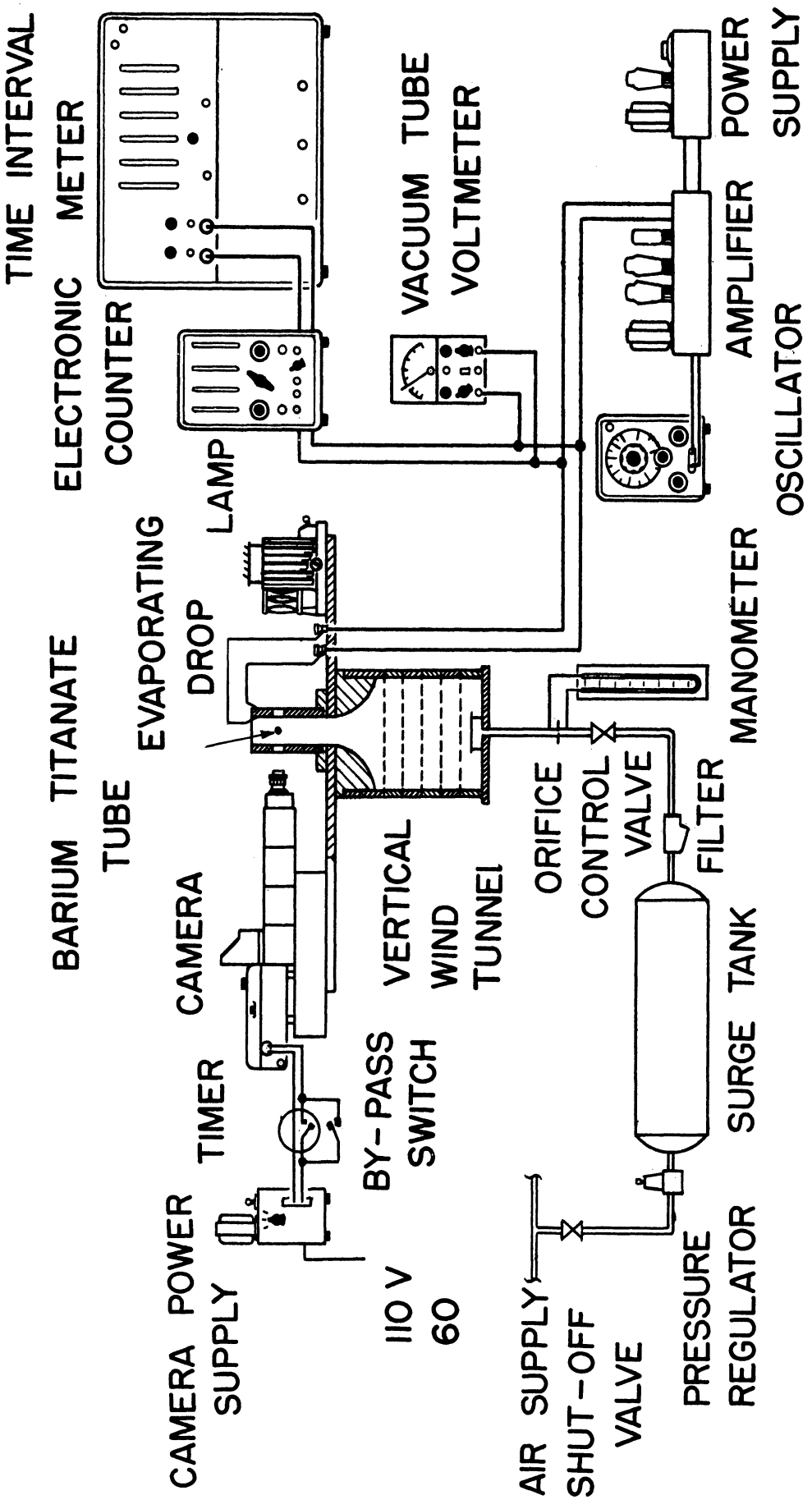

FIG I. SCHEMATIC DIAGRAM OF EXPERIMENTAL EQUIPMENT

The air flow system provides a stream of low turbulence air flowing upward through a cylinder of barium titanate. This cylinder is 4 inches long and 1-5/8 inches inside diameter. This ceramic piezo-electric transducer produces a concentric standing-wave ultrasonic field in the air within the tube. The ultrasonic field, when stationary, i.e., when the wave nodes are fixed, introduces lateral forces on the drop within the tube which holds the drop in a fixed horizontal position. At the same time, the action of the rising air stream on the drop creates an upward drag force which can balance the downward force of gravity. By control of the air velocity and ultrasonic field, a drop may thus be held stationary in space. Motion pictures of the drop were taken at known time intervals to obtain diameter as a function of time.

Efforts were made to burn drops with this equipment by using a heated air stream. This introduced difficulties due to a change in the velocity of sound in the air and a shift in the resonant frequency of the ultrasonic generator. Further, to protect the ceramic from over-heating, it was provided with a coolant jacket, but this substantially reduced the ultrasonic energy transmitted.

RESULTS

Experimental data for evaporating drops were obtained from silhouette photographs taken with a 16-mm motion picture camera. In one series of tests the drops were suspended on fine glass filaments, approximately sixty microns in diameter, in constant velocity air streams. Tests were made at several relative air velocities and sound field intensities. The second series of tests was made with free drops at their terminal velocity in a moving air stream. The drops were actually maintained at a fixed position in space by the combined effects of air drag and ultrasonic forces. Typical sequence photographs for both tests are shown in Figures 2 and 3. The greater reduction in size and reduced drop-shape distortion is evident with free drops.

EVAPORATION OF DROPS WITHOUT ULTRASONIC ENERGY, DROPS ON FILAMENTS

In an attempt to describe the experimental evaporation data obtained for drops on filaments by the widely accepted equation obtained by Godsave[2],

$$D^2 = D_o^2 - \lambda_1 t, \qquad (1)$$

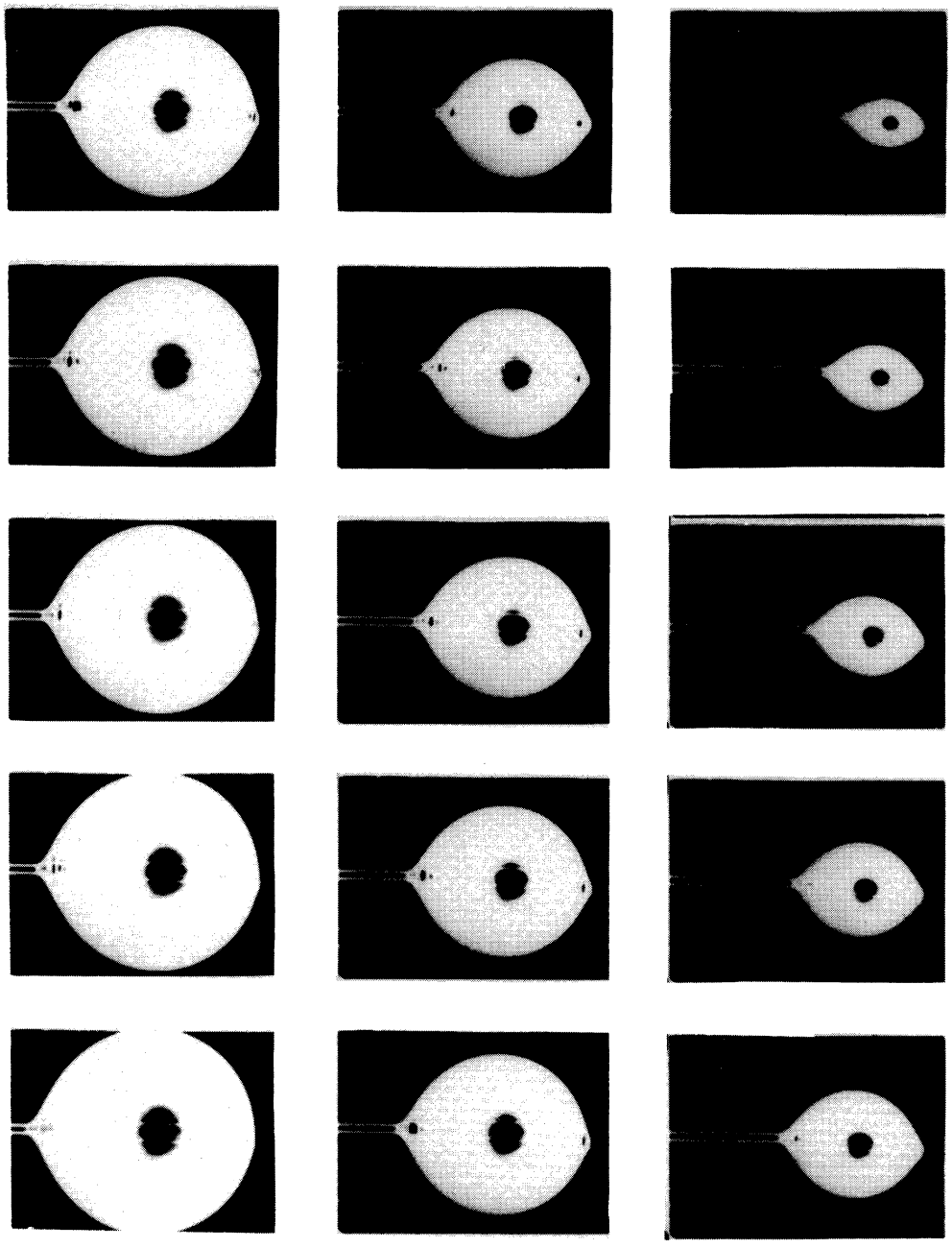

FIG. 2 EVAPORATING SUSPENDED DROP. D_o = 1112 MICRONS

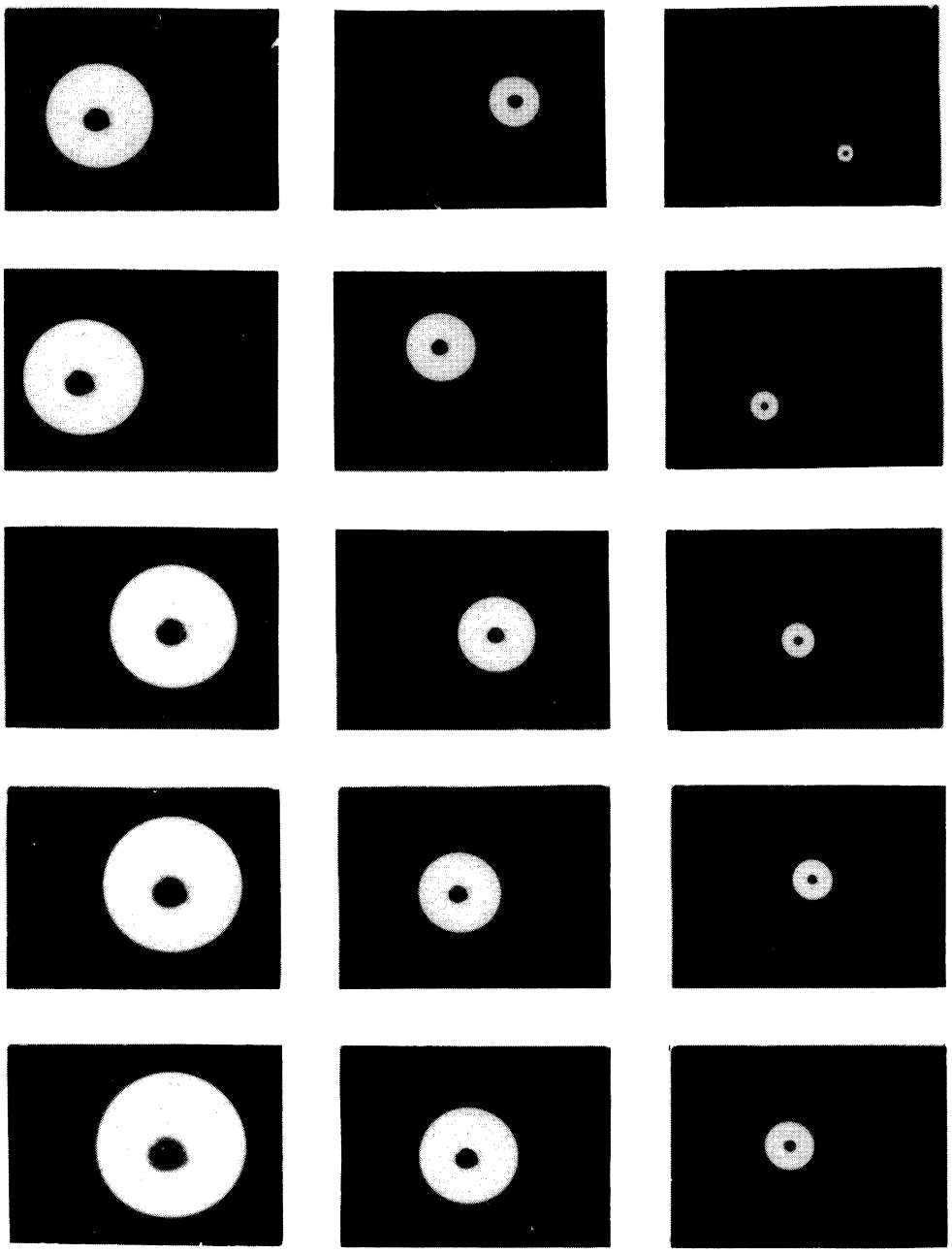

FIG. 3 EVAPORATING FREE DROP. D_o = 1178 MICRONS

the data from twenty-four tests at various relative air velocities were plotted showing D^2 as a function of t. The resulting curves were not straight lines as expected but showed some degree of curvature, the curvature increasing with an increase in relative air velocity. Using measurements from curves giving D as a function of t, it was possible to compute the exponent n to which the diameter had to be raised to make D^n a linear function of t. The evaporation process could then be closely approximated by the equation

$$D^n = D_o^n - \lambda t \qquad (2)$$

where n was found to be a function of relative air velocity as shown in Figure 4. The exponent appears to approach the value 2.0 at zero velocity so that Equation (1) becomes a limiting case of Equation (2).

A mathematical analysis of the evaporation process for constant relative air velocity, based on heat transfer to the drop through a spherically symmetric boundary layer led to quite a different result than presented by Equation (2). The introduction of boundary layer equations developed by Tomotika[3] into the equations for heat transfer led to the following evaporation equation:

$$\Delta D^{3/2} - \frac{3C}{2}\Delta D + 3C^2 \Delta D^{1/2} - 3C^3 \ell n \left[\frac{D_o^{1/2}+C}{D^{1/2}+C}\right] = \frac{6k}{C\rho c} \ell n \left[1 + \frac{c(T_f - T)}{L}\right] t \qquad (3)$$

where

$$\Delta D^n = (D_o^n - D^n) \quad \text{and} \quad C = \frac{2}{f(N_{Pr})^{1/3}(\frac{v}{V})^{1/2}} \qquad (3a)$$

In the analysis, if the assumption is made that the ratio D/D_f remains constant during the entire evaporation process the result reduces to Equation (1).

The result of the analysis can also be expressed in terms of an expression for the Nusselt number

$$N_{Nu} = \alpha[2 + f\,(N_{Pr})^{1/3}\,(N_{Re})^{1/2}] \qquad (4)$$

which is similar to the results obtained by several other investigators.[4-7] The experimental data of this investigation are well correlated by this expression as shown in Figure 5.

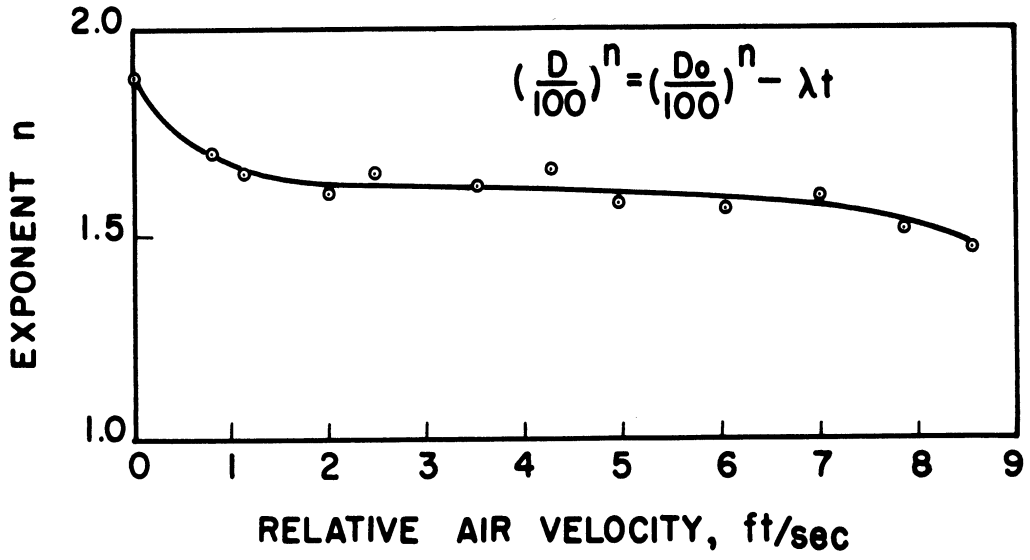

FIG. 4 VARIATION OF EXPONENT n WITH RELATIVE AIR VELOCITY.

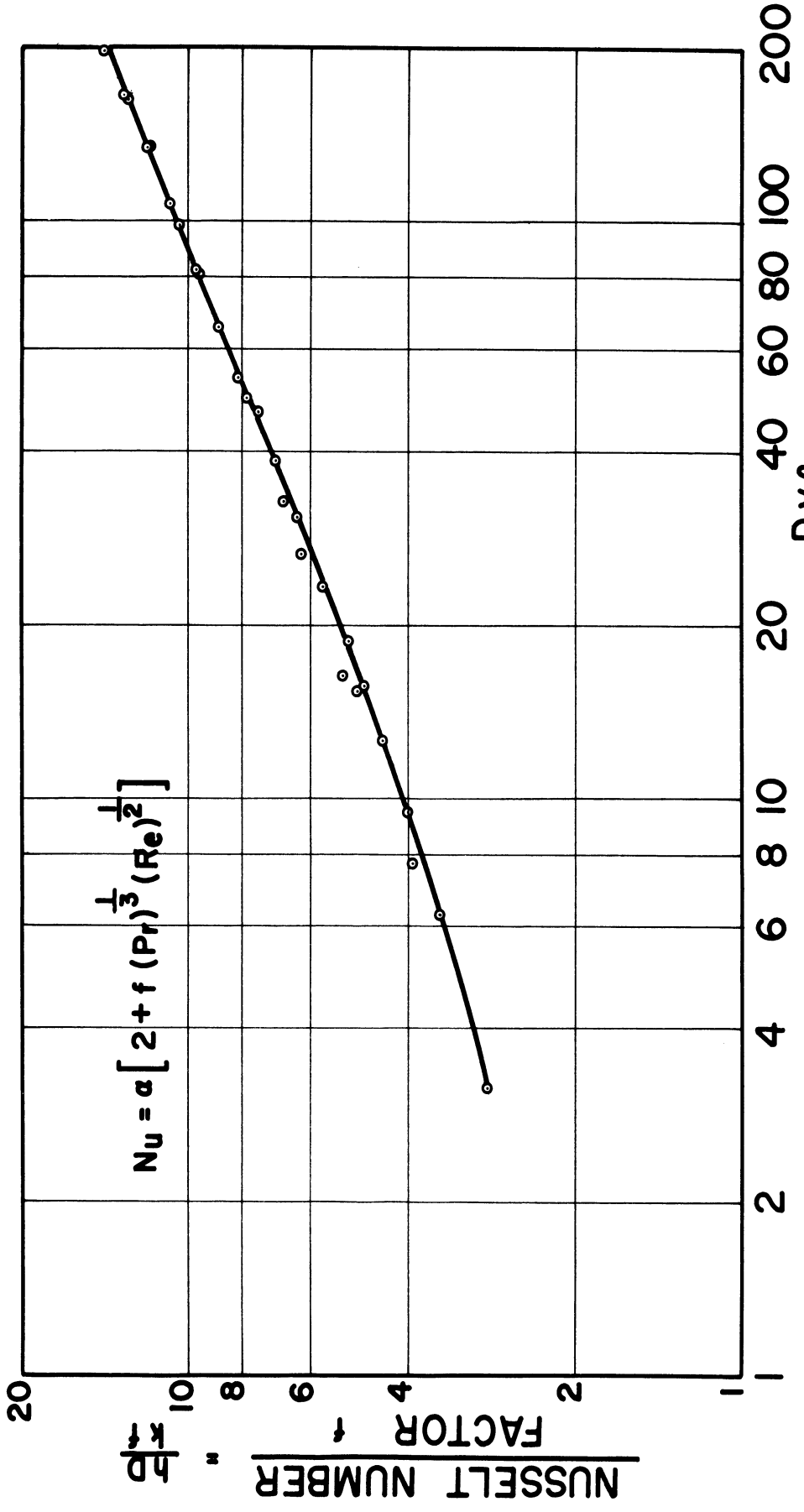

FIG.5 CORRELATION OF EVAPORATION DATA FOR SUSPENDED DROPS

The factor f in Equation (3a) and (4) is a semi-empirical factor which was assumed to vary only with relative velocity. It arises from the analysis of the assumed simplified boundary layer and would be difficult to define accurately in terms of more fundamental properties of the actual physical system.

Good agreement between theory, as represented by Equation (3), and experiment is indicated in Figure 6. The factor f was evaluated at one point on the evaporation curve (D = 600 microns) for each relative air velocity. These values were then used in Equation (3) to predict drop size during evaporation.

EVAPORATION OF DROPS WITH ULTRASONIC ENERGY

Drops on Filaments

Approximately eighty tests were made with evaporating drops on filaments in the presence of an ultrasonic field. Equation (2) was used to compare the evaporation rates obtained from these tests with those obtained with no ultrasonic field. It was found that the field had a pronounced effect on evaporation, especially at low relative air velocities where a maximum increase in the evaporation constant of 58 per cent was obtained. The results of these tests are summarized in Figure 7.

The peculiar rise and fall of the curves at low voltage is believed to be a boundary layer effect, brought about by a change from laminar to turbulent boundary layer with the introduction of the ultrasonic field.

Evaporation rates were found to be extremely sensitive to slight changes in some of the ultrasonic system variables, especially with regard to the location of the drop in relation to the stationary nodes of the ultrasonic field and to variations in the frequency applied to the transducer. Maximum effects on evaporation were obtained with the drops located in the nodes and with the transducer operating at its resonant frequency of approximately 35,000 cycles per second.

Free Drops

A limited number of tests were made with freely suspended drops as illustrated in Figure 3. These tests also indicated an increase in evaporation rate with an increase in ultrasonic energy but experimental difficulties and lack of control of some of the variables in the sound generating system precluded any accurate measurements of evaporation rates.

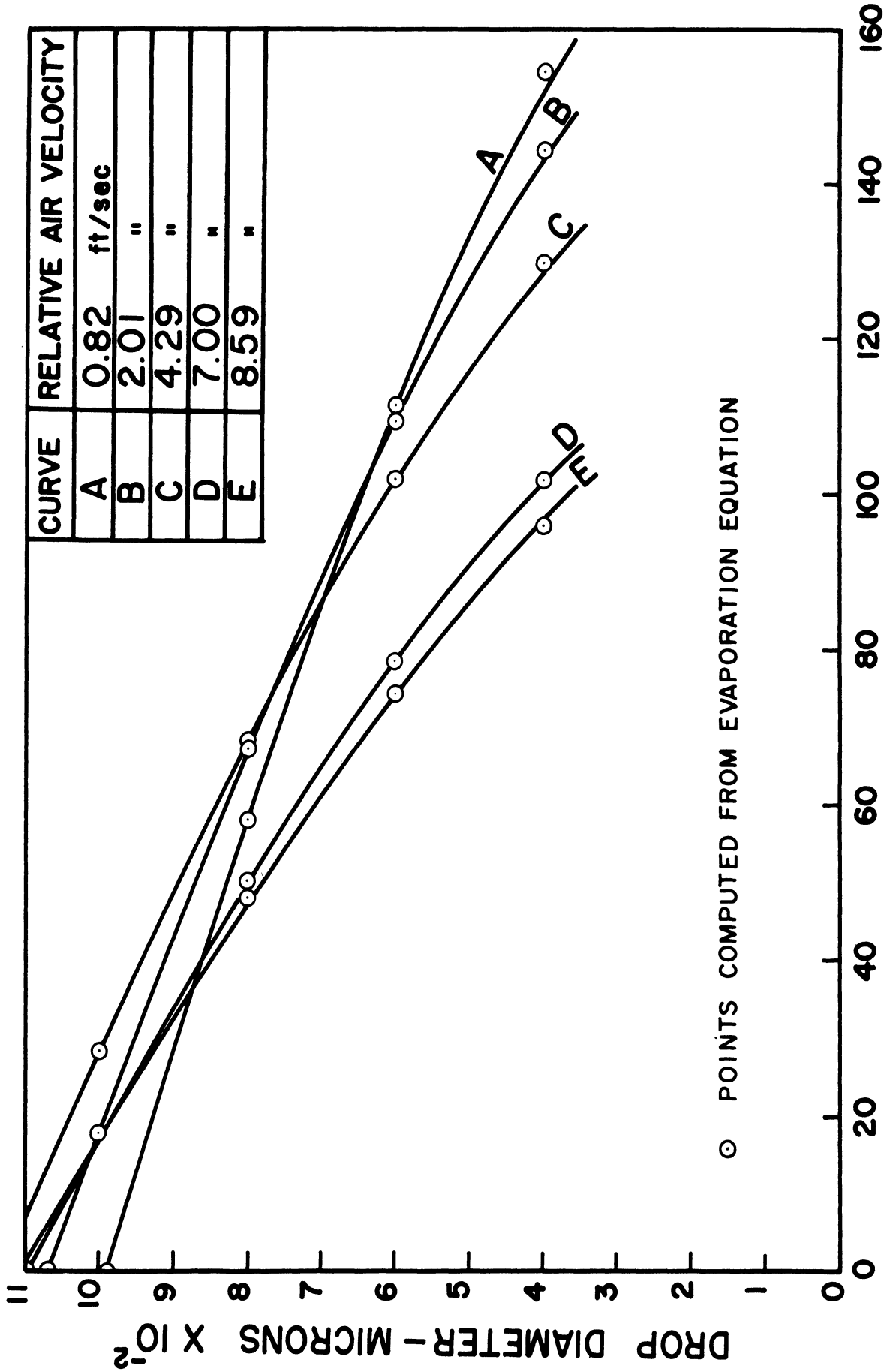

FIG. 6 EXPERIMENTAL CHECK OF EVAPORATION EQUATION.

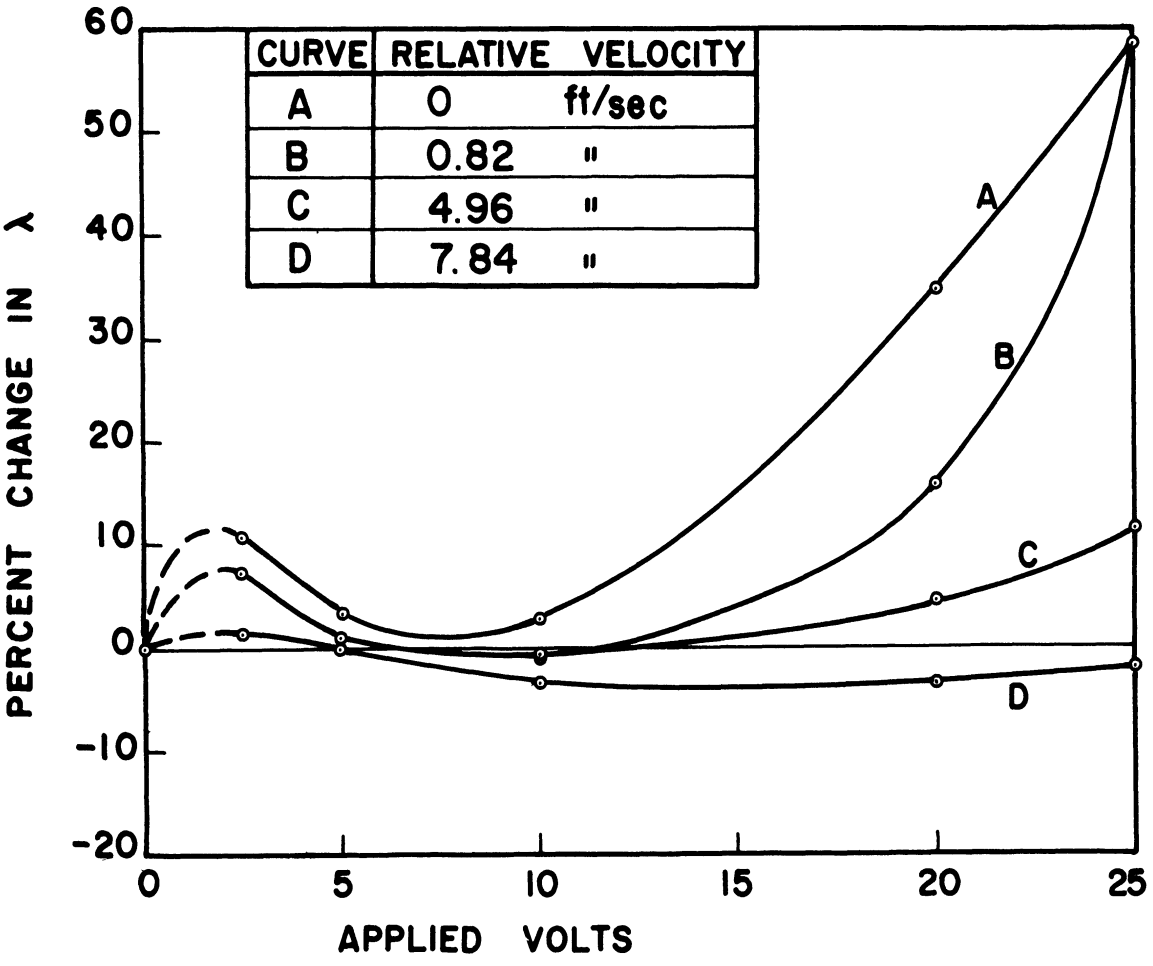

FIG.7 PERCENT CHANGE IN λ DUE TO CHANGE IN FIELD INTENSITY AS MEASURED BY APPLIED VOLTS.

COMBUSTION IN ULTRASONIC AND ELECTROSTATIC FIELDS

Preliminary tests have been conducted with single burning drops and gas flames in an ultrasonic field. An increase in the color intensity of the flame and a large decrease in smokiness was noted in the presence of the field. However, experimental difficulties with the ultrasonic equipment mount rapidly when working with combustion processes.

A preliminary set-up has also been made whereby burning drops and sprays have been subjected to a high frequency electrostatic field produced between two plates. Visual observations and photography reveal that this energy also has a pronounced influence on combustion, which is made evident by shorter flames and reduction in smoke. Further tests are in progress.

CONCLUDING REMARKS

To evaluate the effects of ultrasonic energy on drop evaporation, it was first necessary to obtain evaporation data without this energy. The resulting experimental data were not described well by Equation (1) so new evaporation equations were developed. Equation (2) is entirely empirical while Equation (3) was derived by considering the heat transfer and boundary layer equations for a simplified drop model. Both Equations (2) and (3) adequately defined the experimental rate of evaporation.

When $D_o^{1/2} < C$, which is the case for very small drops ($D_o <$ 100 microns approx.) at very low velocities ($v <$ 1 fps approx.), Equation (3) reduces to

$$\Delta D^2 + \sum_{n=1}^{\infty} (-1)^n \frac{4}{(4+n)c} \Delta D^{\left(\frac{4+n}{2}\right)} = \frac{8k}{\rho c} \ell n \left(1 + \frac{c\Delta T}{L}\right)t. \qquad (5)$$

For relative air velocity approaching zero, the equation is approximated by

$$D_o^2 - D^2 = \frac{8k}{\rho c} \ell n \left(1 + \frac{c\Delta T}{L}\right)t \qquad (6)$$

which is similar to Equation (1).

With the introduction of ultrasonic energy in the form of standing waves, an increase in evaporation rate was obtained. The field appears to be effective in decreasing the boundary layer thickness by molecular agitation, thereby increasing heat and mass transfer rates through increased thermal and concentration gradients. A similar condition is brought about by an increase in relative air velocity. The investigation shows that the effectiveness of the ultrasonic energy for increasing evaporation rates is reduced as the relative velocity increases, as shown in Figure 7.

The experimental apparatus proved quite interesting in its ability to hold drops relatively motionless in space for long periods of time. One drop of kerosene was freely suspended for approximately two hours before the test was stopped. Visual inspection of the drop with a small pocket microscope clearly indicated the internal liquid circulation.

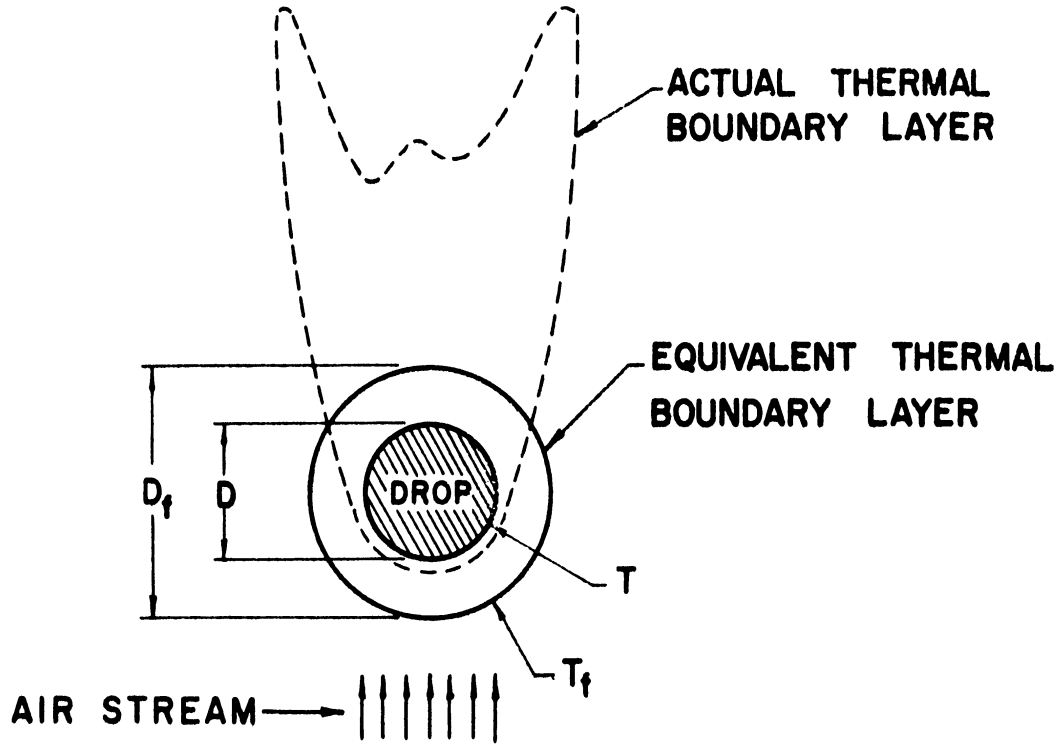

FIG. 8 MODEL OF EVAPORATING DROP.

SYMBOLS

C_1	constant
C	$2/f\ (N_{Pr})^{1/3}\ (\frac{v}{\nu})^{1/2}$
D	diameter of drop
D_f	diameter of outer surface of equivalent thermal boundary layer
D_o	initial drop diameter
L	latent heat of liquid drop
T	temperature of drop surface
T_f	temperature at outer surface of thermal boundary layer
c	specific heat of vapor at constant pressure
f	$3 \sin \Theta/2C_1 f_1$
f_1	proportionality constant
k	thermal conductivity
n	exponent in evaporation equation
n	integer
t	time
v	relative air velocity
α	$\frac{L}{c(T_f-T)}\ \ell n \left[1 + \frac{c(T_f-T)}{L}\right]$
Θ	angle at center of drop measured from forward stagnation point

λ empirical evaporation constant

λ_1 evaporation constant due to Godsave

ν kinematic viscosity

ρ density of liquid drop

$N_{Nu} = \frac{hD}{k}$ = Nusselt number

$N_{Pr} = \frac{c\mu}{k}$ = Prandtl number

$N_{Re} = \frac{Dv}{\nu}$ = Reynolds number

REFERENCES

1. Mirsky, William, "The Evaporation of Single Liquid Drops, Including the Effects of Ultrasonic Energy on Evaporation," Ph.D. Thesis, University of Michigan, 1956.

2. Godsave, G. A. E. ,"Studies of the Combustion of Drops in a Fuel Spray--The Burning of Single Drops of Fuel," Fourth Symposium (International) on Combustion, Baltimore, The Williams and Wilkins Company, 1953.

3. Tomotika, S., "The Laminar Boundary Layer on the Surface of a Sphere in a Uniform Stream," Reports and Memoranda No. 1678, Technical Report of the Aeronautical Research Committee (England), July, 1935.

4. Frossling, N., "Uber die Verdenstung fallender Tropfen," Gerlands Beitrage d. Geophysik, 52, 170, 1938.

5. Kinzer, G.D., and Gunn, R., "The Evaporation, Temperature and Thermal Relaxation-Time of Freely-Falling Waterdrops," Journal of Meteorology, 8, 71, 1951.

6. Ingebo, R. D., Vaporization Rates and Heat-Transfer Coefficients for Pure Liquid Drops, NACA TN-2368, 1951.

7. Ranz, W. E., and Marshall, W. R., "Evaporation from Drops, Part I," Chem. Eng. Prog., 48, 141, 1952; Part II, ibid., p. 173.

GENERATION OF SPRAYS

J. Louis York
Professor of Chemical and Metallurgical Engineering
The University of Michigan

GENERATION OF SPRAYS

J. Louis York

The generation of sprays has been the subject of intensive research at the University of Michigan for over fifteen years. Work has been done in several different departments of the Engineering College, with several different objectives.

There has been no centralized and concerted attack upon the subject, for usually the work was incidental to the solution of other engineering problems. For example, combustion of liquid fuels forced many of us into a study of spray formation, analysis, and control -- because we needed a sound basis for combustion research. Entrainment removal stimulated me to dig deep into sprays -- because I wanted a controlled supply of entrained drops of liquid.

My own introduction was shocking, for I was well along in an experimental program employing spray nozzles as drop suppliers, assuming that the nozzle manufacturer could tell me exactly what his nozzles produced. First one, then all but one of the score or more manufacturers admitted ignorance. The answers were the same: "Sorry, we cannot give you quantitative data on drop sizes." One stood out, however, for he gave me a number. A personal contact with him brought the candid admission, "Chemical engineers always want numbers, so I always give them one -- out of thin air, if necessary!"

We needed desperately to find or to develop a satisfactory analytical technique to tell the true drop sizes. Our research program turned about face, dropped equipment studies, and became an analytical development activity. We still do not have a "satisfactory" analytical procedure, after working for most of those fifteen years on various aspects of the problem, between engineering studies of various kinds.

ANALYTICAL TECHNIQUES

Our criteria for a satisfactory analytical procedure are:

a. accuracy in all drop sizes and concentrations,
b. applicability to sprays in working location,
c. speed and economy.

These are extremely difficult to reconcile in one technique, primarily because the care required for accuracy usually runs counter to speed and economy.

The first decision to be made in development of an analytical technique is on the method of sampling. Physical sampling involves interception, by a target, of all or part of the drops in the spray as it moves past, or as the target is moved through the spray. The spray is a two-phase system, however, consisting of drops in suspension in a fluid phase, usually gas. Removal of both phases in the same proportion as they occur in the spray is satisfactory, except for the eventual separation of the drops from the gas without shattering or coalescing them. This is almost insurmountable, therefore we discarded such a technique early.

If the drops are to be collected in the spray, without removing the gas phase, aerodynamics introduces a sampling bias. The gas flows around the sampler easily, but it drags some of the drops with it. The smaller drops are more easily swept around the sampler, therefore the sampler is usually deficient in the smaller sizes. Figure 1 shows computed values for water drops being sampled by a 1-inch ribbon, such as an ordinary microscopic slide. Note the sharp reduction in effectiveness, or fraction of drops in the sample which should be in the sample, as the drop size decreases and as the velocity decreases.

Two ways to reduce the bias in interception sampling are feasible, one being to reduce the size of the sampling device and the other to operate at high velocities. The latter method is the idea behind the cascade impactor, one version of which is shown in Figure 2. A portion of the suspension of drops in air is drawn through an orifice onto a slide located to force the air to turn at right angles. The larger drops impinge on the first slide, usually operated at lower velocity, the next larger drops on the next slide operating with a higher velocity of impingment, and so on to the smallest drops impinging at near-sonic velocity on the last slide. This system has two disadvantages, it does not guarantee collection of all the drops and at higher velocities some of the drops shatter into smaller ones, thus ruining the analysis. Considerable detailed study of this device has been made at several laboratories, notably Battelle Memorial Institute, and various careful analyses of its inherent errors and calibration procedures have resulted. This effort was expended to take advantage of the speed and economy of the instruments, regardless of its accuracy and complexity of calibration. Little work has been done here on such devices, not only because of the analytical bias discussed, but also because the suspension fed into the inlet involves a sampling bias.

An examination of this sampling-bias problem led us to spread our efforts on techniques with a minimum of such difficulties. We considered the inherent errors of any analytical process to be great enough, without compounding them with sampling bias. We determined upon a simultaneous study of three alternative techniques:

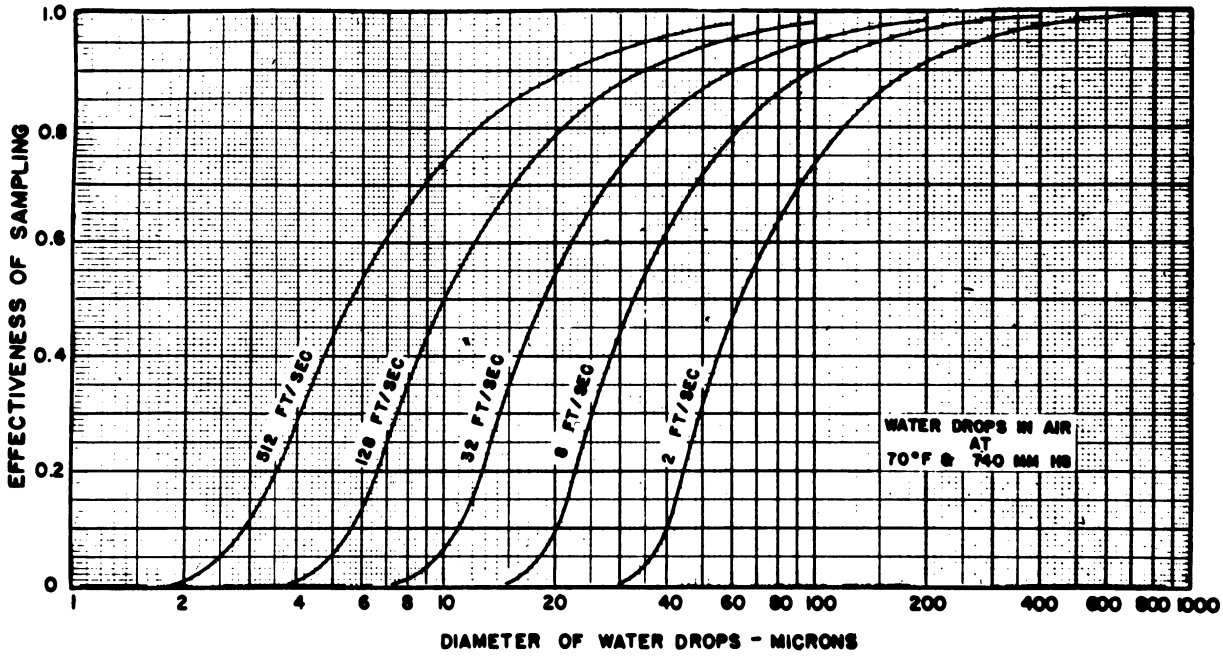

Figure 1. Effectiveness of Sampling by 1-Inch Ribbon

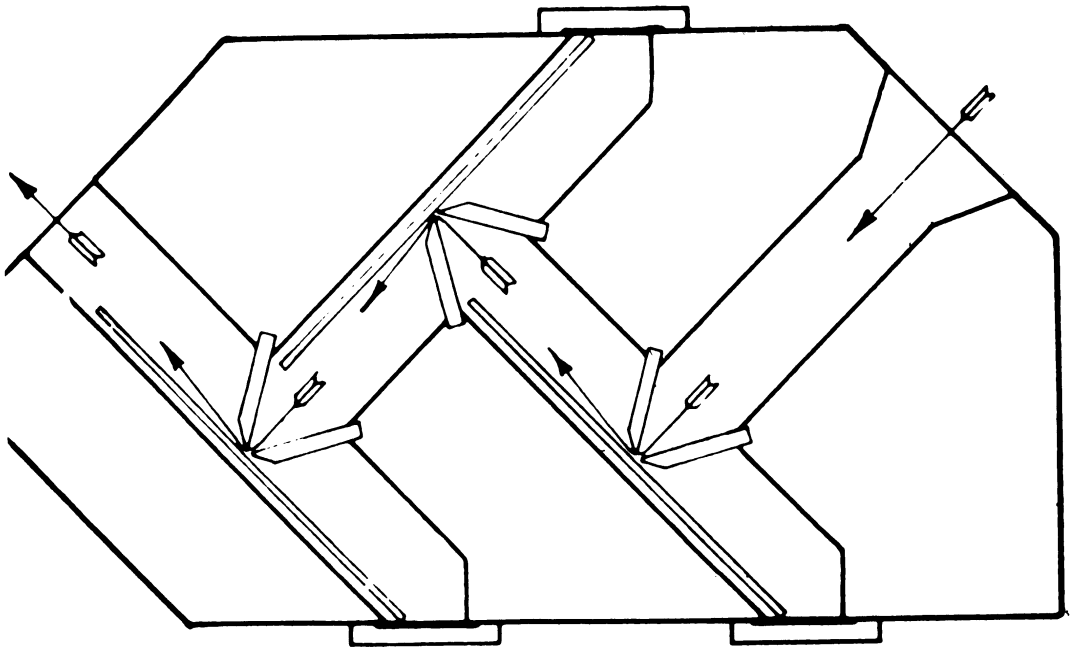

Figure 2. One Form of Cascade Impactor, Showing Path of Air Flow Through It.

1. electronic-probe detectors,
2. light scattering,
3. silhouette flash photography.

The first of these promised speed and economy, along with a small, perhaps negligible bias. The last two involved optical sampling, thus avoiding all bias, but requiring careful calibration and study of accuracy and reproducibility.

As rapidly as these analytical techniques developed, they were put to work on engineering studies. These ranged from combustion through painting and air-pollution control to fuel-injection systems.

Electronic-Probe Detector

Considerable effort was spent on reducing sampling bias by devising a sampler with a smaller cross-section. Figure 3 is a schematic diagram of the principle of the instrument, utilizing a wire or tiny spherical probe as the target for drop impingment. The wire is charged to about 1000 volts potential, and connected to a carefully controlled source to maintain the constant potential. A neutral drop striking the target alters the potential instantaneously, and the circuit proceeds to restore the original potential. Measurement of the restoring current gives a measure of the size of the drop, and a sizing and counting of the electrical pulses gives an analysis of the spray when properly calibrated. The calibration is somewhat difficult, although less so than for the impactor. The latest model built in our laboratories can count up to about 20,000 drops per second, ranging in size from about 40 to 1000 microns. Analytical time is measured in minutes, but considerable calibration must be carried on routinely to account for the inevitable drift in performance of a mass of electronic gear operating at its limit. This unit has not been utilized in spray research because of its high lower limit. It would make a satisfactory control instrument, and could be made to operate on smaller drops with more development.

Light-Scattering

The principles of light-scattering are discussed in another paper of this group, but its application to engineering analysis brings in other aspects. Light-scattering is the only technique capable of measuring drop sizes less than 5 to 10 microns in diameter, but it is unwieldy for large sizes. It is rapid when the drop sizes are all uniform, but it outpaces our ability to feed the information into an electronic computer as the drop sizes spread over a range.

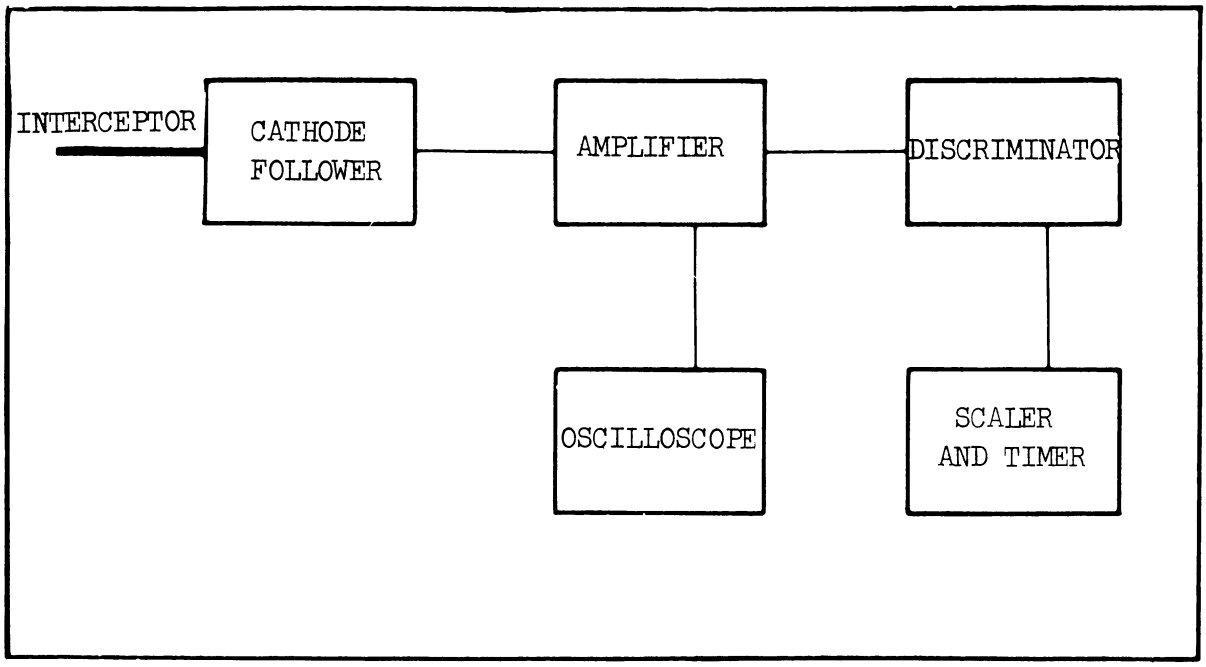

Figure 3. Block Diagram of Electronic-Probe Detector

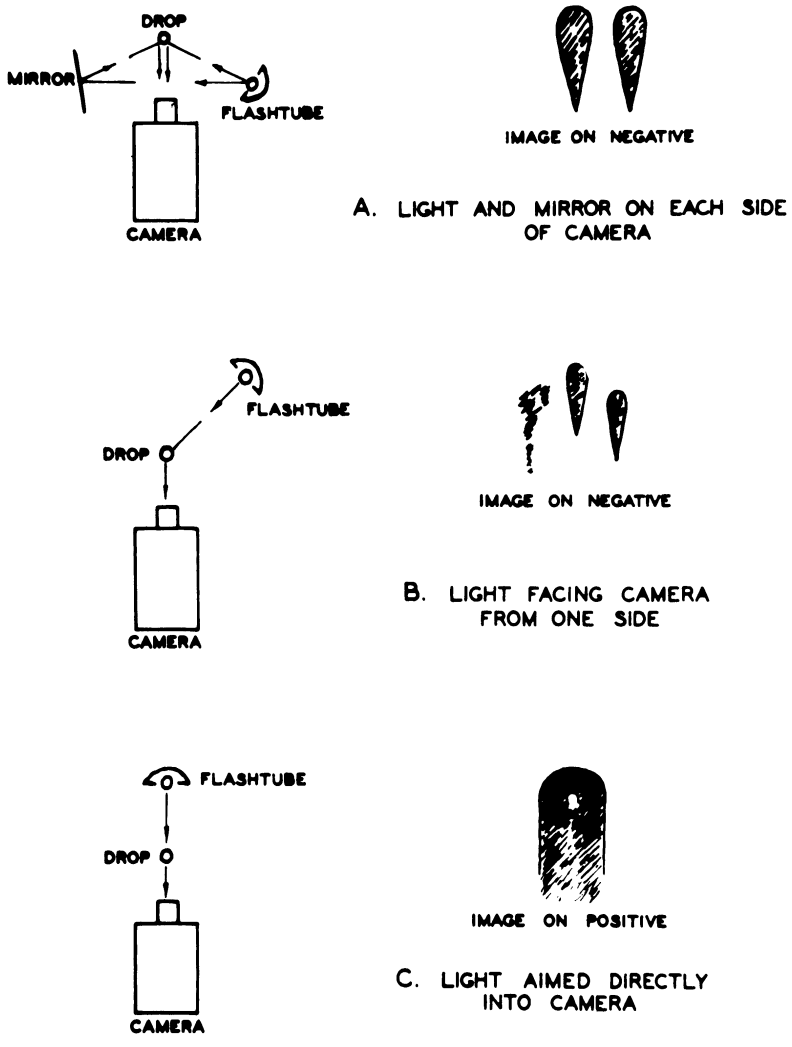

Figure 4. Effect of Light Placement on Drop Image.

Routine drop-size analysis with this technique requires adding supplementary procedures, such as sedimentation rates, to light-transmission data gathered continuously for a considerable time, then feeding that information into a computer already loaded with idealized equations for both light-scattering and sedimentation. Such a procedure requires study of the spray in special equipment, not in working location, and usually with carefully selected fluids rather than the actual fluids. The analysis takes time, and the expense depends upon the availability of a computer and people trained in light-scattering mathematics. The accuracy is good in the limited range suitable for light-scattering studies.

The picture is not entirely dark, however, for some of the recent work conducted by Professors C. M. Sliepcevich* and S. W. Churchill here, especially the work of Dr. J. H. Chin, gives hope that an instantaneous analysis of a broad size range can be obtained. Much more work remains before that procedure is available, however.

Silhouette Flash Photography

The greatest part of our effort was spent on development of a photographic technique to analyze the spray in place without being forced in every case to remove the spray nozzle into a special geometrical situation. Basically, we aimed a short-duration flash unit through a spray directly into a camera, giving a silhouette of the drops passing through the field of focus. Considerable experimenting with lighting was necessary before we found that any angle other than directly into the camera lens gave false images. As shown in Figure 4, the traditional photographic side or back lighting gave images which were really reflections of the light from the drop surfaces, rather than images of the drop itself.

By controlling the light intensity externally to the camera lens, either by using cells of dyed water or crossed Polaroid films, the field of focus could be calibrated and the drops actually in that zone at the instant of picture-taking could be measured. Such techniques permitted computation of the liquid flow from the drop analysis, if desired.

A significant improvement in this process was the addition of a second flash unit, a half-silvered mirror, and a time-delay unit. Double exposures taken by flashing the two lights a known time interval apart allowed computation of the velocity vector in the plane of the film. No other analytical technique provides such information. Figure 5 shows the arrangement for pictures taken by this process.

---

* Professor C.M. Sliepcevich is now at the University of Oklahoma.

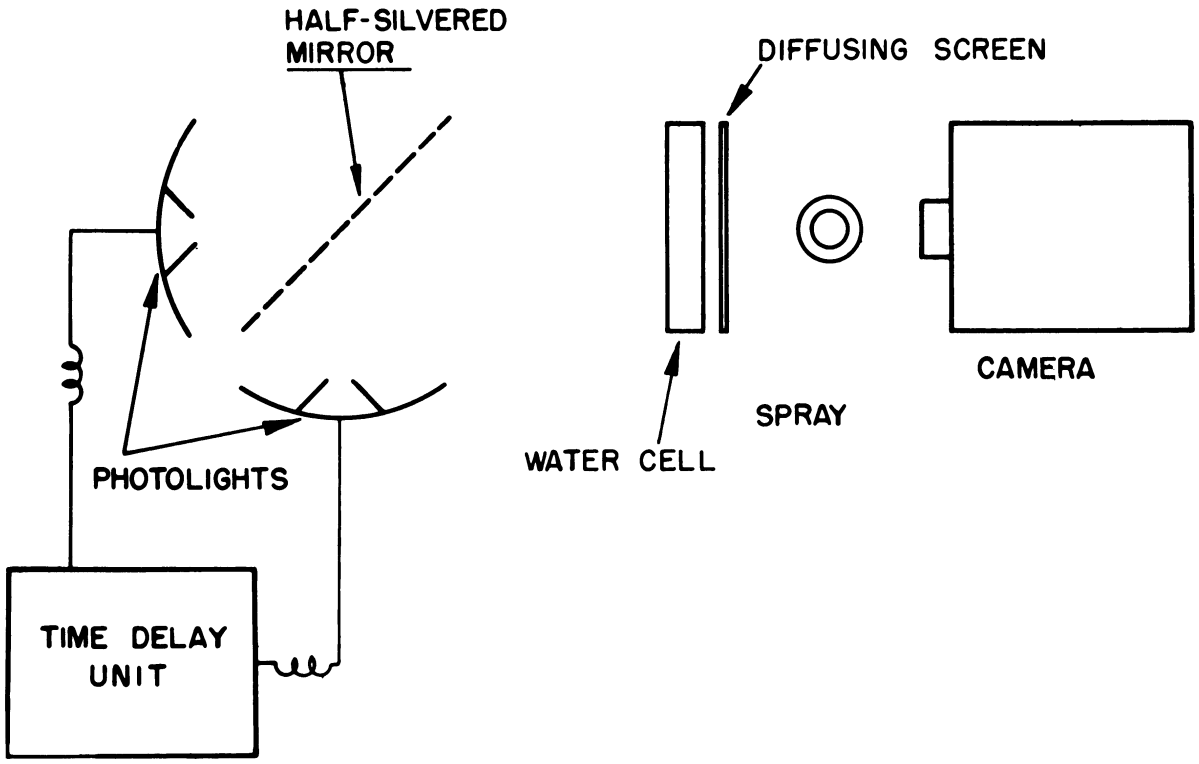

Figure 5. Arrangement for Double-Exposure Flash Photography

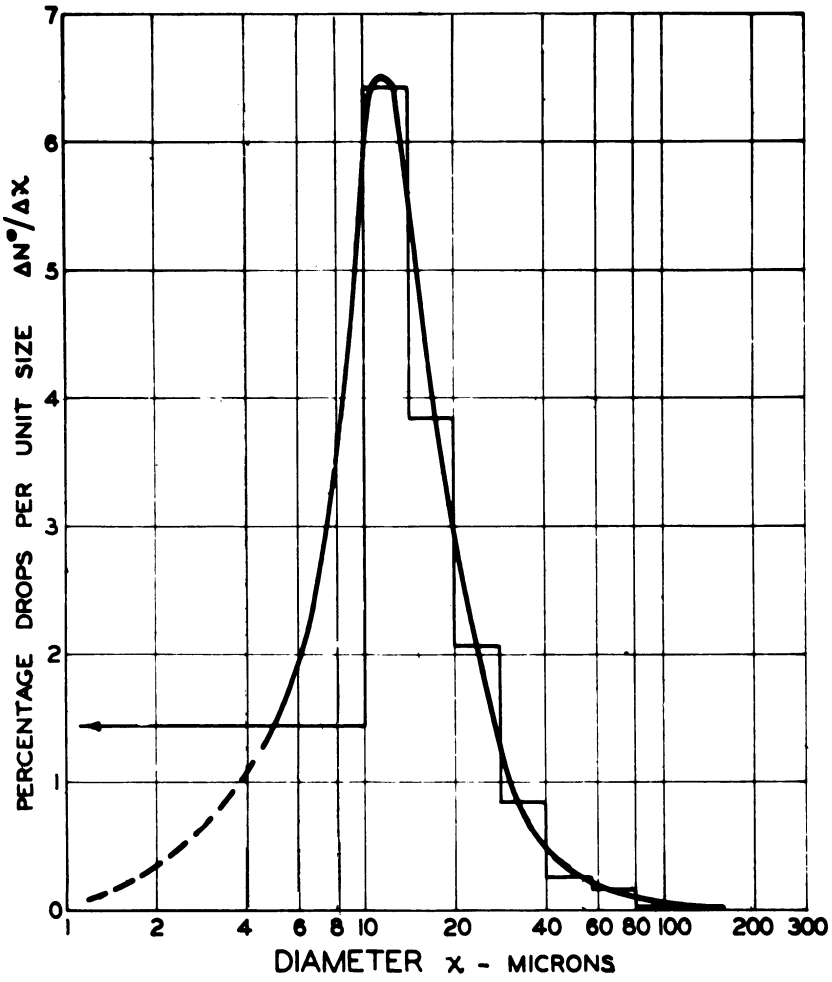

Figure 6. Direct Size-Distribution Curve at One Sample Location

Generally, the silhouette photographic technique is precise, operable down to 5 or ten microns in drop diameter, and capable of yielding more information about the spray than any other technique known. The price for all this is considerable time and manpower for complete analysis and calculation of the results. The technique should be reserved for exploratory and explanatory work, and for careful calibration of more rapid techniques, but we are forced to use it routinely in many cases for lack of a reliable economical alternative or supplement.

SPRAY NOZZLE STUDIES

It would take far too long to discuss all the problems we have investigated in the field of sprays and spray nozzle design, but a few will be shown here to give some highlights and key concepts. Most of our effort has been spent on two types of spray nozzles, air-atomizers and hollow-cone swirl-chamber nozzles, although many other types have entered into our studies.

Air-Atomizing Spray Systems

These studies were all made with the single-flash photographic technique, therefore no velocity data are included. Figures 6, 7, and 8 show typical drop-size analyses for one location in an air-atomized spray. The three curves are computed from the same data, but show three of the typical items of interest in a spray: the distribution of numbers of drops by fraction in each size class, the distribution of surface area by fraction of total surface in each size class, and the distribution of mass by fraction of total mass in each size class. Note the regular shift of the mode of the distribution curve to larger sizes as the property expressed in the ordinate changes.

The data above are all for one location in a spray pattern, and Figure 9 shows the variation in size to be found in an air-atomized spray pattern at various locations and for various mass ratios of air to water. The "average drop size" shown here is that of a drop which has the same ratio of surface per unit mass as all the drops found at that point. This is sometimes called the specific-surface average. The right hand column of curves in Figure 9 shows the way in which the concentration of mass actually varies in the spray for the same changes in mass ratio of air to water. As the air-water ratio increases, both distributions level off to give an essentially uniform spray, but at low ratios the non-uniformity is troublesome.

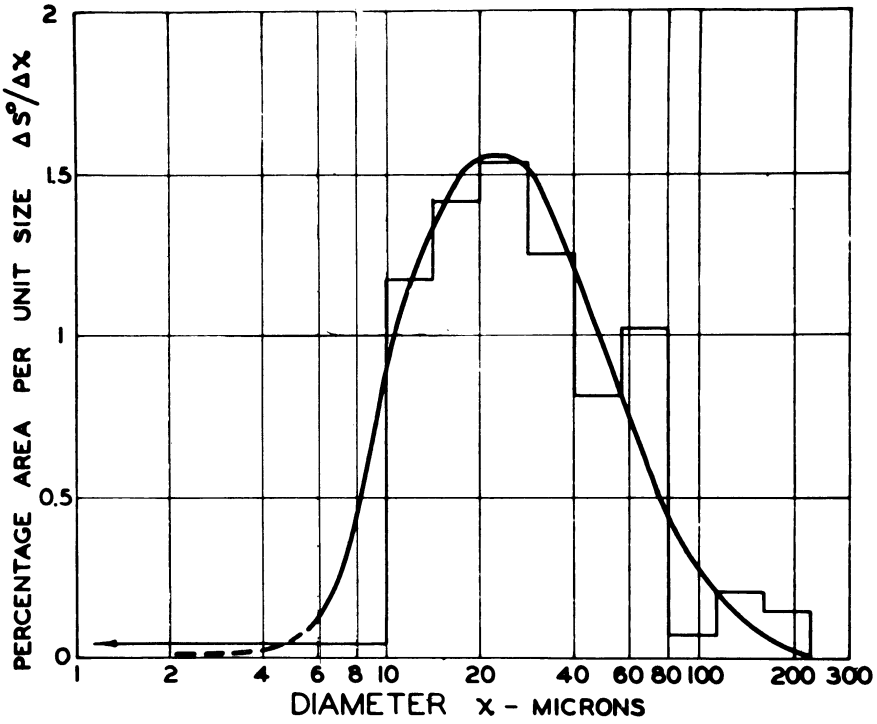

Figure 7. Size-Distribution Based on Surface Area at Same Location as Figure 6.

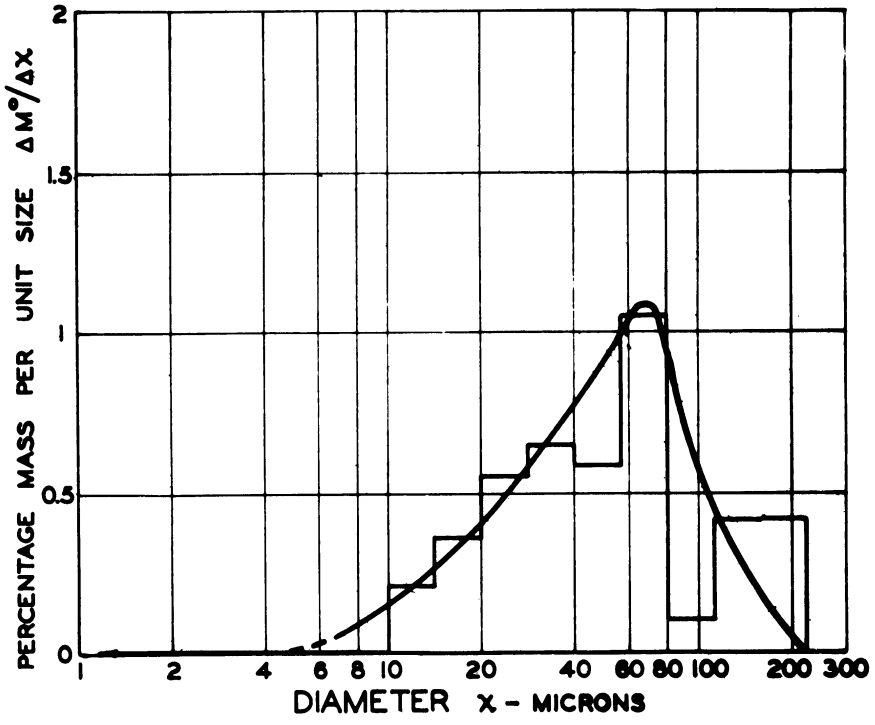

Figure 8. Size-Distribution Based on Mass at Same Location as Figure 6.

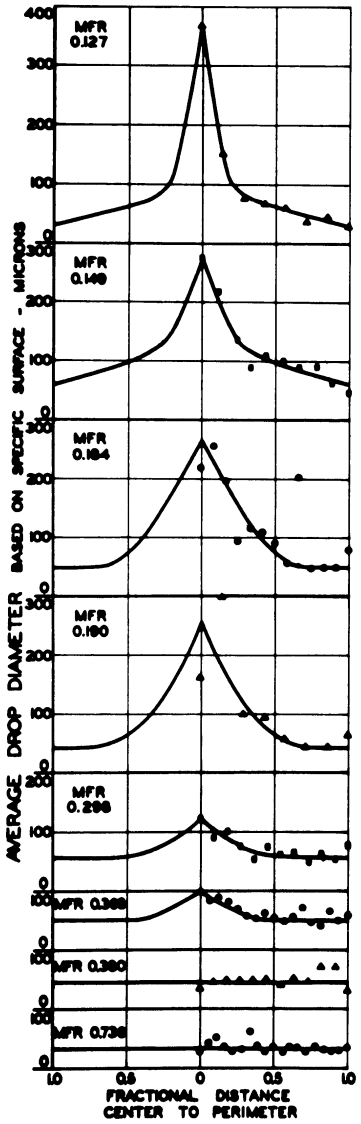

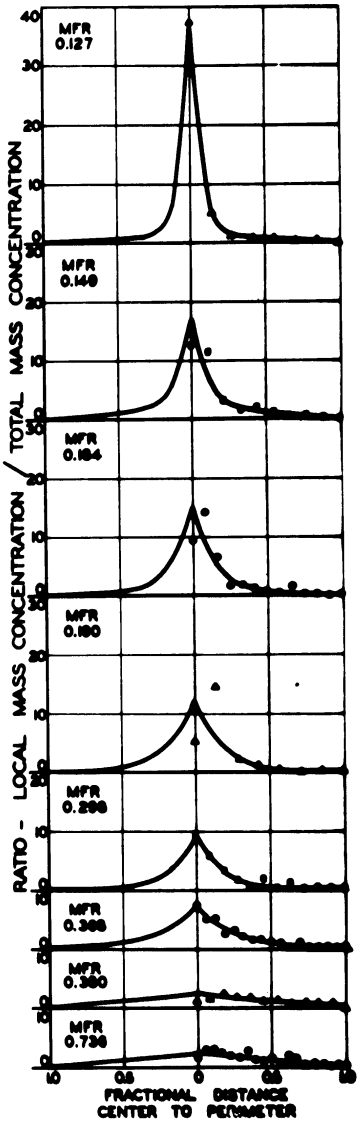

Figure 9

Variation in Drop Diameter Across All Sprays

Variation in Drop Diameter Across All Sprays

MFR: Mass Flow Ratio - Air to Water

Combining analyses across the spray at any one ratio of fluids can give an overall average drop size and overall spray properties. Figure 10 shows the specific surface of the spray formed by air and water as a function of the ratio of the two fluids. Clearly the water phase is being divided more finely as more air is used. But air is not free, and Figure 11 shows the amount of surface created for each pound of air being used as the air-water ratio increases. At a value of about 0.5 pound of air per pound of water the surface creation levels off sharply. This is further summarized by Figure 12, which shows the range of drop sizes, from maximum to minimum in the spray, as a function of the air-water ratio. Note again that at about 0.5 lb/lb the spray seems as well established as is worthwhile. Reference back to Figure 9 also shows that this ratio seems about right for good distribution of material and drop sizes. In other words, for this nozzle design, such an air-water ratio appears ideal. Less air will give less atomization, more air will cost much more without significant gain in performance.

Hollow-Cone Swirl-Chamber Spray Systems

Another common spray nozzle is the one sketched in Figure 13, with the liquid entering tangentially into a cylindrical chamber, from which it leaves by an orifice in the center of one end of the cylinder. The liquid acquires considerable spin with relatively small pressure requirements, and emerges from the orifice as a hollow cone with an air core in the center. The sheet of liquid in the cone must thin down rapidly and breaks up into ligaments and then into drops, forming a substantially hollow ring for the spray cross-section.

The hydraulics of the nozzle are relatively simple in overall factors, although complex in fine detail of turbulence and vectors. The air core persists back to the back wall of the nozzle, even with rather viscous fluids. Analysis of the fluid mechanics of this nozzle shows that the flow-pressure relationship can be predicted with satisfactory accuracy, based simply upon geometrical factors of the nozzle chamber and openings. Figure 14 shows a comparison of various lines predicted for specific nozzles, and experimental data taken for these nozzles.

The general appearance of the spray is shown in Figure 15, (taken at one microsecond) showing water coming from a hollow-cone nozzle. The factors influencing the breakup should permit us to predict the drop sizes, if we could isolate the factors well enough. An extensive study of the fluid mechanics of this situation brought out the relationship between velocities, sheet thickness, surface tension, viscosity, fluid densities, and wavelength of disturbances.

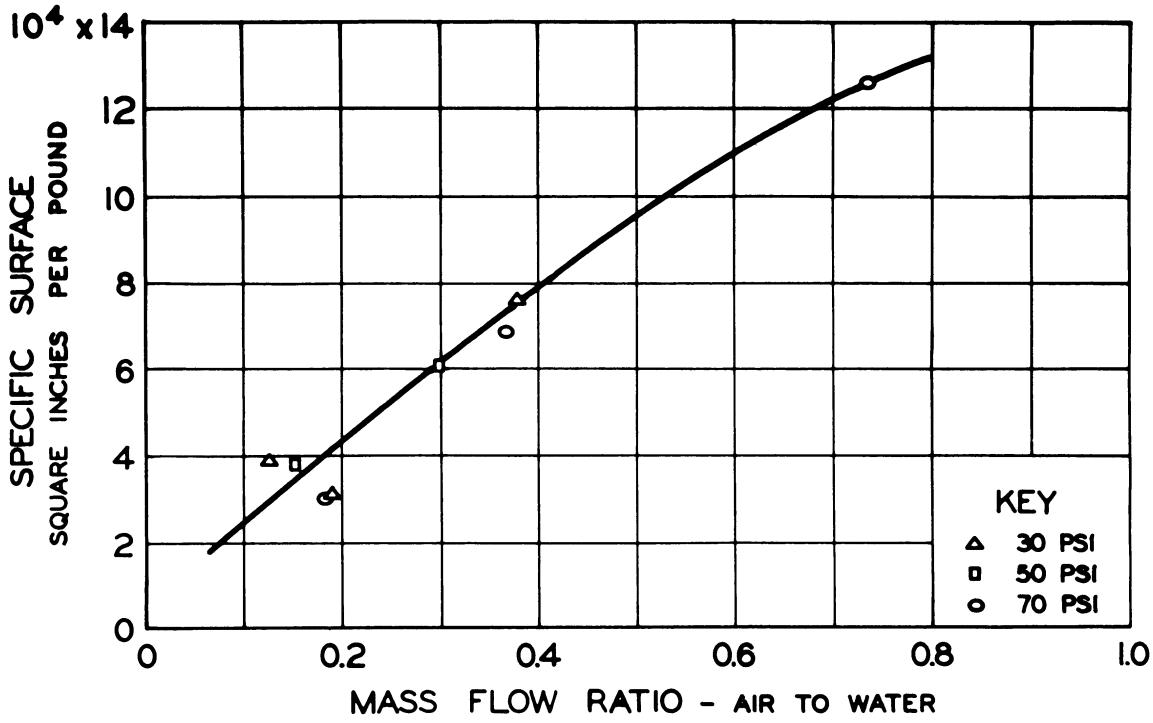

Figure 10. Specific Surface of Spray as a Function of Air Consumption.

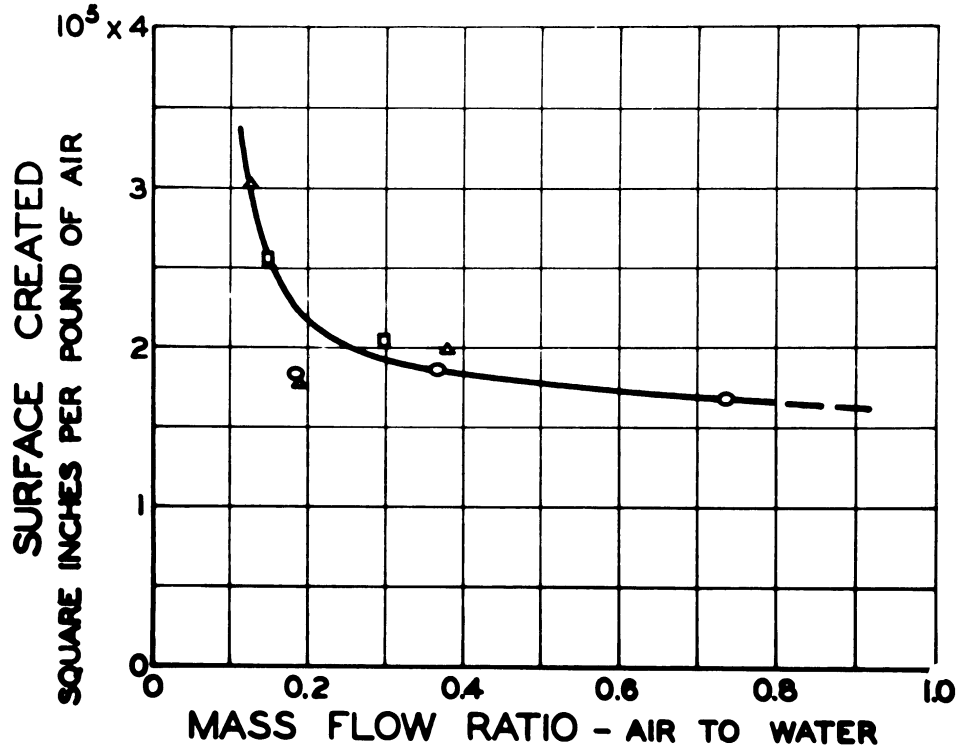

Figure 11. Spray Surface Created Per Pound of Air Consumed.

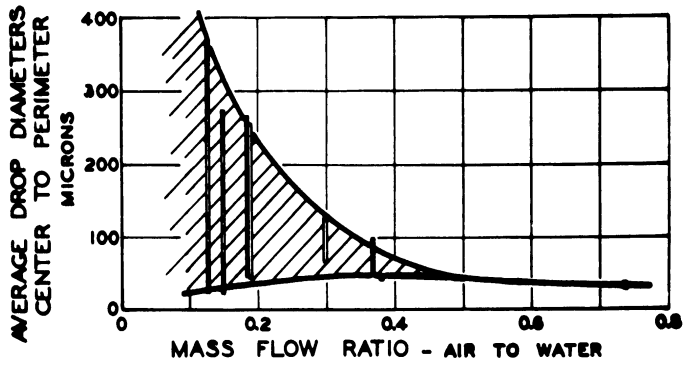

Figure 12. Range of Average Drop Diameters Across Sprays.

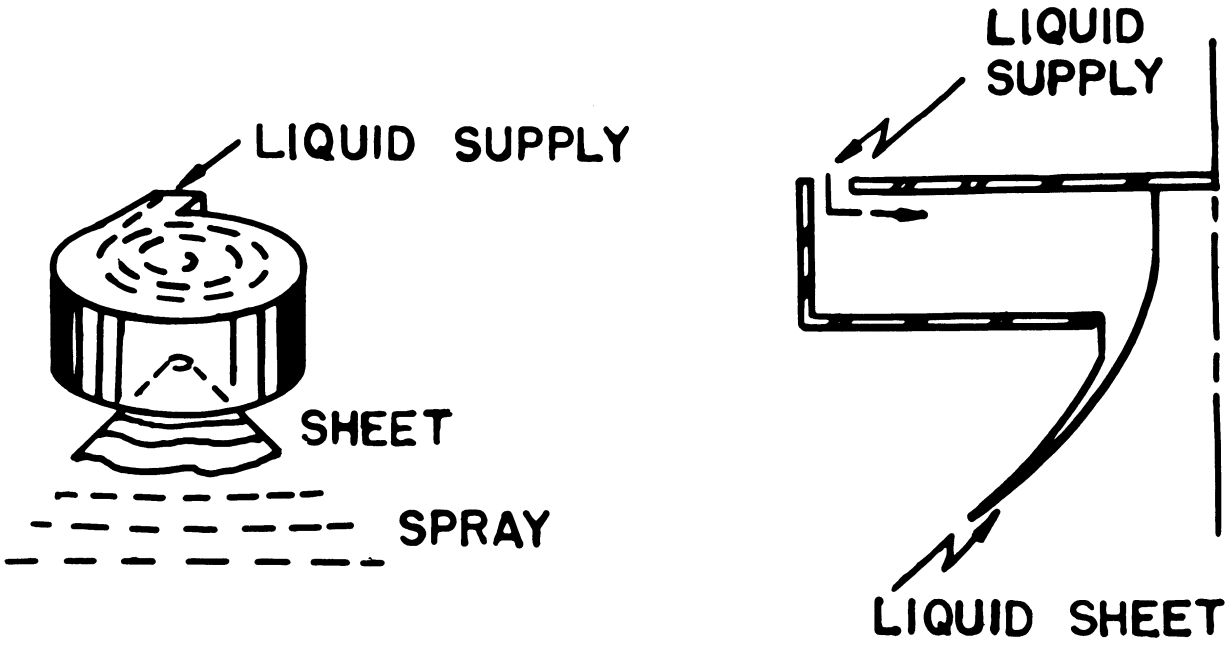

Figure 13. Sketch of Hollow-Cone Swirl-Chamber Spray Nozzle.

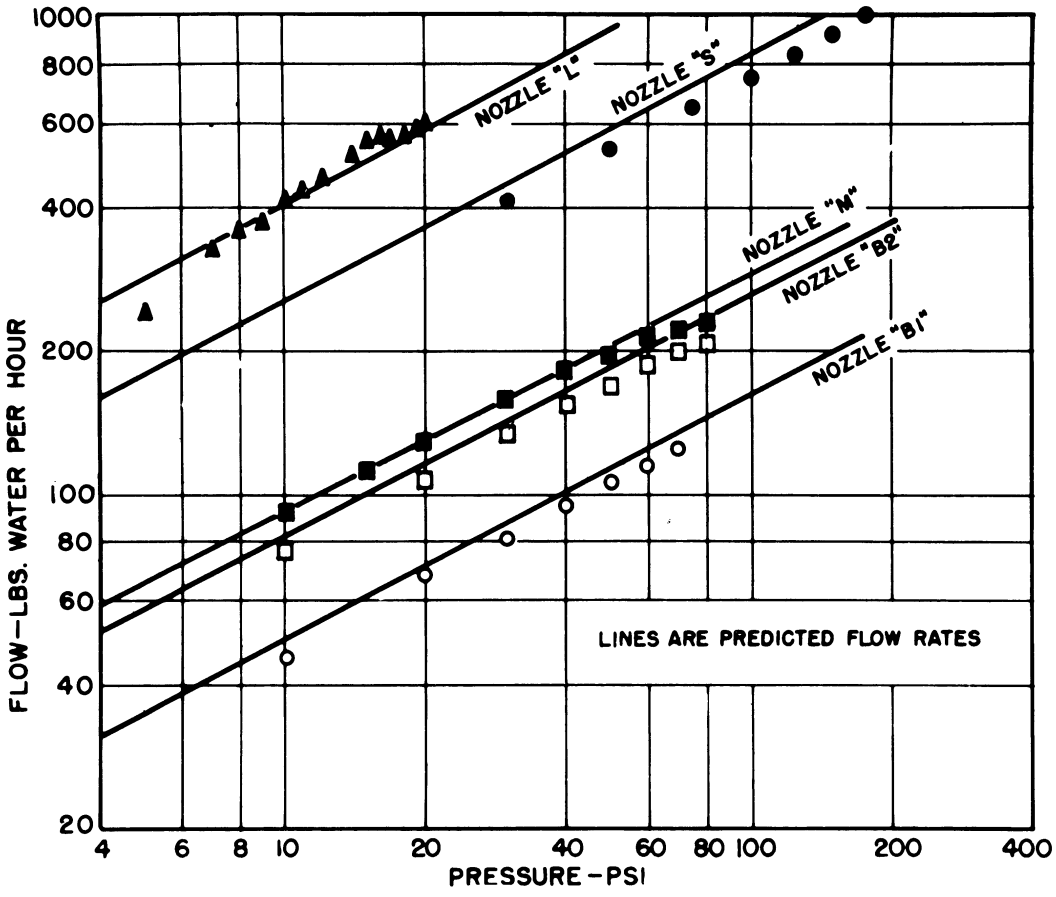

Figure 14. Comparison of Predicted and Measured Flow-Pressure Relationship for Various Hollow-Cone Swirl-Chamber Nozzles.

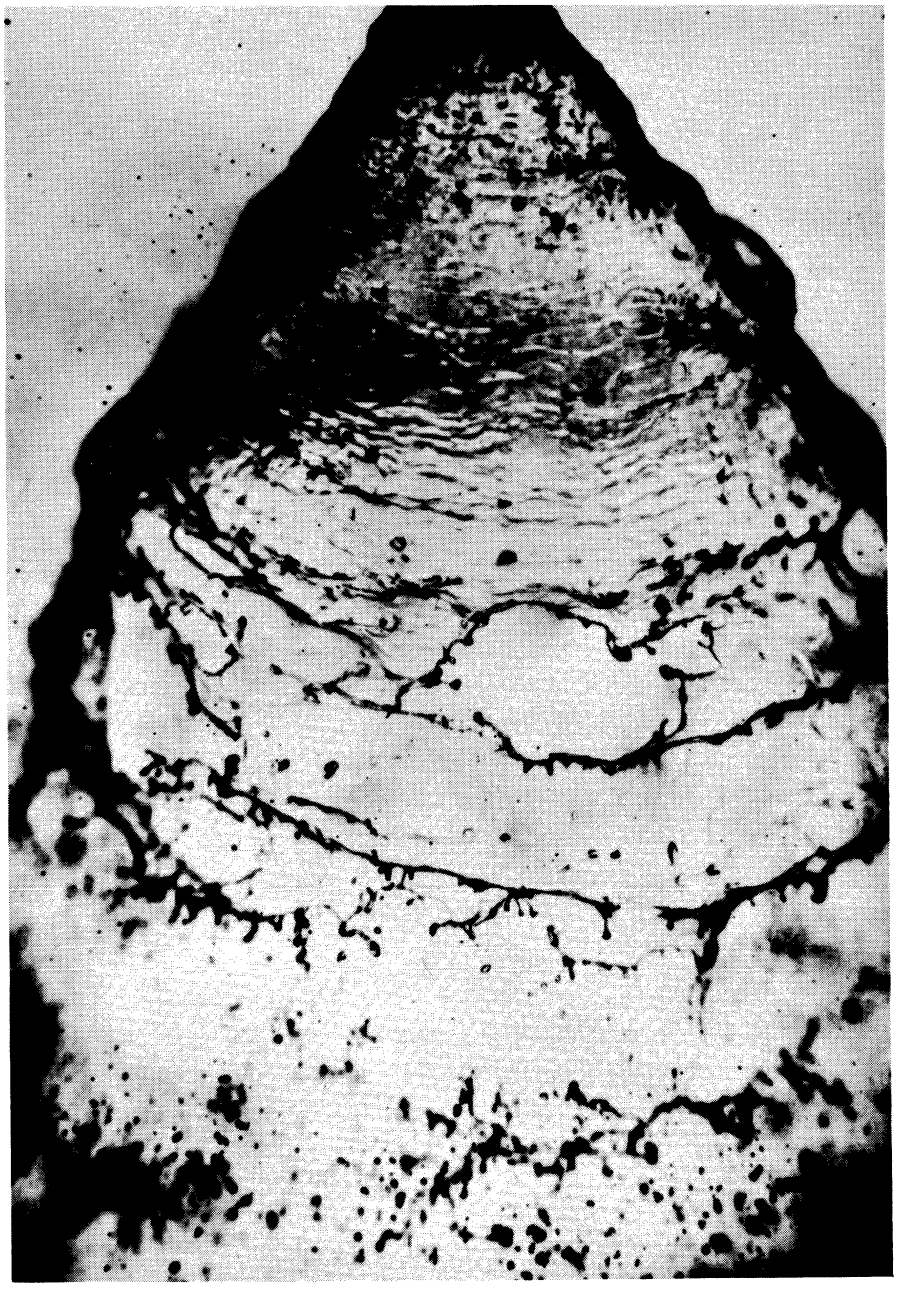

Figure 15. Flash Photograph of Liquid Break-Up From a Hollow-Cone Nozzle.

Figure 16 shows such an analysis, for one particular system, air and water. The parameter is the Weber number:

$$W = \frac{v^2 \rho_w a}{\sigma}$$

where W = Weber Number
v = Relative velocity
ρ_w = Density of water
a = Half thickness of undisturbed sheet
σ = Interfacial tension
λ = Wave length of disturbance
β = Exponential growth rate

The ordinate is called the growth-rate number, because the larger its value, the faster a wave will grow when superimposed upon a sheet of fluid. The abscissa relates the wavelength of the disturbance to the sheet thickness. The striking thing about this curve, computed though it is, is the sharp peak at a particular wavelength-thickness ratio. Such a wave would grow faster than all others and eventually rupture the sheet. Waves of shorter wavelength, such that the curve falls into the region of negative values, would not grow, but would be damped. Examination of Figure 15 shows just that, for the short wavelength disturbances in the sheet as it emerges from the nozzle, where the sheet is thick, are damped out to give a smooth surface part way down the cone. Larger waves eventually rupture the sheet into lacy holes and ligaments running transverse to the direction of fluid motion. This explains why such a spray is never uniform in drop population, but seems gusty with the drops coming in waves of high and low drop population.

The central part of the spray from such a nozzle is low in drop population, as expected, but Figure 17 shows that it also contains a high proportion of smaller drops. The angle of 0° is on the centerline about six inches from the orifice, and 28° is approximately at the zone of highest drop population. The difference in drop size distribution is considerable.

Application of the double-flash technique to such a spray also shows the variation in velocity with both drop size and location in the spray. Figure 18 gives curves from the centerline out to the zone of highest population at 32°. At all locations in this analysis the spread of drop velocities is great, going up to tenfold at the most important location. This variation in velocity is the result of the drop system acting as an ejector, pumping air from the surroundings into the zone of the spray. The drops, or really the sheet of liquid, all emerge from the orifice at essentially a constant velocity, but as the drops give

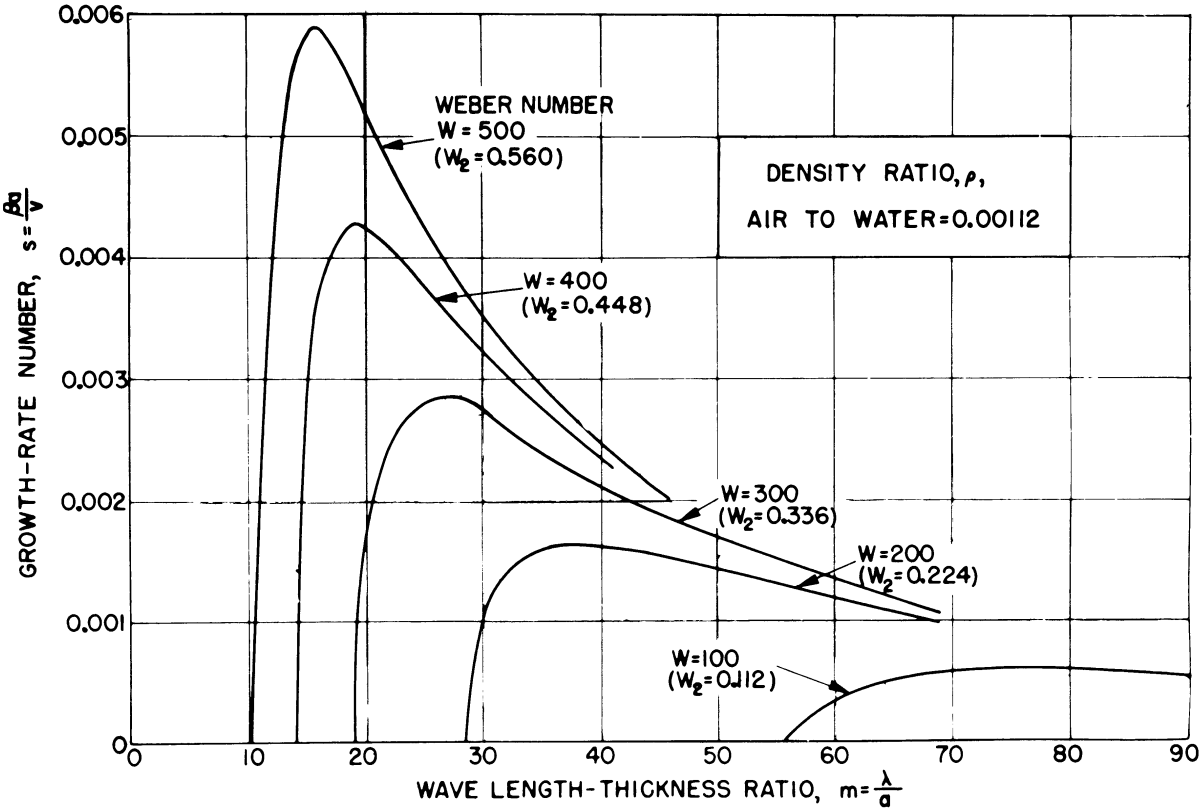

Figure 16. Growth Rate of Waves in Sheets of Liquid Emerging From a Hollow-Cone Nozzle.

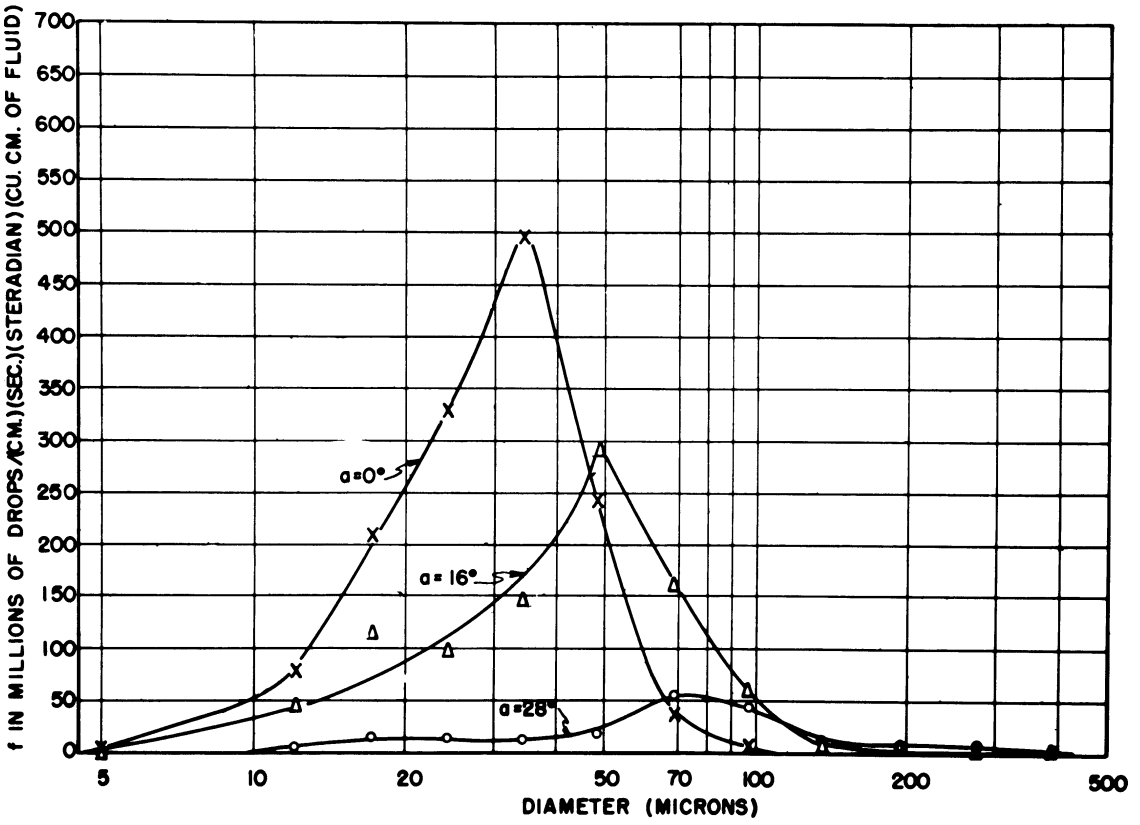

Figure 17. Size-Distribution at Different Angular Locations from Centerline of a Hollow-Cone Spray

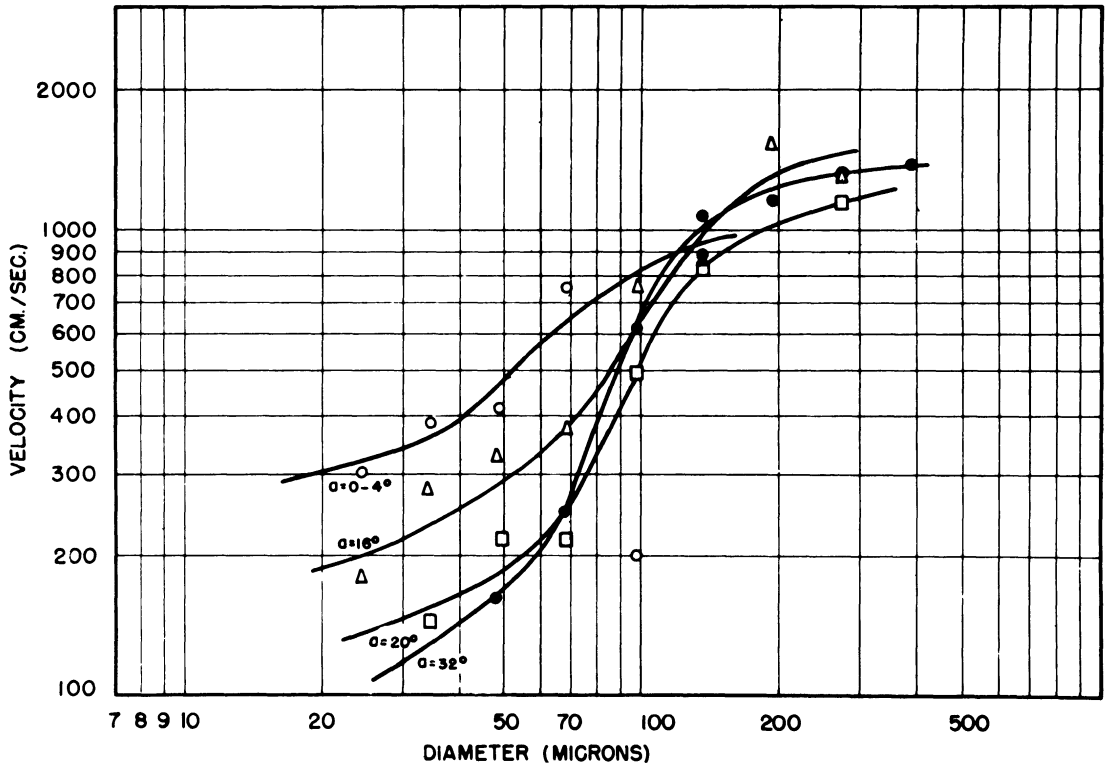

Figure 18. Drop Velocity at Various Locations in Hollow-Cone Spray.

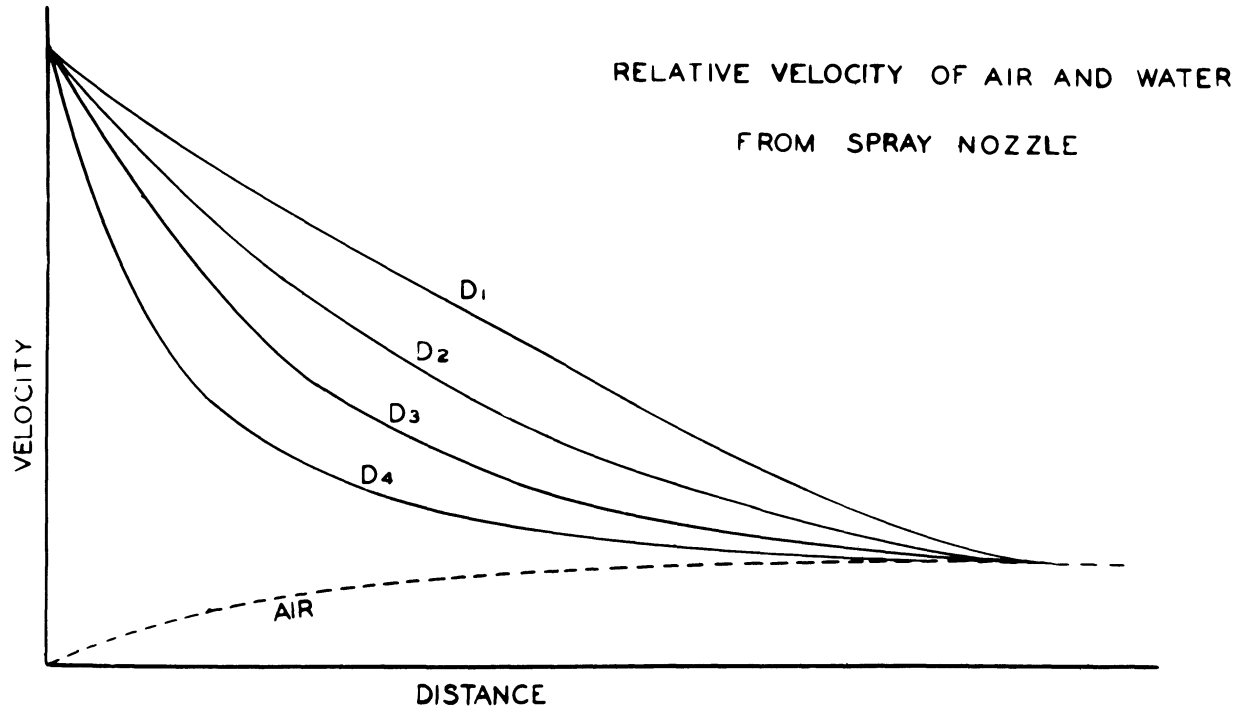

Figure 19. Drop Velocities at Various Distances From Hollow-Cone Nozzle. ($D_1 > D_2 > D_3 > D_4$)

part of their energy to the air around them they slow down and the air speeds up. At a considerable distance from the nozzle a uniform velocity for the entire two-phase system may exist, but not enough information is available to do more than conjecture. Figure 19 represents our thinking on how the velocities vary with distance from the orifice and with drop size. The smaller drops slow down quickly and the larger ones more slowly, thus at some distance out a large spread in velocities will exist.

The effect of physical properties of the liquid on the spray has been the subject of much concern, but it is far from clear yet. For example, Figure 20 shows how a hollow-cone nozzle sprays a thick suspension, almost a paste. The cone is formed, usually with slightly smaller cone angle, and breaks up into holes and ligaments as before. The collapse of the sheet between the holes is much slower than with low-viscosity fluids, therefore the cone has structure for longer distances from the orifice. The energy required to form such a spray is not excessive, as shown in Figure 21. A slurry of sodium bicarbonate in three liquids: water, 0.65 glycerine-0.35 water, and 0.80 glycerine-0.20 water, was sprayed and the zones of spray formation and columnar flow outlined. By increasing the pressure on slurries of low concentration, the spray could be formed easily. At the highest concentrations, approaching a paste with the solid particles all touching one another, the transition region climbs to quite high pressures. We were unable to determine whether it is impossible for these concentrations to be sprayed, but we think they can be.

Our research as discussed here is not all linked into a pretty story, for we opened more doors than we closed with every investigation. We were after specific engineering results in every case, and rarely were able to digress into curious roads of exploration. As time goes on we hope to fill in some of the gaps we found, but we know we shall always have more questions than answers.

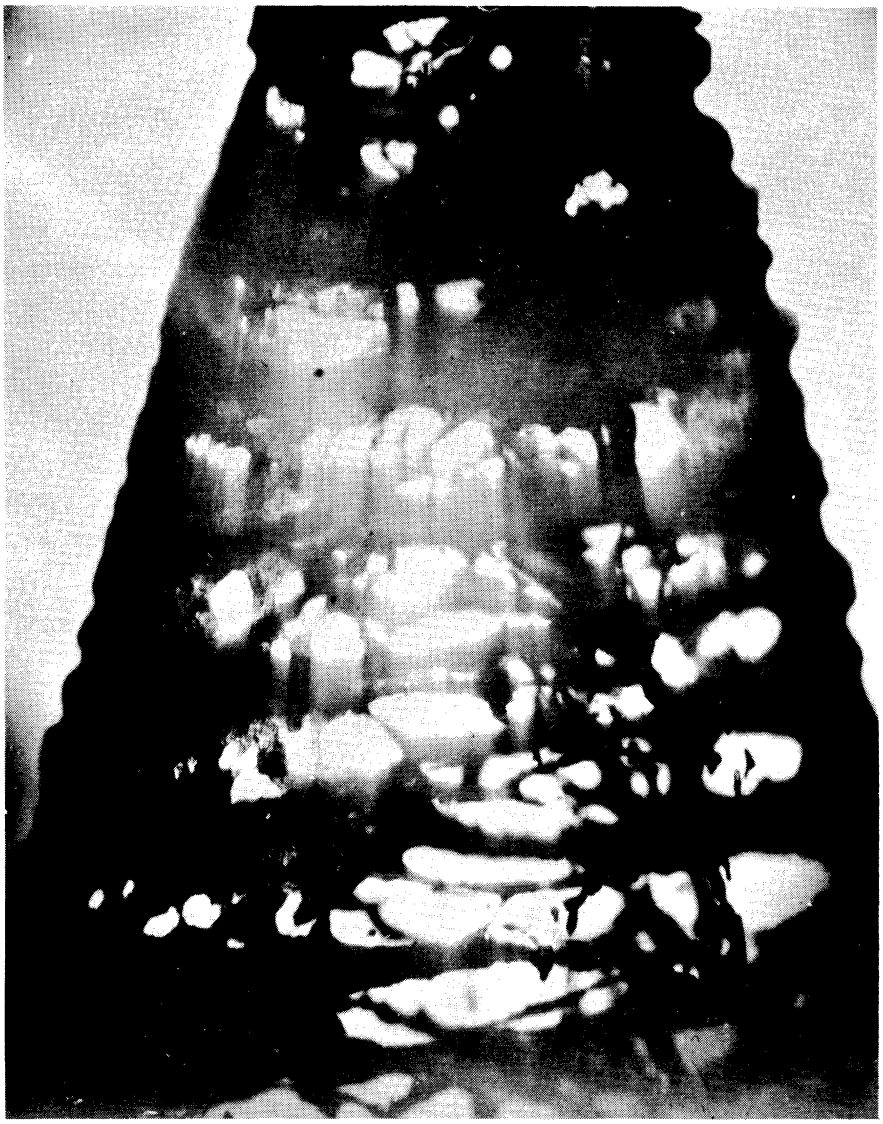

Figure 20. Spray of Paste From Hollow-Cone Nozzle

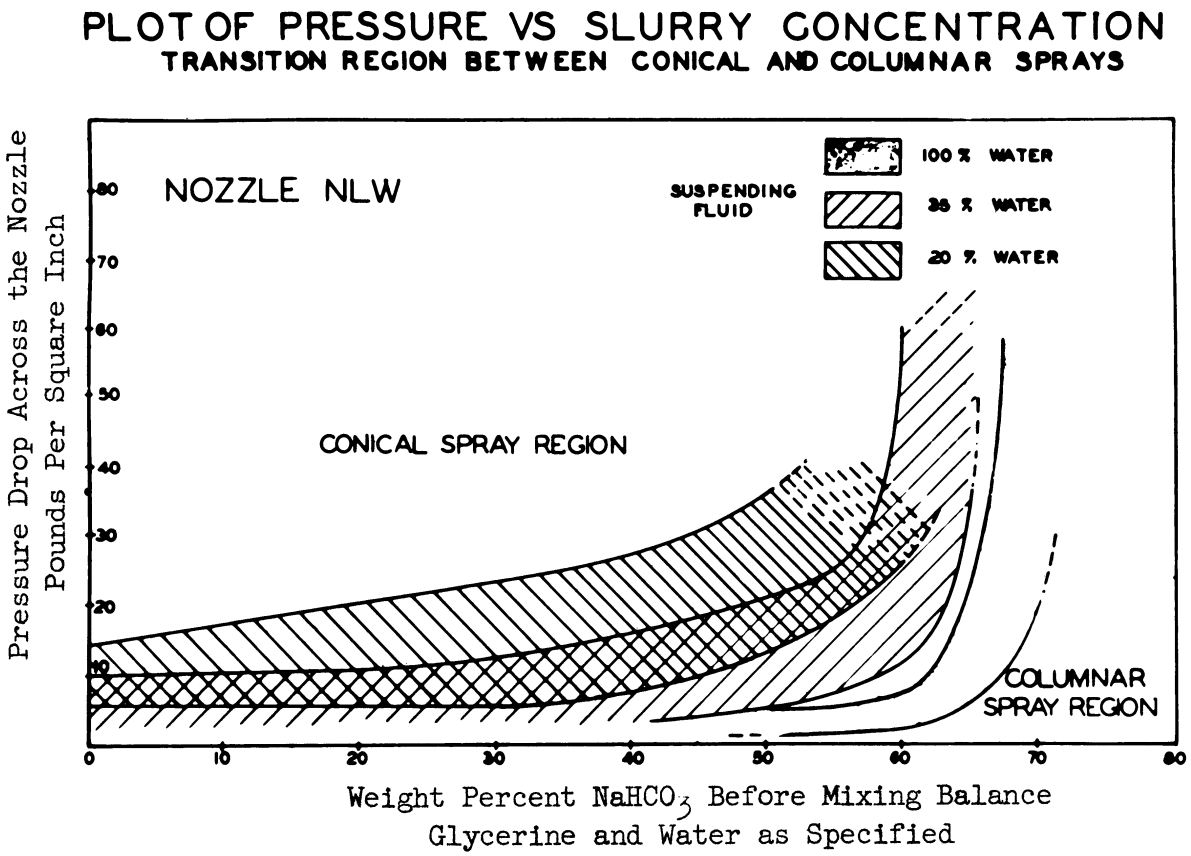

Figure 21. Energy Requirements for Paste Spray From Hollow-Cone Nozzle.

BIBLIOGRAPHY

1. Chin, Jin H., "Particle Size Distributions from Angular Variation of Intensity of Forward-Scattered Light," Ph.D. Thesis, University of Michigan, (1955).

2. Consiglio, Joseph A., "The Effect of Operating Variables on Sprays Produced by a Pressure-Type Nozzle," Ph.D. Thesis, University of Michigan (1953). See also A.I.Ch.E. Journal, 3: 418-427 (1957).

3. Dodge, R. A., Hagerty, W. W., York, J. L., et al., "Continuous Fuel Sprays," parts I, II, III, IV, Air Force Technical Report 6067 (1949-1952).

4. Geist, Jacob M., "An Electronic Spray Analyzer for Electrically Conducting Particles," Ph.D. Thesis, University of Michigan (1950). See also Ind. Eng. Chem., 43: 1371-1377 (1951).

5. Gumprecht, Roland O., "Particle Size Measurements by Light Scattering," Ph.D. Thesis, University of Michigan (1952). See also J. Phys. Chem, 57: 90-97 (1953).

6. York, J. L., and Stubbs, H. E., "Photographic Analysis of Sprays," Trans. A.S.M.E., 74: 1157-1162 (1952).

7. York, J. L., Stubbs, H. E., and Tek, M. R., "The Mechanism of Disintegration of Liquid Sheets," Trans. A.S.M.E., 75: 1279-1286 (1953).

THE FLOW OF PASTES

M. R. Tek
Assistant Professor of Chemical Engineering
The University of Michigan

THE FLOW OF PASTES

M. R. Tek

INTRODUCTION

A paste is a mixture of grandular solids with a continuous liquid phase. Pastes, in general, have high volume fraction solids.

The interest on the quantitative flow behavior of "pastes" has recently been quite apparent in many areas of direct engineering applications. The need for quantitative information on the variables which determine and affect the pressure drop-flow rate relations in multiphase flow systems has been growing along with the advent of many large scale engineering processes. In these operations, "paste-like materials" are in transfer through pipes, orifices, conduits, reactors and special equipment of all types of geometry and flow characteristics. The performance of dry or wet moving catalyst beds such as the one encountered in "cat-cracker" operation, the flow of high density, high solids concentration drilling muds used in oil well drilling operations, fluid flow, mixing, turbulence, heat transfer phenomena encountered in reactor technology applied to semi-liquid, semi-plastic "non-Newtonian" materials are the more prominent examples of "paste-like flow."

When multiphase flow systems are considered from a viewpoint of fluid dynamic behavior the following observations may be made at varying ranges of the bulk density spectrum.

At the density values corresponding to very low volume fraction solids the flow behavior is found to be very close to that of a truly "Newtonian fluid". At increasing solids concentrations, up to a certain point, the Newtonian fluid mechanics would still apply, but the actual numerical value of the viscosity of the liquid phase must be corrected for the effect of the solids present. At even higher densities or volume fraction solids one finds the non-Newtonian flow behavior is basically characterized by a non-linear relationship between the shear stress and the rate of shear. The science of rheology,which basically studies deformation and flow of matter,further classifies the non-Newtonian fluids according to their time-dependent and time-independent behavior. Rheopecticity, thixotropy, pseudo-plasticity, Bingham-plasticity, dilantantcy are all typical examples of non-Newtonian flow behavior.

When the volume fraction solids of a two-phase flow system is further increased to a range, perhaps more adequately described as paste density, a curious, extremely interesting behavior is usually found somewhere between the mechanics of non-Newtonian flow and that of the motion

of dry granular solids. Under these circumstances the knowledge of truly non-Newtonian flow behavior or the scanty information available on the flow of dry granular solids are of little help since the pastes quite often deviate markedly from each of the extreme theoretical models.

The interesting ability of a paste to combine the high density of a solid with the mobility of a fluid suggests the paste flow as a promising mean of transportation of granular solids. From a nuclear engineering viewpoint, on the other hand, a reactor, fueled with paste-like material would appear to combine the desirable controllability of a solid core with the mobility of a fluid.

HIGHLIGHTS OF PASTE FLOW RESEARCH AT THE UNIVERSITY OF MICHIGAN

The engineering research work conducted at the University of Michigan for the past three years has mainly centered around investigating the mechanics of paste flow in simulating paste flow systems by experiments conducted on glass beads, sand, copper-shot, quartz for granular solid materials and water, mineral oil, kerosene for continuous liquids. Co-current co-gravity downward flow through tubes equipped with bottom orifices, low-density, counter gravity upward lift through similar channels, studies of flow rate pressure drop, paste density, manifold performance, velocity profiles have yielded much interesting and valuable data. While research work is still continuing in this general subject and finalized answers to most pertinent questions are not yet quite available, significant and promising progress has been made on some special areas.

Pressure Drop-Flow Rate Relations

Large amounts of data collected in the past indicate that a relatively high density "fluid-like" paste flow can be maintained in square or rectangular vertical flow channels, equipped with bottom orifices. While a generalized pressure drop-flow rate relation through the geometric and physical properties of the flow system has not yet been theoretically or empirically developed, the application of dimensional analysis supplemented with theoretical studies on non-Newtonian flow and experimental data on the flow of granular systems appear the most promising route toward this objective.

Figure 1 represents the sketch of a typical experimental setup used to collect flow rate-pressure drop data across a given orifice or tube. A typical example of pressure drop-flow rate data is indicated in Figure 2.

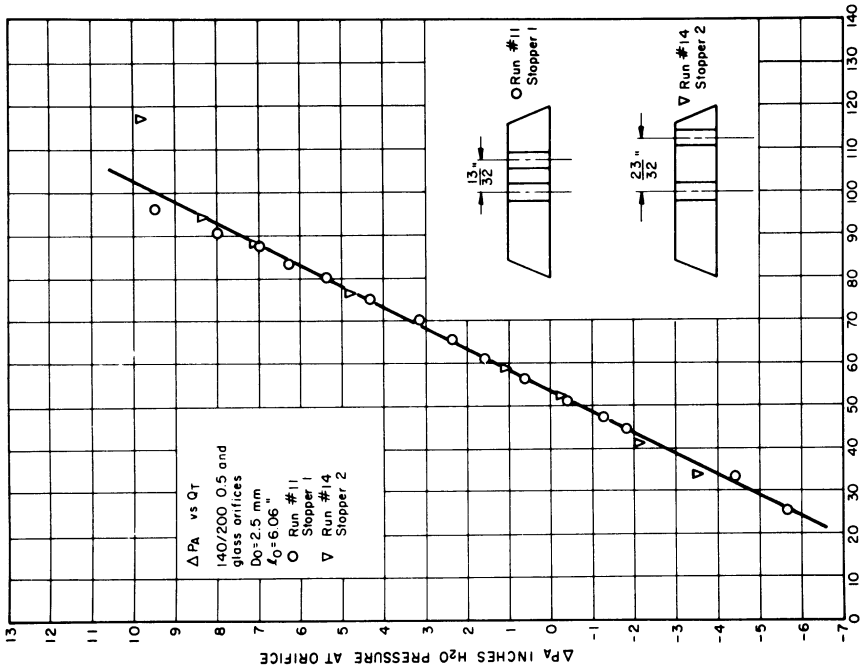

Figure 2.

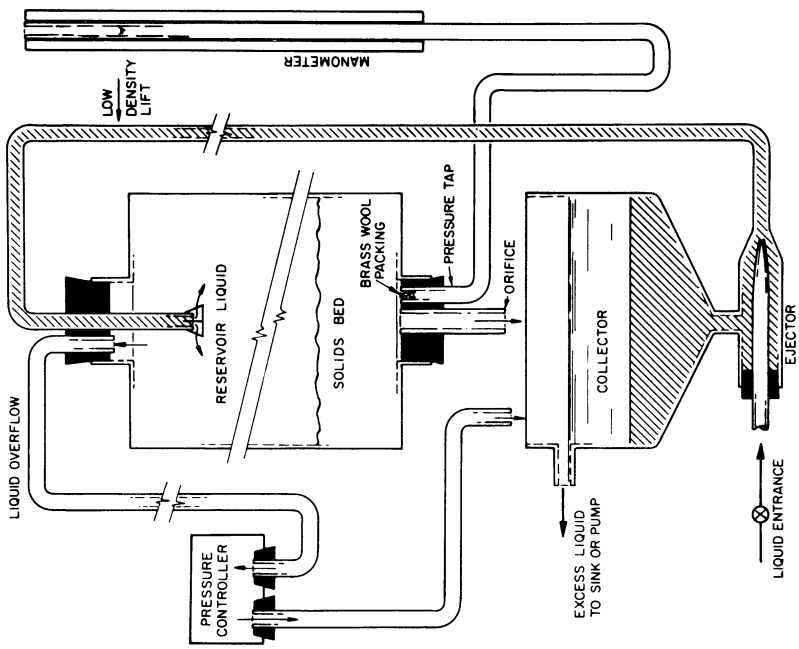

Figure 1.

Paste Deformation Velocity Profile Studies

The fluid deformation attended by the flow of paste in a two dimensional flow channel was quantitatively investigated by using pastes containing colored glass beads and time controlled exposure photography. The channel used for the measurements, rectangular in cross-section, equipped with an orifice in the bottom and loaded with several layers of differently colored glass beads, is indicated in Figures 3, 4, 5 and 6. Figure 3 indicates the static condition just prior to flow with each interface nearly straight and horizontal. In these flow experiments, after preparing the channel for flow, the orifice was unplugged at the bottom and photographs were taken at regular time intervals. The Figures 4, 5 and 6 indicate such photographs taken at about one minute intervals.

From the photographs and the steel ruler mounted along the length of the flow channel and knowing the magnification ratio of the photograph to the model, the relative displacement of each interface was determined as a function of both the space and time variables as the paste continuously deformed during the flow. These measurements give some idea on the development of the velocity profiles at least approximately and during the non-steady state conditions of early flow periods.

In observing the Figures 4, 5 and 6 it may be remarked that at a given height the beads on or nearer the symmetry axis move a great deal more than the ones near the side walls of the channel. A similar observation may be made relative to the displacement of the beads located at a fixed distance from the side walls and away from the orifice. Of these, the beads closer to the orifice move a great deal more than the ones appreciably farther from the orifice. The slope of the deformed interface which is nearly zero along the side walls at short flow durations also gradually increases as the flow develops in the channel. From the measurements made on the location of the interface in two spaces (x and y) and one time manifolds, it appears quite possible to obtain interesting and important data on approximate velocity profiles, pseudo-boundary layer effects, streamlines and equi-potential surfaces.

The encouraging results so far obtained by this photographic technique also suggest that the approach of using individual colored, speckled glass beads and perhaps differently colored dye in the liquid phase should yield further valuable information on how pastes deform under flowing conditions.

The Density of Pastes

The inventory volume or mass of solid particles present in the paste is a direct measure of paste density. In many applications of paste flow systems, and, particularly in the nuclear engineering area, the problem of measurement and variation of paste density becomes important.

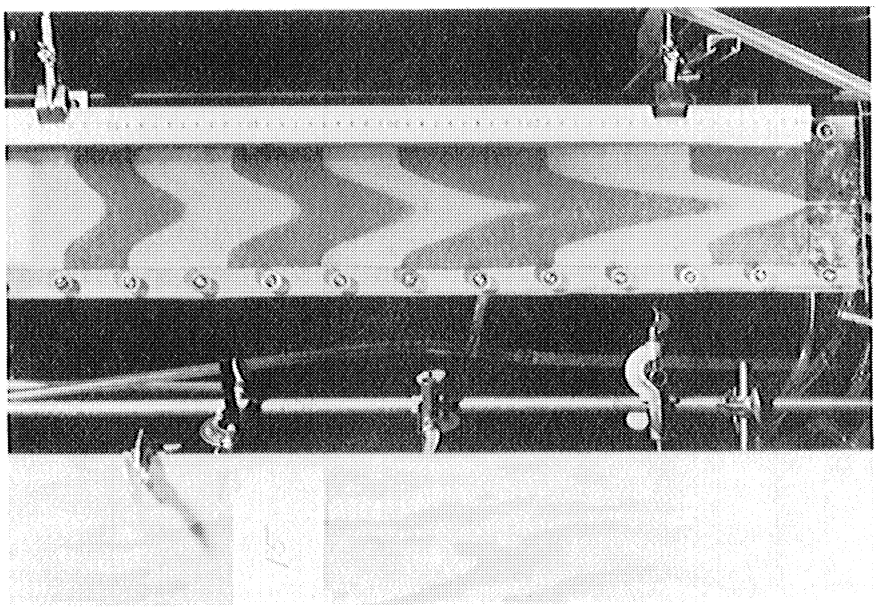

Figure 4.

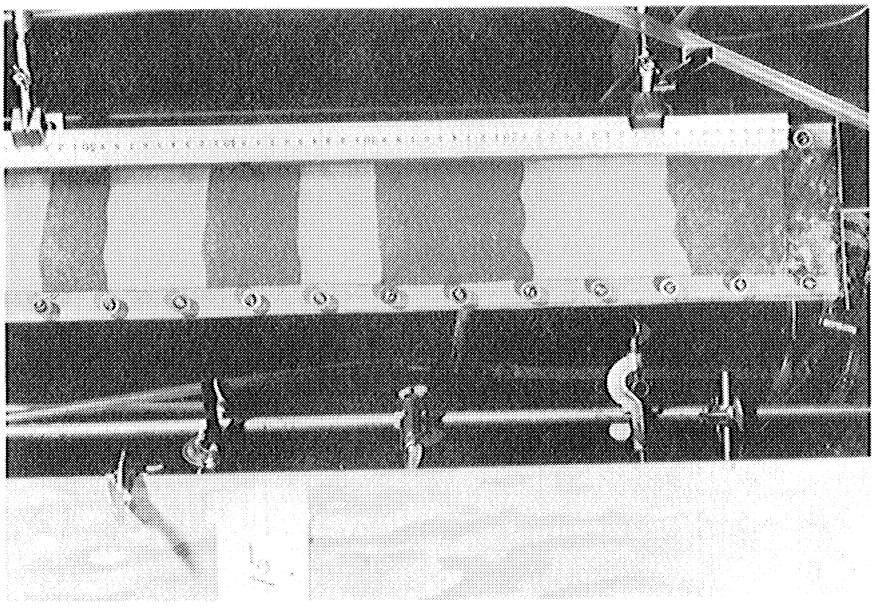

Figure 3.

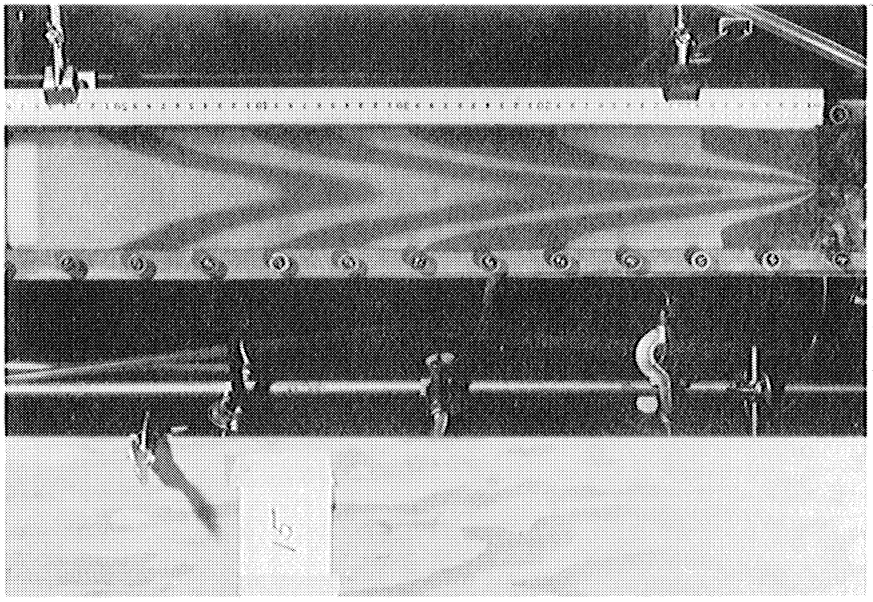

Figure 6.

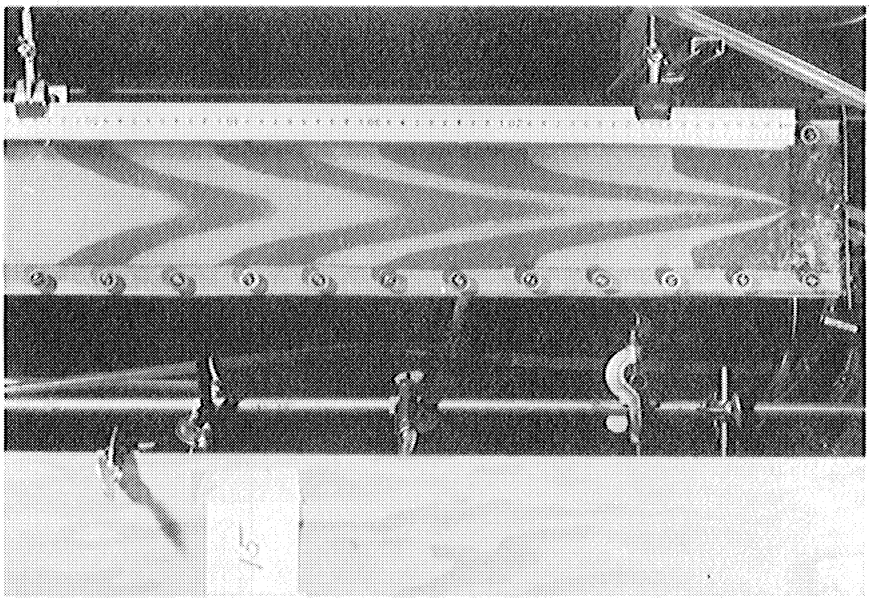

Figure 5.

The density of a paste constituted by solid particles of known size, shape and properties and liquid of known mass and properties may be shown to be a linear function of volume fraction solids. During the earlier studies on paste flow some encouraging preliminary results were obtained in correlating the density of the paste against the electrical resistance measured between two platinum probes submerged in the paste. This method has recently been developed to obtain direct experimental data on static and flowing density of pastes. The effect on the paste density of interrupting a flowing system by stopping the flow was determined in a number of experiments.

In these preliminary experiments it was found that the paste density, expressed as volume fraction solids, can be correlated with the AC impedance by a straight line over the working spectrum of paste porosities ranging from "free-settled" to "tapped-settled" values.

Figure 7 represents the experimental setup used during the calibration and measurement of static and flowing paste densities.

Figure 8 is a photograph of the equipment used in the paste density measurement program.

Figure 9 represents a typical calibration curve where the AC impedance was plotted versus the volume fraction solids.

When calibration curves obtained on the same system at different times are compared it was found that, while these curves shift, they remain remarkably parallel. The parallel shift in these calibration curves, Figures 10 and 11, may be plausibly explained by the fact that the aggregate electrical impedance offered to AC voltage between two probes changes each time with the particular configuration of randomly packed beads. The change in the impedance corresponding to a change in the average packing density between two probes, however, remains constant for a given system.

The data collected so far indicate that the density of a flowing paste does not change by more than about four per cent when the flow is interrupted. Most of the data show a paste density increase of less than one per cent.

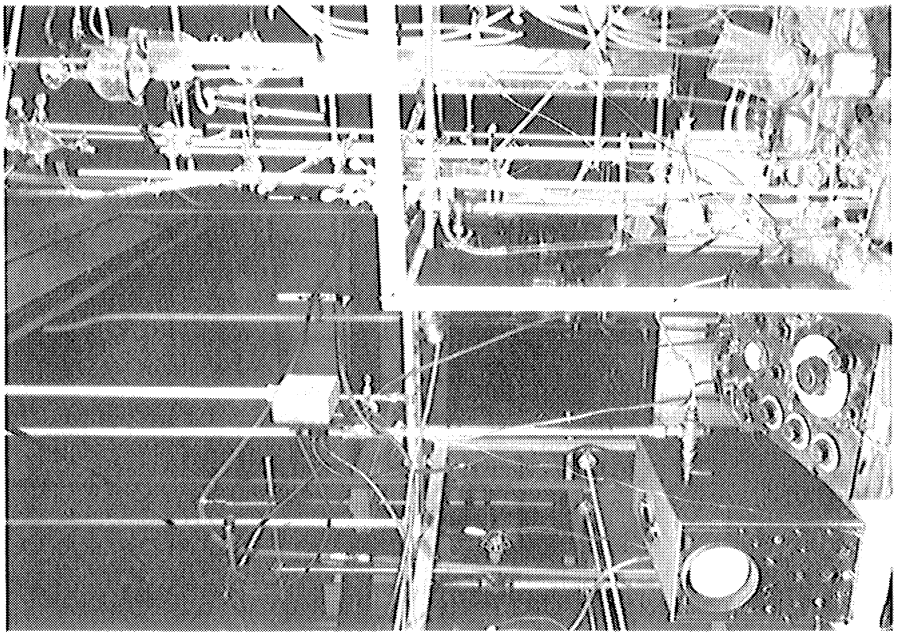

Figure 8.

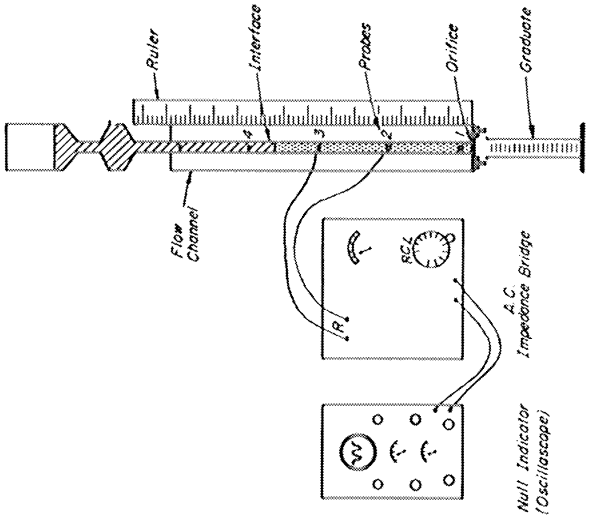

Figure 7.

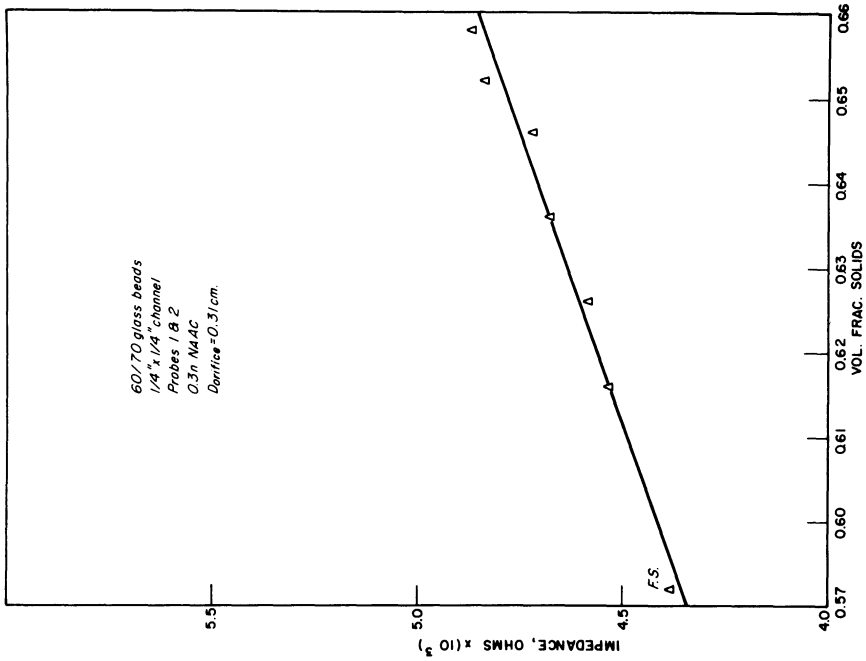

Figure 10.

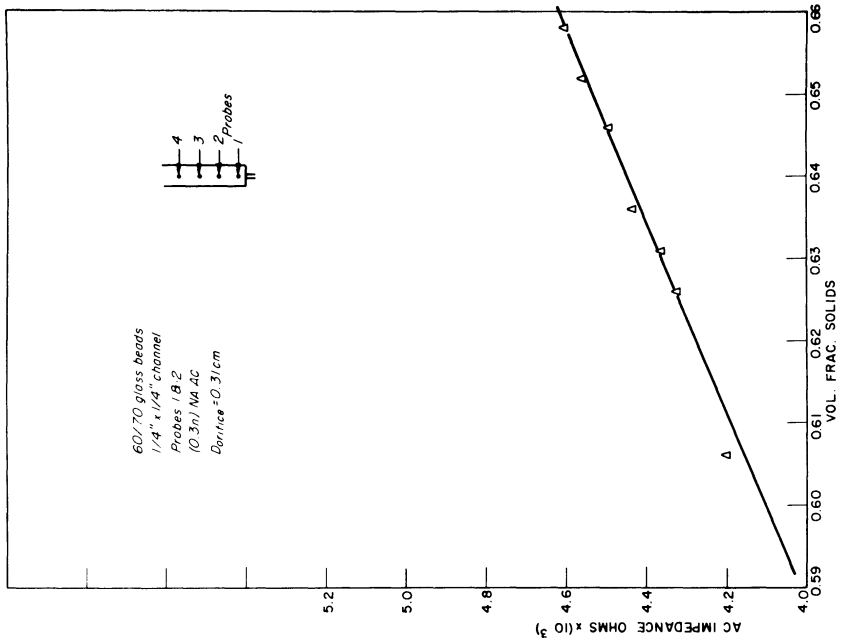

Figure 9.

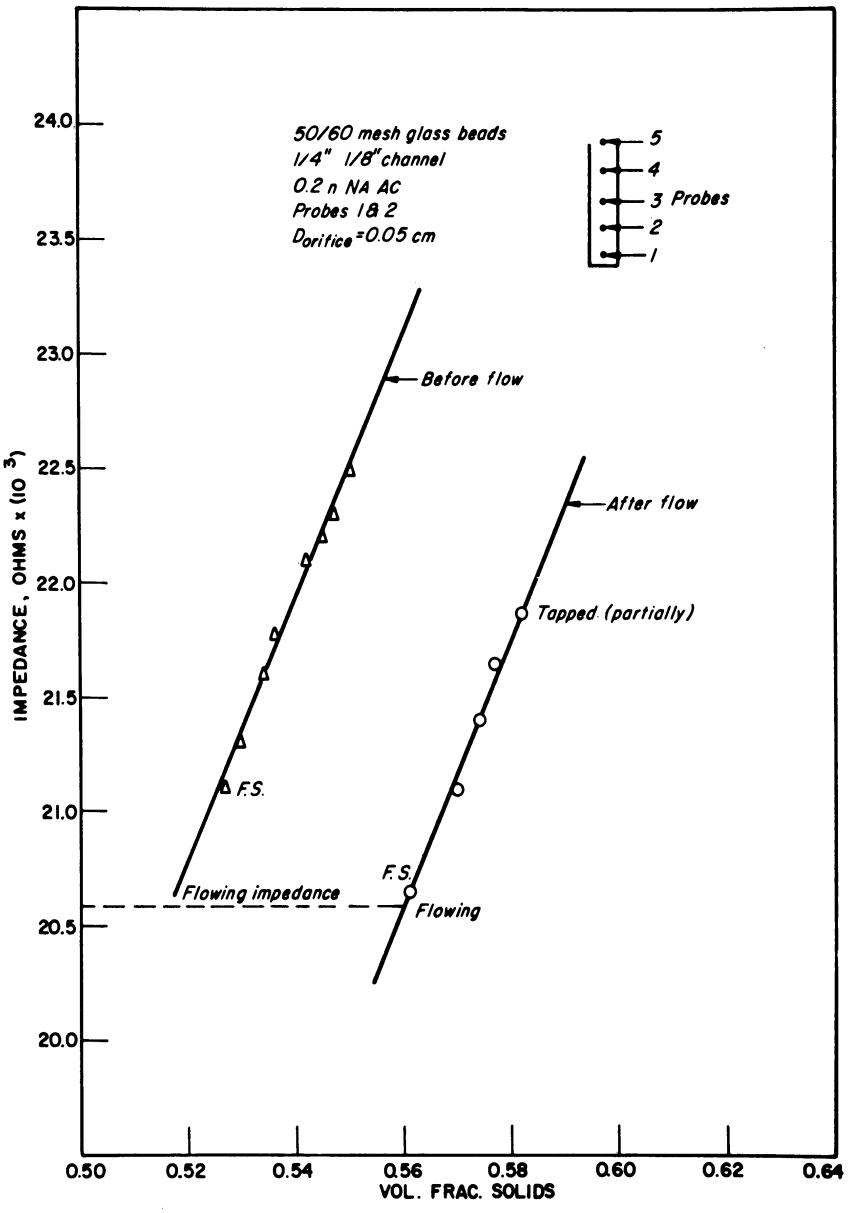
50/60 mesh glass beads
1/4" 1/8" channel
0.2 n NA AC
Probes 1 & 2
$D_{orifice}$ = 0.05 cm
5
4
3 Probes
2
1
Before flow
After flow
Tapped (partially)
F.S.
F.S.
Flowing impedance
Flowing
IMPEDANCE, OHMS x (10^3)
24.0
23.5
23.0
22.5
22.0
21.5
21.0
20.5
20.0
0.50
0.52
0.54
0.56
0.58
0.60
0.62
0.64
VOL. FRAC. SOLIDS

Figure 11.